# „Einfluss von Defekten des Mismatch Reparatur Proteins MLH1 (Mut L Homolog 1) auf Fertilität und Tumorgenese im Mausmodell“

Dissertation zur Erlangung des

naturwissenschaftlichen Doktorgrades

der Julius-Maximilians-Universität Würzburg

vorgelegt von

Cora Reiß

Aus Wiesbaden

Würzburg 2010

Eingereicht am: .....

Mitglieder der Promotionskommission:

Vorsitzender: .....

Gutachter : Prof. Dr. Dr. Manfred Schartl

Gutachter: Prof. Dr. Ricardo Benavente

Tag des Promotionskolloquiums: .....

Doktorurkunde ausgehändigt am: .....

# Inhaltsverzeichnis

*I Einleitung* _____ *- 1 -*

**I.1 Krebsprädispositionsyndrome und genomische Integrität** _____ **- 1 -**

**I.2 Das erbliche, nicht-polypöse Kolonkarzinom (HNPCC)** _____ **- 3 -**

**I.3 Das Mismatch Reparatur System** _____ **- 5 -**

**I.4 MMR defiziente Mausmodelle** _____ **- 9 -**

**I.5 Meiotische Funktion** _____ **- 10 -**

**I.6 MLH1** _____ **- 11 -**

**I.7 Zielsetzung der Arbeit** _____ **- 12 -**

*II Ergebnisse und Diskussion* _____ *- 14 -*

**II. 1. Auswirkungen der MLH1$^{G67R}$ Mutation auf die Meiotischen Mismatch Reparatur Funktionen, Meiose und Tumorgenese im Mausmodell** _____ **- 14 -**

**II.2. Konditionelle Inaktivierung von MLH1 in thymischen und naïven T-Zellen führt zu verminderten Inzidenzen lymphoblastischer Lymphome im Mausmodell** _____ **- 21 -**

**II Nebenprojekt 1: Reaktive Antikörper gegen das hitzeschock Protein 65 aus dem Mycobakterium bovis Bazillus Calmette Guerin prognostizieren den Erfolg der Immuntherapie bei hochgradigen Transitionalzellkarzinomen der Blase.** _____ **- 24 -**

**II. Nebenprojekt 2: STAT3 und SMAD1 Signalgebung in embrynalen Stammzell-ähnlichen Medaka Zellen und Blastula Embryonen** _____ **- 26 -**

*III Zusammenfassung* _____ *- 28 -*

*IV Summary* _____ *- 30 -*

*V Methoden* _____ *- 32 -*

*VI Referenzen* _____ *- 32 -*

*VII Danksagungen* _____ *- 40 -*

*VIII Eidesstattliche Erklärung* _____ *- 42 -*

**Anhang 1: *Mlh1*$^{G67R/G67R}$ Tumortiere**
**Anhang 2: *Mlh1*$^{G67R/-}$Tumortiere**
**Anhang 3: *Mlh1*$^{\Delta Ex4/\Delta Ex4}$ Tumortiere**
**Anhang 4: *Mlh1*$^{T\Delta Ex4/T\Delta Ex4}$ Tumortiere**
**Anhang 5: *Mlh1*$^{T\Delta Ex4/-}$ Tumortiere**
**Anhang 6: *Mlh1*$^{T\Delta Ex4/G67R}$ Tumortiere**

**Anlage 1:** Avdievich, E., Reiss, C., Scherer, S., Zhang, Y., Maier, S., Jin, B., Hou, H., Jr., Rosenwald, A., Riedmiller, H., Kucherlapati, R.,Cohen, P., Edelmann, E. and Kneitz, B. (2008). Distinct effects of the recurrent Mlh1G67R mutation on MMR functions, cancer, and meiosis. Proceedings of the National Academy of Sciences of the United States of America.

**Anlage 2:** Reiss, C., Haneke, T., Völker, H., Spahn, M., Rosenwald, A., Edelmann, E. and Kneitz, B. Conditional inachtivation of MLH1 in thymic and naïve T-cells in mice leads to a limited incidence of lymphoblastic T-cell lymphomas. Leukemia and Lymphoma accepted 2010.

**Anlage 3:** Ardelt, P, Kneitz, B., Adam, P., Reiss, C., Kocot, A., Fensterle, J., Chen, L., Pasqualini, R., Arap, W., Gerharz, E., and Riedmiller, H. (2010). Reactive antibodies against bacillus Calmette-Guerin heat-shock protein-65 potentially predict the outcome of immunotherapy for high-grade transitional cell carcinoma of the bladder. Cancer

**Anlage 4:** Wagner, T., Kraeussling, M., Fedorov, L., Reiss, C., Kneitz, B. and Schartl, M. (2008). STAT3 and SMAD1 signalling in Medaka embryonic stem-like cells and blastula embryos. Stem cells and development.

## Auflistung des Eigenanteils

# I Einleitung

## I.1 *Krebsprädispositionsyndrome und genomische Integrität*

Für den Organismus ist die Aufrechterhaltung der genomischen Integrität jeder einzelnen Zelle essentiell, da Veränderungen des genetischen Materials die Gefahr von malignen Ereignissen bergen. Durch die große Zahl täglich in jeder Zelle auftretender DNA Schäden kann es zur Akkumulation genetischer Veränderungen kommen, die schließlich auch zur Aktivierung von Protoonkogenen, zur Inaktivierung von Tumorsuppressorgenen oder zur Bildung von Fusionsgenen führen. Dies macht deutlich, dass der Erhalt der genomischen Integrität nur möglich ist, wenn es gelingt, eine Vielzahl verschiedener DNA-Schäden effektiv zu beheben oder zumindest deren Weitergabe an Tochterzellen zu verhindern. Je nach Art des DNA Schadens werden unterschiedliche Reparatursysteme aktiviert um die genomische Integrität und somit die korrekte Weitergabe des Erbguts an die Tochterzellen zu gewährleisten. Alternativ aktivieren die DNA Reparatursysteme bei einem starken DNA-Schaden einen Zellzyklusarrest. Falls die Schädigung irreparabel ist, bzw. nicht während des Arrestes behoben werden kann, wird der programmierte Zelltod (Appoptose) eingeleitet um eine Weitergabe des Schadens an die Tochterzellen zu verhindern. Bei defektivem DNA-Reparaturmechanismus kann dies jedoch nicht mehr gewährleistet werden und es kommt zur Entartung der betroffenen Zellen bis hin zur Tumorentstehung. Die Bedeutung der DNA-Reparatursysteme als Wächter der genomischen Integrität wird daraus ersichtlich, dass Defekte in jedem der in Abb. 1 dargestellten DNA Reparatursysteme mit einem Krebsprädispositionssyndrom assoziiert ist.

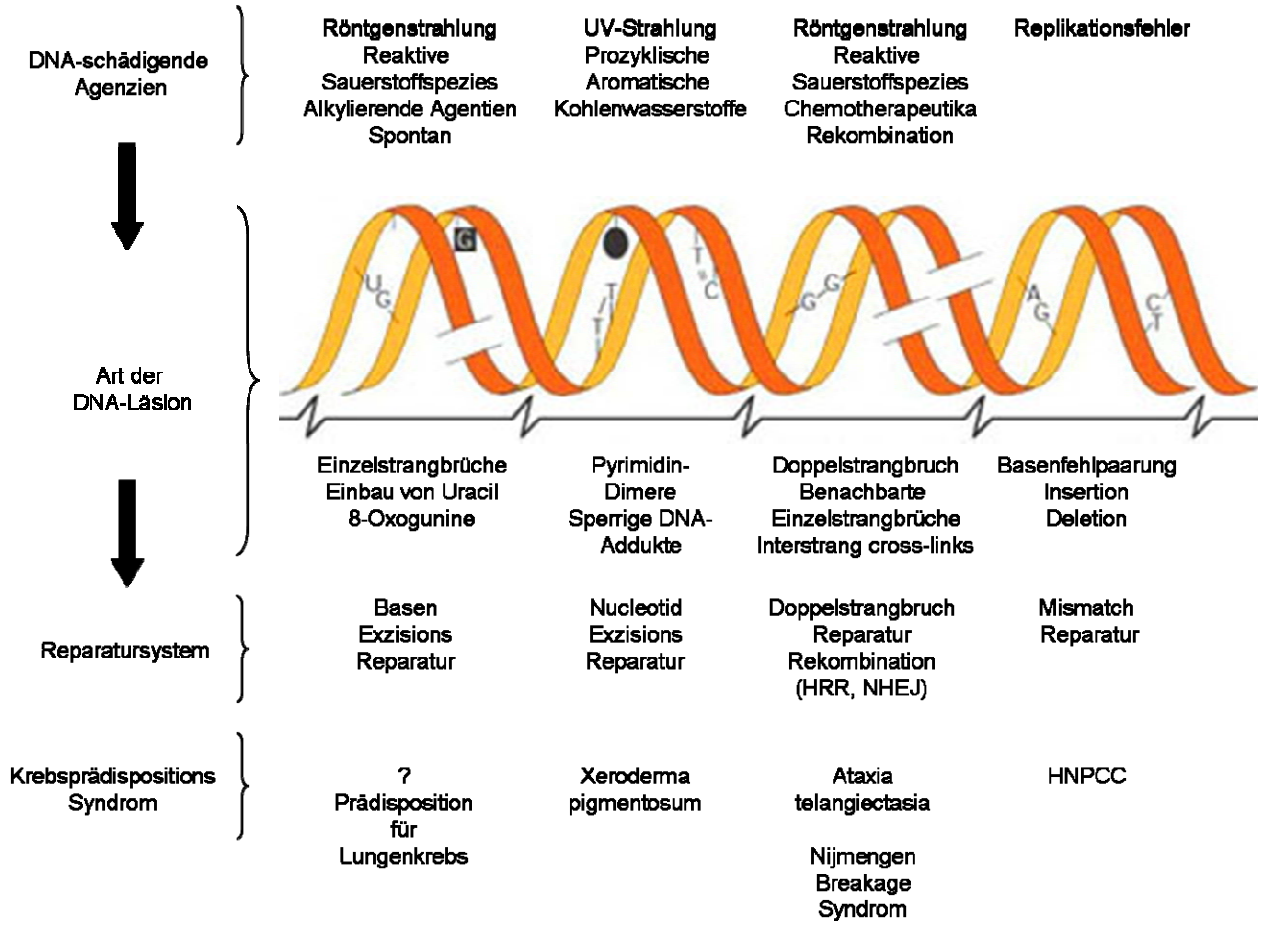


**Abb. 1: Überblick über die wichtigsten DNA-Reparatursysteme.** Aufgezeigt werden mögliche DNA schädigende Agenzien, Art der DNA Läsion sowie die an der Reparatur dieser Schäden beteiligten Systeme und Krebsprädispositions Syndrome bei fehlerhaftem Reparatursystem. Modifiziert nach (Emmert et al., 2006) und (Hoeijmakers, 2001).

So sind bestimmte Polymorphismen im XRCC1-Gens des Basen Exzisions Reparatursystem (BER) mit einer Prädisposition für Lungenkrebs assoziiert (Divine et al., 2001); Mutationen in einem der XP Gene (XPA-XPG) des Nucleotid Exzisions Reparatursystems (NER) führten zu Xeroderma pigmentosum, was mit einem über 1000fach erhöhten Risiko für sonnenlichtinduziete Hauttumoren einher geht (Cleaver, 1968) und eine fehlerhafte Doppelstrangbruchreparatur ist der Grund von Ataxia Telangiectasia (AT) und dem Nijmegen Breakage Syndrom (NBS) die ein erhöhtes Krebsrisiko bedingen (McKinnon and Caldecott, 2007; Taylor et al., 1996). Das vielleicht prominenteste Krebsprädispositionssyndrom aufgrund von DNA Reparaturdefekten stellt das erbliche, nicht-polypöse Kolonkarzinom (HNPCC) dar, welches durch eine fehlerhafte Mismatch Reparatur hervorgerufen wird. Neben diesem „klassischen“ Krebsprädispositions Syndrom sind Mutationen in den MMR Genen für das Muir-Torre Syndrom verantwortlich. Dies wird als Subgruppe von HNPCC eingestuft, bei der Patienten neben viszeralen Tumoren vom HNPCC-Typ auch Hauttumore

entwickeln. Diese spezielle Kombination von Hauttumoren und gleichzeitiger Neigung zu viszeralen Malignomen wurde 1967/68 unabhängig voneinander durch Muir und Torre beschrieben (reviewed durch (Kruse and Ruzicka, 2004)). Eine weitere durch MMR Defekte ausgelöste Erkrankung ist das Turcot Syndrom. Beschrieben wurde es 1959 vom kanadischen Chirurg Turcot. Klinisch wird das nach ihm benannte Syndrom durch das gemeinsame Auftreten von Hirntumoren und multiplen kolorektalen Adenomen definiert. Die Patienten tragen Mutationen in den Genen APC, MLH1, MSH2, MSH6 und PMS2 (Lebrun et al., 2007). Zudem konnte gezeigt werden, dass auch sporadisch auftretende Tumore unterschiedlichster Entitäten mit unterschiedlichen Häufigkeiten Defekte im MMR-System aufweisen (Chao and Lipkin, 2006).

## I.2 *Das erbliche, nicht-polypöse Kolonkarzinom (HNPCC)*

Kolorektalkrebs stellt in Deutschland nach Lungenkrebs bei Männern bzw. Brustkrebs bei Frauen, mit ca. 13% die zweithäufigste Tumorart dar (s. Abb. 2). Hierbei sind 20% der entstehenden Kolorektaltumore erblich bedingt, d.h. die onkogenen genetischen Veränderungen basieren auf Keimbahnmutationen. Hierbei stellt das nicht-polypöse Kolonkarzinom (HNPCC: Heriditary Non-Polyposis Colorectal Cancer), auch Lynch Syndrom genannt, mit 20-35% aller erblichen Kolorektalkarzinome (3-5 % aller Kolorektalkarzinome) die größte Gruppe dar (Lynch, 2003). Patienten mit diesem

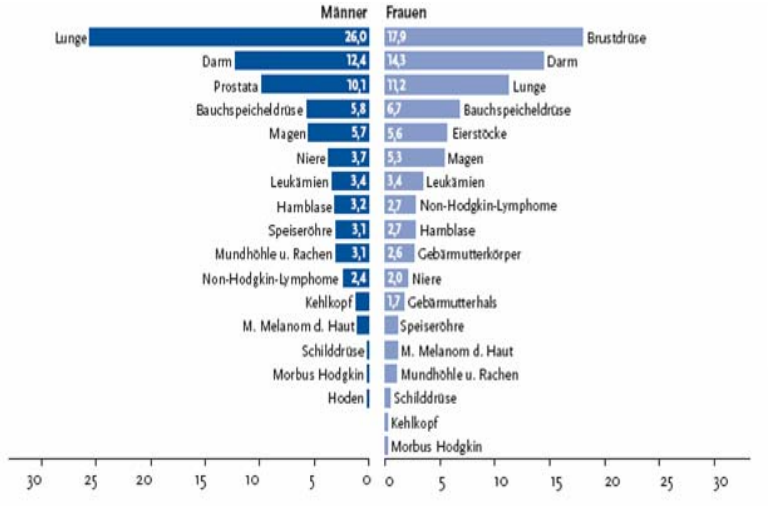


**Abb. 2: Prozentualer Anteil ausgewählter Tumorlokalisationen an allen Krebssterbefällen in Deutschland 2004.**
Aus Krebs in Deutschland 2003 – 2004, Häufigkeiten und Trends. Eine gemeinsame Veröffentlichung des Robert Koch-Instituts und der Gesellschaft der epidemiologischen Krebsregister in Deutschland e.V. 6. überarbeitete Auflage, 2008

Krebsprädispositionssyndrom tragen ein 80 %iges, lebenslanges Risiko Kolonkrebs zu entwickeln (Vasen et al., 1996). Zudem ist das Risiko für andere Krebsarten, wie beispielsweise Endometrium-, Magen-, Dünndarm- oder Ovarialkrebs, stark erhöht (Lynch, 2003). Erstmalig beschrieben wurde ein HNPCC Fall 1913 von dem Pathologen Dr. A.

Warthin, der eine signifikante Anhäufung von Magen-, Kolon- und Endometrialkrebs in einer Familie aufzeigen konnte (Warthin, 1913). Mitte der 60ger Jahre klassifizierte Lynch dieses Phänomen als autosomal dominantes, erbliches Krebsprädispositionssyndrom (Lynch et al., 1966). Zur positiven Identifikation von HNPCC wurden 1990 von einer internationalen HNPCC Kollaborationsgruppe Richtlinien festgelegt; es handelt sich dabei um die sogenannten Amsterdam-Kriterien (Vasen et al., 1999), bei welchen alle Punkte erfüllt sein müssen.

● Drei oder mehr Verwandte mit einem gesicherten HNPCC-assoziierten Karzinom; einer dieser Verwandten sollte in einer Verwandtschaft ersten Grades zu den beiden anderen Erkrankten sein (Eltern, Geschwister, Kinder).

● Das kolorektale Karzinom sollte in zumindest zwei Generationen gefunden werden.

● Eines oder mehrere dieser Karzinome sollten vor dem 50. Lebensjahr diagnostiziert worden sein.

● Eine familiäre adenomatöse Polypose (FAP) muss ausgeschlossen sein.

Die genetische Ursache für HNPCC sind Mutationen in Mismatch-Reparatur Genen. Dies konnte durch positionelles Klonieren in den Jahren 1993-94 von zwei Arbeitsgruppen gezeigt werden (Leach et al., 1993; Papadopoulos et al., 1994). Die am häufigsten mutierten Gene sind h*Msh2* und h*Mlh1* (s. Abb. 3). Das Mutationsspektrum umfasst missense- und nonsense-Mutationen, kleine Insertionen bzw. Deletionen sowie große genomische Deletionen und Duplikationen und Spleißvarianten. Im h*Mlh1* Gen sind ca. 24 % der bisher beschriebenen Mutationen missense Mutationen (Quelle: MMR Gen-Varianten Datenbank); d.h. Punktmutationen, die zu einem Aminosäureaustausch führen. Ein Teil dieser beschriebenen Punktmutationen wurden bereits in *S. cerevisiae* nachgestellt um die genetischen und molekularen Ursachen der durch MMR Defizienz induzierten Tumorgenese zu analysieren (Ellison et al., 2001; Nystrom-Lahti et al., 2002; Shcherbakova and Kunkel, 1999; Shimodaira et al., 1998).

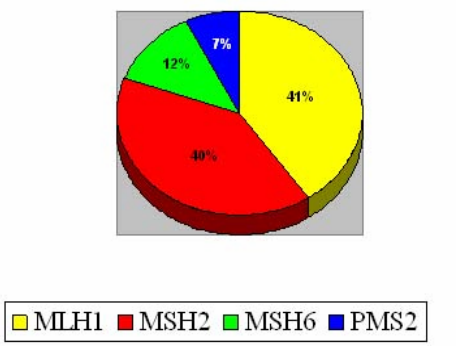


**Abb. 3: Mutationsverteilung der MMR Gene bei HNPCC.** Aus der Mismatch Reparatur Gen Varianten Datenbank; Stand 2007 (Internetadresse: http://www.med.mun.ca/MMRvariants)

Die Pathogenese und Tumorprogression in HNPCC Patienten verläuft anders als in dem von Fearon und Vogelstein (1990) beschriebenen genetischen Mehrschrittmodell für die Karzinogenese von sporadischen kolorektalen Tumoren. Nach dieser führen Aktivierungen von Onkogenen (*ras*) und Funktionsverluste von Tumorsuppressorgenen (*p53*, DCC) dazu, dass aus einem Adenom ein metastasierendes Karzinom entsteht. Entscheidend dabei ist die Anhäufung von mindestens vier bis fünf genetischen Alterationen, während die Reihenfolge der Veränderungen offenbar eine untergeordnete Rolle spielt. Entsprechend der „two hit" Hypothese von Knudson tragen HNPCC Patienten bereits eine Keimbahnmutation auf einem Allel der MMR Gene („first hit"), so dass nur noch ein somatischer Verlust oder eine epigenetische Inaktivierung des wildtypischen Allels („second hit") notwendig ist um einen Verlust der MMR Funktion zu bewirken (Boland, 2000; Peltomäki, 2001; Peltomaki et al., 1993). Hierdurch akkumulieren sich während der Rekombination auftretende Fehler und es kommt zu einer beschleunigten Onkogenese. Besonders betroffen von Replikationsfehlern sind repetetive Sequenzen, wie z.B. die so genannten Mikrosatellitenbereiche. Dies sind repetetive Sequenzen, die über das gesamte Genom verteilt sind. HNPCC Tumore sind besonders durch ihre Mikrosatelliten-instabilität (MSI) gekennzeichnet (Peltomaki et al., 1993). Kurze, repetetive Sequenzen befinden sich zwar größtenteils in nicht codierenden Sequenzen, konnten aber auch in kodierenden Bereichen von Genen nachgewiesen werden, die z. B. in die Signaltransduktion (TGFß-Rezeptor II (Gary et al., 1999); IGF-Rezeptor II (Souza et al., 1996); Pten (Shin et al., 2001)), Apoptose (BAX (Rampino et al., 1997); Caspase 5 (Schwartz et al., 1999)), Transkriptionsregulation (E2F-4 (Ikeda et al., 1998)) und DNA Reparatur (MSH3 und 6 (Yin et al., 1997); MED1 (Riccio et al., 1999)) involviert sind. Diese Sequenzen werden zum Nachweis von Mutationsereignissen in MMR defekten Tumoren genutzt. Es ist jedoch unklar, ob eine erhöhte Mutationsfrequenz in diesen Genen zu einer beschleunigten Karzinogenese führt oder ob eine weitere wichtige Funktion der MMR Proteine, nämlich der Antwort auf DNA Schäden hierbei eine wichtige Rolle spielt.

## I.3 *Das Mismatch Reparatur System*

Das Mismatch Reparatursystem (MMR) ist postreplikativ aktiv und erkennt Basen Fehlpaarungen und Insertions- bzw. Deletions-Loops (IDL), die während der Replikation und homologen Rekombination auftreten (Fishel and Kolodner, 1995; Kolodner and Marsischky, 1999; Modrich and Lahue, 1996). Zudem verhindert es Rekombinationsereignisse zwischen divergierenden DNA Strängen indem es Heteroduplexe entfernt (Abdullah et al., 2004; Wang

et al., 1999). Das MMR System ist vom Bakterium bis zum Menschen hoch konserviert (Buermeyer et al., 1999). Es wurde ursprünglich von E.C. Cox in *E. coli* identifiziert (Cox and Yanofsky, 1967). Er konnte vier „mutator" Gene in *E. coli* Stämmen mit erhöhter Mutationsfrequenz nachweisen. Diese „mutator" Gene *mutS,L,H* und *U* spielen eine zentrale Rolle im prokaryotischen MMR System. Die Erkennung der Basenfehlpaarung bzw. des IDL erfolgt durch die ATPase MutS (Haber and Walker, 1991), die als Homodimer an fehlerhafte DNA bindet. Daraufhin bildet ein Homodimer von MutL eine Komplex mit MutS (Galio et al., 1999) und stimuliert in ATP-abhängiger Weise die Endonucleaseaktivität von MutH. MutH ist für die Unterscheidung zwischen Template- und fehlerhaft neusynthetisiertem Strang verantwortlich und fügt eine Lücke in den Tochterstrang an einer hemimethylierten GATC-Sequenz ein (Buermeyer et al., 1999). Zudem ist MutL zur Bindung von MutU (Helikase/UvrD) an die durch MutL induzierte Lücke notwendig (Yamaguchi et al., 1998). Nach der Entwindung der dsDNA wird unter Beteiligung der ssDNA spezifischen Exonucleasen RecJ, ExoVII, ExoX und ExoI die Basenfehlpaarung bzw. der IDL entfernt (Viswanathan and Lovett, 1998). Zur Resynthese und Ligation des korrigierten Tochterstranges sind das Einzelstrangbindende Protein (SSB: single-strand binding protein), das DNA-Polymerase III-Holoenzym und die DNA-Ligase notwendig (Modrich, 1991).

In Eukaryoten ist das MMR System das am besten charakterisierte Reparatursystem (s. Abb. 4). In der Hefe *S. cerevisiae* konnten sechs MutS-Homologe (MSH1-6) und vier MutL-Homologe (MLH1- 3, PMS1) identifiziert werden. Im Säuger konnten fünf MutS-Homologe (MSH2-6) und vier MutL-Homologe (MLH1 und 3, PMS1 und 2) (Bellacosa, 2001). Homologe zu MutL und MutU konnten bisher jedoch nicht nachgewiesen werden. Die Funktionen und Struktur der identifizierten Mut-Homolog-Gene von Hefe zum Säuger sind hoch konserviert (Harfe and Jinks-Robertson, 2000).

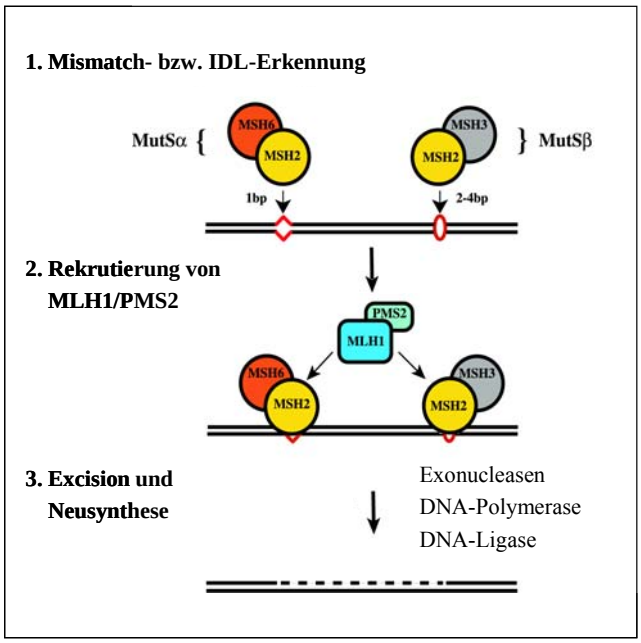


**Abb. 4: Modell des MMR in Eukaryoten:** Fehlpaarungen und/oder IDLs werden von MutSα bzw. MutSß. MutLa vermittelt die Mismatcherkennung mit dem Reparaturmechanismus.

Die Schadenserkennung erfolgt ebenfalls über MutS-Homologe, wobei diese in Eukaryoten jedoch nicht als Homodimere sondern als Heterodimere an den fehlerhaften DNA-Abschnitt binden. Hierbei unterscheidet man zwischen dem MutSα-Komplex, bestehend aus einem MSH2/MSH6 Heterodimer, der bevorzugt Basenfehlpaarungen und 1bp IDL's erkennt (Drummond et al., 1995) und dem MutSß-Komplex, bestehend aus einem MSH2/3 Heterodimer, der >1bp-12bp IDLs erkennt (Palombo et al., 1996). Die Schritte der MMR in Eukaryoten sind in Abb. X dargestellt. Die MMR Erkennung sowie die anschließende Rekrutierung der MutL-Homologen erfolgt ATP-abhängig (Alani et al., 1997; Gu et al., 1998; Habraken et al., 1998). Die MutL Homologen vermitteln Mismatch-Erkennung und Reparaturmechanismus. Hierbei bilden sie ebenfalls Heterodimere; den MutLα-Komplex, bestehend aus einem MLH1/PMS2 Heterodimer und den MutLß-Komplex, bestehend aus einem MLH1/PMS1 Heterodimer, welcher jedoch in der Mismatch Reparatur eine untergeordnete Rolle zu spielen scheint (Guerrette et al., 1999). Nach der Interaktion des MutLα-Komplexes mit den MutS-Homologen werden Faktoren, die zur Strangunterscheidung nötig sind rekrutiert. Wie bereits erwähnt, wird diese Aufgabe in *E. coli* von MutH übernommen, zu dem in Eukaryoten noch kein Äquivalent identifiziert werden konnte. Der Mechanismus, wie die Unterscheidung der beiden Stränge in Eukaryoten stattfindet, ist bisher nicht eindeutig geklärt. Lücken („gaps") zwischen Okazaki-Fragmenten des „lagging"-Strangs oder das freie 3´-Ende des „leading"-Strangs werden als mögliche Unterscheidungsmerkmale diskutiert. Aber auch PCNA (Proliferating Cell Nuklear Antigen), ein Protein, das in der Replikation der DNA eine Rolle spielt und sowohl mit MutS- als auch

mit MutL-Homologen interagiert (Clark et al., 2000; Flores-Rozas et al., 2000; Umar et al., 1996), könnte die Unterscheidung und damit die gerichtete Reparatur gewährleisten. Während der Replikation bindet PCNA die DNA, wobei es eine asymmetrische Struktur annimmt, durch die es möglicherweise in der Lage ist, MMR-Proteine zum neu synthetisierten Tochterstrang zu dirigieren. Der Abbau des Tochterstrangs mit der Fehlpaarung erfolgt durch die Aktivierung der Exonuklease I oder durch die Exonukleaseaktivität der Polymerase d und/oder e. Der resultierende Einzelstrang wird durch die Anlagerung von RPA Proteinen (replicating binding protein A) stabilisiert, während der Tochterstrang durch eine aphidicolin-sensitive Polymerase, wahrscheinlich Polymerase d, resynthetisiert wird. Nach abgeschlossener Synthese wird die verbleibende Lücke durch die DNA Ligase verschlossen.

Eine weitere Funktion der MMR Proteine, neben der eigentlichen Reperatur Funkrion, liegt in einer Induktion der Antwort auf DNA Schäden. Es ist seit längerem bekannt, dass MMR profiziente Zellen sensitiv (Zell-Zyklus-Arrest und Apoptose) gegenüber DNA Schaden induzierender Agenzien reagieren, wohingegen MMR defiziente Zellen eine vergleichsweise hohe Resistenz gegenüber DNA Schäden aufweisen. Dies lässt auf eine prominente Rolle des MMR Systems in dieser biologisch wichtigen Funktion schließen. Zu den Agenzien, deren DNA Schädigungen durch das MMR-System erkannt werden, zählen unter anderem die SN1 methylierenden Agenzien, die sowohl Chemotherapeutika wie Temozolamide, Dacarbazine und Procarbazine als auch Experimentelle Reagenzien wie N-methyl-N'nitrosourea (MNU) und N-methyl-N'-nitro-N-nitroguanidine (MNNG) beinhalten (Ceccotti et al., 1996; Swann et al., 1996) sowie alkylierende Agenzien wie die Chemotherapeutika 6-Thioguanine (6-TG), Cis-diamminedichlorplatinum (II) (Cisplatin) und IR (Aebi et al., 1996; Ceccotti et al., 1996; Fink et al., 1997; Swann et al., 1996). Der genaue Mechanismus, der zum Zell-Zyklus Arrest und letztendlich zur apoptotischen Eliminierung genetisch instabiler Zellen führt, ist bisher nicht klar definiert. Es ist zu vermuten, dass, abhängig von der Art des DNA Schadens und abhängig von der Dosis des DNA Schaden induzierenden Agens (Beardsley et al., 2005; Caporali et al., 2004), zusätzlich auch alternative DNA-Reperatur Mechanismen aktiviert werden, die zudem noch abhängig von der Art des betroffenen Gewebes sind (Hickman and Samson, 1999). Da DNA Schaden induzierende Agenzien zum Teil eine Mehrzahl unterschiedlicher DNA Schäden verursachen, ist zu vermuten, dass mehrere evtl. redundante Mechanismen gleichzeitig aktiviert werden.
Es scheint jedoch klar zu sein, dass Basenfehlpaarungen von MutSα erkannt werden woraufhin MLH1 Proteine rekrutiert werden (Duckett et al., 1999; Yoshioka et al., 2006) und

ein MLH1 abhängiger Import von PMS2 bzw. PMS1 in den Nukleus eingeleitet wird (Luo et al., 2004). Die Art der Beteiligung der MMR Proteine bei der Aktivierung der DNA Schadensantwort wird zurzeit kontrovers diskutiert. Hierbei stehen 2 Modelle zur Diskussion: Die „direct signalling" Hypothese (Fishel, 1999) postuliert, dass die MMR Proteine direkt an der Rekrutierung von proapoptotischen Faktoren beteiligt sind und somit direkt den apoptotischen Zelltod initiieren, während die „futil repair" Hypothese (Karran, 2001) davon ausgeht, dass die MMR Proteine nur indirekt am Zellzyklusarrest und der Apoptoseinduktion beteiligt sind.
Aus der veränderten Toleranz MMR defekter Zellen gegenüber einer Vielzahl von DNA schädigenden Agenzien, die zur Tumortherapie eingesetzt werden, ergibt sich eine klare klinische Relevanz für die Therapie von MMR defizienten Tumoren.

## I.4 *MMR defiziente Mausmodelle*

Um den Einfluss von Defekten des MMR Systems auch *in vivo* auf die Tumorgenese zu analysieren eignet sich besonders das Mausmodell. Hier ist es möglich mittels Gene Targeting gezielt bestimmte Gene zu deletieren. Für alle bekannten MMR Gene wurden bereits knockout Mauslinien generiert. Die Phänotypen dieser Mauslinien sind in Tab.1 zusammengefasst.

| MMR Gen | 50% Überleben (Monate) | Tumor Phänotyp | Meiotischer Phänotyp | Referenz |
|---|---|---|---|---|
| ***Msh2*** | 6 | Lymphome, GI Tumore, Hauttumore | Fertil | Reitmair et al., 1995 |
| *Msh3* | 19 | GI Tumore | Fertil | Wiesendanger et. Al., 2000 |
| *Msh6* | 10 | Lymphome, GI Tumore | Fertil | Wiesendanger et. Al., 2000 |
| ***Mlh1*** | 7 | Lymphome, GI Tumore | Pacytene Arrest | Edelmann et al., 1999; |
| *Pms1* | >15 | Keine | Infertil | Prolla et al., 1998 |
| *Pms2* | 10 | Lymphome | Fertil | Prolla et al., 1998 |
| *Mlh3* | Normal | Keine | Infertil | Lipkin et al., 2002 |
| *Msh4* | Normal | Keine | Früher meiotischer Arrest | Kneitz et al., 2000 |
| *Msh5* | Normal | Keine | Früher meiotischer Arrest | Edelmann et al., 1999 |

**Tab. 1: MMR defiziente Mausmodelle.**
GI: Gastrointestinal Tumor. Modifiziert aus (Heyer et al., 1999).

Hieraus wird ersichtlich, dass sich die knockout Mausmodelle der Mismatch Reparatur Gene durch einen starken Tumorprädispositionsphänotyp auszeichnen (mit Ausnahme der PMS1 defizienten Mauslinie, von der kein Phänotyp beschrieben ist (Prolla et al., 1998)). Tiere mit defektivem MMR System entwickeln bevorzugt gastrointestinale Tumore (Adenome und Karzinome) und Lymphome. Hierbei sind vor allem die MSH2 und MLH1 defizienten

Mauslinien zu erwähnen, die durch eine sehr frühe (50% Überleben sechs bzw. sieben Monate), spontane Entwicklung von GI Tumoren und Lymphomen charakterisiert sind und sich somit als murine Modelle für HNPCC und Lymphomentwicklung eignen (Edelmann et al., 1999b; Prolla et al., 1998; Reitmair et al., 1995). Darüber hinaus konnte in MLH1 und PMS2 defizienten Mauslinien, neben der spontanen Entwicklung von Tumoren, ein meiotischer Phänotyp beschrieben werden (Baker et al., 1995; Edelmann et al., 1996). Tiere dieser Genotypen sind trotz normalen Paarungsverhaltens steril (in der PMS2 defizienten Mauslinie nur die Männchen). Dies lässt darauf schließen, dass MMR Gene während der Evolution des prokaryotischen MutSLH Systems weitere Aufgaben in der meiotischen Zellteilung übernommen haben. Diese Spezifikation der MMR Gene lässt sich auch anhand der MutS Homologen 4 und 5 und des MutL Homologen 3 beobachten. MSH4 und 5 sowie MLH3 defiziente Tiere entwickeln keine Tumore, sind jedoch steril (Edelmann et al., 1999a; Kneitz et al., 2000; Lipkin et al., 2002).

## I.5 *Meiotische Funktion*

Die Meiose ist ein zentraler Bestandteil des Zelldiffernzierungsprozesses der Keimzellentwicklung, die man in allen sexuell reproduzierenden Organismen findet. Hierbei kommt es zu einer Reduktion des Chromosomensatzes von diploid auf haploid und Teile der homologen Chromosomen werden durch genetische Rekombination ausgetauscht. Vor dem Eintritt in die Meiose wird die vorhandene DNA durch eine Replikationsrunde in der S-Phase verdoppelt. Anschließend finden zwei aufeinander folgende Zellteilungen statt, die als Meiose I und II bezeichnet werden.

In der Meiose I durchlaufen die homologen Chromosomen Paarung, Synapsis und Rekombination und werden anschließend voneinander getrennt. Die erste meiotische Teilung wird somit als Reduktionsteilung bezeichnet, da hier die Trennung der „väterlichen“ und „mütterlichen“ Chromosomen stattfindet.

Die Meiose I lässt sich in verschiedene Phasen unterteilen: Prophase, Prometaphase, Metaphase, Anaphase und Telophase. In der Prophase der ersten meiotischen Teilung erfolgt die Paarung, Synapse und Rekombination der homologen Chromosomen. Die Prophase I ist charakterisiert durch ihre lange Dauer, die in der Spermatogenese mehrere Tage, und im Fall der Oogenese mehrere Jahre dauern kann. Aufgrund morphologischer Veränderungen des Zellkerns und der Chromosomen wurde die Prophase I in fünf Stadien unterteilt: Leptotän, Zygotän, Pachytän, Diplotän und Diakinese (Übersicht in (Zickler and Kleckner, 1998)).

Wie bereits erwähnt, zeichnen sich einige der MMR defizienten Mauslinien nicht (nur) durch einen Tumorprädispositionsphänotyp aus; sondern (auch) durch Sterilitäten, welche durch eine beeinträchtigte Meiose hervorgerufen werden, aus.
Für die MutS Homologe MSH4 und 5 konnte sowohl in *S. cerevisiae* (de los Santos et al., 2003) als auch in der Maus (de Vries et al., 1999; Edelmann et al., 1999a; Kneitz et al., 2000) gezeigt werden, dass sie eine wichtige Funktion im meiotischen „Crossing Over" haben. Hierbei vermitteln sie als Heterodimere (Pochart et al., 1997) die Formierung des synaptonemalen Komplexes, der die homologen Chromosomen bis zur Anaphase I zusammenhält. In der Hefe (Novak et al., 2001) und in der Maus konnte gezeigt werden, dass eine MSH4 (Kneitz et al., 2000) bzw. MSH5 (de Vries et al., 1999; Edelmann et al., 1999a) Defizienz zu einer beeinträchtigten Synapsis der homologen Chromosomen führt. Es wird postuliert, dass MSH4/5 Heterodimere die Einzelstranginvasion, die zu der Formierung von „Holliday Junctions" nötig ist, in der frühen Prophase initiiert bzw. stabilisiert. Alternativ zu diesem Modell könnte MSH4/5 auch mit der nachgeschalteten Replikationsmaschinerie interagieren, die nach der Einzelstranginvasion aktiv wird (Hoffmann and Borts, 2004).
Auch die MutL Homologen MLH1 und 3 (und begrenzt auch PMS2) haben eine wichtige meiotische Funktion. In *S. cerevisiae* konnte gezeigt werden, dass MLH1 und 3 defiziente Mauslinien, wie MSH4 und 5 defiziente Linien eine reduzierte Rekombinationsrate aufweisen. Zudem sind MLH1 (Edelmann et al., 1996) und MLH3 (Lipkin et al., 2002) defiziente Mäuse steril (in $Pms2^{-/-}$ Tieren konnte nur in Männchen eine Sterilität nachgewiesen werden (Baker et al., 1995)). MLH1 und 3 kolokalisieren wie MSH4/5 als Heterodimere (Wang et al., 1999) mit den Stellen der „Crossing Over" im Pachytän-Stadium der Prophase I (Moens et al., 2002). Hierbei bindet zunächst MLH3 mit dem MSH4/5 Komplex an einigen - nicht allen- „Holliday Junctions" und rekrutiert MLH1, was zur Einleitung des „Crossing Overs" führt (Kolas and Cohen, 2004).

## I.6 *MLH1*

Das h*Mlh1* Gen besteht aus 19 Exons, die für 756 Aminosäuren kodieren.
Der stark konservierte N-Terminus beherbergt sowohl eine ATPase Domäne als auch einige Reste, die für die Interaktion mit DNA und anderen Proteinen essentiell sind (Guarne et al., 2001). Für die Funktion von MLH1 ist die ATPase-Aktivität ausschlaggebend (Raschle et al., 2002; Tomer et al., 2002). Der evolutionär variablere C-Terminus des MutL-Homologs ist für die Dimerisierung (Kondo et al., 2001; Wu et al., 2003) und die Interaktion mit anderen Proteinen verantwortlich (Schmutte et al., 2001) (s. Abb.5)

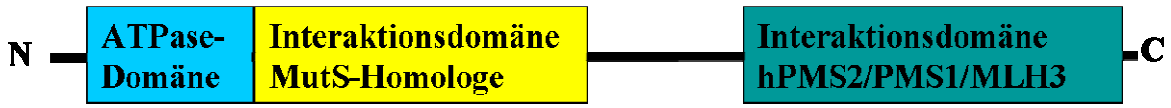


**Abb. 5: Schematische Darstellung der Domänenstruktur des *mMlh1* Gens.**

## I.7 *Zielsetzung der Arbeit*

Die vorliegende Doktorarbeit lässt sich thematisch in zwei Teilprojekte untergliedern, die sich beide mit den Auswirkungen von Defekten des MMR Systems (MLH1) auf die Tumorgenese im Mausmodell befassen.

In meinem ersten Projekt sollte in Fortsetzung meiner Diplomarbeit die *Mlh1*$^{G67R/G67R}$ Mauslinie analysiert werden. Diese Mauslinie trägt eine pathogene Punktmutation in der ATPase Domäne (Codon 67, Austausch von G zu R) des *Mlh1* Gens, die häufig in HNPCC Familien beschrieben wurde und zu einem Verlust der ATPase Funktion führt. Erste funktionelle Analysen an Zellen aus *Mlh1*$^{G67R}$ Mäusen zeigen eine Separation der MLH1 Funktionen. G67R mutante Zellen besitzen eine normale Antwort auf DNA Schäden, wohingegen die DNA Reparatur nicht mehr erfüllt werden kann. Im Folgenden sollte die Tumorgenese in *Mlh1*$^{G67R/G67R}$ Mäusen untersucht werden. Insbesondere interessiert uns welchen Einfluss die MLH1 vermittelte DNA-Schaden induzierte Apoptose auf die Entstehung von Tumoren besitzt. Hierzu sollte die Tumorgenese in *Mlh1* $^{G67R/G67R}$ Mäusen, die keinen Defekt in dieser Funktion besitzt, mit MLH1 defizienten Mäusen verglichen werden. Wir vermuteten aufgrund der intakten DNA-Schadens Funktion eine verlangsamte Tumorgenese in *Mlh1*$^{G67R/G67R}$ Tieren. Des Weiteren sollte der Tumorprädispositionsphänotyp der hemizygoten *Mlh1*$^{G67R/-}$ und der heterozygoten *Mlh1*$^{G67R/+}$ Mauslinie analysiert werden. Die *Mlh1*$^{G67R/-}$ Mauslinie ist durch den Verlust eines *Mlh1* Alleles bei vorhandener G67R Mutation auf dem zweiten Allel gekennzeichnet ist, was die genetische Situation in HNPCC Patienten repräsentiert.

Im zweiten Teilprojekt sollte die MLH1 abhängige Tumorgenese von spezifizierten Geweben bzw. Zelltypen *in vivo* analysiert werden. Hierzu wurde eine konditionell MLH1 defiziente Mauslinie etabliert und charakterisiert, die ein von zwei LoxP Schnittstellen gefloxtes Exon 4 des *Mlh1* Gens trägt. Dies ermöglicht die gewebsspezifische Deletion von MLH1 durch das Einkreuzen von Mauslinie, die Cre unter der Kontrolle definierter Promotoren exprimieren.

Da verschiedene humane Lymphomerkrankungen mit einem Fehlerhaften MMR System assoziiert sind und Lymphome und Leukämien auch teilweise zum HNPCC Spektrum gezählt werden, wurde die MLH1 abhängige Lymphomagenese detaillierter untersucht. Hierzu wurde die *Lck Cre* Mauslinie (Orban PC, 1992) verwendet, die Cre spezifisch in Thymozyten exprimiert. In der entstehenden *Mlh1*$^{T\Delta Ex4/T\Delta Ex4}$ Mauslinie wird MLH1 T-Zell spezifisch deletiert, was eine Analyse der MLH1 abhängigen Lymphomagenese ermöglicht.
Mithilfe dieser transgenen Mauslinien sollten neuartige Modelle entwickelt werden, um die Funktion von MLH1 für die Entstehung von HNPCC ähnlichen Tumoren und spontanen MMR defizienten Lymphomen zu untersuchen. Gleichzeitig sollen diese Modelle genutzt werden, um den Einfluss von MLH1 Mutationen auf die bekannte MLH1 Funktionen zu testen und deren Einfluss auf die Entstehung von Sterilitäten und Tumorgenese darzustellen.

# II Ergebnisse und Diskussion

## *II. 1. Auswirkungen der MLH1$^{G67R}$ Mutation auf die Meiotischen Mismatch Reparatur Funktionen, Meiose und Tumorgenese im Mausmodell*

Ein großer Anteil der in HNPCC Patienten beschriebenen Mutationen im h*Mlh1* Gen sind in der hochkonservierten N-terminalen ATPase Domäne lokalisiert. Hiervon ist die G67R missence Mutation eine physiologisch interessante Missence Mutation. Sie ist im Exon2 der MLH1-ATPase Domäne lokalisiert und führt zu dem Aminosäureaustausch eines konservierten Glycins gegen Alanin (Hutter et al., 1998; Sasaki et al., 1997; Tannergard et al., 1995). Identifiziert wurde diese pathogene Mutation in mehreren HNPCC Patienten aus verschiedenen Ländern, die mikrosatelliten instabile kolorektale Karzinome entwickeln (de la Chapelle, 2004).

Um die Auswirkungen dieser interessanten Punktmutation auf die bekannten MLH1 Funktionen und Tumorgenese im Mausmodell zu untersuchen wurde eine G67R mutante Mauslinie mittels „knockin genetargeting“ Strategie generiert. Da HNPCC Patienten heterozygote Keimbahnmutationen in Mismatchreperaturgenen tragen und ein Verlust des gesunden Allels dem Tumorereignis vorausgeht war es für uns zudem von Interesse diese Situation im Mausmodell nachzustellen. Hierzu wurden *Mlh1*$^{-/-}$ Tiere in die G67R Mutante Mauslinie eingekreuzt und die resultierenden hemizygoten *Mlh1*$^{G67R/-}$ Nachkommen bezüglich ihrer Tumorentwicklung untersucht.

Die Charakterisierung der MLH1$^{G67R}$ mutanten Mauslinie zeigte, dass die G67R missence Mutation keine Auswirkungen auf die mRNA und Protein Expression, sowie auf die Interaktion mit dem Bindungspartner PMS2 hat (Avdievich et al., 2008).

Die Funktionelle Analyse ergab, dass die G67R Mutation zu einer Separation der mitotischen MLH1 Funktionen führte. Es konnte kein Effekt auf die DNA-Schadensantwort nachgewiesen werden wohingegen die Mutation zu einem Verlust der DNA-Reparatur Funktion führte. Diese Separation der mitotischen Funktionen wurde bereist in Mauslinien, die eine Mutation in der ATPase Domäne von MutS Homologen Mismatchreparatur Proteinen *Msh2*$^{G674A}$ und *Msh6*$^{T1217D}$ aufwiesen, beschrieben (Lin et al., 2004; Yang et al., 2004). Der Funktionserhalt der DNA Schadensantwort trotz des Verlustes der ATPase Funktion in diesen drei Mausmodellen stützt die „direct signaling“ Hypothese (Heinen et al.,

2002). Hierbei fungieren die MMR Proteine als Gerüstproteine, welche nachgeschaltete Effektoren der Zellzykluskontrolle und Apoptoseinduktion in räumliche Nähe zum DNA Schaden rekrutierten. Diese Hypothese wird durch die Erkenntnis unterstützt, dass MLH1 mit ATM und MSH2 mit Chk2 interagieren können (Brown et al., 2003). Die Interaktion zwischen Chk2 und ATM führt zur Phosphorylierung der Chk2 Kinase durch ATM und initiiert somit eine Induktion des Zellzyklusarrestes. Des Weiteren wurde eine Interaktion von MSH2 mit p53 beschrieben (Luo et al., 2004), dessen ATM-vermittelte Phosphorylierung die Appoptoseinduktion zur Folge hätte. Die genauen Mechanismen der MMR induzierten DNA Schadensantwort sind jedoch noch nicht hinreichend geklärt und auch alternative Appoptoseinduktionswege wie beispielsweise über p73 sind möglich (Gong JG, 1999; Gong et al., 1999; Shimodaira et al., 2003).

Die Auswirkungen des Verlustes der DNA Reparaturfunktion und des Erhaltes der DNA Schadensantwort auf Tumorentstehung im Mausmodell unterscheiden sich jedoch zwischen *Mlh1*$^{G67R}$ und *Msh2*$^{G674A}$ bzw. *Msh6*$^{T1217D}$ Mauslinien (Lin et al., 2004; Yang et al., 2004). Die Mutationen in den ATPase Domänen der MutS Homologen MSH2 und MSH6 führten im Vergleich zu den *Msh2*$^{-/-}$ bzw. *Msh6*$^{-/-}$ Linien zu einer verlangsamte Tumorgenese. Dahingegen zeigt die MLH1$^{G67R}$ Mutation auch bei gleichzeitigem Verlust des zweiten *Mlh1* Allels keinen Effekt auf den zeitlichen Verlauf der Tumorgenese (Abb. 6). Eine Zusammenfassung aller *Mlh1*$^{G67R/G67R}$ und *Mlh1*$^{G67R/-}$ Tumortiere befindet sich im Anhang 1 und 2. Die vergleichenden Daten bezüglich der Tumorgenese in *Mlh1*$^{-/-}$ Tieren auf demselben genetischen Hintergrund wurden von Dr. Thorsten Haneke und Dr. Burkhard Kneitz zur Verfügung gestellt.

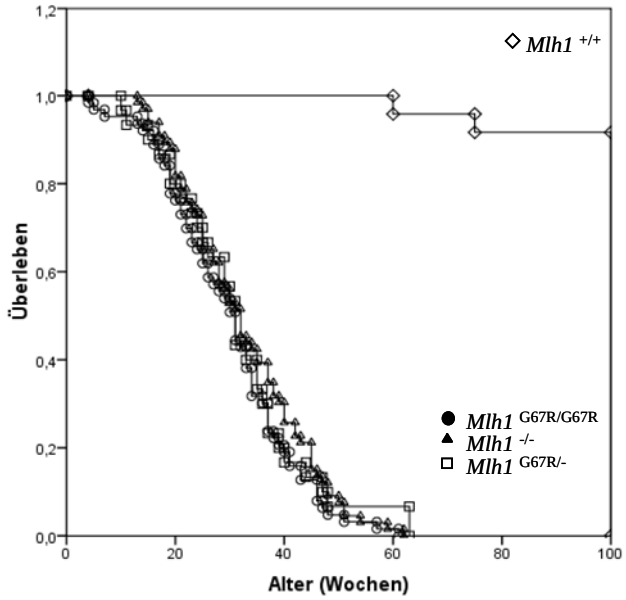


**Abb. 6: Tumorgenese von MLH1$^{G67R}$ Tieren.**

Kaplan-Meier Überlebenskurven von *Mlh1*$^{+/+}$ (n=24), *Mlh1*$^{-/-}$ (n=66), *Mlh1*$^{G67R/G67R}$ (n=60) und *Mlh1*$^{G67R/-}$ (n=28) Mauslinien. Das Gesamtüberleben der MLH1$^{G67R}$ Mauslinien ist im Vergleich zur *Mlh1*$^{+/+}$ Linie hoch signifikant verkürzt (p>0,001; log-rank Test). Es bestehen keine Unterschiede im Überleben von *Mlh1*$^{G67R/G67R}$ und *Mlh1*$^{G67R/-}$ Tieren (p=0, 0,952; log-rank Test) untereinander und im Vergleich zu *Mlh1*$^{-/-}$ Tieren (p=0,915 und p=0,538).

Der Verlust der DNA Reparaturfunktion führt dazu, dass die entstehenden Tumore MLH1$^{G67R}$ mutanter Tiere wie die Tumore MLH1 defizienter Tiere durch einen hohen Grad an Mikrosatelliteinstabilität gekennzeichnet (Tab.2) sind.

| Genotyp | n | MSS | L-MSI | H-MSI |
|---|---|---|---|---|
| *Mlh1*$^{-/-}$ | 28 | 2 (7,1%) | 11 (39,3%) | 15 (53,6%) |
| *Mlh1*$^{G67R/G67R}$ | 44 | 6 (13,6%) | 9 (20,5%) | 29 (65,9%) |
| *Mlh1*$^{G67R/-}$ | 19 | 1 (5,3%) | 4 (21%) | 14 (73,7%) |

**Tab. 2 : Miktosatelliteninstabilität in Tumoren von MLH1$^{G67R}$ Tieren.**

MSS (Mikrosatellitenstabil) Tumore zeigen in keinem der fünf getesteten Mikrosatelliten Veränderungen im Vergleich zu nicht-Tumor DNA; L-MSI (niedrige (low) Mikrosatelliteninstabilität) liegt vor, wenn bis zu zwei der getesteten Mikrosatellitenmarker verändert vorliegen; H-MSI (hohe Mikrosatelliteninstabilität) liegt vor, wenn mehr als zwei Mikrosatellitenmarker alternieren.

Die vorherrschenden Tumorarten in MLH1$^{G67R}$ mutanten Tumortieren sind, wie in *Mlh1*$^{-/-}$ Tumortieren, Lymphome und gastrointestinale Tumore.

Die Tumorgenese verläuft ebenfalls zweiphasig; zunächst erfolgt eine frühe Phase der Lymphomentwicklung gefolgt von einer zweiten Phase der GI-Tumorgenese (siehe zusammenfassend Tabelle 3). Es zeigt sich jedoch in der Tumorgenese der MLH1$^{G67R}$ Mauslinie eine signifikante Verschiebung der Tumorinzidenzen hin zu verminderten gastointestinalen Tumorinzidenzen.

| | *Mlh1* $^{-/-}$ | *Mlh1* $^{G67R/G67R}$ | *Mlh1* $^{G67R/-}$ |
|---|---|---|---|
| Tumor Mäuse (n) : | 66 | 60 | 28 |
| Lymphome (gesammt) | 27 (41%) | 38 (63%) | 17 (61%) |
| GI | 27 (41%) | 13 (22%) | 6 (21%) |
| GI+ Lymphom | 8 (12%) | 5 (8%) | 4 (14%) |
| Haut | 4 (6%) | 4 (7%) | 1 (4%) |
| Medianes Überleben +/- SA (Wochen) | | | |
| Tumor Mäuse | 32 +/- 2,023 | 31 +/- 1,69 | 31 +/- 1,357 |
| Lymphom Mäuse | 21 +/- 1,298 | 22 +/- 1,541 | 29+/- 3,43 |
| GI-Tumor Mäuse | 39 +/- 1,947 | 40 +/- 5,692 | 37 +/- 8,764 |
| Hauttumor Mäuse | 45 +/- 13,5 | 40 +/- 5,715 | 31+/- 0 |

**Tab. 3: Tumor-Verteilung und medianes Überleben in den unterschiedlichen Mauslinien.** MLH1$^{G67R}$ Tiere entwickeln in erster Linie Lymphome und gastrointestinale Tumore (GI), wobei *Mlh1*$^{G67R/G67R}$ und *Mlh1*$^{G67R/-}$ Tiere signifikant weniger GI Tumore als *Mlh1*$^{-/-}$ Tiere entwickeln (p=0,0047 und p=0,0266; T-Test). Die Inzidenzen für GI Tumore unterscheiden sich nicht zwischen *Mlh1*$^{G67R/-}$ und *Mlh1*$^{G67R/G67R}$ Tumortieren (p=0,478; t-Test), doch es ist ein verzögertes medianes Überleben der *Mlh1*$^{G67R/-}$ Lymphomtiere zu beobachten.

Zur detaillierteren Analyse des Tumorprädispositionsphänotyps wurden die Tumortiere in Lymphomtiere und GI-Tumortiere gruppiert und der Entstehungszeitpunkt der Tumore mittels Kaplan-Meier Überlebensanalyse untersucht. Hierbei zeigt sich, dass die Lymphomagenese der *Mlh1*$^{G67R/G67R}$ und *Mlh1*$^{G67R/-}$ Mauslinien im Vergleich zur *Mlh1*$^{-/-}$ Linie leicht bzw. signifikant verlangsamt ist. Zwischen den beiden MLH1$^{G67R}$ Linien bestehen jedoch keine Unterschiede im zeitlichen Auftreten der Lymphome. Die Gruppe der

MLH1$^{G67R}$ GI-Tumortiere weist keine Unterschiede zu *Mlh1*$^{-/-}$ Tieren mit gastrointestinalen Tumoren auf (Abb. 7B).

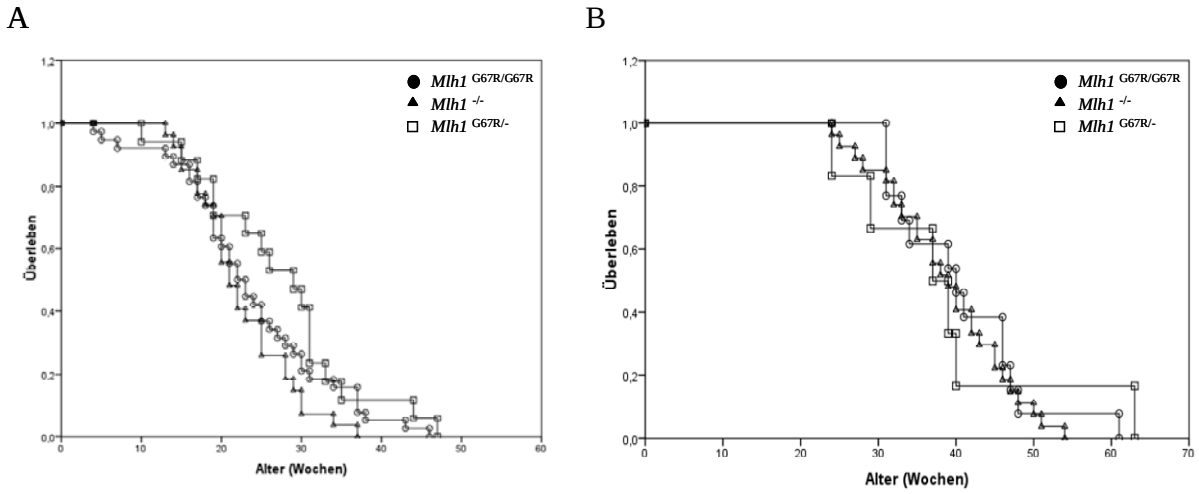


**Abb. 7: Kaplan-Meier Überlebensanalysen für Lymphomagenese und GI-Tumorentwicklung in MLH1$^{G67R}$ Tieren.**

A: Überlebenskurve von Tieren mit lymphoiden Tumoren. Das Überleben von *Mlh1*$^{G67R/G67R}$ Lymphomtieren (n=38) und *Mlh1*$^{G67R/-}$ Lymphomtieren (n=17) ist, im Vergleich zu *Mlh1*$^{-/-}$ Lymphomtieren (n=27) nicht bzw. signifikant verlangsamt (p=0,238 und p=0,026 log-rank Test); es bestehen keine Unterschiede im Überleben von *Mlh1*$^{G67R/G67R}$ und *Mlh1*$^{G67R/-}$ Lymphomtieren (p=0,209; log-rank Test).

B: Überlebenskurve von Tieren mit gastrointestinalen Tumoren. Es bestehen keine Unterschiede im Überleben von *Mlh1*$^{G67R/G67R}$ (n=13), *Mlh1*$^{G67R/-}$ und *Mlh1*$^{-/-}$ (n=27) Tieren mit gastrointestinalen Tumoren (p=0,776; log-rank Test).

Das zeitlich verzögerte Auftreten von Lymphomen ist nicht durch unterschiedliche Inzidenzen von Lymphomsubpopulationen begründet. Dies konnte mittels Immunphänotypisierung der auftretenden Lymphome gezeigt werden. Hierzu wurden FACS-Färbungen mit Lymphozytenspezifischen Antikörpern durchgeführt. Die Unterteilung in Lymphozytensubpopulationen erfolgte aufgrund der Expression von spezifischen Oberflächenmarkern in drei Subkategorien (siehe Tabelle 4):

T-Zell Lymphome, die durch die Expression des CD3 Rezeptors gekennzeichnet sind. In MLH1$^{G67R}$ Tumortieren sind ca. 60% der analysierten Lymphome T-Zell Lymphome. Dies deckt sich mit den in *Mlh1*$^{-/-}$ Tieren ermittelten Befunden, die zeigen, dass ebenfalls ca. 60% der MLH1 defizienten Lymphome, T-Zell Lymphome sind. Auch die weitere Subgruppierung anhand der Expression der Co-Rezeptoren CD4 und CD8 ergab keine unterschiedliche Verteilung in MLH1$^{G67R}$ T-Zell Lymphomen im Vergleich zu *Mlh1*$^{-/-}$ T-Zell Lymphomen.

Die vier T-Zell Lymphom Subgruppen doppelt negative; doppelt positive; CD4 einfach positive und CD8 einfach positive T-Zell Lymphome lagen in beiden Gruppen gleichverteilt vor.

B-Zell Lymphome, die durch die Expression des CD45R Oberflächenantigens gekennzeichnet sind, stellen 11,5% der *Mlh1*$^{G67R/G67R}$ Lymphome.

Hämatopoetische Lymphome, die durch die Expression des TER Oberflächenantigens gekennzeichnet sind, stellen 27% der *Mlh1*$^{G67R/G67R}$ Lymphozytensubpopulationen.

Dies unterscheidet sich zu den in *Mlh1*$^{-/-}$ und *Mlh1*$^{G67R/-}$ Tieren beobachteten Inzidenzen für B-Zell Lymphome (28,6% bzw. 25%) und hämatopoetische Lymphome (11,4% bzw. 10%), nicht signifikant.

| Lymphomart | Immunphänotypisierung | *Mlh1* $^{-/-}$ (n=35) | *Mlh1* $^{G67R/G67R}$ (n=26) | *Mlh1* $^{G67R/-}$ (n=20) |
|---|---|---|---|---|
| T-Zell Lymphom | | 21 (60%) | 16 (61,5%) | 13 (65%) |
| | DN: CD3+CD4-CD8- | 5 (14,3%) | 3 (11,5%) | 4 (20%) |
| | DP: CD3+CD4+CD8+ | 5 (14,3%) | 6 (23%) | 4 (20%) |
| | CD8+: CD3+CD4-CD8+ | 5 (14,3%) | 3 (11,5%) | 1 (5%) |
| | CD4+: CD3+CD4+CD8- | 6 (17,1%) | 4 (15%) | 4 (20%) |
| B-Zell Lymphom | CD3-CD45R+ | 10 (28,6%) | 3 (11,5%) | 5 (25%) |
| Hämatopoetisches Lymphom | CD3-CD45R-TER+ | 4 (11,4%) | 7 (27%) | 2 (10%) |

**Tab. 4: Subklassifizierung der in MLH1$^{G67R}$ Lymphome mittels FACS Analyse.** Kein signifikanter Unterschied in der Verteilung von T-, B- und Hämatopoetischen Lymphomen (p=0,6583; gepaarter T-Test) im Vergleich zu *Mlh1*$^{-/-}$ Lymphomtieren. Kein signifikanter Unterschied in der Verteilung der T-Zell Lymphom Subklassen (DP: Doppelt Positiv; DN: Doppelt Negativ: CD4+: CD4 positiv; CD8+: CD8 positiv) im Vergleich zu *Mlh1*$^{-/-}$ T-Zell Lymphomen (p=0,194; gepaarter T-Test).
(CD3, CD4, CD8: T-Zell Marker; CD45R: B-Zell Marker; TER: Marker für hämatopoetische Zellen.)

Dies lässt den Schluss zu, dass die verlangsamte Lymphomagenese der G67R mutanten Mauslinie durch die geringere Anzahl gastrointestinaler Tumore begründet ist. Es kann nicht ausgeschlossen werden, dass MLH1 defiziente Tiere aufgrund von auftretenden GI-Tumoren aus dem Bestand genommen wurden, die zu einem späteren Zeitpunkt Lymphome entwickelt hätten.

Hieraus lässt sich schlussfolgern, dass die G67R Mutation eine Separation der mitotischen MMR Funktionen zur Folge hat: den Verlust der DNA Reparaturfunktion und den Erhalt einer effektiven Antwort auf DNA Schäden. Die Auswirkungen der Punktmutation auf die Tumorgenese im MLH1$^{G67R}$ Mausmodell unterscheiden sich zu den in punktmutanten MutS Homologen Mauslinien beobachteten. Diese bedingen ebenfalls eine Separation der mitotischen MMR Funktionen. Hierbei führt der Verlust der Reparaturfähigkeit bei gleichzeitigem Erhalt der DNA Schadensantwort zu einer verlangsamten Tumorgenese im Vergleich zu den entsprechenden knockout Tieren. In unserem Modell kann keine verlangsamte Tumorgenese beobachtet werden, es kommt jedoch zu einer Verschiebung der Tumorinzidenzen, was eine gewisse Gewebsspezifität in der Sensitivität auf DNA Schäden vermuten lässt.

Neben den Effekten der MLH1$^{G67R}$ Mutation auf die mitotischen MMR Funktionen und Tumorgenese wurde in der *Mlh1*$^{G67R/G67R}$ Mauslinie ein bemerkenswerter meiotischer Phänotyp festgestellt. Dieser ähnelt stark dem in *Mlh1*$^{-/-}$ Tieren beobachteten. Tiere beider Geschlechter sind aufgrund einer fehlerhaften Chromosomenreifung bzw. Segregation infertil. Die inkorrekte Separation der meiotischen Chromosomen ist durch die fehlende Bindung des MLH1$^{G67R}$ Proteins an die Stellen der „Crossing over“ der homologen Chromosomen im Pachytän Stadium der Prophase I begründet. Im Unterschied zu MLH1 defizienten Prophase I Chromosomen, an denen der meiotischen MLH1 Bindungspartner MLH3 an den Stellen der „Cross over“ lokalisiert (Kolas et al., 2005), kann MLH3 an *Mlh1*$^{G67R/G67R}$ Prophase I Chromosomen nicht nachgewiesen werden. Dies deutet darauf hin, dass MLH3 mit dem G67R mutanten MLH1 Protein dimerisiert, dann jedoch nicht mehr in den MSH4/5 Komplex interagieren kann. Die Vermutung, dass das G67R mutante MLH1 Protein in heterozygoten *Mlh1*$^{G67R/+}$ Tieren mit dem wildtypischen MLH1 Protein um die MLH3 Bindung konkurriert kann nicht bestätigt werden, da *Mlh1*$^{G67R/+}$ Tieren keinen meiotischen Phänotyp zeigen und ihre Wurfgröße und Frequenz nicht von den in C57Bl/6 Tieren beobachteten abweichen.
Bisher konnten auch für HNPCC Patienten, die ebenfalls heterozygote Mutationen im *Mlh1* Gen aufweisen, keine Fälle beschrieben werden, in denen Infertilitäten an Keimbahnmutationen im *Mlh1* Gen gekoppelt sind. Diese stützt zudem die Beobachtung, dass die G67R Mutation keinen dominant-negativen Effekt auf die meiotische MLH1 Funktion hat.

## *II.2. Konditionelle Inaktivierung von MLH1 in thymischen und naïven T-Zellen führt zu verminderten Inzidenzen lymphoblastischer Lymphome im Mausmodell*

MLH1 defiziente Mäuse sind durch einen starken Tumorprädispositionsphänotyp charakterisiert. Sie entwickeln in erster Linie Lymphome und gastrointestinale Tumore. Hierdurch unterscheiden sie sich von HNPCC Patienten, die neben dem 80% erhöhten Risiko für kolorektale Tumore, eine erhöhte Prädisposition für Tumore des Urogenital-Traktes, der Prostata, der Lunge, der Nieren sowie weiterer Gewebe aufweisen (Chao and Lipkin, 2006). Zudem konnte gezeigt werden, dass Tumore unterschiedlichster Gewebe Mikrosatteliten-Instabilitäten aufweisen, was ein Kennzeichen MMR defizienter Tumore ist. Da das mittlere bzw. 50% Überleben MLH1 defizienter Tiere nur 7 Monate beträgt (Edelmann et al., 1999), ist es möglich, dass diese stark verkürzte Lebensspanne dafür verantwortlich ist, dass *Mlh1*$^{-/-}$ Tiere keine bzw. kaum weitere Tumore entwickeln, die zum HNPCC Spektrum gezählt werden können.

Um die Möglichkeit zu erhalten die MLH1 abhängigen Tumorgenese in unterschiedlichen Geweben bzw. Organen, die nicht zum Tumorspektrum der *Mlh1*$^{-/-}$ Mauslinie zählen, zu analysieren, wurde das Cre LoxP Rekombinationssystem genutzt, welches ein ausgezeichnetes gentechnisches Werkzeug zur Generierung konditioneller, d.h. zeit- oder gewebsspezifischer Gendeletion in der Maus darstellen .

Hierzu wurde eine Mauslinie mit gefloxtem Exon 4 des *mMlh1* Gens erzeugt und deren Eignung durch Einkreuzen von ubiquitär Cre exprimierenden Tieren (EIIa-Cre (Lakso et al., 1996)) überprüft. Der Phänotyp der erzeugten *Mlh1*$^{\Delta ex4/\Delta ex4}$ Mauslinie, die durch eine ubiquitäre Deletion des Exon 4 des *Mlh1* Gens vom Zygotenstadium an, charakterisiert ist, entspricht dem der publizierten *Mlh1*$^{-/-}$ Linie, sodass die *Mlh1*$^{flox/flox}$ Mauslinie zur Generierung von Zell- bzw. Gewebsspezifischen MLH1 defizienter Tiere mittels Einkreuzen von spezifisch Cre exprimierenden Mauslinien genutzt werden kann. Eine Zusammenfassung aller *Mlh1*$^{\Delta ex4/\Delta ex4}$ Tumortiere befindet sich im Anhang 3.

Die MMR Defizienz abhängige Lymphomagenese ist von großem Interesse, da Leukämien und Lymphome nicht zum typischen Tumorspektrum von HNPCC Patienten zählen, jedoch in Tumorpatienten mit bialelischen Mutationen der MMR Gene auftreten (Pineda et al., 2008). Homozygote Mutationen sind zudem mit Neurofibromatose Typ 1 korreliert, was frühkindliche B- und T-Zell Leukämien bedingt (Ricciardone et al., 1999; Whiteside et al., 2002). Dies deutet auf eine wichtige Rolle des MMR-Systems in der Unterdrückung von

Lymphomen hin. Des Weiteren wurden Mikrosateliteninstabilitäten, einem Kennzeichen für MMR defektive Tumore, in verschiedenen humanen Lymphomerkrankungen beschrieben (Hangaishi et al., 1997; Kaneko et al., 1995; Wada et al., 1994). Auch das Tumorspektrum der etablierten MLH1 und MSH2 defizienten Mauslinien umfasst neben gastrointestinalen Tumoren Lymphome, die in der gleichen Frequenz auftreten (Edelmann et al., 1996; Reitmair et al., 1995), was diese These unterstützt, dass dem MMR System eine wichtige Rolle in der Suppression von lymphatischen Tumoren zukommt. Im Mausmodell entwickeln MSH2 defiziente Tiere ausschließlich lymphoblastische T-Zell-Lymphome und MLH1 defizienten Tiere zu 70% lymphoblastische T-Zell-Lymphome (unveröffentlichte Daten Dr. Thorsten Haneke und (Avdievich et al., 2008)). Die Homogenität der Lymphome lässt vermuten, dass die maligne Transformation bereits in sehr frühen Stadien der intratymischen T-Zell Entwicklung stattfindet. Um diese Hypothese zu testen wurde die *LckCre* Mauslinie in die $Mlh1^{flox/flox}$ Mauslinie eingekreuzt. Die Expression der Cre-Rekombinase wird in der *LckCre* Mauslinie vom proximalen Lck Promotor reguliert, der in fötalen und adulten unreifen Thymozyten, also bereits in DN Thymozyten aktiv ist (Orban et al., 1992; Reynolds et al., 1990). Die resultierenden $Mlh1^{T\Delta Ex4/T\Delta Ex4}$ Nachkommen sind durch eine T-Zell spezifische MLH1 Defizienz ab dem DP-T-Zell Stadium charakterisiert. Die Analyse der Lymphomagenese von $Mlh1^{T\Delta Ex4/T\Delta Ex4}$ Mäusen zeigte signifikant verminderte Lymphominzidenzen. Auch das Einkreuzen eines MLH1 null Allels und/oder eines $MLH1^{G67R}$ Allels führte zu verminderten Lymphominzidenzen in den resultierenden $Mlh1^{T\Delta Ex4/-}$ und $Mlh1^{T\Delta Ex4/G67R}$ Tieren. Die wenigen $MLH1^{T\Delta Ex4}$ Lymphome konnten als lymphoblastische Lymphome charakterisiert werden und unterscheiden sich auch im Vergleich zu MLH1 defizienten Lymphomen nicht im Entstehungszeitraum und sind ebenfalls durch einen hohen Grad an Mikrosatelliteninstabilität gekennzeichnet. Eine Zusammenfassung aller $Mlh1^{T\Delta Ex4/T\Delta Ex4}$ $Mlh1^{T\Delta Ex4/-}$ und $Mlh1^{T\Delta Ex4/G67R}$ Tiere befindet sich im Anhang 4, 5 und 6.

Diese stark verminderte Lymphominzidenz in $MLH1^{T\Delta Ex4}$ Tieren unterstützt die Hypothese, dass MLH1 bereits in sehr frühen Stadien der intratymischen T-Zell Entwicklung eine Tumorsupressive Funktion besitzt. In $Mlh1^{T\Delta Ex4/T\Delta ex4}$ Thymozyten erfolgt eine effektive Deletion des *Mlh1* Exon 4, in Abhängigkeit der lck getriebenen Cre Expression, erst ab dem doppelt positiven (DP) Stadium der Thymozytenentwicklung. Es ist anzunehmen, dass die MMR vermittelte Suppression der Lymphomentstehung in Zusammenhang mit der massiven Proliferation einhergeht, die in DN T-Zellen stattfindet. Das MMR System ist in Zellen mit einer hohen mitotischen Proliferationsrate von entscheidender Bedeutung, da es

Replikationsfehler behebt und somit einer Akkumulation von Mutationen in Schlüsselgenen verhindert und die genomische Integrität aufrechterhält. Da für B-Zellen gezeigt werden konnte, dass das MMR System bei dem Immunglobulin Gene „Rearrangement“ von entscheidender Bedeutung ist (Larijani et al., 2005) kann es jedoch nicht ausgeschlossen werden, dass ein funktionales MMR System auch für die T-Zell Rezeptor „Rearrangement“ wichtig ist und eine inkorrekte Reorganisation des T-Zell Rezeptors zur Tumorgenese führt.
Der Befund, dass das MMR System äußerst wichtig für die Vermeidung der malignen Transformation in frühen Stadien der Lymphozytenentwicklung, nicht aber in naïven Lymphozyten ist, erklärt das Fehlen von hämatopoetischen Tumoren in HNPCC Patienten. Diese Patienten sind heterozygot für MMR Genmutationen und der Verlust des Wildtypallels tritt später im Leben ein. Zudem ist die thymische T-Zell Entwicklung in Erwachsenen stark reduziert und Lymphozyten sind, anders als das Darmgewebe, kaum endogenen DNA Schädigenden Agenzien ausgesetzt.
Um den genauen Zeitpunkt in der T-Zell Entwicklung terminieren zu können, zu dem MLH1 bzw. das mismatch Reparatursystem die maligne Transformation unreifer Lymphozyten unterdrückt, sind weitere Versuche wie das Einkreuzen von Cre Exprimierenden Mauslinien, die Cre bereits in Lymphozytenvorläufern oder Stammzellen exprimieren, notwendig.

## *II Nebenprojekt 1: Reaktive Antikörper gegen das hitzeschock Protein 65 aus dem Mycobakterium bovis Bazillus Calmette Guerin prognostizieren den Erfolg der Immuntherapie bei hochgradigen Transitionalzellkarzinomen der Blase.*

Das Harnblasenkarzinom stellt nach dem Prostatakarzinom den zweithäufigsten, malignen Tumor des Urogenitaltraktes in Westeuropa und der USA dar (Kaufman et al., 2009). Die Therapie besteht zunächst aus einer histologischen Sicherung durch transurethrale Entfernung des Blasentumors. Die weitere Behandlung ist dann vom Stadium und Grading des Tumors abhängig. Tumore mit einem niedrigen oder mittelgradigen Risiko werden nach 6 Wochen erneut tumorreseziert und als Rezidivprophylaxe eine intravesikale Chemotherapie mit Mitmozyin durchgeführt.

Hochrisikotumore, z.B. das „Carcinoma in situ“, haben ein hohes Rezidiv- sowie Progressionsrisiko zu einem muskelinfiltrierenden Tumor. Als Therapie des Carcinoma in situ und als Rezidivprophylaxe hat sich die wiederholte intravesikale Instillation von Mykobakterium bovi Bazillus Calmette-Guérin (BCG) als Standardtherapie etabliert (Sharma et al., 2007). Durch wiederholte intravesikale Gabe von M. bovis BCG wird eine komplexe immunologische Reaktion in der Blasenwand ausgelöst, die bei 50-75 % der Patienten zur Tumorelimination führt (Alexandroff et al., 1999). Patienten, die nicht auf die BCG-Immuntherapie ansprechen, haben ein hohes Risiko für eine Progression zum muskelinfiltrierenden Tumor sowie zur Metastasierung. Es ist daher wünschenswert den klinischen Erfolg der BCG Therapie möglichst früh vorhersagen oder messbar machen zu können. Ein solcher Marker fehlte und die klinische Diagnostik bzw. Verlaufskontrolle des Urothelkarzinoms beruhten daher auf der invasiven Cystoskopie und der mit einer ungenügenden Spezifität behafteten Urinzytologie.

Ein tumorspezifischer serologischer Marker zur Verlaufskontrolle der BCG Therapie, war daher wünschenswert und wurde durch Charakterisierung der B-Zell Immuantwort identifiziert.

Zunächst wurden Immunglobuline aus Serumproben von Patienten mit Urothelkarzinomen unterschiedlicher Tumorstadien und zu verschiedenen Zeitpunkten der Behandlung aufgereinigt und mittels der Random-Peptide-Phage-Display-Technik die Oligopeptidsequenzen isoliert, gegen die sich die patienteneigene Antikörperantwort (IgG) richtet. Hierbei wurde eine Oligopeptidsequenz (HIGAEGR) als B-Zell-Antigen identifiziert,

gegen das Patienten nach einer erfolgreichen BCG-Therapie Antikörper bilden. Die Bindungsspezifität wurde mittels kompetitiver Bindungsinhibition verifiziert. Als korrespondierendes Antigen zu diesem B-Zell Antigen wurde das *M. bovis* Hitzeschockprotein 65 identifiziert (HSP65). Ein Anstieg sowohl der IgG- als auch IgA-Antikörpertiter gegen *M. bovis* HSP65 nach sechsmaliger Instillation sagt eine erfolgreiche Eradikation des Cis, ein fehlender Anstieg ein Versagen der BCG Immuntherapie vorher.
Die Antikörperbildung gegen das M.-bovis- Hitzeschockprotein 65 stellt daher einen vielversprechenden prädiktiven Marker zur individuellen Vorhersage des Erfolgs der BCG-Immuntherapie, auf serologischem Wege dar.

## *II. Nebenprojekt 2: STAT3 und SMAD1 Signalgebung in embrynalen Stammzell-ähnlichen Medaka Zellen und Blastula Embryonen*

Die Aufrechterhaltung des Pluripotenzstatus bzw. des undifferenzierten Zustandes ist essentiell für die Kultivierung von embryonalen Stammzellen. Das zurzeit am besten charakterisierte ES-Zell System ist dass muriner ES-Zellen. In diesem System konnte gezeigt werden, dass der leukemia-inhibitory Faktor (LIF) den Signalgebers STAT3 (signal transducer and activator of transcription 3) aktiviert (Matsuda et al., 1999). Hierdurch wird ein transkriptionelles Programm initiiert, das den undifferenzierten Status in kultivierten murinen ES-Zellen aufrechterhält (Niwa et al., 1998). Des Weiteren konnte gezeigt werden, dass die Aktivierung des BMP Signalweges über SMAD Proteine die Expression von ID Genen („Inhibitor of Differentiation“) induziert und hierdurch den undifferenzierten ES-Zell Status stabilisiert (Hollnagel et al., 1999). Hierbei arbeiten beide Signalwege sowohl kooperativ als auch kompetitiv. Die mittels BMP induzierten ID Gene inhibieren die Differenzierung von ES Zellen zur nuronalen Linie, die nur partiell über den STAT3 Signalweg verhindert wird. STAT3 wiederum inhibiert die BMP induzierte Mesoderm- und Endoderm-Differenzierung (Ying et al., 2003). Neben den STAT und BMP Signalwegen sind noch weitere Signalübertragunswege wie WNT, PI3K und Notch beschrieben, die ebenfalls an der Kontrolle der Pluripotenz in murinen ES-Zellen beteiligt sind (Boiani and Scholer, 2005; Liu et al., 2007).

Im Gegensatz zu murinen ES-Zelllinien kann die pluripotenz-erhaltenden Effekte der STAT und BMP Signalwege in ES-Zelllinien, die aus Mensch und Affen isoliert wurden, nicht nachgewiesen werden (Humphrey et al., 2004; Sumi et al., 2004). Diese wesentlichen Unterschiede zwischen zwei so nahe verwandten Spezies wie Mensch und Maus in der Kontrolle der Pluripotenz sind durch spezies-spezifische Unterschiede in der und nicht durch artifizielle Zellkultureffekte begründet. Dies kann durch vergleichende Untersuchungen an Medaka (*Oryzias latipes*) und murinen Stammzellkulturen und Blastozysten nachgewiesen werden (Wagner et al., 2008).

Die subzelluläre Lokalisation der Signalüberträger STAT3 und SMAD1 korrelierten mit dem Aktivierungsstatus des jeweiligen Signalübertragunswegs (Kretzschmar et al., 2004; Sapkota et al., 2007). In Medaka lokalisiert STAT3 sowohl in ES-Zell-ähnlichen Mes1 Zellen als auch in Blastula Embryos nur im Cytoplasma, wohingegen es in murinen ES-Zellen und Blasozysten nukleär nachgewiesen werden kann. Hiermit konnte gezeigt werden, dass der

STAT3 Signalweg für die Aufrechterhaltung der Pluripotenz in Medaka entbehrlich ist. Anders verhält es sich für SMAD1, welches in Mes1 Zellen und in Medaka Blastula Embryos im Zellkern lokalisiert. Dies spricht gegen das Konzept der gegenseitigen Regulation der STAT/BMP Signalwege (Ying et al., 2003), das für murinen ES-Zellen postuliert wird. Nicht ausgeschlossen ist allerdings, dass alternative Signalwege die BMP-induzierte Differenzierung inhibieren.

Der Teleost Medaka ist evolutionär sehr weit entfernt von Mensch und Maus einzusiedeln. Da sowohl im humanen System als auch in Medaka STAT Signalgebung keine übergeordnete Rolle in der Aufrechterhaltung der Pluripotenz spielen, scheint somit die starke Abhängigkeit von einem aktiven STAT Signalweg, wie sie in murinen ES-Zellen beschrieben ist, die Ausnahme der Regel zu sein.

# III Zusammenfasung

Mutationen im humanen DNA Mismatch-Reparatur (MMR) Gens *Mlh1* sind mit dem erblichen, nicht-polypösen Kolonkarzinom (Lynch Syndrom, HNPCC) und einem signifikanten Anteil sporadischer kolorektaler Tumore assoziiert. Zudem konnten MMR Defekte in sporadischen und erblichen Lymphom Erkrankungen beschrieben werden.
In Zellen resultiert die Inaktivierung des *Mlh1* Gens in der Akkumulation von somatischen Mutationen im Genom und einer erhöhten Resistenz gegenüber den genotoxischen Effekten einer Vielzahl von DNA schädigenden Agenzien. Mäuse, die ein Null Allel für das MMR Gen *Mlh1* tragen zeigen einen starken Tumorprädispositions Phänotyp. Sie entwickeln vorrangig B- und T-Zell Lymphome und mit geringerer Haufigkeit gastrointestinale Tumore. Zusätzlich sind $Mlh1^{-/-}$ Mäuse durch einen meiotischen Phänotyp charakterisiert, der zu Sterilitäten in beiden Geschlechtern führt.

Um die Effekte von *Mlh1* missense Mutationen auf die Tumoranfälligkeit zu untersuchen, erzeugten wir eine Mauslinie, die die häufig in HNPCC Patienten beschriebene $MLH1^{G67R}$ Mutation tragen, die in einer der ATP Bindungs-Domänen von MLH1 lokalisiert ist. Auch wenn die $MLH1^{G67R}$ Mutation in homozygot mutanten Mäusen in einer DNA Reparatur Defizienz resultierte hatte sie keinen Effekt auf die MMR vermittelte zelluläre Antwort auf DNA Schäden. Hierzu gehörte die apoptotische Antwort von Epithelzellen der intestinalen Mucosa auf Cisplatin, die in $Mlh1^{-/-}$ Mäusen defektiv jedoch in $Mlh1^{G67R/G67R}$ Mäusen normal ausfiel. $Mlh1^{G67R/G67R}$ mutante Mäuse zeigten wie $Mlh1^{-/-}$ Tiere einen starken Tumorprädispositions Phänotyp. Sie entwickelten jedoch im Vergleich zu $Mlh1^{-/-}$ Tieren signifikant weniger gastrointestinale Tumore, was darauf hinweist, dass *Mlh1* missense Mutationen die Tumor supprimierende MMR Funktion in einer Gewebs-spezifischen Weise beeinflussen können. Darüber hinaus sind $Mlh1^{G67R/G67R}$ Mäuse, aufgrund der fehlenden Bindungsfähigkeit des $MLH1^{G67R}$ Proteins an die meiotischen Chromosomen im Pachytän Stadium, steril. Dies zeigt, dass die ATPase Aktivität von MLH1 für die Fertilität in Säugern essentiell ist.
Diese Untersuchungen belegen, dass die $Mlh1^{G67R}$ Mutation die biologischen MLH1 Funktionen differentiell mit einem eindeutigen Phänotyp beeinflusst.

Um die Rolle von MLH1 für die Lymphomagenese detaillierter untersuchen zu können, generierten wir ein neues Mausmodell mit einem konditionellen *Mlh1* Allel ($Mlh1^{flox/flox}$). Das

Einkreuzen von transgenen *EIIa-Cre* Mausen in die *Mlh1*$^{flox/flox}$ Mauslinie führte zur konstitutiven Inaktivierung von MLH1. Die resultierende *Mlh1*$^{\Delta ex4/\Delta ex4}$ Mauslinie zeichnete sich durch MMR Defizienz und einen zu *Mlh1*$^{-/-}$ Tieren vergleichbaren Tumorprädispositions Phänotyp aus. Zur T-Zell spezifischen MMR Inaktivierung kombinierten wir das *Mlh1*$^{flox/flox}$ Allel mit dem *Lck-Cre* Transgen. In den resultierenden *Mlh1*$^{T\Delta ex4/T\Delta ex4}$ Mäusen ist die MLH1 Inaktivierung auf doppelt positive und einzel positive Thymozyten und naïve periphere T-Zellen beschränkt. Die Entwicklung von T-Zell Lymphomen in *Mlh1*$^{T\Delta ex4/T\Delta ex4}$ Mäusen ist im Vergleich zu *Mlh1*$^{-/-}$ Mäusen signifikant reduziert, was eine wichtige, Lymphom supprimierende MMR Funktion in frühen Stadien der T-Zell Entwicklung oder in lymphoiden Vorläuferzellen impliziert.

# IV Summary

Mutations in the human DNA mismatch repair (MMR) gene *Mlh1* are associated with hereditary nonpolyposis colorectal cancer (Lynch syndrome, HNPCC) and a significant proportion of sporadic colorectal cancer. Furthermore, MMR defects have also been observed in sporadic and hereditary lymphoid malignancies.

In cells the inactivation of MLH1 results in the accumulation of somatic mutations in the genome and an increased resistance to the genotoxic effects of a variety of DNA damaging agents. Mice carrying a null allele for the MMR gene *Mlh1* show a strong tumor predisposition phenotype. They are preferentially prone to the development of lymphomas of B- and T-cell origin and to a lesser extent gastrointestinal tumors. Additionally *Mlh1*$^{-/-}$ mice are characterized by a meiotic phenotype leading to male and female sterility.

To study the effect of *Mlh1* missense mutations on cancer susceptibility, we generated a mouse line carrying the recurrent MLH1$^{G67R}$ mutation that is located in one of the ATP-binding domains of MLH1. Although the MLH1$^{G67R}$ mutation resulted in DNA repair deficiency in homozygous mutant mice, it did not affect the MMR-mediated cellular response to DNA damage, including the apoptotic response of epithelial cells in the intestinal mucosa to cisplatin, which was defective in *Mlh1*$^{-/-}$ mice but remained normal in *Mlh1*$^{G67R/G67R}$ mice. Similar to *Mlh1*$^{-/-}$ mice, *Mlh1*$^{G67R/G67R}$ mutant mice displayed a strong cancer predisposition phenotype. However, in contrast to *Mlh1*$^{-/-}$ mice, *Mlh1*$^{G67R/G67R}$ mutant mice developed significantly fewer intestinal tumors, indicating that *Mlh1* missense mutations can affect MMR tumor suppressor functions in a tissue-specific manner. In addition, *Mlh1*$^{G67R/G67R}$ mice were sterile because of the inability of the mutant Mlh1$^{G67R}$ protein to interact with meiotic chromosomes at pachynema, demonstrating that the ATPase activity of MLH1 is essential for fertility in mammals.

These studies demonstrate that the Mlh1$^{G67R}$ mutation differentially affects the biological functions associated with MLH1 with distinct phenotypic effects.

To study the role of MLH1 for lymphomagenesis in more detail, we generated a new mouse model carrying a conditional *Mlh1* allele (*Mlh1*$^{flox/flox}$). Mating of these mice with *EIIa*-Cre recombinase transgenic mice allowed the constitutive inactivation of MLH1 and the resulting

Summary

*Mlh1*$^{\Delta ex4/\Delta ex4}$ mouse line displays complete MMR deficiency and a cancer predisposition phenotype similar to *Mlh1*$^{-/-}$ mice. For T-cell specific MMR inactivation we combined the *Mlh1*$^{flox/flox}$ allele with the *Lck-Cre* Transgene. In the resulting *Mlh1*$^{T\Delta ex4/T\Delta ex4}$ mice, MLH1 inactivation is limited to double positive and single positive thymocytes and naïve peripheral T-cells. The development of T-cell lymphomas in *Mlh1*$^{T\Delta ex4/T\Delta ex4}$ mice is significantly reduced compared to *Mlh1*$^{-/-}$ mice implicating that MMR functions either at very early stages during T-cell development or even earlier in lymphoid precursor cells to suppress lymphomagenesis.

# V Methoden

Alle von mir während meiner Promotion verwendeten Methoden sind in den Veröffentlichungen genauer beschrieben.

# VI Referenzen


Abdullah, M. F., Hoffmann, E. R., Cotton, V. E., and Borts, R. H. (2004). A role for the MutL homologue MLH2 in controlling heteroduplex formation and in regulating between two different crossover pathways in budding yeast. Cytogenetic and genome research *107*, 180-190.

Aebi, S., Kurdi-Haidar, B., Gordon, R., Cenni, B., Zheng, H., Fink, D., Christen, R. D., Boland, C. R., Koi, M., Fishel, R., and Howell, S. B. (1996). Loss of DNA mismatch repair in acquired resistance to cisplatin. Cancer Res *56*, 3087-3090.

Alani, E., Sokolsky, T., Studamire, B., Miret, J. J., and Lahue, R. S. (1997). Genetic and biochemical analysis of Msh2p-Msh6p: role of ATP hydrolysis and Msh2p-Msh6p subunit interactions in mismatch base pair recognition. Mol Cell Biol *17*, 2436-2447.

Alexandroff, A. B., Jackson, A. M., O'Donnell, M. A., and James, K. (1999). BCG immunotherapy of bladder cancer: 20 years on. Lancet *353*, 1689-1694.

Avdievich, E., Reiss, C., Scherer, S. J., Zhang, Y., Maier, S. M., Jin, B., Hou, H., Jr., Rosenwald, A., Riedmiller, H., Kucherlapati, R., *et al.* (2008). Distinct effects of the recurrent Mlh1G67R mutation on MMR functions, cancer, and meiosis. Proceedings of the National Academy of Sciences of the United States of America *105*, 4247-4252.

Baker, S. M., Bronner, C. E., Zhang, L., Plug, A. W., Robatzek, M., Warren, G., Elliott, E. A., Yu, J., Ashley, T., Arnheim, N., *et al.* (1995). Male mice defective in the DNA mismatch repair gene PMS2 exhibit abnormal chromosome synapsis in meiosis. Cell *82*, 309-319.

Beardsley, D. I., Kim, W. J., and Brown, K. D. (2005). N-methyl-N'-nitro-N-nitrosoguanidine activates cell-cycle arrest through distinct mechanisms activated in a dose-dependent manner. Mol Pharmacol *68*, 1049-1060.

Bellacosa, A. (2001). Functional interactions and signaling properties of mammalian DNA mismatch repair proteins. Cell Death and Differentiation *8*, 1076-1092.

Boiani, M., and Scholer, H. R. (2005). Regulatory networks in embryo-derived pluripotent stem cells. Nature reviews *6*, 872-884.

Boland, C. (2000). Molecular genetics of hereditary nonpolyposis colorectal cancer. Annals of the New York Academy of Sciences *910*, 50-59.

Brown, K. D., Rathi, A., Kamath, R., Beardsley, D. I., Zhan, Q., Mannino, J. L., and Baskaran, R. (2003). The mismatch repair system is required for S-phase checkpoint activation. Nat Genet *33*, 80-84.

Buermeyer, A. B., Deschenes, S. M., Baker, S. M., and Liskay, R. M. (1999). Mammalian DNA mismatch repair. Annu Rev Genet *33*, 533-564.

Caporali, S., Falcinelli, S., Starace, G., Russo, M. T., Bonmassar, E., Jiricny, J., and D'Atri, S. (2004). DNA damage induced by temozolomide signals to both ATM and ATR: role of the mismatch repair system. Mol Pharmacol *66*, 478-491.

Ceccotti, S., Aquilina, G., Macpherson, P., Yamada, M., Karran, P., and Bignami, M. (1996). Processing of O6-methylguanine by mismatch correction in human cell extracts. Curr Biol *6*, 1528-1531.

Chao, E. C., and Lipkin, S. M. (2006). Molecular models for the tissue specificity of DNA mismatch repair-deficient carcinogenesis. Nucleic Acids Res *34*, 840-852.

Clark, A. B., Valle, F., Drotschmann, K., Gary, R. K., and Kunkel, T. A. (2000). Functional interaction of proliferating cell nuclear antigen with MSH2-MSH6 and MSH2-MSH3 complexes. The Journal of biological chemistry *275*, 36498-36501.
Cleaver, J. (1968). Defective repair replication of DNA in xeroderma pigmentosum. Nature *218*, 652-656.
Cox, E. C., and Yanofsky, C. (1967). Altered base ratios in the DNA of an Escherichia coli mutator strain. Proceedings of the National Academy of Sciences of the United States of America *58*, 1895-1902.
de la Chapelle, A. (2004). Genetic predisposition to colorectal cancer. Nat Rev Cancer *4*, 769-780.
de los Santos, T., Hunter, N., Lee, C., Larkin, B., Loidl, J., and Hollingsworth, N. M. (2003). The Mus81/Mms4 endonuclease acts independently of double-Holliday junction resolution to promote a distinct subset of crossovers during meiosis in budding yeast. Genetics *164*, 81-94.
de Vries, S. S., Baart, E. B., Dekker, M., Siezen, A., de Rooij, D. G., de Boer, P., and te Riele, H. (1999). Mouse MutS-like protein Msh5 is required for proper chromosome synapsis in male and female meiosis. Genes & development *13*, 523-531.
Divine, K. K., Gilliland, F. D., Crowell, R. E., Stidley, C. A., Bocklage, T. J., Cook, D. L., and Belinsky, S. A. (2001). The XRCC1 399 glutamine allele is a risk factor for adenocarcinoma of the lung. Mutat Res *461*, 273-278.
Drummond, J. T., Li, G. M., Longley, M. J., and Modrich, P. (1995). Isolation of an hMSH2-p160 heterodimer that restores DNA mismatch repair to tumor cells. Science *268*, 1909-1912.
Duckett, D. R., Bronstein, S. M., Taya, Y., and Modrich, P. (1999). hMutSalpha- and hMutLalpha-dependent phosphorylation of p53 in response to DNA methylator damage. Proceedings of the National Academy of Sciences of the United States of America *96*, 12384-12388.
Edelmann, W., Cohen, P. E., Kane, M., Lau, K., Morrow, B., Bennett, S., Umar, A., Kunkel, T., Cattoretti, G., Chaganti, R., *et al.* (1996). Meiotic pachytene arrest in MLH1-deficient mice. Cell *85*, 1125-1134.
Edelmann, W., Cohen, P. E., Kneitz, B., Winand, N., Lia, M., Heyer, J., Kolodner, R., Pollard, J. W., and Kucherlapati, R. (1999a). Mammalian MutS homologue 5 is required for chromosome pairing in meiosis. Nat Genet *21*, 123-127.
Edelmann, W., Yang, K., Kuraguchi, M., Heyer, J., Lia, M., Kneitz, B., Fan, K., Brown, A. M., Lipkin, M., and Kucherlapati, R. (1999b). Tumorigenesis in Mlh1 and Mlh1/Apc1638N mutant mice. Cancer Res *59*, 1301-1307.
Ellison, A. R., Lofing, J., and Bitter, G. A. (2001). Functional analysis of human MLH1 and MSH2 missense variants and hybrid human-yeast MLH1 proteins in Saccharomyces cerevisiae. Human molecular genetics *10*, 1889-1900.
Emmert, S., Leibeling, D., and Runger, T. M. (2006). Syndromes with genetic instability: model diseases for (skin) cancerogenesis. J Dtsch Dermatol Ges *4*, 721-731.
Fink, D., Zheng, H., Nebel, S., Norris, P. S., Aebi, S., Lin, T. P., Nehme, A., Christen, R. D., Haas, M., MacLeod, C. L., and Howell, S. B. (1997). In vitro and in vivo resistance to cisplatin in cells that have lost DNA mismatch repair. Cancer Res *57*, 1841-1845.
Fishel, R. (1999). Signaling mismatch repair in cancer. Nature Medicine *5*, 1239-1241.
Fishel, R., and Kolodner, R. D. (1995). Identification of mismatch repair genes and their role in the development of cancer. Current opinion in genetics & development *5*, 382-395.
Flores-Rozas, H., Clark, D., and Kolodner, R. D. (2000). Proliferating cell nuclear antigen and Msh2p-Msh6p interact to form an active mispair recognition complex. Nat Genet *26*, 375-378.
Galio, L., Bouquet, C., and Brooks, P. (1999). ATP hydrolysis-dependent formation of a dynamic ternary nucleoprotein complex with MutS and MutL. Nucleic Acids Res *27*, 2325-2331.

Gary, R., Kim, K., Cornelius, H. L., Park, M. S., and Matsumoto, Y. (1999). Proliferating cell nuclear antigen facilitates excision in long-patch base excision repair. The Journal of biological chemistry *274*, 4354-4363.
Gong JG, C. A., Yang HQ, Melino G, Kaelin WG Jr, Levrero M, Wang JY. (1999). The tyrosine kinase c-Abl regulates p73 in apoptotic response to cisplatin-induced DNA damage. Nature *399*, 806-809.
Gong, J. G., Costanzo, A., Yang, H. Q., Melino, G., Kaelin, W. G., Jr., Levrero, M., and Wang, J. Y. (1999). The tyrosine kinase c-Abl regulates p73 in apoptotic response to cisplatin-induced DNA damage. Nature *399*, 806-809.
Gu, L., Hong, Y., McCulloch, S., Watanabe, H., and Li, G. M. (1998). ATP-dependent interaction of human mismatch repair proteins and dual role of PCNA in mismatch repair. Nucleic Acids Res *26*, 1173-1178.
Guarne, A., Junop, M. S., and Yang, W. (2001). Structure and function of the N-terminal 40 kDa fragment of human PMS2: a monomeric GHL ATPase. Embo J *20*, 5521-5531.
Guerrette, S., Acharya, S., and Fishel, R. (1999). The interaction of the human MutL homologues in hereditary nonpolyposis colon cancer. The Journal of biological chemistry *274*, 6336-6341.
Haber, L. T., and Walker, G. C. (1991). Altering the conserved nucleotide binding motif in the Salmonella typhimurium MutS mismatch repair protein affects both its ATPase and mismatch binding activities. Embo J *10*, 2707-2715.
Habraken, Y., Sung, P., Prakash, L., and Prakash, S. (1998). ATP-dependent assembly of a ternary complex consisting of a DNA mismatch and the yeast MSH2-MSH6 and MLH1-PMS1 protein complexes. The Journal of biological chemistry *273*, 9837-9841.
Hangaishi, A., Ogawa, S., Mitani, K., Hosoya, N., Chiba, S., Yazaki, Y., and Hirai, H. (1997). Mutations and loss of expression of a mismatch repair gene, hMLH1, in leukemia and lymphoma cell lines. Blood *89*, 1740-1747.
Harfe, B. D., and Jinks-Robertson, S. (2000). DNA mismatch repair and genetic instability. Annu Rev Genet *34*, 359-399.
Heinen, C. D., Schmutte, C., and Fishel, R. (2002). DNA repair and tumorigenesis: lessons from hereditary cancer syndromes. Cancer biology & therapy *1*, 477-485.
Heyer, J., Yang, K., Lipkin, M., Edelmann, W., and Kucherlapati, R. (1999). Mouse models for colorectal cancer. Oncogene *18*, 5325-5333.
Hickman, M. J., and Samson, L. D. (1999). Role of DNA mismatch repair and p53 in signaling induction of apoptosis by alkylating agents. Proceedings of the National Academy of Sciences of the United States of America *96*, 10764-10769.
Hoeijmakers, J. H. (2001). Genome maintenance mechanisms for preventing cancer. Nature *411*, 721-731.
Hoffmann, E. R., and Borts, R. H. (2004). Meiotic recombination intermediates and mismatch repair proteins. Cytogenetic and genome research *107*, 232-248.
Hollnagel, A., Oehlmann, V., Heymer, J., Ruther, U., and Nordheim, A. (1999). Id genes are direct targets of bone morphogenetic protein induction in embryonic stem cells. The Journal of biological chemistry *274*, 19838-19845.
Humphrey, R. K., Beattie, G. M., Lopez, A. D., Bucay, N., King, C. C., Firpo, M. T., Rose-John, S., and Hayek, A. (2004). Maintenance of pluripotency in human embryonic stem cells is STAT3 independent. Stem cells (Dayton, Ohio) *22*, 522-530.
Hutter, P., Couturier, A., Membrez, V., Joris, F., Sappino, A. P., and Chappuis, P. O. (1998). Excess of hMLH1 germline mutations in Swiss families with hereditary non-polyposis colorectal cancer. International journal of cancer *78*, 680-684.
Ikeda, M., Orimo, H., Moriyama, H., Nakajima, E., Matsubara, N., Mibu, R., Tanaka, N., Shimada, T., Kimura, A., and Shimizu, K. (1998). Close correlation between mutations of

E2F4 and hMSH3 genes in colorectal cancers with microsatellite instability. Cancer Res *58*, 594-598.
Kaneko, H., Horiike, S., Inazawa, J., Nakai, H., and Misawa, S. (1995). Microsatellite instability is an early genetic event in myelodysplastic syndrome. Blood *86*, 1236-1237.
Karran, P. (2001). Mechanisms of tolerance to DNA damaging therapeutic drugs. Carcinogenesis *22*, 1931-1937.
Kaufman, D. S., Shipley, W. U., and Feldman, A. S. (2009). Bladder cancer. Lancet *374*, 239-249.
Kneitz, B., Cohen, P. E., Avdievich, E., Zhu, L., Kane, M. F., Hou, H., Jr., Kolodner, R. D., Kucherlapati, R., Pollard, J. W., and Edelmann, W. (2000). MutS homolog 4 localization to meiotic chromosomes is required for chromosome pairing during meiosis in male and female mice. Genes & development *14*, 1085-1097.
Kolas, N. K., and Cohen, P. E. (2004). Novel and diverse functions of the DNA mismatch repair family in mammalian meiosis and recombination. Cytogenetic and genome research *107*, 216-231.
Kolas, N. K., Svetlanov, A., Lenzi, M. L., Macaluso, F. P., Lipkin, S. M., Liskay, R. M., Greally, J., Edelmann, W., and Cohen, P. E. (2005). Localization of MMR proteins on meiotic chromosomes in mice indicates distinct functions during prophase I. The Journal of cell biology *171*, 447-458.
Kolodner, R. D., and Marsischky, G. T. (1999). Eukaryotic DNA mismatch repair. Current opinion in genetics & development *9*, 89-96.
Kondo, E., Horii, A., and Fukushige, S. (2001). The interacting domains of three MutL heterodimers in man: hMLH1 interacts with 36 homologous amino acid residues within hMLH3, hPMS1 and hPMS2. Nucleic Acids Res *29*, 1695-1702.
Kretzschmar, A. K., Dinger, M. C., Henze, C., Brocke-Heidrich, K., and Horn, F. (2004). Analysis of Stat3 (signal transducer and activator of transcription 3) dimerization by fluorescence resonance energy transfer in living cells. The Biochemical journal *377*, 289-297.
Kruse, R., and Ruzicka, T. (2004). DNA mismatch repair and the significance of a sebaceous skin tumor for visceral cancer prevention. Trends in molecular medicine *10*, 136-141.
Lakso, M., Pichel, J. G., Gorman, J. R., Sauer, B., Okamoto, Y., Lee, E., Alt, F. W., and Westphal, H. (1996). Efficient in vivo manipulation of mouse genomic sequences at the zygote stage. Proceedings of the National Academy of Sciences of the United States of America *93*, 5860-5865.
Larijani, M., Zaheen, A., Frieder, D., Wang, Y., Wu, G. E., Edelmann, W., and Martin, A. (2005). Lack of MSH2 involvement differentiates V(D)J recombination from other non-homologous end joining events. Nucleic Acids Res *33*, 6733-6742.
Leach, F. S., Nicolaides, N. C., Papadopoulos, N., Liu, B., Jen, J., Parsons, R., Peltomaki, P., Sistonen, P., Aaltonen, L. A., Nystrom-Lahti, M., and et al. (1993). Mutations of a mutS homolog in hereditary nonpolyposis colorectal cancer. Cell *75*, 1215-1225.
Lebrun, C., Olschwang, S., Jeannin, S., Vandenbos, F., Sobol, H., and Frenay, M. (2007). Turcot syndrome confirmed with molecular analysis. Eur J Neurol *14*, 470-472.
Lin, D. P., Wang, Y., Scherer, S. J., Clark, A. B., Yang, K., Avdievich, E., Jin, B., Werling, U., Parris, T., Kurihara, N., *et al.* (2004). An Msh2 point mutation uncouples DNA mismatch repair and apoptosis. Cancer Res *64*, 517-522.
Lipkin, S. M., Moens, P. B., Wang, V., Lenzi, M., Shanmugarajah, D., Gilgeous, A., Thomas, J., Cheng, J., Touchman, J. W., Green, E. D., *et al.* (2002). Meiotic arrest and aneuploidy in MLH3-deficient mice. Nat Genet *31*, 385-390.
Liu, N., Lu, M., Tian, X., and Han, Z. (2007). Molecular mechanisms involved in self-renewal and pluripotency of embryonic stem cells. Journal of cellular physiology *211*, 279-286.

Luo, Y., Lin, F. T., and Lin, W. C. (2004). ATM-mediated stabilization of hMutL DNA mismatch repair proteins augments p53 activation during DNA damage. Mol Cell Biol *24*, 6430-6444.
Lynch, H. T., Shaw, M. W., Magnuson, C. W., Larsen, A. L., and Krush, A. J. (1966). Hereditary factors in cancer. Study of two large midwestern kindreds. Archives of internal medicine *117*, 206-212.
Lynch, H. T. R., BD; Weismann, S; Coronell, SM; Kinarsky, Y; Lynch, JF; Shaw, TG; Rubinstein, WS. (2003). Hereditary Nonpolyposis Colorectal Carcinoma (HNPCC) and HNPCC-Like Families: Problems in Diagnosis, Surveillance, and Management. . Cancer *100*, 53-64.
Matsuda, T., Nakamura, T., Nakao, K., Arai, T., Katsuki, M., Heike, T., and Yokota, T. (1999). STAT3 activation is sufficient to maintain an undifferentiated state of mouse embryonic stem cells. Embo J *18*, 4261-4269.
McKinnon, P. J., and Caldecott, K. W. (2007). DNA strand break repair and human genetic disease. Annu Rev Genomics Hum Genet *8*, 37-55.
Modrich, P. (1991). Mechanisms and biological effects of mismatch repair. Annual Review of Genetics *25*, 229-255.
Modrich, P., and Lahue, R. (1996). Mismatch repair in replication fidelity, genetic recombination, and cancer biology. Annu Rev Biochem *65*, 101-133.
Moens, P. B., Kolas, N. K., Tarsounas, M., Marcon, E., Cohen, P. E., and Spyropoulos, B. (2002). The time course and chromosomal localization of recombination-related proteins at meiosis in the mouse are compatible with models that can resolve the early DNA-DNA interactions without reciprocal recombination. J Cell Sci *115*, 1611-1622.
Niwa, H., Burdon, T., Chambers, I., and Smith, A. (1998). Self-renewal of pluripotent embryonic stem cells is mediated via activation of STAT3. Genes & development *12*, 2048-2060.
Novak, J. E., Ross-Macdonald, P. B., and Roeder, G. S. (2001). The budding yeast Msh4 protein functions in chromosome synapsis and the regulation of crossover distribution. Genetics *158*, 1013-1025.
Nystrom-Lahti, M., Perrera, C., Raschle, M., Panyushkina-Seiler, E., Marra, G., Curci, A., Quaresima, B., Costanzo, F., D'Urso, M., Venuta, S., and Jiricny, J. (2002). Functional analysis of MLH1 mutations linked to hereditary nonpolyposis colon cancer. Genes Chromosomes Cancer *33*, 160-167.
Orban PC, C. D., Marth JD. (1992). Tissue- and site-specific DNA recombination in transgenic mice. Proceedings of the Nationel Academy of Sciences *89*, 6861-6865.
Orban, P. C., Chui, D., and Marth, J. D. (1992). Tissue- and site-specific DNA recombination in transgenic mice. Proceedings of the National Academy of Sciences of the United States of America *89*, 6861-6865.
Palombo, F., Iaccarino, I., Nakajima, E., Ikejima, M., Shimada, T., and Jiricny, J. (1996). hMutSbeta, a heterodimer of hMSH2 and hMSH3, binds to insertion/deletion loops in DNA. Curr Biol *6*, 1181-1184.
Papadopoulos, N., Nicolaides, N. C., Wei, Y. F., Ruben, S. M., Carter, K. C., Rosen, C. A., Haseltine, W. A., Fleischmann, R. D., Fraser, C. M., Adams, M. D., and et al. (1994). Mutation of a mutL homolog in hereditary colon cancer. Science *263*, 1625-1629.
Peltomäki, P. (2001). DNA mismatch repair and cancer. Mutation Research *488*, 77-85.
Peltomaki, P., Lothe, R. A., Aaltonen, L. A., Pylkkanen, L., Nystrom-Lahti, M., Seruca, R., David, L., Holm, R., Ryberg, D., Haugen, A., and et al. (1993). Microsatellite instability is associated with tumors that characterize the hereditary non-polyposis colorectal carcinoma syndrome. Cancer Res *53*, 5853-5855.
Pineda, M., Castellsague, E., Musulen, E., Llort, G., Frebourg, T., Baert-Desurmont, S., Gonzalez, S., Capella, G., and Blanco, I. (2008). Non-Hodgkin lymphoma related to

hereditary nonpolyposis colorectal cancer in a patient with a novel heterozygous complex deletion in the MSH2 gene. Genes Chromosomes Cancer *47*, 326-332.
Pochart, P., Woltering, D., and Hollingsworth, N. M. (1997). Conserved properties between functionally distinct MutS homologs in yeast. The Journal of biological chemistry *272*, 30345-30349.
Prolla, T. A., Baker, S. M., Harris, A. C., Tsao, J. L., Yao, X., Bronner, C. E., Zheng, B., Gordon, M., Reneker, J., Arnheim, N., *et al.* (1998). Tumour susceptibility and spontaneous mutation in mice deficient in Mlh1, Pms1 and Pms2 DNA mismatch repair. Nat Genet *18*, 276-279.
Rampino, N., Yamamoto, H., Ionov, Y., Li, Y., Sawai, H., Reed, J. C., and Perucho, M. (1997). Somatic frameshift mutations in the BAX gene in colon cancers of the microsatellite mutator phenotype. Science *275*, 967-969.
Raschle, M., Dufner, P., Marra, G., and Jiricny, J. (2002). Mutations within the hMLH1 and hPMS2 subunits of the human MutLalpha mismatch repair factor affect its ATPase activity, but not its ability to interact with hMutSalpha. The Journal of biological chemistry *277*, 21810-21820.
Reitmair, A. H., Schmits, R., Ewel, A., Bapat, B., Redston, M., Mitri, A., Waterhouse, P., Mittrucker, H. W., Wakeham, A., Liu, B., and et al. (1995). MSH2 deficient mice are viable and susceptible to lymphoid tumours. Nat Genet *11*, 64-70.
Reynolds, P. J., Lesley, J., Trotter, J., Schulte, R., Hyman, R., and Sefton, B. M. (1990). Changes in the relative abundance of type I and type II lck mRNA transcripts suggest differential promoter usage during T-cell development. Mol Cell Biol *10*, 4266-4270.
Ricciardone, M. D., Ozcelik, T., Cevher, B., Ozdag, H., Tuncer, M., Gurgey, A., Uzunalimoglu, O., Cetinkaya, H., Tanyeli, A., Erken, E., and Ozturk, M. (1999). Human MLH1 deficiency predisposes to hematological malignancy and neurofibromatosis type 1. Cancer Res *59*, 290-293.
Riccio, A., Aaltonen, L. A., Godwin, A. K., Loukola, A., Percesepe, A., Salovaara, R., Masciullo, V., Genuardi, M., Paravatou-Petsotas, M., Bassi, D. E., *et al.* (1999). The DNA repair gene MBD4 (MED1) is mutated in human carcinomas with microsatellite instability. Nat Genet *23*, 266-268.
Sapkota, G., Alarcon, C., Spagnoli, F. M., Brivanlou, A. H., and Massague, J. (2007). Balancing BMP signaling through integrated inputs into the Smad1 linker. Mol Cell *25*, 441-454.
Sasaki, S., Tokino, T., Miyatsu, T., Muto, T., and Nakamura, Y. (1997). Mutational analysis of the hMLH1 gene using an automated two-dimensional DNA typing system. Hum Mutat *9*, 164-171.
Schmutte, C., Sadoff, M. M., Shim, K. S., Acharya, S., and Fishel, R. (2001). The interaction of DNA mismatch repair proteins with human exonuclease I. The Journal of biological chemistry *276*, 33011-33018.
Schwartz, S., Jr., Yamamoto, H., Navarro, M., Maestro, M., Reventos, J., and Perucho, M. (1999). Frameshift mutations at mononucleotide repeats in caspase-5 and other target genes in endometrial and gastrointestinal cancer of the microsatellite mutator phenotype. Cancer Res *59*, 2995-3002.
Sharma, P., Old, L. J., and Allison, J. P. (2007). Immunotherapeutic strategies for high-risk bladder cancer. Seminars in oncology *34*, 165-172.
Shcherbakova, P. V., and Kunkel, T. A. (1999). Mutator phenotypes conferred by MLH1 overexpression and by heterozygosity for mlh1 mutations. Mol Cell Biol *19*, 3177-3183.
Shimodaira, H., Filosi, N., Shibata, H., Suzuki, T., Radice, P., Kanamaru, R., Friend, S. H., Kolodner, R. D., and Ishioka, C. (1998). Functional analysis of human MLH1 mutations in Saccharomyces cerevisiae. Nat Genet *19*, 384-389.

Shimodaira, H., Yoshioka-Yamashita, A., Kolodner, R. D., and Wang, J. Y. (2003). Interaction of mismatch repair protein PMS2 and the p53-related transcription factor p73 in apoptosis response to cisplatin. Proceedings of the National Academy of Sciences of the United States of America *100*, 2420-2425.
Shin, K. H., Park, Y. J., and Park, J. G. (2001). PTEN gene mutations in colorectal cancers displaying microsatellite instability. Cancer letters *174*, 189-194.
Souza, R. F., Appel, R., Yin, J., Wang, S., Smolinski, K. N., Abraham, J. M., Zou, T. T., Shi, Y. Q., Lei, J., Cottrell, J., *et al.* (1996). Microsatellite instability in the insulin-like growth factor II receptor gene in gastrointestinal tumours. Nat Genet *14*, 255-257.
Sumi, T., Fujimoto, Y., Nakatsuji, N., and Suemori, H. (2004). STAT3 is dispensable for maintenance of self-renewal in nonhuman primate embryonic stem cells. Stem cells (Dayton, Ohio) *22*, 861-872.
Swann, P. F., Waters, T. R., Moulton, D. C., Xu, Y. Z., Zheng, Q., Edwards, M., and Mace, R. (1996). Role of postreplicative DNA mismatch repair in the cytotoxic action of thioguanine. Science *273*, 1109-1111.
Tannergard, P., Lipford, J. R., Kolodner, R., Frodin, J. E., Nordenskjold, M., and Lindblom, A. (1995). Mutation screening in the hMLH1 gene in Swedish hereditary nonpolyposis colon cancer families. Cancer Res *55*, 6092-6096.
Taylor, A. M., Metcalfe, J. A., Thick, J., and Mak, Y. F. (1996). Leukemia and lymphoma in ataxia telangiectasia. Blood *87*, 423-438.
Tomer, G., Buermeyer, A. B., Nguyen, M. M., and Liskay, R. M. (2002). Contribution of human mlh1 and pms2 ATPase activities to DNA mismatch repair. The Journal of biological chemistry *277*, 21801-21809.
Umar, A., Buermeyer, A. B., Simon, J. A., Thomas, D. C., Clark, A. B., Liskay, R. M., and Kunkel, T. A. (1996). Requirement for PCNA in DNA mismatch repair at a step preceding DNA resynthesis. Cell *87*, 65-73.
Vasen, H. F., Watson, P., Mecklin, J. P., and Lynch, H. T. (1999). New clinical criteria for hereditary nonpolyposis colorectal cancer (HNPCC, Lynch syndrome) proposed by the International Collaborative group on HNPCC. Gastroenterology *116*, 1453-1456.
Vasen, H. F., Wijnen, J. T., Menko, F. H., Kleibeuker, J. H., Taal, B. G., Griffioen, G., Nagengast, F. M., Meijers-Heijboer, E. H., Bertario, L., Varesco, L., *et al.* (1996). Cancer risk in families with hereditary nonpolyposis colorectal cancer diagnosed by mutation analysis. Gastroenterology *110*, 1020-1027.
Viswanathan, M., and Lovett, S. T. (1998). Single-strand DNA-specific exonucleases in Escherichia coli. Roles in repair and mutation avoidance. Genetics *149*, 7-16.
Wada, C., Shionoya, S., Fujino, Y., Tokuhiro, H., Akahoshi, T., Uchida, T., and Ohtani, H. (1994). Genomic instability of microsatellite repeats and its association with the evolution of chronic myelogenous leukemia. Blood *83*, 3449-3456.
Wagner, T. U., Kraeussling, M., Fedorov, L. M., Reiss, C., Kneitz, B., and Schartl, M. (2008). STAT3 and SMAD1 signalling in Medaka embryonic stem-like cells and blastula embryos. Stem cells and development.
Wang, T. F., Kleckner, N., and Hunter, N. (1999). Functional specificity of MutL homologs in yeast: evidence for three Mlh1-based heterocomplexes with distinct roles during meiosis in recombination and mismatch correction. Proceedings of the National Academy of Sciences of the United States of America *96*, 13914-13919.
Warthin, A. (1913). Heredity with reference to carcinoma. *Arc Intern Med 12*, 546-555.
Whiteside, D., McLeod, R., Graham, G., Steckley, J. L., Booth, K., Somerville, M. J., and Andrew, S. E. (2002). A homozygous germ-line mutation in the human MSH2 gene predisposes to hematological malignancy and multiple cafe-au-lait spots. Cancer Res *62*, 359-362.

Wu, X., Platt, J. L., and Cascalho, M. (2003). Dimerization of MLH1 and PMS2 limits nuclear localization of MutLalpha. Mol Cell Biol *23*, 3320-3328.
Yamaguchi, M., Dao, V., and Modrich, P. (1998). MutS and MutL activate DNA helicase II in a mismatch-dependent manner. The Journal of biological chemistry *273*, 9197-9201.
Yang, G., Scherer, S. J., Shell, S. S., Yang, K., Kim, M., Lipkin, M., Kucherlapati, R., Kolodner, R. D., and Edelmann, W. (2004). Dominant effects of an Msh6 missense mutation on DNA repair and cancer susceptibility. Cancer Cell *6*, 139-150.
Yin, J., Kong, D., Wang, S., Zou, T. T., Souza, R. F., Smolinski, K. N., Lynch, P. M., Hamilton, S. R., Sugimura, H., Powell, S. M., *et al.* (1997). Mutation of hMSH3 and hMSH6 mismatch repair genes in genetically unstable human colorectal and gastric carcinomas. Hum Mutat *10*, 474-478.
Ying, Q. L., Nichols, J., Chambers, I., and Smith, A. (2003). BMP induction of Id proteins suppresses differentiation and sustains embryonic stem cell self-renewal in collaboration with STAT3. Cell *115*, 281-292.
Yoshioka, K., Yoshioka, Y., and Hsieh, P. (2006). ATR kinase activation mediated by MutSalpha and MutLalpha in response to cytotoxic O6-methylguanine adducts. Mol Cell *22*, 501-510.
Zickler, D., and Kleckner, N. (1998). The leptotene-zygotene transition of meiosis. Annu Rev Genet *32*, 619-697.

# VII Danksagungen

Während der letzten Jahre haben mich viele Menschen durch mein Leben begleitet, ohne die das gelingen dieser Arbeit nicht möglich gewesen wäre. Sie eröffneten mir Möglichkeiten, stärkten mir den Rücken, halfen mir wenn es nötig war und glaubten an mich.

Deshalb möchte ich mich bei all Jenen Bedanken, die mich während meiner Doktorarbeit unterstützt haben.

Mein besonderer Dank gilt Pof. Dr. Dr. M. Schartl, der es mir ermöglicht hat meine Promotion an seinem Lehrstuhl anfertigen zu können der mir ideale Rahmenbedingungen und eine sehr gute Ausstattung bot. Insbesondere Danke ich Ihm für die Unterstützung die er mir bezüglich meines Aufenthaltes in New York als Gastwissenschaftler zukommen lies, für die Übernahme der Erstkorrektur und das Interesse an meinen Projekten.

Mein herzlichster Dank auch an Prof. Dr. Benavente für die unkomplizierte Übernahme des Zweitgutachtens.

Bei meinem Betreuer Dr. Burkhard Kneitz möchte ich mich aufrichtig für die Bereitstellung des interessanten Themengebietes, seine Unterstützung und Betreuung, den wissenschaftlichen Freiraum, das gute, freundschaftliche Arbeitsklima, die Möglichkeit an verschiedenen Kongressen teilnehmen zu dürfen und vieles mehr bedanken.

Ich möchte mich herzlich bei meinen Kollaborationspartnern aus New York bedanken, die ich zum Teil auch persönlich kennen lerne durfte. Hierbei möchte ich besonders Prof. Dr. W. Edelmann, Dr. P. Cohen und Dr. E. Avdievich, die maßgeblich an der erfolgreichen Publikation der G67R mutanten Mauslinie beteiligt waren, erwähnen.

Prof. Dr. A. Rosenwald möchte ich für die histologische Diagnostik der Tumore und die Betreuung während meiner Zugehörigkeit im Graduiertenkolleg 639 „Genomische Instabillität“ danken.

Ich danke dem Graduiertenkolleg 639 „Genomische Instabillität“ und dem IZKF Würzburg für die finanzielle Unterstützung. Hier gilt mein besonderer Dank Prof. Dr. Manfred Gessler, der mich ebenfalls bezüglich meines Auslandsaufenthaltes unterstützte.

Den Mitgliedern der Arbeitsgruppe Kneitz Martina Döhler, Thorsten Haneke, Lev Fedorov, Kathrin Borschert, Susanne Emmerling, Peter Ardelt, Antje Sauer, Vera Schwarz und Barbara Dexler danke ich für ihre Unterstützung, die freundschaftliche Arbeitsatmosphäre, den guten Kaffe, das offene Ohr, ihre Geduld und Hilfsbereitschaft. Danke!

Meinen Freunden außerhalb des Labors möchte ich ebenfalls auf diesem Weg meinen Dank aussprechen. Beginnen möchte ich mit jenen, deren Freundschaf all die Kilometer und Jahre,

die ich fern der Heimat verbringe unbeschadet überdauert. Mädels ihr seid wunderbar und die besten Freunde, die man sich wünschen kann! Ich weiß, das ich mich in allen Lebenslagen auf Euch verlassen kann, immer zuhause willkommen bin und mit Euch noch sehr viel Spaß haben werde. Ich hab Euch unheimlich lieb!

Ich möchte mich auch bei all meinen „neuen“ Freunden, die ich in Würzburg finden durfte bedanken, die mir Ihre Zeit, Ihr Ohr und Ihre Freundschaft schenken. Ich glaube, dass auch diese Freundschaften dazu gemacht sind Raum und Zeit zu überstehen. Danke Anna und Martina!

Mein größtes Dankeschön geht an meine Familie. Ich weiß nicht wo ich anfangen soll mich bei Euch zu bedanken…Da es nicht genügend Worte gibt Euch für all das zu Danken, was Ihr für mich getan habt und in Zukunft tun werdet, lasse ich dies einfach.

Ich Liebe Euch – und Danke!

# VIII Eidesstattliche Erklärung

Hiermit erkläre ich an Eides statt, dass ich die vorliegende Dissertation selbstständig verfasst habe und dabei keine anderen, als die von mir angegebenen Hilfsmittel und Quellen benutzt habe. Zitate sind als solche gekennzeichnet.

Ich erkläre weiterhin, dass die vorliegende Dissertation weder in gleicher noch in ähnlicher Form bereits in einem anderen Prüfungsverfahren vorgelegen hat.

Zudem erkläre ich, dass ich außer den mit dem Zulassungsantrag urkundlich vorgelegten Graden, keine weiteren akademischen Grade erworben, oder zu erwerben versucht habe.

Würzburg, August 2010 Cora Reiß

Anhang 1: *Mlh1* $^{G67R/G67R}$ Tumortiere

| Nr | Alter (Wochen) | Tumorart | FACS-Analyse | Gewebe | L24372 | Aa006036 | D17mit91 | D7mit132 | U12235 | Instabile MS | MSI |
|---|---|---|---|---|---|---|---|---|---|---|---|
| 73 | 26 | Dessiminiertes Lymphom | CD8+ T-Zell Lymphom | Thymus | 0 | -1 | 0 | -1 | -1 | 3 | High |
| | | 1*GI | | Milz | 0 | -1 | 0 | -1 | 0 | 2 | High |
| 74 | 30 | Periphäres Lymphom | unreifes B-Zell-Lymphom | LK | 0 | -2 | -1 | -1 | -1 | 4 | High |
| 93 | 28 | Thymisches Lymphom | DP T-Zell-Lymphom | Thymus | -1 | -1 | 0 | 0 | -1 | 3 | High |
| 94 | 47 | 1*GI | | n.A. | - | - | - | - | - | | |
| 101 | 25 | Thymisches Lymphom | DN T-Zell-Lymphom | Thymus | -1 | -1 | -1 | 0 | -1 | 4 | High |
| 102 | 24 | Lymphom | n.A. | n.A. | - | - | - | - | - | | |
| 103 | 31 | Dessiminiertes Lymphom | CD8+ T-Zell Lymphom | LK | -1 | -2 | 0 | 0 | -2 | 3 | High |
| 109 | 30 | Lymphom | n.A. | n.A. | - | - | - | - | - | | |
| 120 | 33 | Periphäres Lymphom | Hämatopoetisches Lymphom | Milz | 0 | 0 | 0 | 0 | 0 | 0 | No |
| | | 2* GI | | LK | -1 | -1 | -1 | 0 | 0 | 3 | High |
| | | | | GI | -1 | -2 | 0 | -1 | -2 | 4 | High |
| 132 | 37 | Thymisches Lymphom | n.A. | n.A. | - | - | - | - | - | | |
| 133 | 43 | 5*GI | | GI | -1 | 0 | -1 | 0 | 0 | 2 | High |
| | | Dessiminiertes Lymphom | Hämatopoetisches Lymphom | LK | 0 | 0 | 0 | 0 | 0 | 0 | No |
| 138 | 41 | Hauttumor | | Haut | 0 | 0 | 0 | 1 | -1 | 2 | High |
| 145 | 22 | Thymisches Lymphom | DP T-Zell-Lymphom | Thymus | -1 | 1 | -2 | +2 | -1 | 5 | High |
| 148 | 34 | Dessiminiertes Lymphom | DN T-Zell-Lymphom | Thymus | 0 | -1 | +1 | 0 | 0 | 3 | High |
| 168 | 39 | 1*GI | | GI | 0 | -1 | -1 | 1 | 1 | 4 | High |
| 169 | 33 | Verstorben o.B. | | | - | - | - | - | - | | |
| 173 | 34 | Hauttumor | | Haut | 0 | 0 | 0 | 0 | 0 | 0 | No |
| 177 | 43 | Periphäres Lymphom | Hämatopoetisches Lymphom | LK | -1 | 0 | 0 | 0 | -1 | 2 | High |
| | | | | Milz | 0 | -1 | 0 | -1 | 0 | 2 | High |
| 180 | 23 | Thymisches Lymphom | DP T-Zell-Lymphom | Thymus | -1 | -2 | 1 | 0 | -1 | 4 | High |
| 190 | 46 | 3*GI | | GI | -2 | -2 | 0 | 0 | -2 | 3 | High |
| | | | | Milz | 0 | 0 | 0 | 0 | -2 | 1 | Low |
| 195 | 46 | Periphäres Lymphom | Hämatopoetisches Lymphom | Milz | 0 | 0 | 0 | 0 | 0 | 0 | No |
| 196 | 51 | Uteruskarzinom, Hauttumor | | Haut | -1 | -1 | 0 | 0 | 0 | 2 | High |
| 199 | 31 | 1*GI | | GI | 0 | -1 | -1 | 0 | 0 | 2 | High |
| | | Hauttumor | | Haut | 0 | -1 | -2 | 0 | 0 | 2 | High |

| Nr | Alter (Wochen) | Tumorart | FACS-Analyse | Gewebe | L24372 | Aa006036 | D17mit91 | D7mit132 | U12235 | Instabile MS | MSI |
|---|---|---|---|---|---|---|---|---|---|---|---|
| 200 | 5 | Lymphom | n.A. | n.A. | - | - | - | - | - | | |
| 206 | 37 | Periphäres Lymphom | unreifes B-Zell-Lymphom | LK | +1 | -1 | 0 | -2 | -2 | 4 | High |
| | | | | Thymus | +1 | 0 | -1 | -1 | -2 | 4 | High |
| 218 | 40 | 1*GI | | GI | -1 | 0 | 0 | -1 | 0 | 2 | High |
| 225 | 16 | Thymisches Lymphom | CD4+ T-Zell-Lymphom | Thymus | -1 | -1 | 0 | 0 | -1 | 3 | High |
| 226 | 37 | 2* GI | | GI | -1 | 0 | 0 | -1 | -1 | 3 | High |
| | | Periphäres Lymphom | Hämatopoetisches Lymphom | Milz | 0 | 0 | 0 | 0 | 0 | 0 | No |
| 227 | 48 | 2*GI | | GI | -1 | 0 | 0 | -1 | 0 | 2 | High |
| 232 | 17 | Dessiminiertes Lymphom | DP T-Zell-Lymphom | Thymus | 0 | 0 | -1 | 0 | -1 | 2 | High |
| | | | | LK | 0 | 0 | -1 | 0 | -1 | 2 | High |
| 236 | 21 | Dessiminiertes Lymphom | DP T-Zell-Lymphom | Thymus | -1 | 0 | -1 | 1 | -1 | 4 | High |
| | | | | Milz | -1 | -1 | -1 | 1 | 0 | 4 | High |
| 240 | 31 | 4*GI | | GI | 0 | -1 | 0 | -1 | -1 | 3 | High |
| 253 | 27 | Periphäres Lymphom | n.A. | LK | -1 | -1 | -1 | -1 | 0 | 4 | High |
| 258 | 34 | Verstorben o.B. | | | - | - | - | - | - | | |
| 259 | 38 | Periphäres Lymphom | n.A. | LK | 0 | 0 | 0 | 0 | 0 | 0 | No |
| 263 | 31 | 1*GI | | GI | -2 | -2 | 0 | 0 | 0 | 2 | High |
| 263 | 17 | Thymisches Lymphom | DN T-Zell-Lymphom | Thymus | -1 | 0 | 0 | 0 | -1 | 2 | High |
| 266 | 20 | Verstorben o.B. | | | - | - | - | - | - | | |
| 269 | 37 | Periphäres Lymphom | unreifes B-Zell-Lymphom | LK | 0 | 0 | 0 | 0 | 0 | 0 | No |
| 271 | 46 | 2*GI | | n.A. | - | - | - | - | - | | |
| 272 | 32 | Analkarzinom, | | Karzinom | 0 | -1 | 0 | -1 | -1 | 3 | High |
| | | Periphäres Lymphom | n.A. | LK | 0 | -1 | 0 | 0 | 0 | 1 | Low |
| 276 | 26 | Lymphom | n.A. | n.A. | - | - | - | - | - | | |
| 278 | 18 | Thymisches Lymphom | CD8+ T-Zell Lymphom | Thymus | -1 | 0 | 0 | -1 | -1 | 3 | High |
| 297 | 13 | Lymphom | n.A. | n.A. | - | - | - | - | - | | |
| 318 | 19 | Thymisches Lymphom | CD8+ T-Zell Lymphom | Thymus | 0 | -2 | 0 | -1 | -2 | 3 | High |
| 327 | 29 | Periphäres Lymphom | Hämatopoetisches Lymphom | Milz | 0 | 0 | 0 | 0 | 0 | 0 | No |
| | | Thymisches Lymphom | CD4+ T-Zell-Lymphom | Thymus | -1 | 0 | -1 | 1 | -1 | 4 | High |
| 328 | 34 | 2*GI | | n.A. | - | - | - | - | - | | |
| 331 | 19 | Thymisches Lymphom | CD4+ T-Zell-Lymphom | Thymus | -1 | 0 | -1 | -1 | -1 | 4 | High |
| 340 | 41 | 1*GI | | n.A. | - | - | - | - | - | | |
| 348 | 25 | Thymisches Lymphom | DP T-Zell-Lymphom | Thymus | 0 | -1 | 0 | 0 | 0 | 1 | Low |

| Nr | Alter (Wochen) | Tumorart | FACS-Analyse | Gewebe | L24372 | Aa006036 | D17mit91 | D7mit132 | U12235 | Instabile MS | MSI |
|---|---|---|---|---|---|---|---|---|---|---|---|
| 350 | 68 | Lymphom | n.A. | n.A. | - | - | - | - | - | | |
| 361 | 20 | Thymisches Lymphom | Hämatopoetisches Lymphom | Thymus | - | - | - | - | - | | |
| 363 | 7 | Lymphom | n.A. | n.A. | - | - | - | - | - | | |
| 374 | 61 | 2*GI | | GI | -1 | -1 | -1 | 0 | 0 | 3 | High |
| 375 | 33 | 2*GI | | GI | - | - | - | - | - | | |
| 396 | 57 | Verstorben o.B. | | | - | - | - | - | - | | |
| 402 | 19 | Dessiminiertes Lymphom | n.A. | LK | -1 | 0 | -1 | -1 | -1 | 4 | High |
| | | | | Thymus | 0 | 0 | -1 | -1 | 0 | 2 | High |
| 412 | 22 | Lymphom | n.A. | n.A. | - | - | - | - | - | | |
| 438 | 16 | Lymphom | n.A. | n.A. | - | - | - | - | - | | |
| 444 | 19 | Lymphom | n.A. | n.A. | - | - | - | - | - | | |
| 445 | 36 | Verstorben o.B. | | | - | - | - | - | - | | |
| 476 | 4 | Lymphom | n.A. | n.A. | - | - | - | - | - | | |
| 486 | 21 | Thymisches Lymphom | n.A. | Thymus | -1 | -1 | -1 | 0 | -1 | 4 | High |
| 487 | 23 | Thymisches Lymphom | n.A. | Thymus | -1 | -1 | 1 | 0 | 0 | 3 | High |
| 488 | 14 | Dessiminiertes Lymphom | n.A. | Thymus | 0 | 0 | 1 | 0 | 0 | 1 | Low |
| | | | | LK | 0 | 0 | 1 | 0 | 0 | 1 | Low |

+1: Insertion eines Nukleotids

-1: Deletion eines Nukleotids

Anhang 2: *Mlh1* $^{G67R/-}$ Tumortiere

| Nr | Alter (Wochen) | Tumorart | FACS-Analyse | Gewebe | L24372 | Aa006036 | D17mit91 | D7mit132 | U12235 | Instabile MS | MSI |
|---|---|---|---|---|---|---|---|---|---|---|---|
| 11 | 31 | Hauttumor | | Thymus | -1 | -1 | 0 | -1 | -1 | 4 | High |
| | | Dessiminiertes Lymphom | DN T-Zell-Lymphom | Haut | 0 | 0 | -1 | -1 | -1 | 3 | High |
| 14 | 63 | Periphäres Lymphom | unreifes B-Zell-Lymphom | LK | -1 | -2 | 0 | -1 | -2 | 3 | High |
| 30 | 37 | 3* GI | | Milz | 0 | 0 | 0 | 0 | 0 | 0 | No |
| | | Periphäres Lymphom | n.A. | GI | -1 | -2 | -1 | 0 | 0 | 3 | High |
| 31 | 29 | Periphäres Lymphom | unreifes B-Zell-Lymphom | LK | 0 | -1 | 0 | -1 | 0 | 2 | Low |
| 33 | 37 | Hauttumor | | Haut | -1 | -1 | 0 | -1 | -2 | 4 | High |
| | | 1*GI | | GI | -1 | -2 | -1 | 0 | -2 | 4 | High |
| 35 | 31 | Dessiminiertes Lymphom | n.A. | LK | 1 | -1 | -1 | 0 | -1 | 4 | High |
| | | | | Milz | 0 | -1 | 0 | 2 | -1 | 3 | High |
| 60 | 26 | Thymisches Lymphom | DPT-Zell-Lymphom | Thymus | 0 | -1 | 0 | -2 | 0 | 2 | Low |
| 66 | 21 | Dessiminiertes Lymphom | DN T-Zell-Lymphom | LK | -2 | -2 | -1 | +1 | -1 | 5 | High |
| | | 1*GI | | GI | -1 | -1 | 0 | 0 | -1 | 3 | High |
| 67 | 29 | 1*GI | | n.A. | - | - | - | - | - | - | - |
| 73 | 47 | Periphäres Lymphom | unreifes B-Zell-Lymphom | LK | -1 | -2 | 0 | -2 | 0 | 3 | High |
| 91 | 30 | Periphäres Lymphom | unreifes B-Zell-Lymphom | Milz | 0 | -1 | -1 | 0 | -2 | 3 | High |
| | | | | LK | 0 | -2 | -1 | 0 | -2 | 3 | High |
| 92 | 40 | 2*GI | | GI | -1 | -1 | 0 | -1 | -1 | 4 | High |
| 93 | 39 | 1*GI | | GI | -1 | -1 | 0 | -1 | -1 | 4 | High |
| 97 | 48 | Dessiminiertes Lymphom | CD4+ T-Zell-Lymphom | n.A. | - | - | - | - | - | - | - |
| | | 2*GI | | n.A. | - | - | - | - | - | - | - |
| 99 | 19 | Dessiminiertes Lymphom | DN T-Zell-Lymphom | LK | +1 | -1 | 0 | 0 | -1 | 3 | High |
| 100 | 25 | Periphäres Lymphom | n.A. | LK | 0 | 0 | 0 | -1 | 0 | 1 | Low |
| 177 | 35 | Periphäres Lymphom | n.A. | n.A. | - | - | - | - | - | - | - |
| 180 | 10 | Dessiminiertes Lymphom | DP T-Zell-Lymphom | Thymus | 0 | -1 | 1 | -1 | -1 | 3 | High |

| Nr | Alter (Wochen) | Tumorart | FACS-Analyse | Gewebe | L24372 | Aa006036 | D17mit91 | D7mit132 | U12235 | Instabile MS | MSI |
|---|---|---|---|---|---|---|---|---|---|---|---|
| 181 | 23 | Dessiminiertes Lymphom | CD4+ T-Zell-Lymphom | LK | -1 | 0 | 0 | 0 | -1 | 2 | Low |
| 192 | 19 | Thymisches Lymphom | DP T-Zell-Lymphom | Thymus | 0 | -1 | -1 | 0 | -1 | 3 | High |
| 201 | 11 | Niere | | n.A. | - | - | - | - | - | - | - |
| 204 | 44 | Thymisches Lymphom | CD4+ T-Zell-Lymphom | n.A. | - | - | - | - | - | - | - |
| | | Periphäres Lymphom | unreifes B-Zell-Lymphom | n.A. | - | - | - | - | - | - | - |
| 209 | 15 | Thymisches Lymphom | CD8+ T-Zell-Lymphom | n.A. | - | - | - | - | - | - | - |
| 222 | 17 | Thymisches Lymphom | CD4+ T-Zell-Lymphom | n.A. | - | - | - | - | - | - | - |
| 224 | 24 | 1*GI | | n.A. | - | - | - | - | - | - | - |
| 257 | 35 | 3*GI | | n.A. | - | - | - | - | - | - | - |
| | | Dessiminiertes Lymphom | DN T-Zell-Lymphom | n.A. | - | - | - | - | - | - | - |
| 259 | 31 | Periphäres Lymphom | unreifes B-Zell-Lymphom | n.A. | - | - | - | - | - | - | - |
| 286 | 33 | Thymisches Lymphom | DP T-Zell-Lymphom | n.A. | - | - | - | - | - | - | - |
| 292 | 36 | Niere | | n.A. | - | - | - | - | - | - | - |
| 293 | 63 | Periphäres Lymphom | n.A. | n.A. | - | - | - | - | - | - | - |

+1: Insertion eines Nukleotids

-1: Deletion eines Nukleotids

Anhang 3: *Mlh1* $^{\Delta ex4/\Delta Ex4}$

| Nr | Alter (Wochen) | Tumorart | FACS-Analyse | Gewebe | L24372 | Aa006036 | D17mit91 | D7mit132 | U12235 | Instabile MS | MSI |
|---|---|---|---|---|---|---|---|---|---|---|---|
| 24 | 23 | Thymisches Lymphom | n.A. | - | - | - | - | - | - | - | - |
| 42 | 43 | 1* GI | - | - | - | - | - | - | - | - | - |
| 48 | 56 | GI | - | - | - | - | - | - | - | - | - |
| 59 | 29 | Verstorben o.B. | - | - | - | - | - | - | - | - | - |
| 76 | 19 | Dessiminiertes Lymphom | - | - | - | - | - | - | - | - | - |
| 88 | 27 | Periphäres Lymphom | - | LK | 0 | -1 | 0 | 0 | 0 | 1 | Low |
| 89 | 21 | Periphäres Lymphom | - | - | - | - | - | - | - | - | - |
| 91 | 41 | Hauttumor | - | - | - | - | - | - | - | - | - |
| 93 | 18 | Lymphom | - | - | - | - | - | - | - | - | - |
| 121 | 54 | 1*GI | - | GI | -1 | -1 | -1 | -1 | -1 | 5 | High |
|  |  | Periphäres Lymphom | - | LK | -1 | -1 | -1 | 0 | -1 | 4 | High |
| 130 | 17 | Lymphom | - | - | - | - | - | - | - | - | - |
| 145 | 30 | 1* GI und Hauttumor | - | - | - | - | - | - | - | - | - |
| 149 | 19 | Periphäres Lymphom | - | Leber | 0 | 0 | 0 | 0 | -1 | 1 | Low |
|  |  |  | - | Milz | 0 | 0 | 0 | 0 | -1 | 1 | Low |
| 150 | 58 | Periphäres Lymphom | - | LK | 0 | 0 | 0 | 0 | 0 | 0 | No |
| 151 | 13 | Thymisches Lymphom | - | Thymus | - | - | - | - | - | - | - |
| 152 | 48 | 1*GI | - | GI | 0 | -1 | 0 | 0 | -1 | 2 | High |
| 159 | 49 | 2*GI | - | GI | 0 | -1 | 0 | 0 | -1 | 2 | High |
| 181 | 1 | Periphäres Lymphom | - | LK | -1 | -1 | 0 | -1 | 0 | 3 | High |
| 182 | 63 | 2* GI | - | GI | - | - | - | - | - | - | - |
| 187 | 15 | Dessiminiertes Lymphom | - | Thymus | 0 | -1 | 0 | +1 | -1 | 3 | High |
|  |  |  | - | Milz | +1 | -1 | 0 | +1 | -1 | 4 | High |
| 197 | 55 | 4*GI | - | GI | -1 | 0 | -1 | -1 | -1 | 4 | High |
| 201 | 31 | Verstorben o.B. | - | - | - | - | - | - | - | - | - |
| 208 | 18 | Dessiminiertes Lymphom | - | - | - | - | - | - | - | - | - |
| 210 | 26 | Periphäres Lymphom | - | - | - | - | - | - | - | - | - |
| 221 | 34 | Verstorben o.B. | - | - | - | - | - | - | - | - | - |
| 224 | 38 | 2*GI | - | GI | 0 | 0 | 0 | 0 | -1 | 1 | Low |
| 227 | 25 | Verstorben o.B. | - | - | - | - | - | - | - | - | - |

| Nr | Alter (Wochen) | Tumorart | FACS-Analyse | Gewebe | L24372 | Aa006036 | D17mit91 | D7mit132 | U12235 | Instabile MS | MSI |
|---|---|---|---|---|---|---|---|---|---|---|---|
| 243 | 77 | 2*GI | - | LK | - | - | - | - | - | - | - |
| | | Periphäres Lymphom | - | GI | - | - | - | - | - | - | - |
| 294 | 10 | Thymisches Lymphom | - | - | - | - | - | - | - | - | - |
| 321 | 19 | Thymisches Lymphom | - | Thymus | -1 | 0 | -1 | 0 | -1 | 3 | High |
| 354 | 17 | Thymisches Lymphom | - | Thymus | -1 | 0 | -1 | -1 | 0 | 3 | High |
| 738 | 34 | 3* GI und Thymisches Lymphom | - | - | - | - | - | - | - | - | - |
| 740 | 38 | 2*Hauttumor + GI | - | GI | - | - | - | - | - | - | - |
| | | | - | Haut | -1 | 0 | 0 | 0 | -1 | 2 | Hgih |
| 742 | 9 | Dessiminiertes Lymphom | - | - | - | - | - | - | - | - | - |
| 744 | 25 | Dessiminiertes Lymphom | - | Thymus | -1 | 0 | 0 | -1 | -1 | 2 | High |

+1: Insertion eines Nukleotids

-1: Deletion eines Nukleotids

Anhang 4: *Mlh1* $^{T\,\Delta Ex4/T\Delta Ex4}$ Tumortiere

| Nr | Sektion nach (Wochen) | Tumorart | FACS-Analyse | Gewebe | L24372 | Aa006036 | D17mit91 | D7mit132 | U12235 | Instabile MS | MSI |
|---|---|---|---|---|---|---|---|---|---|---|---|
| 1 | 75 | Verstorben o.B. | - | - | - | - | - | - | - | - | - |
| 2 | 82 | Tumor frei | - | - | - | - | - | - | - | - | - |
| 3 | 82 | Tumor frei | - | - | - | - | - | - | - | - | - |
| 4 | 82 | Tumor frei | - | - | - | - | - | - | - | - | - |
| 7 | 81 | Tumor frei | - | - | - | - | - | - | - | - | - |
| 8 | 82 | Tumor frei | - | - | - | - | - | - | - | - | - |
| 13 | 65 | Tumor frei | - | - | - | - | - | - | - | - | - |
| 16 | 65 | Tumor frei | - | - | - | - | - | - | - | - | - |
| 17 | 65 | Tumor frei | - | - | - | - | - | - | - | - | - |
| 19 | 63 | Tumor frei | - | - | - | - | - | - | - | - | - |
| 21 | 68 | Tumor frei | - | - | - | - | - | - | - | - | - |
| 22 | 63 | Tumor frei | - | - | - | - | - | - | - | - | - |
| 23 | 63 | Tumor frei | - | - | - | - | - | - | - | - | - |
| 26 | 56 | Tumor frei | - | - | - | - | - | - | - | - | - |
| 27 | 63 | Tumor frei | - | - | - | - | - | - | - | - | - |
| 28 | 68 | Tumor frei | - | - | - | - | - | - | - | - | - |
| 29 | 58 | Tumor frei | - | - | - | - | - | - | - | - | - |
| 30 | 58 | Tumor frei | - | - | - | - | - | - | - | - | - |
| 31 | 24 | Thymisches Lymphom | DP T-Zell-Lymphom | Thymus | 0 | 0 | 0 | 0 | -1 | 1 | Low |
| 33 | 51 | Tumor frei | - | - | - | - | - | - | - | - | - |
| 34 | 61 | Tumor frei | - | - | - | - | - | - | - | - | - |
| 57 | 47 | Tumor frei | - | - | - | - | - | - | - | - | - |
| 60 | 47 | Tumor frei | - | - | - | - | - | - | - | - | - |
| 63 | 44 | Tumor frei | - | - | - | - | - | - | - | - | - |
| 64 | 44 | Tumor frei | - | - | - | - | - | - | - | - | - |
| 65 | 44 | Tumor frei | - | - | - | - | - | - | - | - | - |
| 108 | 44 | Tumor frei | - | - | - | - | - | - | - | - | - |
| 109 | 15 | Dessiminiertes Lymphom | DP T-Zell-Lymphom | Thymus | -1 | 0 | 0 | -1 | -1 | 3 | High |
| | | | | LK | -1 | 0 | 0 | -1 | -1 | 3 | High |

| Nr | Sektion nach (Wochen) | Tumorart | FACS-Analyse | Gewebe | L24372 | Aa006036 | D17mit91 | D7mit132 | U12235 | Instabile MS | MSI |
|---|---|---|---|---|---|---|---|---|---|---|---|
| 110 | 44 | Tumor frei | - | - | - | - | - | - | - | - | - |
| 123 | 48 | Tumor frei | - | - | - | - | - | - | - | - | - |
| 124 | 48 | Tumor frei | - | - | - | - | - | - | - | - | - |
| 125 | 48 | Tumor frei | - | - | - | - | - | - | - | - | - |
| 126 | 48 | Tumor frei | - | - | - | - | - | - | - | - | - |
| 127 | 48 | Tumor frei | - | - | - | - | - | - | - | - | - |
| 129 | 48 | Tumor frei | - | - | - | - | - | - | - | - | - |
| 130 | 48 | Tumor frei | - | - | - | - | - | - | - | - | - |
| 132 | 48 | Tumor frei | - | - | - | - | - | - | - | - | - |
| 134 | 46 | Tumor frei | - | - | - | - | - | - | - | - | - |
| 136 | 46 | Tumor frei | - | - | - | - | - | - | - | - | - |
| 136 | 60 | Tumor frei | - | - | - | - | - | - | - | - | - |
| 137 | 66 | Tumor frei | - | - | - | - | - | - | - | - | - |
| 138 | 56 | Tumor frei | - | - | - | - | - | - | - | - | - |
| 139 | 47 | Verstorben o.B. | - | - | - | - | - | - | - | - | - |
| 140 | 35 | Sektion ohne Befund | - | - | - | - | - | - | - | - | - |
| 141 | 60 | Tumor frei | - | - | - | - | - | - | - | - | - |
| 142 | 60 | Tumor frei | - | - | - | - | - | - | - | - | - |
| 143 | 53 | Tumor frei | - | - | - | - | - | - | - | - | - |
| 144 | 26 | Sektion ohne Befund | - | - | - | - | - | - | - | - | - |
| 145 | 43 | Tumor frei | - | - | - | - | - | - | - | - | - |
| 147 | 43 | Tumor frei | - | - | - | - | - | - | - | - | - |
| 148 | 43 | Tumor frei | - | - | - | - | - | - | - | - | - |
| 149 | 43 | Tumor frei | - | - | - | - | - | - | - | - | - |
| 150 | 43 | Tumor frei | - | - | - | - | - | - | - | - | - |
| 151 | 43 | Tumor frei | - | - | - | - | - | - | - | - | - |
| 152 | 43 | Tumor frei | - | - | - | - | - | - | - | - | - |
| 153 | 43 | Tumor frei | - | - | - | - | - | - | - | - | - |
| 154 | 43 | Tumor frei | - | - | - | - | - | - | - | - | - |
| 177 | 27 | Dessiminiertes Lymphom | DP T-Zell-Lymphom | Thymus | 0 | 0 | 0 | 0 | 0 | 0 | No |
| | | | | LK | 0 | 0 | 0 | 0 | 0 | 0 | No |

| Nr | Sektion nach (Wochen) | Tumorart | FACS-Analyse | Gewebe | L24372 | Aa006036 | D17mit91 | D7mit132 | U12235 | Instabile MS | MSI |
|---|---|---|---|---|---|---|---|---|---|---|---|
| 313 | 100 | Tumor frei | - | - | - | - | - | - | - | - | - |
| 322 | 80 | Tumor frei | - | - | - | - | - | - | - | - | - |
| 323 | 87 | Tumor frei | - | - | - | - | - | - | - | - | - |
| 327 | 88 | Tumor frei | - | - | - | - | - | - | - | - | - |
| 330 | 93 | Tumor frei | - | - | - | - | - | - | - | - | - |
| 332 | 20 | Thymisches Lymphom | DN T-Zell-Lymphom | Thymus | -1 | 0 | 0 | 0 | 0 | 1 | Low |

+1: Insertion eines Nukleotids

-1: Deletion eines Nukleotids

Anhang 5: *Mlh1* $^{T\,\Delta Ex4/-}$ Tumortiere

| Nr | Sektion nach (Wochen) | Tumorart | FACS-Analyse | Gewebe | L24372 | Aa006036 | D17mit91 | D7mit132 | U12235 | Instabile MS | MSI |
|---|---|---|---|---|---|---|---|---|---|---|---|
| 401 | 42 | Tumor frei | - | - | - | - | - | - | - | - | - |
| 402 | 65 | Tumor frei | - | - | - | - | - | - | - | - | - |
| 1 | 41 | Tumor frei | - | - | - | - | - | - | - | - | - |
| 3 | 60 | Tumor frei | - | - | - | - | - | - | - | - | - |
| 4 | 60 | Tumor frei | - | - | - | - | - | - | - | - | - |
| 5 | 16 | Periphäres Lymphom | DP T-Zell-Lymphom | Milz | 0 | -1 | 0 | 0 | -1 | 2 | High |
| 6 | 56 | Tumor frei | - | - | - | - | - | - | - | - | - |
| 10 | 60 | Tumor frei | - | - | - | - | - | - | - | - | - |
| 11 | 39 | Verstorben o.B. | - | - | - | - | - | - | - | - | - |
| 23 | 47 | Tumor frei | - | - | - | - | - | - | - | - | - |

Anhang 6: Mlh1$^{T\Delta Ex4/G67R}$ Vesuchstiere

| Nr | Sektion nach (Wochen) | Tumorart | FACS-Analyse | Gewebe | L24372 | Aa006036 | D17mit91 | D7mit132 | U12235 | Instabile MS | MSI |
|---|---|---|---|---|---|---|---|---|---|---|---|
| 1 | 23 | Dessiminiertes Lymphom | DP T-Zell-Lymphom | Thymus | -1 | -1 | 0 | 0 | -1 | 3 | High |
| | | | | LK | -1 | -1 | 0 | 0 | -1 | 3 | High |
| 2 | 58 | Tumor frei | - | - | - | - | - | - | - | - | - |
| 3 | 58 | Tumor frei | - | - | - | - | - | - | - | - | - |
| 4 | 59 | Tumor frei | - | - | - | - | - | - | - | - | - |
| 6 | 59 | Tumor frei | - | - | - | - | - | - | - | - | - |
| 12 | 25 | Hautprobleme, Tumor frei | - | - | - | - | - | - | - | - | - |
| 18 | 22 | Thymisches Lymphom | DP T-Zell-Lymphom | Thymus | 0 | 0 | 0 | 0 | -1 | 1 | Low |
| 20 | 43 | Tumor frei | - | - | - | - | - | - | - | - | - |
| 21 | 20 | Periphäres Lymphom | B-Zell-Lymphom | LK | 0 | 0 | 0 | 0 | 0 | 0 | No |
| 22 | 35 | Tumor frei | - | - | - | - | - | - | - | - | - |
| 23 | 49 | Tumor frei | - | - | - | - | - | - | - | - | - |
| 46 | 49 | Tumor frei | - | - | - | - | - | - | - | - | - |
| 48 | 44 | Tumor frei | - | - | - | - | - | - | - | - | - |
| 49 | 49 | Tumor frei | - | - | - | - | - | - | - | - | - |
| 50 | 49 | Tumor frei | - | - | - | - | - | - | - | - | - |
| 55 | 49 | Tumor frei | - | - | - | - | - | - | - | - | - |
| 60 | 17 | verstorben | - | - | - | - | - | - | - | - | - |
| 65 | 46 | Tumor frei | - | - | - | - | - | - | - | - | - |
| 67 | 46 | Tumor frei | - | - | - | - | - | - | - | - | - |
| 68 | 42 | Tumor frei | - | - | - | - | - | - | - | - | - |
| 71 | 42 | Tumor frei | - | - | - | - | - | - | - | - | - |
| 73 | 43 | Tumor frei | - | - | - | - | - | - | - | - | - |
| 75 | 42 | Tumor frei | - | - | - | - | - | - | - | - | - |
| 76 | 42 | Tumor frei | - | - | - | - | - | - | - | - | - |
| 78 | 42 | Tumor frei | - | - | - | - | - | - | - | - | - |
| 80 | 40 | Tumor frei | - | - | - | - | - | - | - | - | - |
| 84 | 40 | Tumor frei | - | - | - | - | - | - | - | - | - |
| 85 | 40 | Tumor frei | - | - | - | - | - | - | - | - | - |

+1: Insertion eines Nukleotids

-1: Deletion eines Nukleotids

# Distinct effects of the recurrent Mlh1$^{G67R}$ mutation on MMR functions, cancer, and meiosis

Publiziert **2008 in Proc Natl Acad Sci U S A. 105(11):4247-52.**

# Distinct effects of the recurrent Mlh1$^{G67R}$ mutation on MMR functions, cancer, and meiosis

**Elena Avdievich*, Cora Reiss†, Stefan J. Scherer*, Yongwei Zhang*, Sandra M. Maier‡, Bo Jin*, Harry Hou, Jr.*,**
**Andreas Rosenwald†, Hubertus Riedmiller§, Raju Kucherlapati¶, Paula E. Cohen_, Winfried Edelmann*,**,**
**and Burkhard Kneitz§††**
*Department of Cell Biology and Cancer Center, Albert Einstein College of Medicine, Bronx, NY 10461; ‡Department of Oncology, Montefiore Medical
Center, Bronx, NY 10467; †Theodor Boveri Institute for Bioscience and §Department of Urology, Medical School, Julius Maximilians University,
97074 Wu¨ rzburg, Germany; ¶Harvard Medical School–Partners Healthcare Center for Genetics and Genomics, Harvard Medical School,
Boston, MA 02115; and _Department of Biomedical Sciences, Cornell University, Ithaca, NY 14853

Mutations in the human DNA mismatch repair (MMR) gene MLH1 are associated with hereditary nonpolyposis colorectal cancer (Lynch syndrome, HNPCC) and a significant proportion of sporadiccolorectal cancer. The inactivation of MLH1 results in the accumulation of somatic mutations in the genome of tumor cells and resistance to the genotoxic effects of a variety of DNA damaging agents. To study the effect of MLH1 missense mutations on cancer susceptibility, we generated a mouse line carrying the recurrent Mlh1$^{G67R}$ mutation that is located in one of the ATP-binding domains of Mlh1. Although the Mlh1$^{G67R}$ mutation resulted in DNA repair deficiency in homozygous mutant mice, it did not affect the MMR-mediated cellular response to DNA damage, including the apoptotic response of epithelial cells in the intestinal mucosa to cisplatin, which was defective in Mlh1$^{-/-}$ mice but remained normal in Mlh1$^{G67R/G67R}$ mice. Similar to Mlh1$^{-/-}$ mice, Mlh1$^{G67R/G67R}$ mutant mice displayed a strong cancer predisposition phenotype. However, in contrast to Mlh1$^{-/-}$ mice, Mlh1$^{G67R/G67R}$ mutant mice developed significantly fewer intestinal tumors, indicating that Mlh1 missense mutations can affect MMR tumor suppressor functions in a tissue-specific manner. In addition, Mlh1$^{G67R/G67R}$ mice were sterile because of the inability of the mutant Mlh1$^{G67R}$ protein to interact with meiotic chromosomes at pachynema, demonstrating that the ATPase activity of Mlh1 is essential for fertility in mammals.

**M**utations in the human DNA mismatch repair (MMR) genes *MSH2*, *MSH6* (MutS homolog), and *MLH1* (MutL homolog 1) are the cause of the majority of hereditary nonpolyposis colorectal cancer (Lynch syndrome, HNPCC) cases and also a significant number of sporadic cancers (1, 2). The DNA MMR system plays a critical role in the maintenance of genome integrity and functions in the postreplicative repair of base substitution mutations as well as small insertions/deletions (IDLs) caused by erroneous replication (3). In addition, studies in yeast and mice indicate that several of theMMRproteins have essential meiotic functions (4, 5). In eukaryotic cells, MMR is initiated by subsets of MutS homologs (MSH) that form heterodimeric complexes: MSH2–MSH6 (MutSα) and MSH2– MSH3 (MutSß). The MutSα complex recognizes base–base mispairs and single-base IDLs, whereas the MutSß complex detects single-base and larger IDLs to initiate the

repair process. As a result of mismatch recognition, the MutSα and MutSß complexes undergo ATP-hydrolysis-dependent conformational transitions and recruit a heterodimeric complex of the MutL homologs MLH1 and PMS2 (MutLα). This interaction between MutS and the MutL complexes is essential for the activation of subsequent MMR steps, i.e., the excision of the mispairs and IDLs and the resynthesis of the excised DNA strand (6–8). Similar to MutS complexes, the mediation of repair excision and resynthesis by MutLα requires ATP binding and hydrolysis (9–11).

In addition to repairing mismatched bases, MMR also contributes to genome stability by stimulating DNA damageinduced apoptosis as part of the cytotoxic response to DNAdamaging agents. Although MMR-proficient cells respond to exposure to DNA-damaging agents such as cisplatin by signalling cell cycle arrest at the G2 checkpoint followed by apoptosis, MMR-deficient human tumor cells are defective in this response (8, 12, 13). As a result, they display increased resistance to the genotoxic effects of DNA damage-inducing agents. It has been proposed that both the DNA repair and DNA damage-response functions of MMR are important for the suppression of tumorigenesis. On the one hand, defects in MMR are associated with an increased mutator phenotype, resulting in the accumulation of mutations in tumor-suppressor genes and oncogenes and leading to the initiation of tumorigenesis (14, 15). Alternatively, defects in the MMR-dependent DNA damage response could lead to a failure in clearing DNA damage-bearing cells, which may confer a selective advantage in tumor cells (13, 16, 17). Consistent with this notion, *Msh2G674A* and *Msh6T1217D* mutant mice, which carry separation of function mutations that inactivate DNA repair but leave the DNA damage-response function intact, have delayed tumor onset compared with $Msh2^{-/-}$ and $Msh6^{-/-}$ mice, which are defective in both MMR functions (18, 19).

Although the majority of MMR mutations found in Lynch syndrome (HNPCC) patients are frameshift or nonsense mutations that result in an inactive protein, a significant number of MMR mutations are missense mutations [~25% of *MSH2* or *MLH1* mutations and ~45% of *MSH6* mutations (20)]. The impact of these missense mutations on the individual MMR functions and their significance for cancer predisposition often remain uncertain. The generation and analysis of mouse lines with MMR point mutations that model Lynch syndrome (HNPCC) mutations provides the opportunity to determine their impact on DNA repair and DNA damage response on the organismal level and assess their impact on carcinogenesis. Here, we report on a knockin mouse line with the first missense mutation in a MutL homolog. This mouse line carries a germ-linemutation that models the recurrent $MLH1^{G67R}$ variant found in several Lynch syndrome (HNPCC) families from different countries (1). Patients carrying the $MLH1^{G67R}$ mutation develop colorectal cancers that are characterized by microsatellite instability (MSI) (21). Consistent with the cancer phenotype in these Lynch syndrome (HNPCC) patients, $Mlh1^{G67R/G67R}$ mice display a strong cancer phenotype. However, in contrast to $Mlh1^{-/-}$ mice, the tumor incidence in $Mlh1^{G67R/G67R}$ mice is significantly different, with a lower incidence of gastrointestinal tumors. This change appears to be caused by the different effects the $Mlh1^{G67R}$ mutation exerts on the DNA repair and damageresponse functions in the intestinal mucosa. In addition, the $Mlh1^{G67R}$ mutation causes infertility in both male and female mice that is caused by the inability of the mutant $Mlh1^{G67R}$ protein to localize to meiotic chromosomes. These studies demonstrate that the $Mlh1^{G67R}$ mutation differentially affects the biological functions associated with Mlh1 with distinct phenotypic effects.

## Results

### *Generation and Cancer Susceptibility Phenotype of $Mlh1^{G67R}$ Mutant Mice.*

The Mlh1$^{G67R}$ mouse line was created by a knockin genetargeting strategy [Fig. 1 a–c and supporting information (SI) Fig. 8 in SI Appendix]. Western blot analysis revealed slightly reduced levels of cellular Mlh1$^{G67R}$ protein, indicating that the mutation affected protein stability (Fig. 1d). However, similar to WT Mlh1, the mutant Mlh1$^{G67R}$ protein was still capable of interacting with Pms2 as assessed by coimmunoprecipitation of Flag-tagged Mlh1$^{G67R}$ and HA-tagged Pms2 protein expressed in 293T cells (SI Fig. 9 in SI Appendix). Analysis of heterozygous or homozygous F2 animals revealed no developmental abnormalities. Cohorts of Mlh1$^{G67R/G67R}$, Mlh1$^{G67R/+}$, Mlh1$^{-/-}$, and Mlh1$^{+/+}$ mice were monitored for survival and cancer susceptibility. Both Mlh1$^{G67R/G67R}$ and Mlh1$^{-/-}$ mice showed severely reduced survival, with only 50% of animals surviving 30 weeks of age, and all animals had died by 64 weeks of age. In contrast, 100% of Mlh1$^{-/-}$ and 96% of Mlh1$^{G67R/+}$ mice survived this period (Fig. 2a and data not shown). There was no difference in survival between Mlh1$^{G67R/G67R}$ and Mlh1$^{-/-}$ mice. The reduced survival in the Mlh1$^{G67R/G67R}$ and Mlh1$^{-/-}$ mutant mice was caused by an increase in cancer predisposition. The histopathological analysis of moribund mice revealed that among 66 Mlh1$^{-/-}$ mice, 35 had developed T and B cell lymphoma, 35 had developed small intestinal tumors (among these, 8 mice developed both lymphoma and intestinal tumors), and 4 mice developed squamous basal cell carcinoma of the skin. The analysis of 49 Mlh1$^{G67R/G67R}$ mice revealed a similar tumor spectrum; however, we found a significant reduction in the number of mice with intestinal tumors (Fig. 2b). Although 34 mice had developed T and B cell lymphoma, only 16 mice developed small intestinal tumors (among these, 5 mice developed both types of tumors). Histopathological analysis revealed that, of 31 intestinal tumors in Mlh1$^{-/-}$ mice, 19 were adenocarcinoma, and 12 were adenoma, whereas, of 18 intestinal tumors in Mlh1$^{G67R/G67R}$ mice, 11 were adenocarcinomas, and 7 were adenomas. In addition, four Mlh1$^{G67R/G67R}$ mice had also developed squamous basal cell carcinoma of the skin. Six Mlh1$^{G67R/G67R}$ mice died prematurely, but their tumors were not available for analysis.

*MSI in Mlh1$^{G67R/G67R}$ Mice.*

To determine the MMR defect caused by the Mlh1$^{G67R}$ mutation, we assessed the in vivo mutator phenotype in Mlh1$^{G67R/G67R}$ mutant mice by analyzing MSI in tail genomic DNA (SI Fig. 10a in SI Appendix). At the dinucleotide marker D17Mit123, 25.4% of alleles tested were unstable in Mlh1$^{-/-}$ mice, and 21.9% of alleles were unstable in Mlh1$^{G67R/G67R}$ mice. In contrast, only 6.6% of alleles in Mlh1$^{-/-}$ genomes were unstable, indicating highly significant increases in mutation frequency in the genomes of Mlh1$^{-/-}$ and Mlh1$^{G67R/G67R}$ mice at this marker ($P < 0.0001$ compared with Mlh1$^{-/-}$) (SI Fig. 10b in SI Appendix). Similarly, the same marker showed significantly increased instability in intestinal epithelial cells of Mlh1$^{-/-}$ and Mlh1$^{G67R/G67R}$ mice (24.0% and 23.4%, respectively) compared with WT mice (4.2%) ($P < 0.0001$) (SI Fig. 10c in SI Appendix). The analysis of five different microsatellite markers in the genomes of intestinal and lymphatic tumors showed that 80% of Mlh1$^{G67R/G67R}$ tumors displayed a high MSI phenotype (22 of 28), with three or more microsatellites being unstable (data not shown). As expected from previous studies, the majority (79%, 25 of 32) of Mlh1$^{-/-}$ tumors displayed an MSI high phenotype (24, 25).

*In Vitro DNA Damage Response in Mlh1 Mutant Mouse Embryonic Fibroblast (MEF) Cells.*

To study the impact of the Mlh1$^{G67R}$ mutation on the DNA damage response, we exposed Mlh1$^{+/+}$, Mlh1$^{-/-}$, and Mlh1$^{G67R/G67R}$ primary MEF strains to cisplatin. Consistent with previous results, Mlh1$^{-/-}$ MEFs showed increased resistance to treatment with cisplatin (Fig. 3 a and b) (26). In contrast, both Mlh1$^{+/+}$ and Mlh1$^{G67R/G67R}$ MEF cells displayed similar sensitivity to cisplatin exposure. The differences in sensitivity between the Mlh1$^{-/-}$ and Mlh1$^{G67R/G67R}$ cells and Mlh1$^{+/+}$ cells were highly significant ($P < 0.0001$). The cisplatin sensitivity in Mlh1$^{+/+}$ and Mlh1$^{G67R/G67R}$ cells was associated with a significant increase in apoptosis (Fig. 3c) ($P < 0.0001$

for both $Mlh1^{+/+}$ and $Mlh1^{G67R/G67R}$ compared with untreated cells). In contrast, no significant increase in the number of apoptotic cells was seen in $Mlh1^{-/-}$ cells compared with untreated cells. In addition, consistent with previous reports (26), $Mlh1^{-/-}$ cells showed a defective cell cycle arrest after cisplatin treatment as shown by the reduced proportion of G2/M cells after damage-induced cell stress, whereas both $Mlh1^{+/+}$ and $Mlh1^{G67R/G67R}$ cells displayed normal G2/M arrest (Fig. 3d). Furthermore, in vitro-activated primary T cells of Mlh1-/- mice displayed increased resistance against cisplatin, as shown by increased survival and reduced apoptosis, whereas T cell blasts of both $Mlh1^{+/+}$ and $Mlh1^{G67R/G67R}$ mice were sensitive to cisplatin-induced cell death (SI Fig. 11 in SI Appendix).

*In Vivo DNA Damage Response in Intestinal Epithelia of Mlh1 Mutant Mice.*

We next analyzed the in vivo response to cisplatin in the intestinal epithelium of Mlh1 mutant mice. $Mlh1^{+/+}$, $Mlh1^{-/-}$, and $Mlh1^{G67R/G67R}$ mice were injected with cisplatin or PBS, and the apoptotic response of intestinal epithelial cells was measured by TUNEL. Consistent with the results in MEF cells, $Mlh1^{+/+}$ and $Mlh1^{G67R/G67R}$ epithelial cells in the small and large intestines of cisplatin-treated mice displayed a significant increase in TUNEL-positive cells compared with the intestines of PBS treated mice (Fig. 4 a and b). In contrast, cisplatin treatment of $Mlh1^{-/-}$ mice resulted in only a moderate increase in the number of apoptotic cells.

*Meiotic Defects in Mutant $Mlh1^{G67R/G67R}$ Males.*

$Mlh1^{G67R/G67R}$ male and female mice were infertile. The seminiferous tubules in testes from $Mlh1^{G67R/G67R}$ males were severely depleted in spermatogenic cells compared with their WT littermates (Fig. 5 a–d). Spermatogonia and early spermatocytes were visible proximal to the basement membrane within the tubules of $Mlh1^{G67R/G67R}$ testes and progressed through pachynema in a normal fashion. By metaphase, however, spermatocytes from $Mlh1^{G67R/G67R}$ males displayed abnormal spindle structures with chromosomes misaligned across the spindles (Fig. 5d, arrows). Further analysis of metaphase chromosomes in $Mlh1^{G67R/G67R}$ animals revealed mainly univalent chromosomes with only a few bivalents (Fig. 5f, arrow), indicating that the chromosomes undergo premature separation before aligning at the metaphase plate. These results suggest that the $Mlh1^{G67R}$ mutation causes the loss of chiasmata at or before metaphase I, and, as a result, most of the $Mlh1^{G67R/G67R}$ spermatocytes failed to progress beyond metaphase and became apoptotic. In contrast, in $Mlh1^{+/+}$ males the seminiferous epithelium displayed a normal range of spermatogenic cells and contained mature spermatozoa within their lumen, indicating normal progression through metaphase and full completion of spermatogenesis (Fig. 5 a, b, and e). We monitored meiotic progression in adult WT and $Mlh1^{G67R/G67R}$ males by analyzing the assembly of synaptonemal complex proteins, Sycp1 and Sycp3, during prophase I. Although the meiotic chromosomes in $Mlh1^{G67R/G67R}$ mice display the typical pachytene-to-diplotene configurations similar to WT (Fig. 6 a and b), some spermatocytes from these mutant animals display premature separation of some of the chromosomes (Fig. 6 c and d) as well as abnormal intrahomolog associations at late pachytene and diplotene (Fig. 6 e and f ). We also examined the localization of Mlh1 to meiotic foci in WT and mutant animals. Although Mlh1 containing foci, which represent sites of crossing-over, were found at the predicted frequency and localization in WT mice (Fig. 7a), the analysis of $Mlh1^{G67R/G76R}$ males revealed either the complete loss or a decrease in the frequency and intensity of $Mlh1^{G67R}$ staining (Fig. 7 b and c). The frequency of Mlh1 foci in $Mlh1^{G67R/G67R}$ mice ranged from 20% to 77% of that observed in WT mice (data not shown). This analysis also showed a complete absence of Mlh3 staining in pachytene spreads of $Mlh1^{G67R/G67R}$ animals, whereas WT animals displayed normal staining (Fig. 7 d–f ).

## Discussion

We generated a mouse line carrying the $Mlh1^{G67R}$ missense mutation that corresponds to a recurrent mutation in Lynch syndrome (HNPCC) patients and studied the consequences on individual MMR functions, cancer susceptibility, and fertility. The $Mlh1^{G67R}$ mutation had distinct effects on the DNA repair and damage-response functions of Mlh1. Similar to the $Msh2^{G674A}$ and $Msh6^{T1217D}$ missense mutations that we previously analyzed in mice, these functions are clearly distinguishable by the $Mlh1^{G67R}$ mutation. In homozygous mutant $Msh2^{G674A}$ and $Msh6^{T1217D}$ animals, the tumor onset was delayed compared with $Msh2^{-/-}$ and $Msh6^{-/-}$ mice (18, 19), consistent with the idea that the MMR-dependent DNA damage-induced apoptotic response could play an important tumor-suppressing role in the initial stages of tumorigenesis (13). Similar to $Mlh1^{-/-}$ mice, $Mlh1^{G67R/G67R}$ mice were characterized by a strong cancer predisposition phenotype. However, the number of intestinal tumors in $Mlh1^{G67R/G67R}$ mice was significantly reduced compared with $Mlh1^{-/-}$ mice. We observed the retention of a robust apoptotic response to cisplatin exposure in the epithelial mucosa of $Mlh1^{G67R/G67R}$ animals similar to WT mice, whereas this response was severely affected in $Mlh1^{-/-}$ animals. Similarly, WT and $Mlh1^{G67R/G67R}$ T lymphocytes displayed a robust cisplatin response, whereas T lymphocytes in $Mlh1^{-/-}$ mice showed increased resistance to cisplatin (Fig. 3 and SI Fig. 10 in SI Appendix). However, in contrast to intestinal epithelial cells, in T lymphocytes, the difference in the DNA damage response was not associated with a reduction in the incidence of lymphomas, although the time of death due to lymphoma was slightly delayed in Mlh1G67R/G67R mice (data not shown). These results demonstrate that the effect of missense mutations on MMR functions can affect cancer susceptibility in a tissue-specific manner in mice. They also suggest that the MMR-dependent DNA damageresponse in patients carrying the $MLH1^{G67R}$ might differ compared with patients carrying complete MLH1 loss-of-function mutations, and it is possible that some Lynch syndrome (HNPCC)-associated cancers with missense mutations respond more favorably to chemotherapeutic treatment. The G67R mutation affected the stability of the mutant protein and led to slightly reduced cellular levels of $Mlh1^{G67R}$ protein. This finding is consistent with the observation that ectopic expression of human $MLH1^{G67R}$ in N-methyl-Nnitrosourea (MNU)-resistant A2780MNU ovarian carcinoma cells did only yield reduced levels of protein compared with WT MLH1. In addition, ectopic expression of $MLH1^{G67R}$ in A2780MNU cells did not restore sensitivity to MNU (27). We found that the cells from different tissues in $Mlh1^{G67R/G67R}$ mutant mice remained sensitive to cisplatin exposure. It is possible that primary cells and transformed cancer cells derived from different tissue behave differently in the MMR-dependent DNA damage response. The $Mlh1^{G67R}$ mutation caused a strong DNA repair defect as indicated by the high MSI in the tissues and tumors of $Mlh1^{G67R/G67R}$ mice, which is consistent with studies in bacteria, yeast, and human cells and further demonstrates that normal ATPase activity is essential for the activation of the repair processes that facilitate the removal of mismatched bases (9, 11, 28–32). However, because the $Mlh1^{G67R}$ mutation did not significantly affect the MMR-dependent cytotoxic response, normal Mlh1-mediated ATP processing is apparently not essential for the DNA damage-signaling function of Mlh1 in mammalian tissues. Different models have been proposed to explain the role o fMMRproteins in DNA damage response: The futile cycle model proposes that MMR engages in futile repair cycles after treatment with alkylating agents that ultimately lead to the formation of double-strand breaks that signal cell-cycle arrest and apoptosis (33). A second model suggests that MMR proteins function as damage sensors and directly link cell cycle and apoptotic mediators to the site of DNA damage (13, 34, 35). The molecular analysis of the $Mlh1^{G67R}$ mouse line showed that the Mlh1G67R mutation resulted in reduced levels of $Mlh1^{G67R}$ protein but had no effect on the stability of other proteins such as Pms2 and p73 (data not shown) with which it interacts during MMR and

poptosis signaling (36, 37). The presence of $Mlh1^{G67R}$ protein that has lost its ability to mediate excision repair but is still capable of DNA damage signaling is consistent with the idea that the MutSα and MutLα complexes can act as molecular scaffolds to recruit downstream effectors to sites of DNA damage. In this model, MutSα and MutLα bind to either mismatched or damaged bases. Depending on the DNA ligand, the MutSα and MutLα complexes then recruit either DNA repair factors to mediate either excision repair or downstream effectors such as ATR (ataxia-, telangiectasia-, and Rad3- related) and ATRIP (ATR-interacting protein) or p73 to mediate cell-cycle arrest and apoptosis (37, 38). This scenario would also predict that, although the $Mlh1^{G67R}$ mutation prevents MutLα from functional interaction with downstream repair factors to initiate mismatch excision similar to other previously reported ATPase mutations in Mlh1 or Pms2 (9, 11), it should still allow the interaction of MutLα with ATM/ ATRIP, p73, or other factors to signal cell-cycle arrest and apoptosis. Recently it was discovered that MutLα contains a latent endonuclease activity that depends on the DQHA(X)2E(X)4E motif in Pms2 (39, 40), and it was shown that this activity is important in the cellular response to 6-thioguanine exposure (41). It has also been reported that mutations in the ATPase centers of both MLH1 and PMS2 impair MutLα endonuclease activity (39). Our results suggest that either the Mlh1G67R mutation does not completely impair the ATPase activity of MutLα or the endonuclease activity may not be required for the cisplatin response. These predictions can be tested in future studies. In mice, Mlh1 also has distinct functions in meiotic recombination, mismatch repair, and, possibly, DNA damage response. The $Mlh1^{G67R}$ mutation caused a strong meiotic defect that resulted in male and female sterility. The histopathological analysis of meiotic progression in $Mlh1^{G67R/G67R}$ male mice revealed that, similar to $Mlh1^{-/-}$ mice, spermatogenesis proceeded normally through pachynema but failed to progress through metaphase I (42, 43). Consistent with this observation, cytogenetic analysis of prophase I chromosomes in $Mlh1^{G67R/G67R}$ males showed normal synapsis and typical pachytene and diplotene configurations of the chromosomes, however, a significant number of nuclei also showed premature desynapsis of chromosomes. In addition, metaphase chromosomes also showed premature separation of chromosomes, suggesting that the Mlh1G67R protein interfered with meiotic recombination. Consistent with this idea, mutations affecting the ATPase domain of yeast MLH1 resulted in reduced meiotic crossing-over (44). Localization studies showed that this meiotic defect in $Mlh1^{G67R/G67R}$ mice was caused by the inability of the mutant protein to efficiently localize to meiotic chromosomes. Therefore, at the cytogenetic level the $Mlh1^{G67R}$ mutation resulted in an ‘‘Mlh1 knockout’’ phenotype. Interestingly, the meiotic defect is different in $Mlh1^{-/-}$ mice, in that Mlh3 localization to chromosomes is absent in $Mlh1^{G67R/G67R}$ mice, whereas Mlh3 localization occurs in $Mlh1^{-/-}$ mice (45). Mlh1 and Mlh3 are known to form a heterodimeric complex (termed MutLψ) (5) whose function is essential for meiotic progression, and our studies demonstrate that the $Mlh1^{G67R}$ mutation interferes with the function of this complex and its chromosomal localization. It is possible that the mutant $Mlh1^{G67R}$ also interferes with MutLψ function in heterozygous mice, and it will be interesting to evaluate the possibility of more subtle meiotic defects in heterozygous animals, which may provide a model for human aneuploidy.

## Materials and Methods

*PCR Genotyping of $Mlh1^{G67R}$ Mutant Mice.*

Genomic tail DNA was PCR amplified by using forward primer 5’-TGC-TGA-AAG GAC-TGC-CCT AC-3’ and reverseprimer 5’-GCC-CTC-CTG-AAT-GAC-CAA-TA-3’, and the 880-bp PCR was subsequently digested with EcoRI.

*Western Blot Analysis.*

Thymocyte cell extracts (50 μg of protein) were separated on two 10% SDS/PAGE gels. Protein was transferred onto Protran membranes, and the membranes were incubated either with rabbit polyclonal antibodies directed against Mlh1 (AB 9144; Abcam) or Msh2 (PharMingen).

*Histopathological Analysis of Tumors.*

Gastrointestinal tumors were dissected, fixed in 10% neutral buffered formalin, and processed for paraffin embedding and H&E staining. Lymphomas were analyzed for surface markers by three-color flow cytometry.

*MSI Analysis.*

Genomic DNA from tail and intestinal mucosa was analyzed at dinucleotide markers D17Mit123 and D7Mit91 as described (22). For tumor tissue, three mononucleotide markers (U12235, Aa006036, and L24372) and two dinucleotide markers (D7Mit91 and D17Mit123) were analyzed. PCR was performed by using Cy5-end-labeled primers (30 cycles of 95°C for 30 s, 60°C for 1 min, and 72°C for 2 min). PCR products were separated on denaturing acrylamide gels and autoradiographed.

*Cytotoxicity Assays.*

MEFs were exposed to cisplatin and MTT [3-(4,5-dimethylthiazol-2-yl)-2,5-diphenyltetrazolium bromide] assays were performed according to standard procedures. MEFs were seeded at 2 * 104 cells per well in a 24-well plate. The cells were exposed to various concentrations of cisplatin and analyzed after 24, 48, and 72 h of treatment. The percentage of cell survival was calculated as (treated cells per untreated cells * 100). The apoptotic response to drug exposure was measured by TUNEL (Promega). The experiments were performed for three different MEF strains for each Mlh1 genotype and repeated at least three times for each strain.

In Vivo DNA Damage Response.

Three animals of each $Mlh1^{+/+}$, $Mlh1^{-/-}$, and $Mlh1^{G67R/G67R}$ genotype were injected intraperitoneally with cisplatin (10mg/kg of body weight) or saline solution. All animals were killed 24 h after injection, and their intestines were fixed in 10% formamide. Paraffinembedded histological sections from small and large intestines were stained with TUNEL (Promega). The number of TUNEL-positive cells per 50 crypts in the small and large intestines were counted, and the means of three mice in each group were calculated.

*Cell Cycle Analysis.*

MEF cells (1.0 * 106) were either treated with 40 μM cisplatin for 36 h or left untreated. The cells were subsequently fixed in 70% ethanol, stained with propidium iodide (PI), and analyzed by flow cytometry.

*Analysis of Meiotic Prophase I.*

The testes from male mice were fixed in Bouin's or 10% formalin, embedded in paraffin, and sectioned. Chromosome spreads were prepared as described (23) and subjected to indirect immunofluorescence using antibodies against synaptonemal complex proteins (Sycp1 and Sycp3), MutL homologs (Mlh1 and Mlh3), and centromers (CREST). Secondary antibodies were conjugated to Cy3, Cy5, or fluoroscein (Jackson Immunochemicals). Images were visualized with the aid of a Zeiss Axioimager Z1 equipped with a cooledCCD Axiocam MRM camera, and processed by using Axiovision 4.0 software (Zeiss).

**ACKNOWLEDGMENTS.**

We thank Martina Doehler for excellent technical support. This work was supported by National Institutes of Health Grants CA76329, CA102705, and CA93484 (to W.E.), CA84301 (to W.E. and R.K.), and HD41012 (to P.E.C.) and Center Grant CA13330 (to the Albert Einstein College of Medicine) and an Irma T. Hirschl Career Scientist Award (to W.E.). B.K., A.R., and C.R. were supported by Interdisziplina¨ res Zentrum fu¨ r Klinische Forschung

and Deutsche Forschungsgemeinschaft graduate college 639 grants.

1. Peltomaki P, Vasen HF (1997) Mutations predisposing to hereditary nonpolyposis colorectal cancer: Database and results of a collaborative study. The International Collaborative Group on Hereditary Nonpolyposis Colorectal Cancer. Gastroenterology 113:1146–1158.
2. Yan H, et al. (2000) Conversion of diploidy to haploidy. Nature 403:723–724.
3. Kunkel TA, Erie DA (2005) DNA mismatch repair. Annu Rev Biochem 74:681–710.
4. Schofield MJ, Hsieh P (2003) DNA mismatch repair: Molecular mechanisms and biological function. Annu Rev Microbiol 57:579–608.
5. Kolas NK, Cohen PE (2004) Novel and diverse functions of the DNA mismatch repair family in mammalian meiosis and recombination. Cytogenet Genome Res 107:216– 231.
6. Buermeyer AB, Deschˆ nes SM, Baker SM, Liskay RM (1999) Mammalian mismatch repair. Annu Rev Genet 33:533–564.
7. Kolodner RD, Marsischky GT (1999) Eukaryotic DNA mismatch repair. Curr Opin Genet Dev 9:89–96.
8. Iyer RR, Pluciennik A, Burdett V, Modrich PL (2006)DNAmismatch repair: functions and mechanisms. Chem Rev 106:302–323.
9. Raschle M, Dufner P, Marra G, Jiricny J (2002) Mutations within the hMLH1 and hPMS2 subunits of the human MutLalpha mismatch repair factor affect its ATPase activity, but not its ability to interact with hMutSalpha. J Biol Chem 277:21810–21820.
10. Hall MC, Shcherbakova PV, Kunkel TA (2002) Differential ATP binding and intrinsic ATP hydrolysis by amino-terminal domains of the yeast Mlh1 and Pms1 proteins. J Biol Chem 277:3673–3679.
11. Tomer G, Buermeyer AB, Nguyen MM, Liskay RM (2002) Contribution of human mlh1 and pms2 ATPase activities to DNA mismatch repair. J Biol Chem 277:21801–21809.
12. Stojic L, et al. (2004) Mismatch repair-dependent G2 checkpoint induced by low doses of SN1 type methylating agents requires the ATR kinase. Genes Dev 18:1331–1344.
13. Fishel R (2001) The selection for mismatch repair defects in hereditary nonpolyposis colorectal cancer: revising the mutator hypothesis. Cancer Res 61:7369–7374.
14. Kinzler KW, Vogelstein B (1996) Lessons from hereditary colorectal cancer. Cell 87:159–170.
15. Loeb LA (2001) A mutator phenotype in cancer. Cancer Res 61:3230–3239.
16. Nowell PC (1976) The clonal evolution of tumor cell populations. Science 194:23–28.
17. Tomlinson I, BodmerW(1999) Selection, the mutation rate and cancer: Ensuring that the tail does not wag the dog. Nat Med 5:11–12.
18. Lin DP, et al. (2004) An Msh2 point mutation uncouples DNA mismatch repair and apoptosis. Cancer Res 64:517–522.
19. Yang G, et al. (2004) Dominant effects of an Msh6 missense mutation on DNA repair and cancer susceptibility. Cancer Cell 6:139–150.
20. de la Chapelle A (2004) Genetic predisposition to colorectal cancer. Nat Rev Cancer 4:769–780.
21. Alazzouzi H, et al. (2005) Low levels of microsatellite instability characterize MLH1 and MSH2 HNPCC carriers before tumor diagnosis. Hum Mol Genet 14:235–239.
22. WeiK, et al. (2003) Inactivation of Exonuclease 1 inmice results inDNAmismatch repair defects, increased cancer susceptibility, and male and female sterility. Genes Dev 17:603–614.

23. Kolas NK, et al. (2005) Localization of MMR proteins on meiotic chromosomes in mice indicates distinct functions during prophase I J Cell Biol 171:447–458.
24. Prolla TA, et al. (1998) Tumour susceptibility and spontaneous mutation in mice deficient in Mlh1, Pms1 and Pms2 DNA mismatch repair. Nat Genet 18:276–279.
25. Edelmann W, et al. (1999) Tumorigenesis in Mlh1 and Mlh1/Apc1638N mutant mice. Cancer Res 59:1301–1307.
26. Gong JG, et al. (1999) The tyrosine kinase c-Abl regulates p73 in apoptotic response to cisplatin-induced DNA damage. Nature 399:806–809.
27. Blasi MF, et al. (2006) A human cell-based assay to evaluate the effects of alterations in the MLH1 mismatch repair gene. Cancer Res 66:9036–9044.
28. Kondo E, Suzuki H, Horii A, Fukushige S (2003) A yeast two-hybrid assay provides a simple way to evaluate the vast majority of hMLH1 germ-line mutations. Cancer Res 63:3302–3308.
29. Ellison AR, Lofing J, Bitter GA (2004) Human MutL homolog (MLH1) function in DNA mismatch repair: A prospective screen for missense mutations in the ATPase domain. Nucleic Acids Res 32:5321–5338.
30. Junop MS, Yang W, Funchain P, Clendenin W, Miller JH (2003) In vitro and in vivo studies of MutS, MutL and MutH mutants: Correlation of mismatch repair and DNA recombination. DNA Repair 2:387–405.
31. Prolla TA, Pang Q, Alani E, Kolodner RD, Liskay RM (1994) MLH1, PMS1, and MSH2 interactions during the initiation of DNA mismatch repair in yeast. Science 265:1091– 1093.
32. Raevaara TE, et al. (2005) Functional significance and clinical phenotype of nontruncating mismatch repair variants of MLH1. Gastroenterology 129:537–549.
33. Karran P, Bignami M (1994) DNA damage tolerance, mismatch repair and genome instability. BioEssays 16:833–839.
34. LiGM(1999) The role of mismatch repair inDNAdamage-induced apoptosis. Oncol Res 11:393–400.
35. Kat A, et al. (1993) An alkylation-tolerant, mutator human cell line is deficient in strand-specific mismatch repair. Proc Natl Acad Sci USA 90:6424–6428.
36. Buermeyer AB, Wilson-Van Patten C, Baker SM, Liskay RM (1999) The human MLH1 cDNA complements DNA mismatch repair defects in Mlh1-deficient mouse embryonic fibroblasts. Cancer Res 59:538–541.
37. Shimodaira H, Yoshioka-Yamashita A, Kolodner RD, Wang JY (2003) Interaction of mismatch repair protein PMS2 and the p53-related transcription factor p73 in apoptosis response to cisplatin. Proc Natl Acad Sci USA 100:2420–2425.
38. Yoshioka K, Yoshioka Y, Hsieh P (2006) ATR kinase activation mediated by MutSalpha and MutLalpha in response to cytotoxic O6-methylguanine adducts. Mol Cell 22:501– 510.
39. Kadyrov FA, Dzantiev L, Constantin N, Modrich P (2006) Endonucleolytic function of MutLalpha in human mismatch repair. Cell 126:297–308.
40. Kadyrov FA, et al. (2007) Saccharomyces cerevisiae MutLa is a mismatch repair endonuclease. J Biol Chem 282:37181–37190.
41. Erdeniz N, Nguyen M, Deschenes SM, Liskay RM (2007) Mutations affecting a putative MutLalpha endonuclease motif impact multiple mismatch repair functions. DNA Repair 6:1463–1470.
42. Edelmann W, et al. (1996) Meiotic pachytene arrest in MLH1-deficient mice. Cell 85:1125–1134.
43. Baker SM, et al. (1996) Involvement of mouse Mlh1 inDNAmismatch repair and meiotic crossing over. Nat Genet 13:336–342.

44. Hoffmann ER, Shcherbakova PV, Kunkel TA, Borts RH (2003) MLH1 mutations differentially affect meiotic functions in Saccharomyces cerevisiae. Genetics 163:515–526.
45. Lipkin SM (2002) Meiotic arrest and aneuploidy in MLH3-deficient mice. Nat Genet 31:385–390.

**Figure Legends**

Fig. 1 : The generation of $Mlh1^{G67R}$ mutant mice. (a) Domain structure of Mlh1. The location of the G67R mutation is indicated. (b) Schematic representation of the modified $Mlh1^{G67R}$ genomic locus and sequence characteristics of the G67R mutation. (c) PCR genotyping of tail DNA from $Mlh1^{G67R}$ mutant mice. $Mlh1^{G67R/+}$, heterozygous mice; $Mlh1^{G67R/G67R}$, homozygous mutant mice. After EcoRI restriction digestion of the PCR product, the WT allele is indicated by an 880-bp fragment and the $Mlh1^{G67R}$ mutant allele by 470- and 410-bp restriction fragments. (d) Western blot analyses of thymocyte cell extracts using anti-Mlh1 and anti-Msh2 antibodies.*, Unspecific protein recognized by the Mlh1 antisera.

Fig. 2. Survival and tumor incidence in Mlh1 mutant mice. (a) Survival of Mlh1 mutant mice. Significantly reduced survival of $Mlh1^{-/-}$ and $Mlh1^{G67R/G76R}$ mice compared with WT mice ($P < 0.0001$; log-rank test) is shown. There was no difference in survival between $Mlh1^{-/-}$ and $Mlh1^{G67R/G76R}$ mice ($P = 0.915$; log-rank test). (b) Tumor incidence in $Mlh1^{-/-}$ and $Mlh1^{G67R/G67R}$ mutant mice. Reduced gastrointestinal (GI) tumor incidence in $Mlh1^{G67R/G67R}$ mice ($P = 0.0296$) is shown.

Fig. 3. Cisplatin sensitivity and apoptosis in $Mlh1^{G67R/G67R}$ MEF cells. MEF strains of the various Mlh1 genotypes were exposed to cisplatin for different time periods or at varying concentrations. (a) Survival of cells after exposure with 40 μM cisplatin at different time intervals. (b) Survival of cells after 48-h exposure at different cisplatin concentrations. (c) Apoptotic response to cisplatin treatment (20 μM cisplatin for 24 h) measured by TUNEL. (d) G2/M cell-cycle arrest in $Mlh1^{G67R/G67R}$ MEF cells. The percentage of cells in G0/G1 and G2/M were calculated for three different MEF strains for indicated genotypes. The results are shown as the fold increase of G2/M cells in treated over untreated MEFs for each genotype.

Fig. 4. Cisplatin-induced apoptotic response of epithelial cells in the intestinal mucosa in Mlh1 mutant mice. TUNEL-positive cells 24 h after cisplatin exposure (10 mg/kg of body weight). (a) Small intestine. (b) Large intestine.

Fig. 5. Analysis of $Mlh1^{G67R/G67R}$ mutant testes reveals spermatogenic failure at or before metaphase of the first meiotic division. (a–d)H&Estaining of testis sections from WT (a and b) and $Mlh1^{G67R/G67R}$ (c and d) males, showing normal progression of spermatogenesis in WT and failure to progress beyond metaphase I in mutant adult testes. Aberrant spindle configurations are observed in testis sections from males (arrows). (Scale bar, 100_m.) (e and f ) Metaphase spreads from WT (e) and $Mlh1^{G67R/G67R}$ ( f ) spermatocytes show abnormal metaphase configurations in the mutant mice. Almost all chromosomes are univalent, with only very few crossovers remaining (arrow) in $Mlh1^{G67R/G67R}$ spermatocytes.

Fig. 6. Premature chromosome desynapsis in $Mlh1^{G67R/G67R}$ mice. Sycp1 (red) and Sycp3 (green) staining shows pachytene to diplotene chromosome configurations in WT (a) and $Mlh1^{G67R/G67R}$ (b–f) mouse spermatocytes. Mutant animals show premature separation of some chromosomes,

particularly the XY in midpachynema (MP) and longer chromosomes in late pachynema (LP) to early diplonema (arrowheads in c) with abnormal intrahomolog associations being evident at late pachynema and diplonema (Dipl) (arrowheads in e and f ). Broken synaptonemal complexes are also common (arrows in c and e). (See also larger images in SI Fig. 12 in SI Appendix).

Fig. 7. Localization of Mlh1 (a–c) and Mlh3 (d–f) on meiotic chromosomes. (a–c) Localization of Mlh1 (green foci) on pachytene chromosome spreads from WT (a) and $Mlh1^{G67R/G67R}$ (b and c) males reveals a dramatic decrease in frequency and intensity of Mlh1 staining in the $Mlh1^{G67R/G67R}$ mutant animals. Many cells show a complete absence of Mlh1G67R staining (data not shown), but others show distinct $Mlh1^{G67R}$ reduction as exemplified in b and c. (d–f) Mlh3 staining (green foci) of WT (d) and $Mlh1^{G67R/G67R}$ (e and f ) males reveals a complete absence of Mlh3 staining in pachytene spreads from Mlh1G67R/G67R mutant animals. (See also larger images in SI Fig. 13 in SI Appendix). Synaptonemal complexes are stained with anti Sycp3 antiserum (red), and centromeres are detected by CREST autoimmune serum (blue).

**Supplemental Figures**

**Fig. 8.** Gene targeting strategy for the generation of $Mlh1^{G67R}$ mutant mice. The *Mlh1* genomic locus spanning exons 1 to 6, the p$Mlh1^{G67R}$ targeting vector and the $Mlh1^{G67R}$ targeted locus are shown. The deletion of the PGKhygromycin cassette by Cre-loxP-mediated recombination after mating of male chimeric mice to *ZP3-Cre* recombinase transgenic female mice to generate the $Mlh1^{G67R}$ floxed locus is indicated. Solid boxes indicate exons and solid triangles indicate LoxP sites. Lower panel: Southern blot analysis of targeted ES cell lines: The *Mlh1* WT (+/+) allele is indicated by a 5.2-kb *Eco*RI restriction fragment and the targeted $Mlh1^{G67R}$ locus by a 3.5-kb *Eco*RI fragment. The relative position of the hybridization probe is indicated by a solid line.

**Fig. 9.** Interaction of Mlh1 and $Mlh1^{G67R}$ with Pms2. 3xFlag-tagged-Mlh1 or 3xFlag-tagged-$Mlh1^{G67R}$ were transiently co-expressed with HA-tagged-Pms2 in 293T cells and their interaction analyzed by co-immunoprecipitation 48 hours post-transfection in the presence of 150 mM NaCl according to standard procedures.

(*a*) Protein extracts from cells expressing 1) 3xFlag-tagged-Mlh1 and 2) 3xFlag-tagged-$Mlh1^{G67R}$ were subjected to co-immunoprecipitation using anti-Flag-coated beads. The presence of HA-tagged-Pms2 in the precipitate was tested by Western blot analysis using anti-HA antisera. 3) HA-tagged-Pms2 in total lysate of cells transfected with 3xFlag-tagged-Mlh1 and 4) 3xFlag-tagged-$Mlh1^{G67R}$ expression constructs.

(*b*) Protein extracts from cells expressing 1) 3xFlag-tagged-Mlh1 and 2) 3xFlag-tagged-$Mlh1^{G67R}$ were subjected to co-immunoprecipitation using anti-HA-coated beads. The presence of 3xFlag-tagged-Mlh1 and 3xFlag-tagged-$Mlh1^{G67R}$ in the precipitate was tested by Western blot analysis using anti-Flag antisera. 3) 3xFlag-tagged-Mlh1 in total lysate from cells transfected with 3xFlag-tagged-Mlh1 and 4) 3xFlag-tagged-$Mlh1^{G67R}$ in total lysate from cells transfected with 3xFlag-tagged-$Mlh1^{G67R}$.

**Fig. 10.** MSI in *Mlh1* mutant tissue. *(a)* Instability at the *D17Mit123* locus. Shown are representative examples of extensions and contractions caused by Mlh1-deficiency. *(b)* Comparison of MSI in $Mlh1^{+/+}$ (WT), $Mlh1^{-/-}$ and $Mlh1^{G67R/G67R}$ ($Mlh1^{GR/GR}$) mutant MEFs. *(c)*

Comparison of MSI in WT, *Mlh1*$^{-/-}$ and *Mlh1*$^{G67R/G67R}$ (*Mlh1*$^{GR/GR}$) mutant intestinal epithelial cells. Statistical analysis by Fisher's exact test.

**Fig. 11.** DNA damage response in activated T lymphocytes. (*a)* Survival of activated T cells after exposure with 20 μM cisplatin at different time intervals. Primary lymphocytes were prepared from lymph nodes of mice with different Mlh1 genotypes. T cells were purified using the MACS magnetic cell sorting system (Miltenyi) according to the manufacturer's protocols. Isolated T cells of the different *Mlh1* genotypes were (pre) activated by plate bound anti-CD3e (2 μg/ml) and soluble CD28 (0.5 μg/ml) for 24 hours and subsequently exposed to cisplatin for indicated time periods. Cell survival was measured by tryphan blue exclusion and by an in vitro cytotoxicity assay (Cell Titer 96, Promega) according to manufacturer's protocols. The percentage of cell survival was calculated as (treated cells/untreated cells x 100). The experiments were performed for T cell isolations from three individual mice for each *Mlh1* genotype and repeated two times for each strain. (*b)* Apoptotic response to cisplatin treatment (20 μM cisplatin for 24h). Apoptotic T cells were measured using the Annexin V- Fitc Kit (Bender MedSystems, Vienna) by flow cytometry analysis. The mean percentages of apoptotic cells in three independent T cell cultures of each genotype are shown. The cumulative results of two independent experiments are shown.

# Fig.1

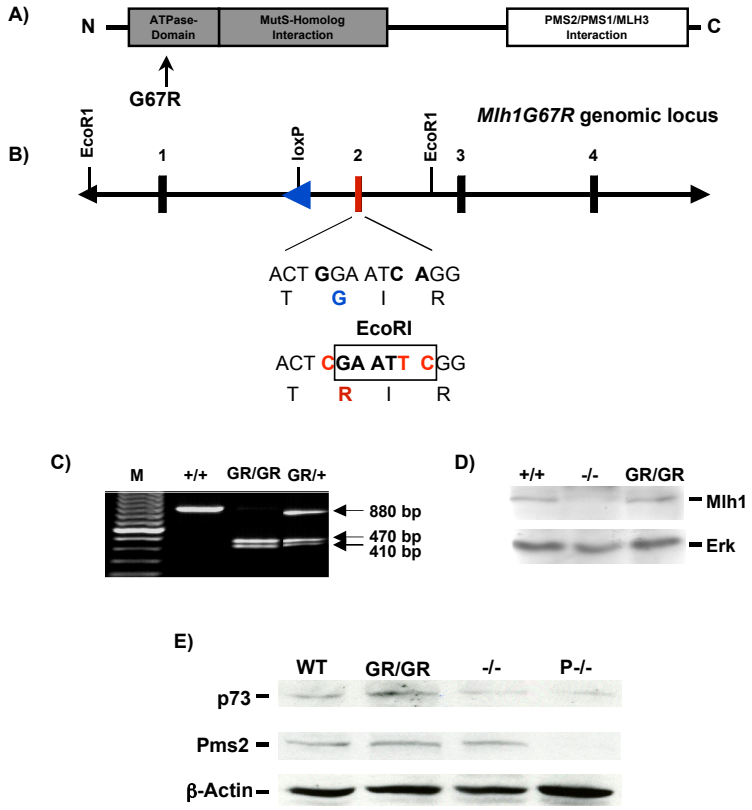
A)
N
ATPase-Domain
MutS-Homolog Interaction
PMS2/PMS1/MLH3 Interaction
C
G67R
B)
Mlh1G67R genomic locus
EcoR1
1
loxP
2
EcoR1
3
4
ACT GGA ATC AGG
T G I R
EcoRI
ACT CGA ATT CGG
T R I R
C)
M
+/+
GR/GR
GR/+
880 bp
470 bp
410 bp
D)
+/+
-/-
GR/GR
Mlh1
Erk
E)
WT
GR/GR
-/-
P-/-
p73
Pms2
β-Actin

# Fig. 2

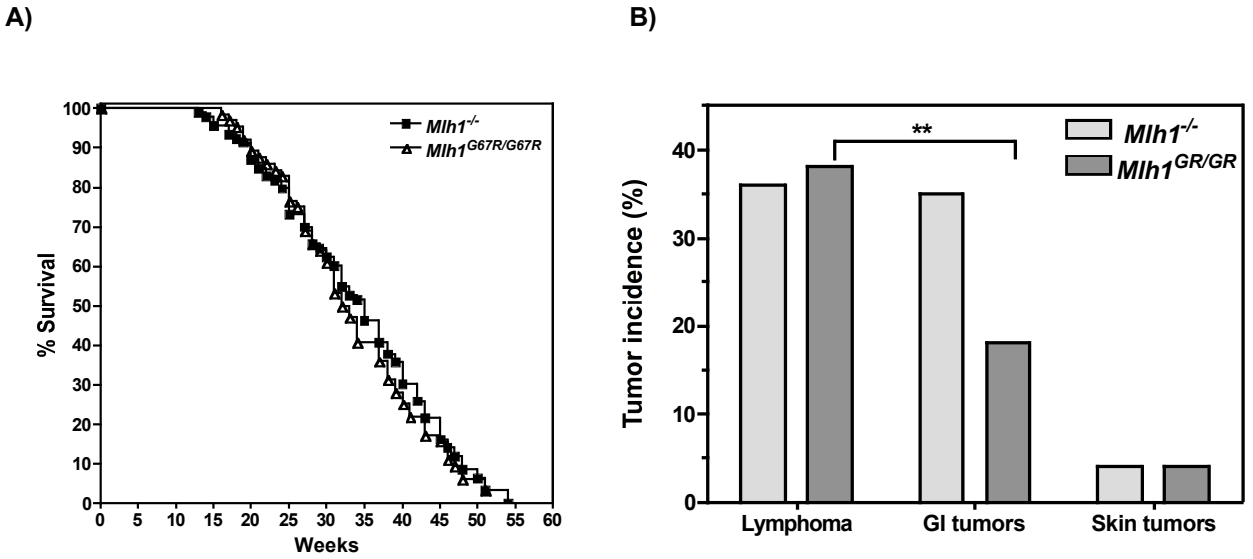
A)
B)
% Survival
Weeks
Mlh1-/-
Mlh1G67R/G67R
Tumor incidence (%)
**
Mlh1-/-
Mlh1GR/GR
Lymphoma
GI tumors
Skin tumors

# Fig. 3

A

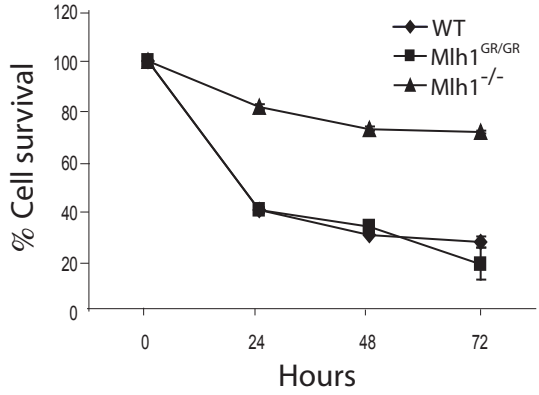
WT
Mlh1GR/GR
Mlh1-/-
% Cell survival
120
100
80
60
40
20
0
0
24
48
72
Hours

B

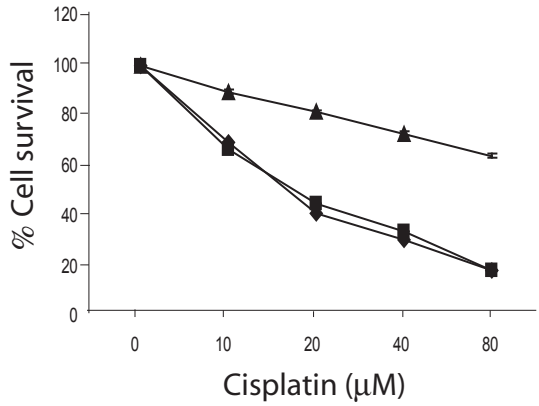
% Cell survival
120
100
80
60
40
20
0
0
10
20
40
80
Cisplatin (μM)

C

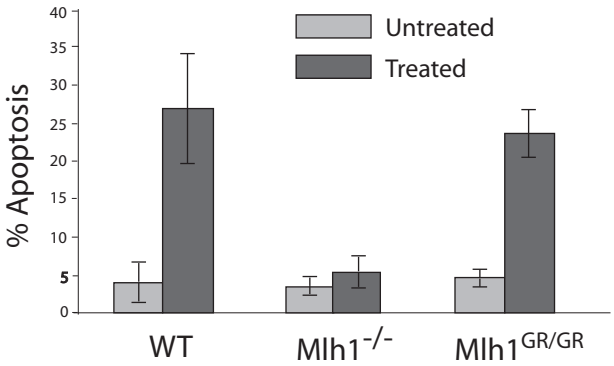
Untreated
Treated
% Apoptosis
40
35
30
25
20
15
10
5
0
WT
Mlh1-/-
Mlh1GR/GR

D

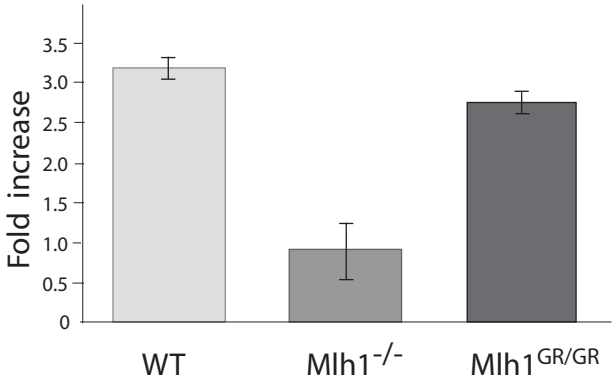
Fold increase
3.5
3.0
2.5
2.0
1.5
1.0
0.5
0
WT
Mlh1-/-
Mlh1GR/GR

A

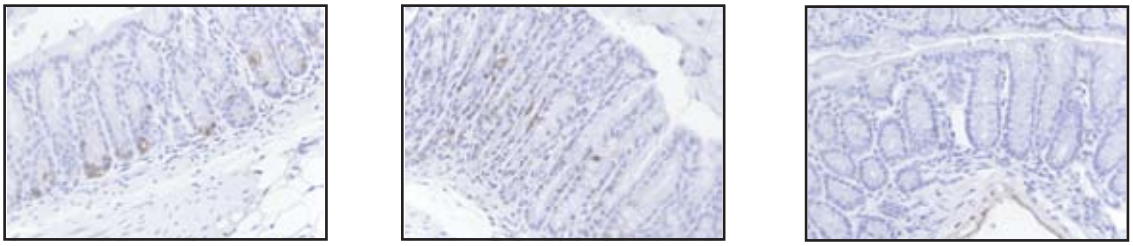
WT
Mlh1-/-
Mlh1GR/GR

B

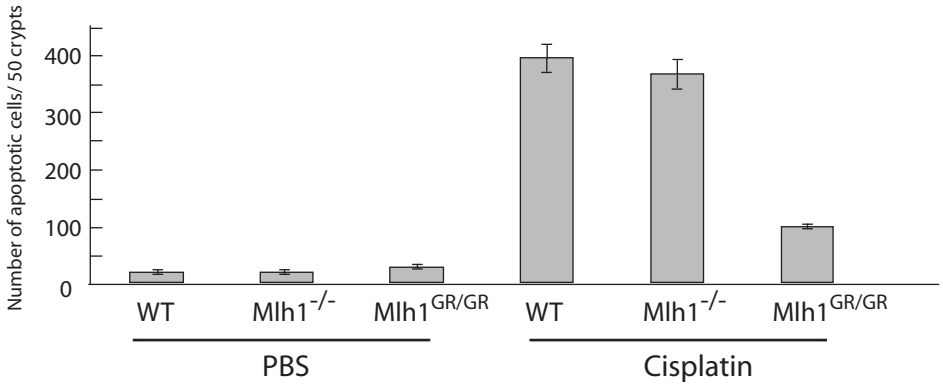
Number of apoptotic cells/ 50 crypts
0
100
200
300
400
WT
Mlh1-/-
Mlh1GR/GR
WT
Mlh1-/-
Mlh1GR/GR
PBS
Cisplatin

C

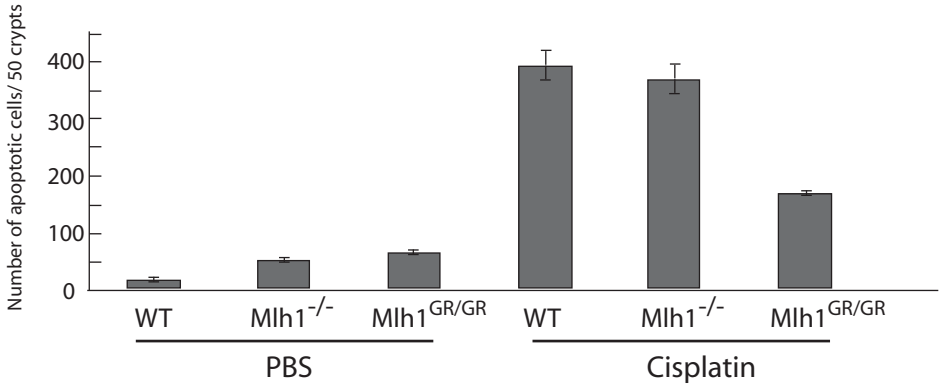
Number of apoptotic cells/ 50 crypts
0
100
200
300
400
WT
Mlh1-/-
Mlh1GR/GR
WT
Mlh1-/-
Mlh1GR/GR
PBS
Cisplatin

**Fig. 5**

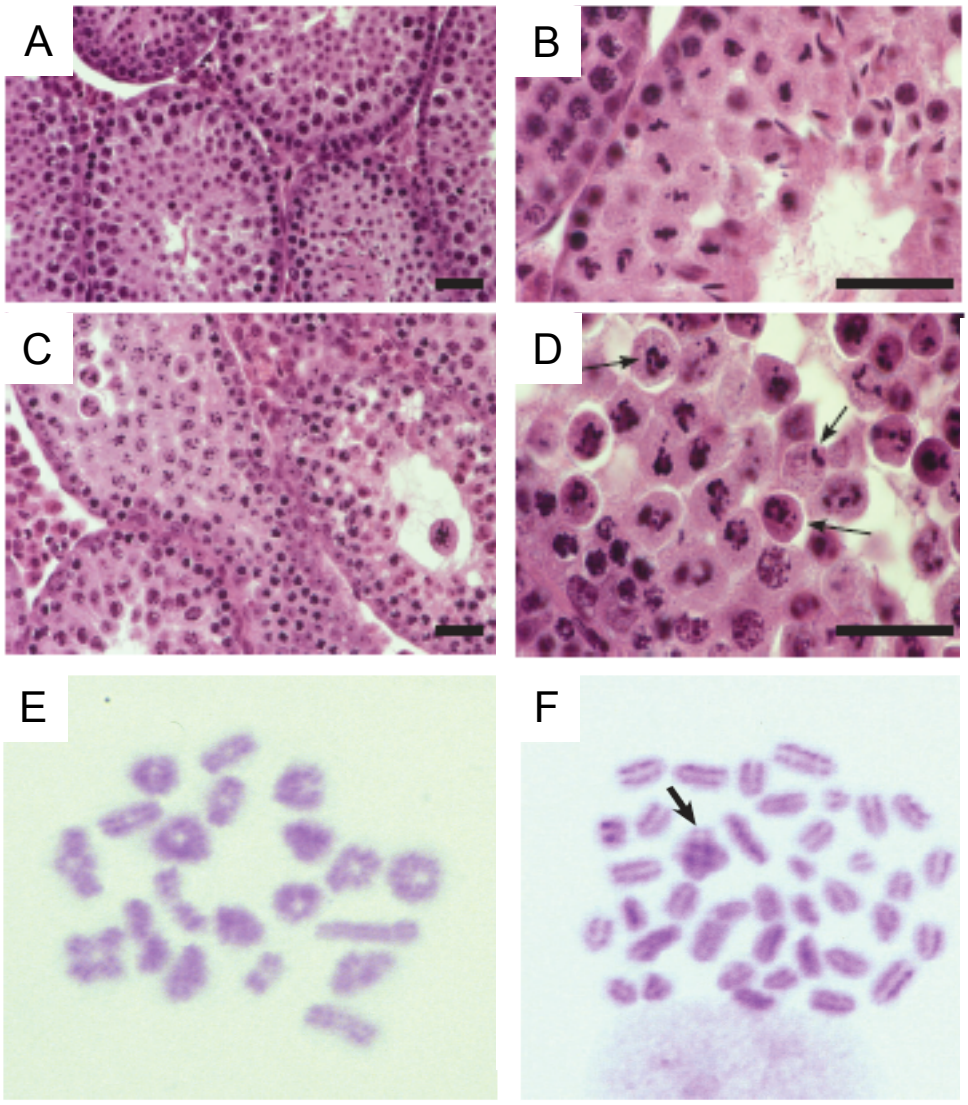

**Fig. 6**

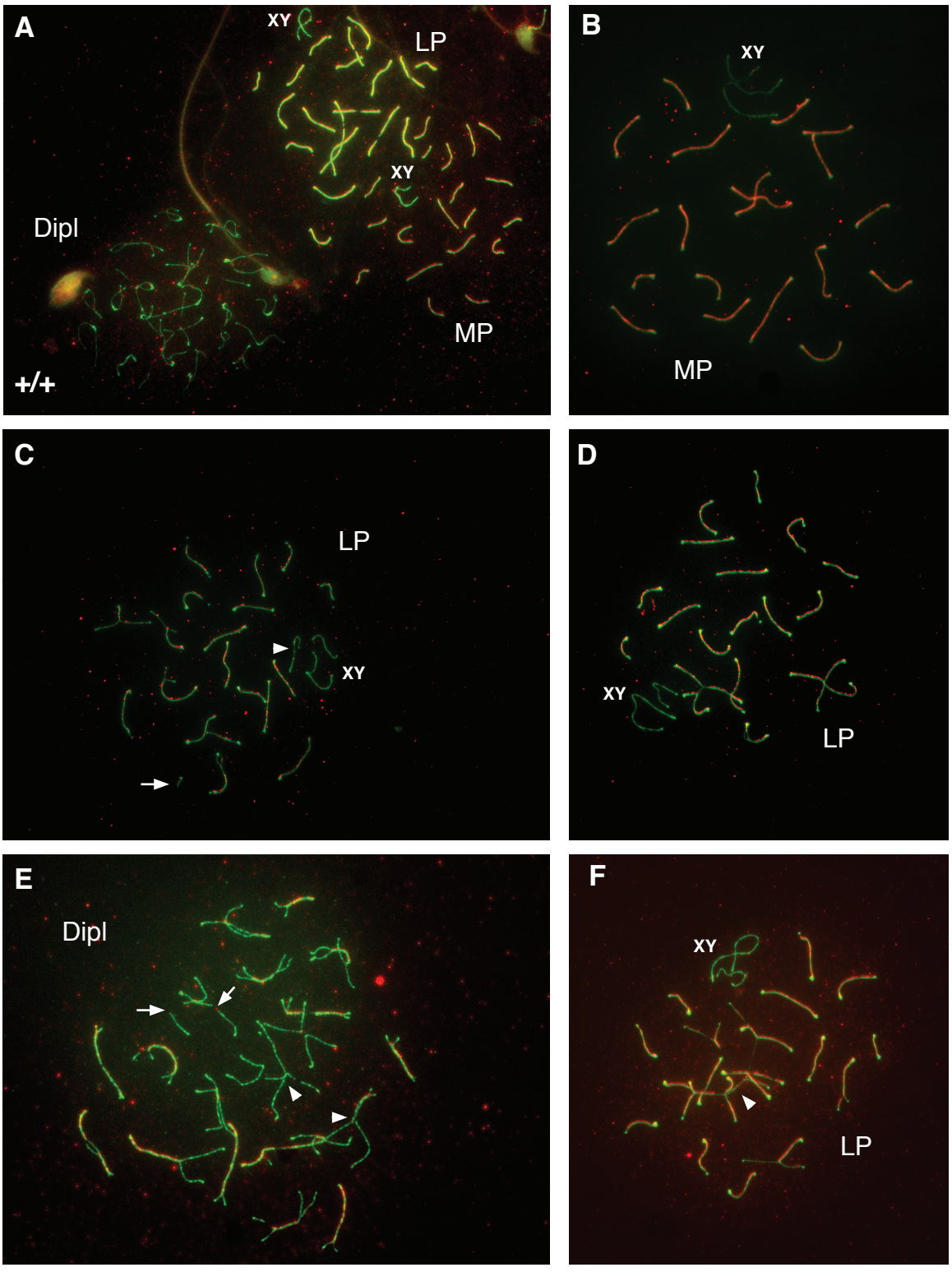

**Fig. 7**

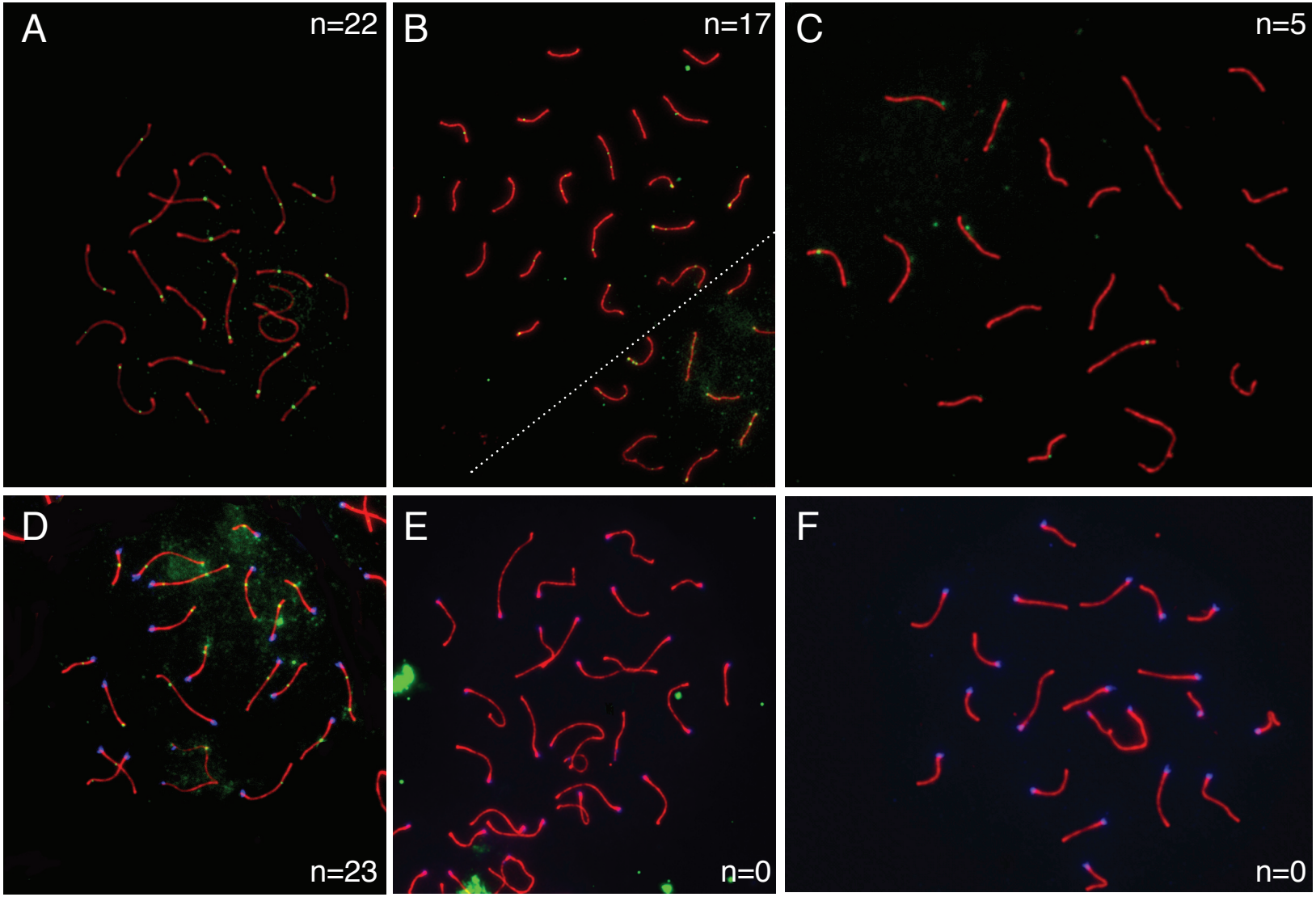

SI Figure 8

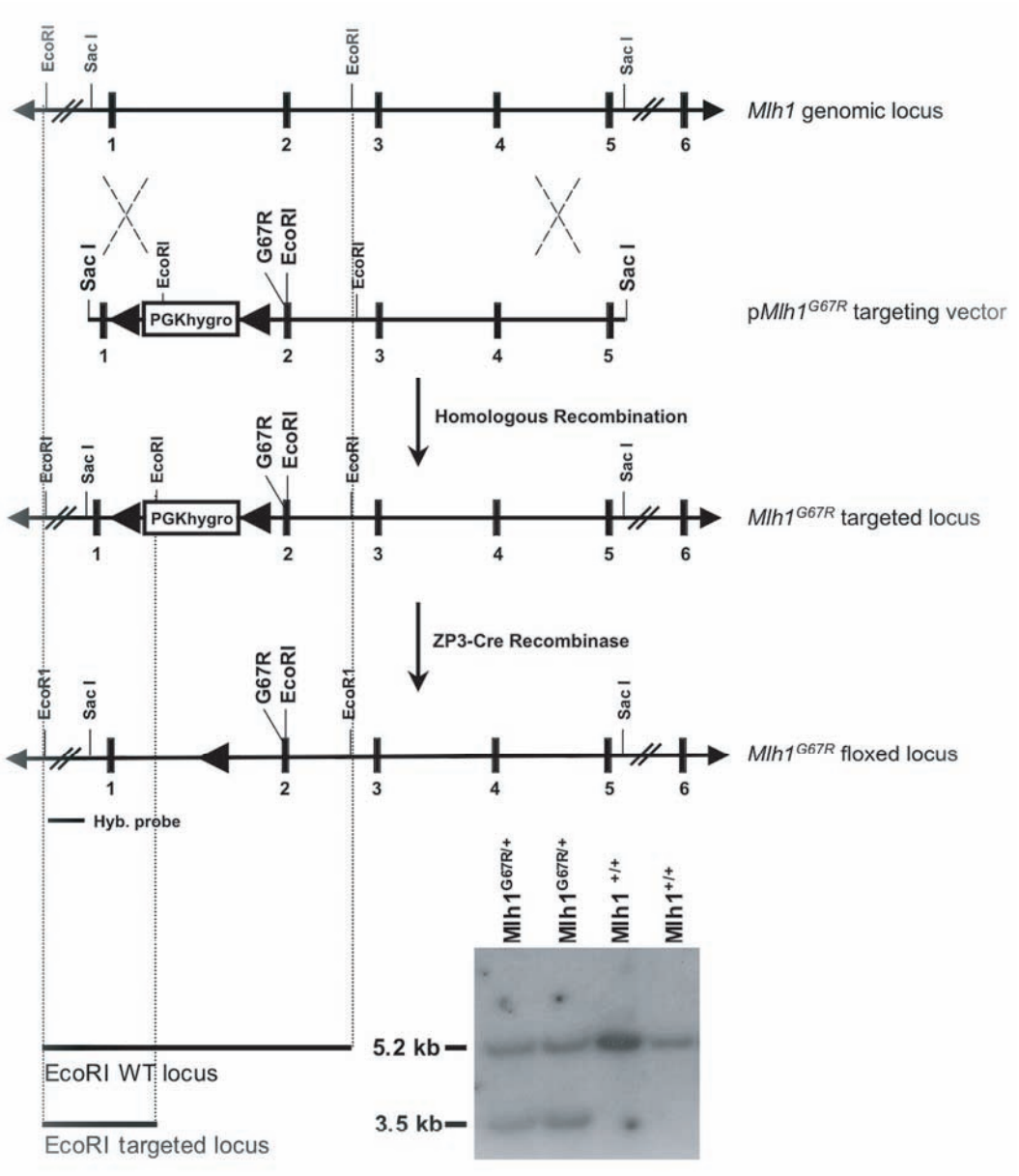
EcoRI
Sac I
EcoRI
Sac I
Mlh1 genomic locus
1
2
3
4
5
6
Sac I
EcoRI
G67R
EcoRI
EcoRI
Sac I
PGKhygro
pMlh1G67R targeting vector
Homologous Recombination
Mlh1G67R targeted locus
ZP3-Cre Recombinase
Mlh1G67R floxed locus
Hyb. probe
Mlh1G67R/+
Mlh1G67R/+
Mlh1 +/+
Mlh1+/+
5.2 kb
3.5 kb
EcoRI WT locus
EcoRI targeted locus

SI Figure 9

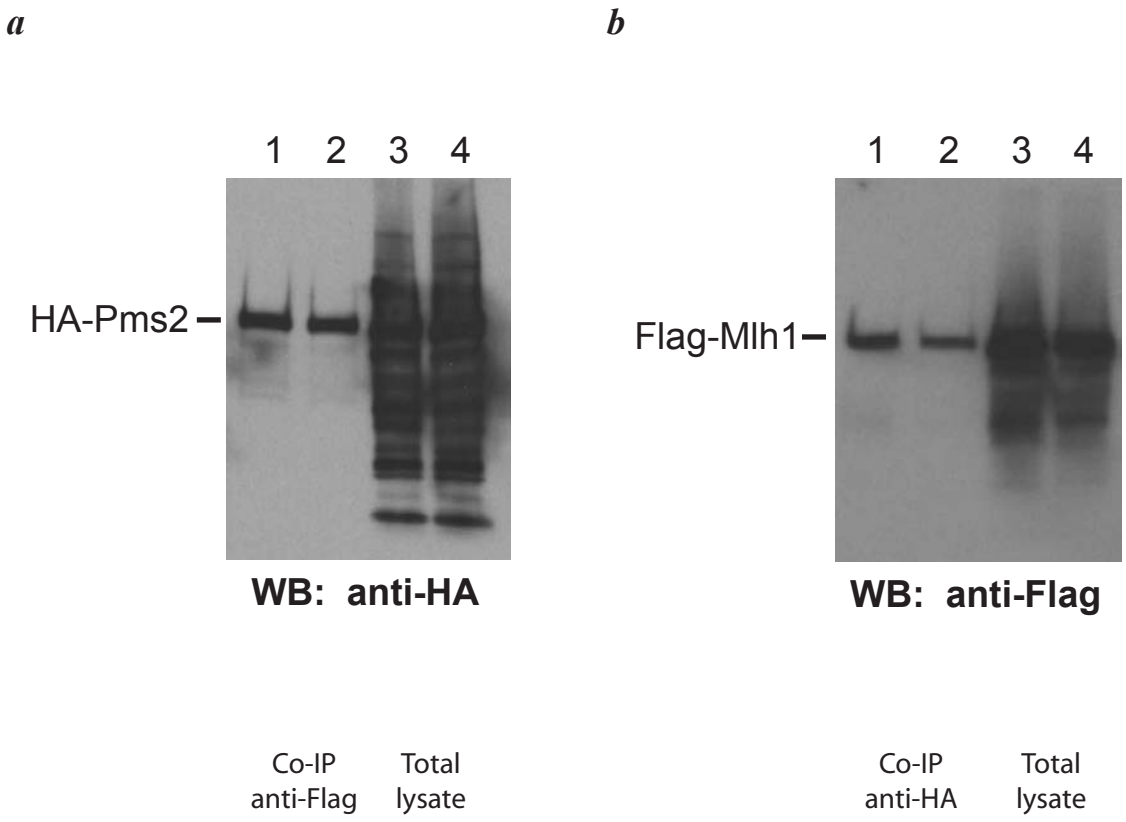
a
1 2 3 4
HA-Pms2
WB: anti-HA
Co-IP anti-Flag
Total lysate
b
1 2 3 4
Flag-Mlh1
WB: anti-Flag
Co-IP anti-HA
Total lysate

SI Figure 10

*a*

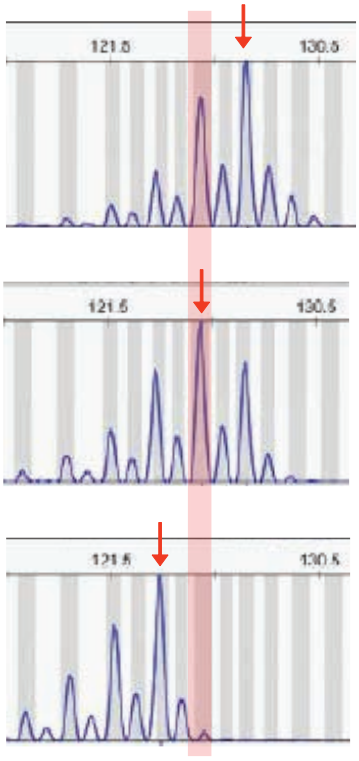


expansion

normal

contraction

*b*

| Genotype | Frequency | |
|---|---|---|
| WT | 6.6% (15/229) | |
| *Mlh1*$^{-/-}$ | 25.4% (48/189) | p<0.0001 (compared to WT) |
| *Mlh1*$^{GR/GR}$ | 21.9% (50/228) | p<0.0001 (compared to WT) |

*c*

| Genotype | Frequency | |
|---|---|---|
| WT | 4.2% (2/48) | |
| *Mlh1*$^{-/-}$ | 24.0% (23/96) | p<0.0001 (compared to WT) |
| *Mlh1*$^{GR/GR}$ | 23.4% (22/94) | p<0.0001 (compared to WT) |

SI Figure 11

***a***

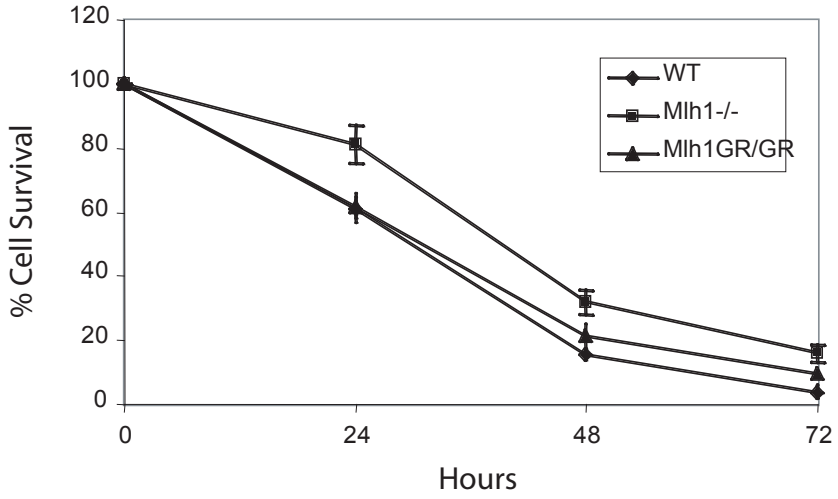


***b***

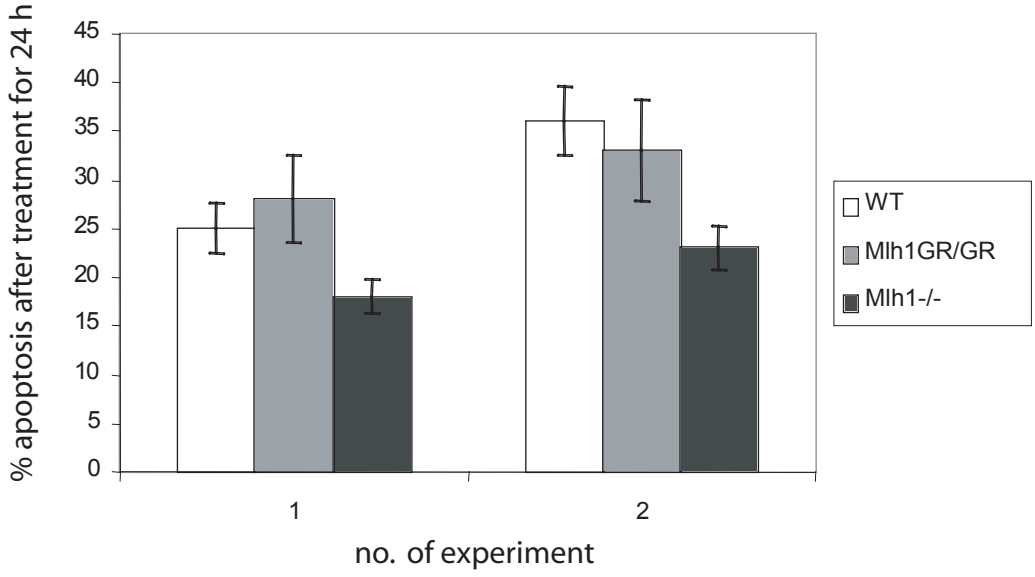

SI Figure 12

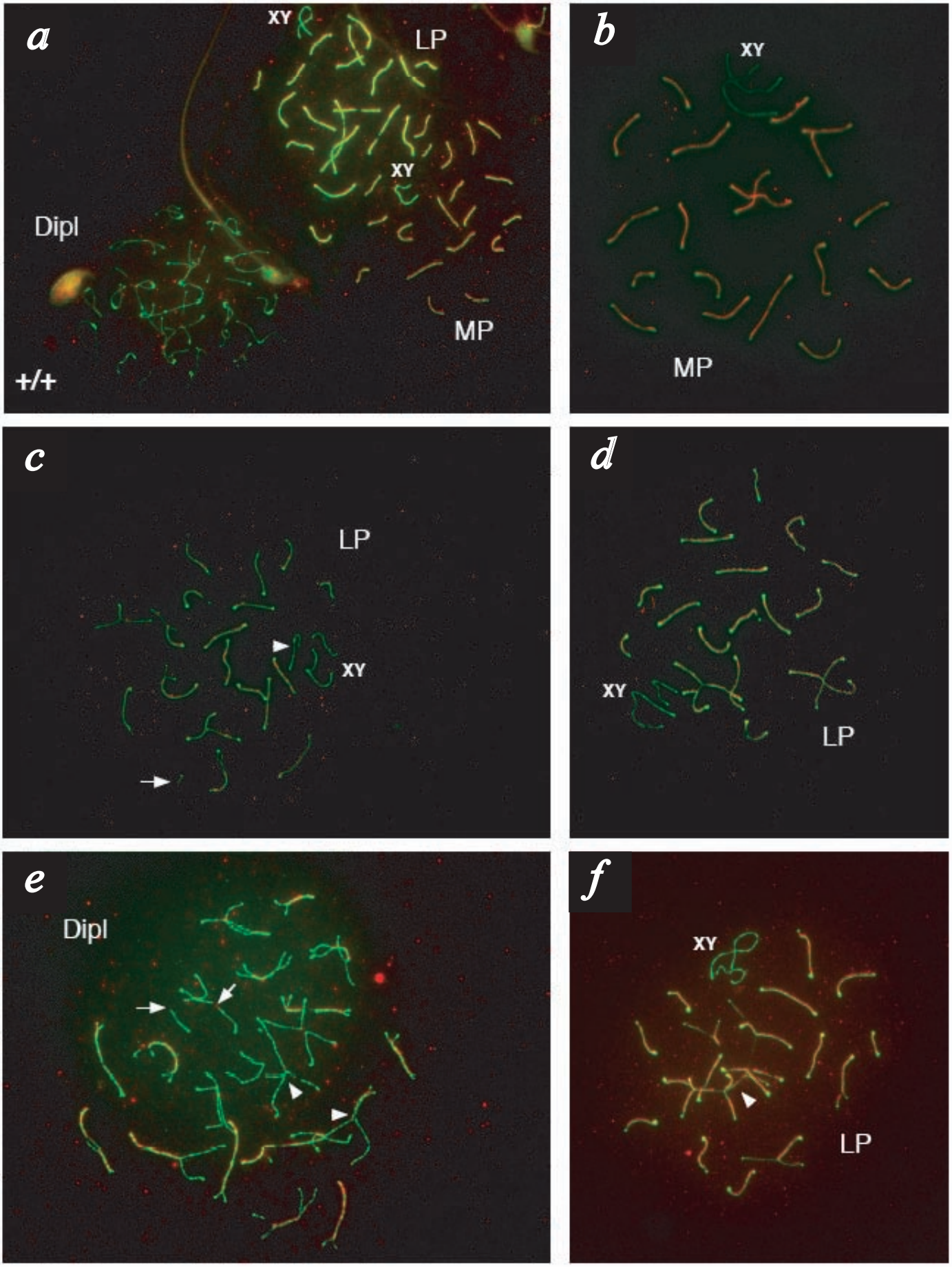

SI Figure 13

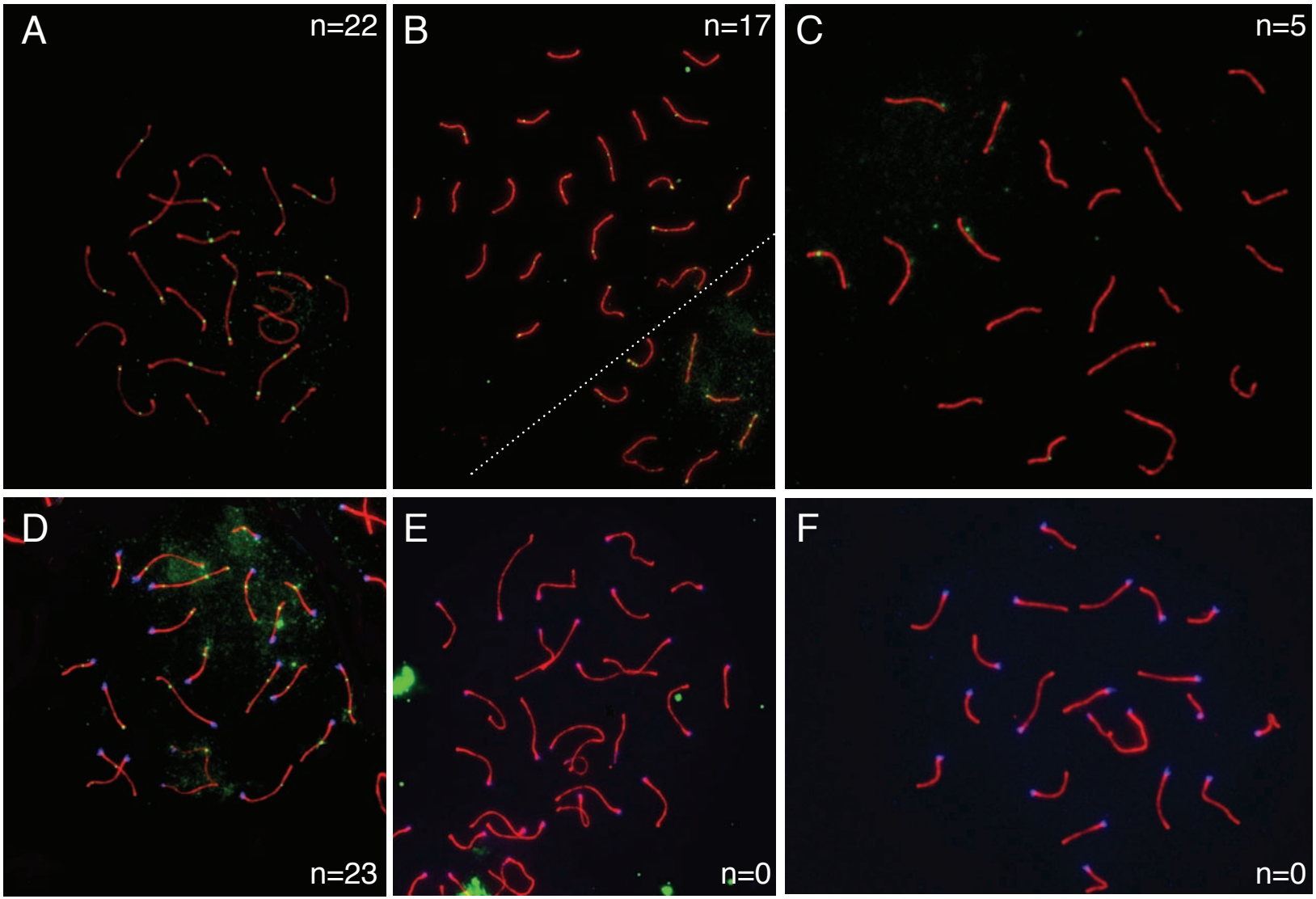

# Conditional inactivation of MLH1 in thymic and naïve T-cells in mice leads to a limited incidence of lymphoblastic T-cell lymphomas

Publiziert 2010 in. Leukemia and Lymphoma, 51(10):1875-86.

# Conditional inactivation of MLH1 in thymic and naïve T-cells in mice leads to a limited incidence of lymphoblastic T-cell lymphomas

Cora Reiss[1,2]*, Torsten Haneke[1], Hans-Ulrich Völker[3], Martin Spahn[5], Andreas Rosenwald[3], Winfried Edelmann[4] and Burkhard Kneitz[1,5]*

[1] Physiological Chemistry I, University of Würzburg, Germany; [2] Institute of Clinical Biochemistry and Pathobiochemistry, University of Würzburg, Germany; [3] Institute of Pathology, University of Würzburg; [4] Department of Cell Biology and Cancer Center, Albert Einstein College of Medicine, Bronx, NY 10461, [5] Department of Urology and Pediatric Urology, University of Würzburg; Germany

* To whom correspondence may be addressed to:

Cora Reiss: Institute of Clinical Biochemistry and Pathobiochemistry
Julius Maximilians University
D-97080 Würzburg, Germany
E-mail: reiss@klin-biochem.uni-wuerzburg.de
Tel: + 49 931 3183180

Burkhard Kneitz: Department of Urology
Medical School Julius Maximilians University
Oberdürrbacher Str. 8
D-97074 Würzburg, Germany
E-mail: kneitz_b@klinik.uni-wuerzburg.de
Tel: + 49 931 201 32700

Keywords: mismatch repair, MLH1, lymphoblastic T-cell lymphoma, conditional mouse model, lck-Cre

MLH1 deficiency in T-cell lymphomas

ABSTRACT:

Defects in the mismatch repair system (MMR) underlie hereditary non-polypsosis colorectal cancer (HNPCC)/Lynch syndrome and also a significant number of sporadic colorectal cancers. Mice carrying a null allele for the MMR gene *Mlh1* are preferentially prone to the development of lymphomas of B- and T-cell origin and to a lesser extent gastrointestinal tumors. Consistent with these findings in mice, MMR defects have also been observed in sporadic and hereditary hematological malignancies. To study the role of MLH1 for lymphomagenesis in more detail, we generated a new mouse model carrying a conditional *Mlh1* allele ($Mlh1^{flox/flox}$). Mating of these mice with *EIIa*-Cre recombinase transgenic mice allowed the constitutive inactivation of MLH1 and the resulting $Mlh1^{\Delta ex4/\Delta ex4}$ mouse line displays complete MMR deficiency and a cancer predisposition phenotype similar to $Mlh1^{-/-}$ mice. For T-cell specific MMR inactivation we combined the $Mlh1^{flox/flox}$ allele with the *Lck-Cre* Transgene. In the resulting $Mlh1^{T\Delta ex4/T\Delta ex4}$ mice, MLH1 inactivation is limited to DP/SP thymocytes and naïve peripheral T-cells. The development of T-cell lymphomas in $Mlh1^{T\Delta ex4/T\Delta ex4}$ mice is significantly reduced compared to $Mlh1^{-/-}$ mice implicating that MMR functions either at very early stages during T-cell development or even earlier in lymphoid precursor cells to suppress lymphomagenesis.

INTRODUCTION

Mutations in the human mismatch repair (MMR) genes are the major cause of hereditary nonpolyposis colorectal cancer (HNPCC)/Lynch syndrome [1; 2]. HNPCC/Lynch syndrome patients carry heterozygous germ line mutations in MMR genes and develop colorectal cancers and also various other types of cancers. Although hematological malignancies are not part of the typical tumor spectra of HNPCC/Lynch syndrome, they are common in patients with biallelic mutations in MMR genes indicating an important role of MMR in the suppression of lymphomagenesis [3]. Tumors with defective MMR acquire deletion and insertion mutations at a high frequency, particularly within microsatellite repeat sequences.

This molecular phenotype is referred to as microsatellite instability (MSI) [4]. In addition to HNPCC/Lynch syndrome, MSI has also been observed in a variety of sporadic cancers [5; 6] including hematopoetic malignancies such as chronic myeloid leukemia (CML), myelodysplastic syndrome (MDS), chronic lymphocytic leukemia (CLL), Burkitt's lymphoma and human immunodeficiency virus (HIV)-associated lymphomas [7; 8; 9]. Additionally, homozygous mutations of MMR genes are also correlated with neurofibromatosis type 1 (NF1) which causes an early onset of childhood T- or B-cell leukemias [10; 11]. The most frequently mutated genes in tumor patients with MMR defects are the MutS homologs MSH2 [12; 13], MSH6 [14] and the Mut L homolog MLH1 [2].

Recent studies on MLH1 deficient mice and cells demonstrate that MLH1 has at least three main functions. First, the mismatch repair function which protects mammalian genomes against genomic instability of the MIN type by repairing distinct DNA defects that result from erroneous DNA replication [15; 16]. Secondly, MLH1 mediates the DNA damage induced apoptosis as part of the cellular response to endogenous and exogenous agents [17; 18]. Thirdly, MLH1 also plays a role in reciprocal recombination events during meiosis and MLH1 deficient mice are sterile [19]. The tumor suppressor function of MLH1 was clearly demonstrated in MLH1 deficient mice that are characterized by an early and spontaneous onset of lymphomas and HNPCC/Lynch syndrome-like cancers [20; 21].

Here, we describe the first conditional MLH1 mouse line (*Mlh1*$^{flox}$) that permits the tissue specific modeling of MMR-defective tumorigenesis. Using this model we study at which stage of lymphocyte ontogeny to the loss of MMR function mediates transformation and what role the rate of cell divisions in these developing lymphocytes plays for MMR-dependent lymphomagenesis. For these studies, we generated a T-cell specific MLH1 deficient mouse line (*Mlh1*$^{T\Delta ex4/T\Delta ex4}$) by crossing *Mlh1*$^{flox}$ mice with mice expressing the Cre recombinase under the T-cell specific *Lck* promoter and analyzed the MLH1-dependent lymphomagenesis.

We show that the T-cell specific MLH1 deletion in double positive and single positive (DP/SP) thymocytes and naïve peripheral T-cells leads in only a very limited number of mice to the development of lymphoblastic lymphomas. Lymphoma incidences in these mice are strongly reduced compared to *Mlh1*$^{-/-}$ mice. This result indicates that loss of MMR function has to occur either at very early T-cell developmental stages or even earlier in lymphoid precursor cells to induce lymphomagenesis and might explain the limited incidences of hematological malignancies in HNPCC patients.

## MATERIAL AND METHODS

### Mice:

*Mlh1*$^{flox}$ mice were generated using a gene targeting approach. A 5.2-kb *Sac* genomic fragment containing *Mlh1* exons 2 to 6 derived from a 129SvEv BAC genomic DNA library was subcloned into pUC19. A single *NotI* side was inserted into intron 3 by site directed mutagenesis. Using this single *Not I* side a LoxP cassette was cloned into *Mlh1* intron 3 followed by the introduction of a loxP- PGKhygro- loxP selection cassette into *Mlh1* intron 4. The vector was linearized and transfected into WW6 embryonic cells as described previously [21]. Two correctly targeted ES cell clones were microinjected into blastocysts, generating highly chimeric mice, which transmitted the conditional *Mlh1* locus through their germ line. Chimeric male mice were bred to C57Bl/6J females to generate *Mlh1*$^{loxPhygro}$ F1 offspring. The PGKhygro cassette was subsequently deleted *in vivo* by crossing *Mlh1*$^{loxPhygro}$ heterozygotes with *Cre* expressing *EIIa* deleter mice [22]. Offspring from this crosses-breeding were genotyped by PCR and sequence analyses to confirm the integrity of the *Mlh1*$^{flox}$ allele.

Heterozygous *Mlh1*$^{lox/+}$ males and females of the F1 generation to generate homozygous *Mlh1*$^{flox/flox}$ mice. To generate Cre expressing *Mlh1*$^{flox/flox}$ mice homozygous *Mlh1*$^{flox/flox}$ mice were mated with two Cre expressing mouse lines. *Mlh1*$^{flox/flox}$ mice were crossed with EIIa-

Cre recombinase transgenic mice to obtain *Mlh1*$^{\Delta ex4/+}$ mice. Subsequent homozygous *Mlh1*$^{\Delta ex4/\Delta ex4}$ mice were generated by intercrossing heterozygous offspring. To generate *Mlh1*$^{T\Delta ex4/T\Delta ex4}$ mice, we mated *Mlh1*$^{flox/flox}$ mice with Lck-Cre recombinase transgenic mice. [23]. The resulting heterozygous *Mlh1*$^{T\Delta ex4/+}$ mice were interbred to produce *Mlh1*$^{T\Delta ex4/T\Delta ex4}$ mice.

The *Cre* expressing mouse lines were obtained from Jackson Lab, Bar Harbor, Maine, USA. The following mouse strains were used: B6.FVB-TgC5379Lmgd/J (EIIa-cre) and NOD.Cg-Tg548Jxm/AchJ (Lck-cre). The *Mlh1*$^{-/-}$ animals used in this study were generated by crossing *Mlh1* heterozygote males and females in order to generate homozygous, heterozygous, and wild-type mice as described previously [21]. All procedures were in accordance with Institutional Animal Care.

PCR Analysis

*Mlh1*$^{flox/floxP}$ mice genotyping was performed by PCR using two primers: P1 forward 5'-ggc-aag-cat-atg-tgg-c-3', and P2 reverse, 5'-gcc-aca-tgg-cct-tgc-c-3'. The primers amplified a 410 bp product in the absence of the LoxP site; in the presence of the LoxP site a 600 bp product.

The presence of the *Cre*-recombinase gene was detected using the primers pmc-cre2: 5'-ggc-att-tct-ggg-gat-tgc-3' and pmc-cre3: 5'-cag-acc-agg-cca-ggt-atc-tc-3'.

The detection of the *Mlh1* Δexon4 locus was performed by PCR using two primers: P1 forward primer and P3 reverse, 5'-tca-ggc-ctc-tca-ggg-tac-cag-3'. The primers amplified a 750 bp product for the *Mlh1* genomic locus and a 350 bp product for the Δexon4 locus.

Western Blot Analysis

Thymocyte cell extracts (50 μg of protein) were separated on 10% SDS/PAGE gels. The proteins were transferred onto Protran membranes (Whatmann), and the membranes were incubated either with rabbit polyclonal antibodies directed against MLH1 (AB 9144; Abcam) or MSH2 (PharMingen) as a loading control.

RNA Isolation and RT-PCR

Total RNA was isolated from cells using TRIzol Reagent (Invitrogen, Karlsruhe, Germany) and converted to first-strand cDNA using the ImProm-II™ Reverse Transcription System (Promega, Mannheim, Germany) before amplification with specific primers. The resulting PCR products were resolved on 0,9% agarose gels. The primer pairs used for amplification were the following:*Mlh1* cEx2 (forward), 5'-atg-gca-ctg-gaa-tca-gga-ag-3', *Mlh1* cEx5 (reverse), 5'-gtt-gcc-tgc-aca-ggg-ttt-ag-3' and *Gapdh* (forward), 5'-cgg-agt-caa-cgg-att-tgg-tcg-tat -3'; *Gapdh* (reverse), 5'-agc-ctt-ctc-cat-ggt-ggt-gaa-gac-3'

Real Time PCR

Real-time RT-PCR was conducted in an ABI 7300 Real-Time System in a final volume of 20 µl. The reaction mix contained 0,25 mM of dNTPs; 3 U Taq polymerase, primers at a concentration of 10 pM each, 1*Sybr Green mix (Thermo scientific) as well as 100 ng of cDNA. Standard PCR program was carried out with 40 cycles of denaturation at 95°C for 15 sec, followed by annealing (58°C) and elongation (72°C) for 30 sec. The following primers were used for amplification:

*Hprt* forward, 5'-tgt-tgt-tgg-ata-tgc-cct-tg-3'and reverse, 5'-act-ggc-aac-atc-aac-agg-act-3' ; *Cre* forward, 5'-cga-acg-cac-tga-ttt-cga-c-3' and reverse, 5'-ggc-aac-acc-att-ttt-tct-gac-3'; *Mlh1* forward, 5'-atg-tgg-ccc-atg-tca-cta-tt-3' and reverse, 5'-aaa-aag-gtc-ttc-cac-cgt-ga-3'. Differences in cDNA concentrations were adjusted by normalizing to *Hprt*.

Microsatellite Instability (MSI) in Tumors

Mutations in microsatellite sequences were assayed by PCR in tumor DNA and nontumor DNA as control. DNA was isolated using the DNeasy tissue Kit (Quiagen, Hilden, Germany). Cycling reactions were performed with five end-Cy5-labeled primers: three mononucleotide markers (*U12235*, *Aa006036* and *L24372*) and two dinucleotide markers (*D7Mit91* and *D17Mit123*). The analysis of the markers was performed using a single round of amplification: 30 cycles of 95°C for 30 s, 60°C for 1 min and 72°C for 2 min. The PCR products were separated by electrophoresis on denaturing acrylamide gels (Amersham

Bioscience, Freiburg, Germany) and autoradiographed for analysis. The results were analyzed using DNA Fragment Manager V 1.1 (Amersham Pharmacia Biotech, Freiburg, Germany)

Isolation of DN and DP Thymocytes

$5*10^6$ thymocytes were magnetically labeled with MACS CD4 and CD8 micro beads and separated with MACS LD columns (Milteny Biotec, Bergisch Gladbach, Germany) using the manufactures protocol.

Statistics

Statistical evaluation was performed with SPSS (V12) using the log rank and t-test.

RESULTS

Generation of *Mlh1*$^{loxPhygro}$ Mice

To address the role of MLH1 in the development of tissue specific tumors, we generated mice harboring a conditional knockout allele for *Mlh1*. Using a gene targeting strategy we flanked the *Mlh1* exon 4 encoding functional parts of the ATPase domain with loxP sites (Figure 1A). Homozygous mutant *Mlh1*$^{loxPhygro}$ mice were born according to a normal Mendelian ratio. Genotyping of the offspring was performed by PCR using two primers flanking the additional 3 prime LoxP site (Figure 1B). To confirm the targeting event in the *Mlh1*$^{loxPhygro}$ mouse line, we sequenced the *Mlh1* intron 3 of these mice. The sequence analysis revealed that the 3' LoxP site was located at the expected locus (Supplemental Figure1). Homozygous *Mlh1*$^{loxPhygro}$ mice displayed no developmental abnormalities, were fertile in both genders and showed no tumor predisposition phenotype.

Cre Mediated Inactivation of MLH1 in *EIIa-Cre Mlh1*$^{LoxPhygro}$ Mice

To remove the selection marker and to generate a knockout allele for MLH1, *Mlh1*$^{loxPhygro}$ mice were crossed with *EIIa-Cre* transgenic mice that express the *Cre* recombinase gene under the control of the adenoviral *EIIa* promotor. This causes a robust *Cre* expression in early mouse embryos from the zygote stage on. The offspring of this breeding were used to

generate *Mlh1*$^{flox/flox}$ mice in which the hygromycin cassette was removed; these mice were viable, fertile and showed none of the phenotypes seen in *Mlh1*$^{-/-}$ mice (Table I). Additionally, we generated mice containing the *Mlh1* exon 4 deletion allele (*Mlh1*$^{\Delta ex4/\Delta ex4}$) (Figure 2A). PCR analysis using two primers flanking exon 4 of the *Mlh1* gene revealed that the PCR product in *Mlh1*$^{\Delta ex4/\Delta ex4}$ mice is about 400bp smaller than the PCR product in *Mlh1*$^{+/+}$ mice, indicating an efficient deletion of *Mlh1* exon 4 (Figure 2B). Western blot analysis of thymocyte cell extracts derived from *Mlh1*$^{\Delta ex4/\Delta ex4}$ cells showed that the MLH1 protein was efficiently deleted by the Cre-mediated recombination of the floxed *Mlh1* locus (Figure 2C). *Mlh1*$^{\Delta ex4/\Delta ex4}$ mice were born according to normal Mendelian ratio. Mating of female or male *Mlh1*$^{\Delta ex4/\Delta ex4}$ mice with *Mlh1*$^{+/+}$ mice of the opposite gender yielded no offspring, indicating that homozygous *Mlh1*$^{\Delta ex4/\Delta ex4}$ mice were infertile in both genders.

Survival, Tumor Development and Microsatellite Instability in *Mlh1*$^{\Delta ex4/\Delta ex4}$ Mice

To confirm that the *Mlh1*$^{\Delta ex4}$ allele encoded a true null allele we analyzed the tumor phenotype of *Mlh1*$^{\Delta ex4/\Delta ex4}$ mice and compared it to the tumor phenotype of *Mlh1*$^{-/-}$mice. Cohorts of *Mlh1*$^{-/-}$, *Mlh1*$^{flox/flox}$ and *Mlh1*$^{\Delta ex4/\Delta ex4}$ mice were monitored for a period of 80 weeks with regard to their survival and cancer susceptibility. Although the survival of *Mlh1*$^{\Delta ex4/\Delta ex4}$ and *Mlh1*$^{-/-}$ mice did not differ significantly (p= 0,224, log-rank test; Figure 3A), it was significantly reduced compared to the *Mlh1*$^{flox/flox}$ littermates (p< 0.01, log-rank test; Figure 3A). This reduced overall survival of *Mlh1*$^{\Delta ex4/\Delta ex4}$ mice was caused by an increased cancer predisposition. Most of the *Mlh1*$^{\Delta ex4/\Delta ex4}$ animals developed lymphomas (51%), a smaller number of animals developed gastrointestinal adenocarcinomas (29%) and two animals (6%) developed both lymphoma and gastrointestinal adenocarcinoma within 80 weeks of life. Four of the *Mlh1*$^{\Delta ex4/\Delta ex4}$ mice died without any obvious cancer phenotype (Supplemental Table I). The tumor incidences of the *Mlh1*$^{\Delta ex4/\Delta ex4}$ mice were very similar to those seen in the *Mlh1*$^{-/-}$ mice (p=0,373; t-Test).

To characterize the MMR defect caused by the deletion of exon 4 we studied the MSI phenotype in intestinal and lymphatic tumors from *Mlh1*$^{\Delta ex4/\Delta ex4}$ and *Mlh1*$^{-/-}$ mice. Genomic DNA from tumor and non-tumor tissue was analyzed using a panel of five different microsatellite markers (two dinucleotide markers *D17Mit132* and *D7Mit9;1* three mononucleotide markers *U12235*, *Aa006036* and *L24372*). This analysis showed that 70% (12 of 17) of *Mlh1*$^{\Delta ex4/\Delta ex4}$ tumors and 80% (25 of 32) of *Mlh1*$^{-/-}$ tumors displayed an MSI high phenotype with two or more microsatellites being unstable (Figure 3D).

From these results we concluded that the Cre mediated recombination of the floxed *Mlh1* locus leads to an *Mlh1* null allele causing a tumor predisposition phenotype comparable to the phenotype observed in *Mlh1*$^{-/-}$ mice.

Lck-Cre Mediated Inactivation of MLH1 in T-cells of *Mlh1*$^{T\Delta ex4/T\Delta ex4}$ Mice

To more precisely investigate the tumor suppressor function of MLH1 during T-cell development, we deleted MLH1 specifically in T-cells. Homozygous *Mlh1*$^{flox/flox}$ mice were bred with Lck-Cre recombinase transgenic mice to generate T-cell specific MLH1-deficient mice (*Mlh1*$^{T\Delta ex4/T\Delta ex4}$). In order to determine whether the Cre-mediated recombination of the *Mlh1* locus had indeed occurred specifically in thymocytes, thymic and intestinal DNA from *Mlh1*$^{\Delta ex4/\Delta ex4}$, *Mlh1*$^{T\Delta ex4/T\Delta ex4}$ and *Mlh1*$^{+/+}$ mice were screened for the Δexon4 locus using the PCR method described above. Figure 2B shows the occurrence of the deletion of exon 4 in thymocyte as well as intestinal DNA derived from *Mlh1*$^{\Delta ex4/\Delta ex4}$ mice, whereas the Δexon4 locus is only present in thymocytes of *Mlh1*$^{T\Delta ex4/T\Delta ex4}$ mice. Furthermore, Western blot analyses (Figure 2C), showed that the excision of exon 4 of the *Mlh1* gene leads to the loss of MLH1 protein with high efficiency in thymocytes. These results confirm that a complete Cre-mediated excision of the floxed *Mlh1* allele had occurred in *Mlh1*$^{T\Delta ex4/T\Delta ex4}$ thymocytes.

Using these T-cell specific MLH1 deficient *Mlh1*$^{T\Delta ex4/T\Delta ex4}$ mice, we also examined whether the loss of MLH1 functions such as DNA repair and damage response, affects T-cell development and the intrinsic maintenance of peripheral T-cells. The number of nucleated

cells in lymphoid organs such as thymus, spleen, and lymph nodes in healthy three months old *Mlh1*$^{T\Delta ex4/T\Delta ex4}$ mice were the same as those in *Mlh1*$^{+/+}$ mice. Flow-cytometric analysis of these organs revealed that the CD3-positive T-cell population and CD4/CD8 ratios in T-cells of *Mlh1*$^{T\Delta ex4/T\Delta ex4}$ mice were not altered compared to *Mlh1*$^{+/+}$ mice (data not shown). These results indicate that MLH1 functions are not critically involved in development and maintenance of T-cells.

Lymphomagenesis in *Mlh1*$^{T\Delta ex4/T\Delta ex4}$ Mice

To clarify whether the T-cell specific loss of MLH1 in *Mlh1*$^{T\Delta ex4/T\Delta ex4}$ mice leads to the development of T-cell lymphomas, we monitored cohorts of *Mlh1*$^{flox/flox}$, *Mlh1*$^{-/-}$, *Mlh1*$^{\Delta ex4/\Delta ex4}$ and *Mlh1*$^{T\Delta ex4/T\Delta ex4}$ mice up to 40 weeks of age with regard to their survival and cancer susceptibility. *Mlh1*$^{-/-}$ mice developed preferentially B and T-cell lymphomas (43%) in the first 40 weeks of life while older mice were also prone to gastrointestinal tumors. None of the *Mlh1*$^{flox/flox}$ control mice developed lymphoma or any other type of tumors over this period of time (Table I; Figure 3B). Only 6% (4 of 65) of the *Mlh1*$^{T\Delta ex4/T\Delta ex4}$ mice developed lymphomas, indicating that the T-cell specific deletion of MLH1 leads only in rare cases to lymphomagenesis in mice. This very low incidence of T-cell lymphoma was significantly different to the lymphoma incidences observed in the cohort of *Mlh1*$^{-/-}$ mice, in which 26% of mice developed lymphoma in the same period of time ($p>0,001$) (Table I; Figure 3C). H&E staining and histopathological analysis revealed that the majority of tumors were lymphoblastic lymphomas (94.6% of tumors) characterized by monotonous sheets of poorly differentiated lymphoid cells with enlarged nuclei, reduced cytoplasm, numerous mitotic figures and a "starry sky" appearance (data not shown). To further characterize the tumors arising in *Mlh1*$^{T\Delta ex4/T\Delta ex4}$ and *Mlh1*$^{-/-}$ mice we immunophenotyped the lymphomas by FACS analysis. All *Mlh1*$^{T\Delta ex4/T\Delta ex4}$ lymphomas were immunophenotyped as T-cell lymphomas using T- and B-cell specific antibodies. The majority of the lymphomas in *Mlh1*$^{T\Delta ex4/T\Delta ex4}$ mice (3 out of 4) could be classified as double positive T-cell lymphomas by the expression of the αβ

T cell receptor (TCRαβ) and both coreceptors CD4 and CD8. Only one lymphoma was classified as double negative T-cell lymphoma (Supplemental Table II). The prevalence of DP T-cell lymphomas was not observed in *Mlh1*$^{-/-}$ mice. *Mlh1*$^{-/-}$ mice developed B- and T-cell lymphomas. T-cell lymphomas (TCRαβ$^{+}$CD45R$^{-}$) of *Mlh1*$^{-/-}$ mice showed a distribution of several immunophenotypes: CD4$^{+}$ or CD8$^{+}$ single positive (SP), CD4/CD8 double positive (DP) and CD4/CD8 double negative (DN).

Although the lymphoma incidences observed in *Mlh1*$^{T\Delta ex4/T\Delta ex4}$ mice were significantly reduced, the onset of lymphoma progression remained unaffected (Figure 3C) as indicated by the Kaplan Meier estimates. The survival of *Mlh1*$^{T\Delta ex4/T\Delta ex4}$, *Mlh1*$^{\Delta ex4/\Delta ex4}$ *and Mlh1*$^{-/-}$ lymphoma mice showed no significant differences in this time period (p=0,291; log-rank test). To determine whether the tumorigenesis observed in *Mlh1*$^{T\Delta ex4/T\Delta ex4}$ is caused by MMR defects similar to *Mlh1*$^{\Delta ex4/\Delta ex4}$ and *Mlh1*$^{-/-}$ mice, the MSI status of the available lymphatic tumors from *Mlh1*$^{T\Delta ex4/T\Delta ex4}$ mice were analyzed as described above. This analysis showed that 3 of 4 (75%) of *Mlh1*$^{T\Delta ex4/T\Delta ex4}$ tumors displayed MSI. As expected from previous studies [21], the majority (79%) of *Mlh1*$^{-/-}$ tumors displayed a MSI high phenotype (Figure 3D).

Deletion of MLH1 is Completed in DP Thymocytes of *Mlh1*$^{T\Delta ex4/T\Delta ex4}$ Mice

In order to further clarify the time point of *Mlh1* deletion in thymocyte development, whole cell lysates of thymocytes at different stages of development were sub-fractioned and analyzed for the Δexon 4 locus by RT-PCR. The major stages of T-cell development in the thymus can be delineated by the expression of CD4, CD8, and TCRαβ, which define the TCRαβ$^{-}$CD4$^{-}$CD8$^{-}$ double negative, TCRαβ$^{+}$ CD4$^{+}$CD8$^{+}$ double-positive, CD4$^{+}$ or CD8$^{+}$ single-positive, and CD4$^{-}$CD8$^{-}$TCRγδ$^{+}$ subsets. After the maturation and differentiation steps are completed, SP thymocytes emigrate from the thymus to peripheral lymphoid organs as naïve T-cells. Therefore we separated DN and DP plus SP thymocytes out of thymi as well as naïve peripheral T-cells derived from *Mlh1*$^{T\Delta ex4/T\Delta ex4}$ mice (Figure 4A). RT-PCR analysis using two primers flanking exon 4 of the *Mlh1* transcript showed a high efficiency (80%) of

Cre mediated deletion of exon 4 in whole mount thymocytes of *Mlh1*$^{T\Delta ex4/T\Delta ex4}$ mice. Deletion was completed in >50% of immature DN cells, and nondeleted alleles were hardly detectable by PCR in DP/SP thymocytes. Deletion was also completed in >90% of peripheral T-cells from *Mlh1*$^{T\Delta ex4/T\Delta ex4}$ mice. Both RT-PCR products present in DN thymocytes were sequenced. Sequence alignment revealed that the shortened PCR product was a result of the excision of exon 4 (Supplementary Figure 2). Real time PCR analysis confirmed these variations at the level of *Mlh1* expression in thymocyte subpopulations (Figure 5A). We examined *Mlh1*$^{T\Delta ex4/T\Delta ex4}$ and *Mlh1*$^{+/+}$ thymocyte subpopulations with regard to their *Mlh1* and *Cre* expression status. The analysis revealed that *Mlh1*$^{+/+}$ thymocyte subpopulations showed a constant level of *Mlh1* transcript. *Mlh1* mRNA expression is highly significantly downregulated in all *Mlh1*$^{T\Delta ex4/T\Delta ex4}$ thymocyte subpopulations as compared to *Mlh1*$^{+/+}$ control populations (p>0,001; t-test). However *Mlh1*$^{T\Delta ex4/T\Delta ex4}$ DN thymocytes showed significantly higher *Mlh1* expression (p=0,031; t-test) compared to *Mlh1*$^{T\Delta ex4/T\Delta ex4}$ DP plus SP thymocytes indicating an incomplete deletion of MLH1 in this thymic subpopulation (Figure 5A). Next we associated the *Mlh1* expression in *Mlh1*$^{T\Delta ex4/T\Delta ex4}$ DP/SP thymocyte subpopulations with their Cre expression. As expected, DP/SP thymocyte subpopulations showed a strong Cre expression. In contrast DN thymocytes, which were characterized by an incomplete MLH1 deletion, showed a significantly reduced expression of *Cre* (p<0,001; paired t-test) (Figure 5B). Thus, the targeted deletion of *Mlh1* occurred in association to the expression of the *Cre* recombinase gene driven by the *lck* promoter. In summary, this data indicate that the highly efficient Cre mediated deletion of *Mlh1* exon 4 possibly begins at the DN cells stage and is almost completed in the DP stage of thymocyte development.

## DISCUSSION

### Generation of Conditional *Mlh1* Mice

Mutations in the human DNA mismatch repair (MMR) gene MLH1 are associated with hereditary non-polyposis colorectal cancer (Lynch syndrome, HNPCC) and a significant proportion of sporadic cancer [24]. The inactivation of MLH1 results in the accumulation of somatic mutations in the genome of tumor cells [25] and this mutator phenotype is characterized by widespread microsatellite instability in the hereditary non-polyposis colorectal cancer syndrome. Nevertheless MMR genes are expressed in all mitoticly active tissues and MMR mediated cancer development is found in a large variety of sporadic cancers [5; 6; 26]. To study the impact of MLH1 for tumor development and meiosis, mice carrying a null or a G67R mutant *Mlh1* allele were previously generated. Both mutant mouse lines showed that *Mlh1* has distinct functions in meiotic recombination, mismatch repair, and DNA damage response [21]. To avoid overlaying effects of tumorigenesis in different organ systems we generated a conditional MLH1 mouse line. The resulting $Mlh1^{\text{flox/flox}}$ mice showed no tumor predisposition or infertility and can therefore be used to study tissue-specific MMR-dependent tumorigenesis or infertility. To confirm that Cre mediated deletion of exon 4, located in the ATP binding side of the *Mlh1* gene, leads to the loss of MLH1 function, we mated $Mlh1^{LoxP/\text{LoxP}}$ mice with the deleter mouse line *EIIa-Cre*. Similar to $Mlh1^{-/-}$ mice, the resulting $Mlh1^{\Delta\text{ex4}/\Delta\text{ex4}}$ mice were characterized by a strong cancer predisposition phenotype. In addition the $\text{MLH1}^{\Delta ex4}$ mutation caused a meiotic defect that resulted in male and female sterility. From these results we concluded that EIIa mediated Cre expression in $Mlh1^{\text{flox/flox}}$ mice leads to an efficient deletion of exon 4 resulting in a phenotype very similar to the phenotype in MLH1-deficient mice.

T-cell Lymphomagenesis Caused by MLH1 Deficiency

Evidence for the impact of MMR-deficiency on lymphomagenesis was previously found in different MMR knockout mouse models and in humans [10; 11; 21; 27]. We and others have shown that MLH1 deficient mice spontaneously develop lymphomas of B- and T-cell origin [20; 21]. In MLH1 deficient mice the onset of lymphomas begins at three months of age and

the 50% survival time is approximately nine months. The spontaneous tumor spectrum of *Mlh1*$^{-/-}$ mice has been altered by breeding these mice with *Apc*$^{+/-}$/Min mice, resulting in an increased intestinal tumor incidence, intestinal tumor multiplicity per animal, and reduced survival [20]. In contrast, MMR deficient mice exposed to genotoxic agents show an accelerated onset of lymphomagenesis with dramatically increased incidence [28]. These results support the idea that in the constitutive absence of mismatch repair, mice are prone to develop predominantly hematological malignancies that are either spontaneous or induced. Furthermore, MSH2 deficient thymic lymphomas represent a single histopathological entity of lymphoblastic T-cell lymphomas characterized by a starry sky appearance, enlarged nuclei, reduced cytoplasm, and numerous mitotic figures [20; 27]. We could confirm that T-cell lymphomas arising in MLH1 deficient mice represent a very similar phenotype of lymphoblastic T-cell lymphomas. This homogeneity of MMR defective lymphomas suggests that specific recurring genetic events, which might take place at an early maturation step in intrathymic T-cell development, underlie the lymphocyte transformation. Data from two previous studies indicate that the mismatch repair function is critical in preventing the development of lymphoblastic lymphoma arising from very early lymphocyte precursors [29; 30]. These studies support a role for MMR in maintaining the genomic integrity of very early lymphocytes precursors. By analogy, this situation also applies to T-cell development, wherein thymic lymphomas have been observed to arise at high rates in various MMR deficient backgrounds. Nevertheless it is unknown, whether the mechanism of transformation is similar between thymocytes and pro/pre B-cells.

T-cell Lymphomagenesis is Limited in *Mlh1*$^{T\Delta ex4/T\Delta ex4}$ Mice

Based on the finding that lymphomas in MMR deficient mice uniformly develop from early T-cells we hypothesized that loss of MMR activity at later stages of T-cell development may not play a major role for the induction of lymphomagenesis. This hypothesis was confirmed by the observation that *Mlh1*$^{T\Delta ex4/T\Delta ex4}$ mice displayed a strongly reduced T-cell lymphoma

development compared to *Mlh1*$^{-/-}$ or *Mlh1*$^{\Delta ex4/\Delta ex4}$mice. We could further show that the highly limited development of T-cell lymphomas might depend on the time point of Lck driven Cre activity in developing T-cells. Shimizu and colleges reported recently that Lck expression in DN thymocytes is significantly lower than in DP and SP thymocytes in *plckGFPTg* mice [31]. Consistent with this finding, our analysis revealed that Lck-*Cre* driven deletion of *Mlh1* exon 4 is less efficient in DN compared to DP/SP thymocytes. From these results we concluded that MMR mediated suppression of lymphomagenesis is specifically important before or at the time point of the transition from DN to DP thymocytes. Due to the function of MMR in the repair of replication errors in mitotic cells, it was suggested that the prevalence of lymphoblastic lymphomas in MMR defective mice depends on the high mitotic proliferation rate of developing lymphocytes and on the accumulation of mutations in key downstream genes. It was previously shown that MSH2 deficient mice uniformly develop thymic T-cell lymphomas representing counterparts of human lymphoblastic lymphomas [27]. Athymic MSH2 deficient mice however develop lymphomas of early B-cell origin, but no T-cell lymphomas [29]. We confirmed these result in MLH1/RAG combined deficient mice, which were also characterized by the uniform development of lymphoblastic B-cell lymphomas (unpublished result). The lack of T-cell lymphomas in athymic or RAG deficient MMR defective mice indicates that loss of MMR activity in stem cells or early precursor T-cells is not sufficient for the development of lymphoblastic T-cell lymphomas, if the following maturation and proliferation of the developing T-cells is impaired. These data revealed that MMR mediated transformation of T-cells has to be linked to a high mitotic proliferation rate. One can further speculate that MLH1 is crucial during the first massive proliferation step in T-cell development (transition from DN1 to DN2 thymocytes) to maintain genomic integrity [32]. Our finding that loss of MMR activity in thymocytes starting at the transition from DN to DP leads to hematological malignancies on very rare occasions however let us assume that malignant transformation in MMR defective T-cells depends not only on the cell proliferation

rate. This suggestion is supported by the prevalence of DP lymphoblastic T -cell lymphomas among the limited number of tumors arising in *Mlh1*$^{T\Delta ex4/T\Delta ex4}$ mice. Therefore our results let suggest that the malignant transformation might be additionally linked to a specific process normally occurring within T-cell progenitors or stem cells that depend on proper MMR function. Evidence was shown that in the absence of mismatch repair, B-cell immunoglobulin gene rearrangement is impaired [29]. Further analysis of T cell receptor rearrangements in MLH1 defective lymphomas may help to clarify if rearrangement of the T-cell receptor is incorrectly regulated in the absence of MMR activity, leading to tumorigenesis. Also investigation using our conditional mouse model may further help to determine the precise stage of development at which these lymphoblastic lymphomas arise.

Analogous to the mouse models with homozygousity for a MMR defect, several human NF1 patients with germline mutations in both copies of any one of the mismatch repair genes, MLH1, MSH2, or PMS2, have presented with early-onset childhood T- or B-cell malignancies [10; 11]. Altered mismatch repair gene expression, mismatch repair gene mutation, and/or microsatellite instability has been observed in varying proportions of human hematological neoplasms [5], consistent with the idea that loss of mismatch repair plays a significant role in human hematological malignancy. In contrast to HNPCC/Lynch syndrome patients with homozygous mutations in mismatch repair genes, patients with heterozygous mismatch repair mutations do not develop early-onset T- or B-cell malignancies. Our results showed that the effect of the loss of mismatch repair in lymphocytes is highly dependent on the stage in T-cell development at which the loss occurs. In heterozygous HNPCC/Lynch syndrome patients the loss of the wild-type allele resulting in complete mismatch repair inactivity occurs later in life. The affected tissues, especially the colon, include tissues with a relatively high exposure to exogenous DNA damaging agents and may therefore be at a higher risk for additional mutations. The reduced thymic T-cell development in adult humans

and the limited exposure to DNA damaging agents might therefore explain the tumor spectrum observed in heterozygous HNPPC patients.

In summary, our results indicates that MMR is critical in preventing lymphomagenesis resulting from very early lymphocyte precursors, but that it plays no major role in preventing lymphomagenesis arising from DP/SP thymocytes or naïve peripheral T-cells.

ACKNOWLEDGEMENTS

This work was supported by grants from the "Interdisziplinäres Zentrum für Klinische Forschung (IZKF)" at the Department of Medicine, University of Würzburg, Germany and the DFG graduate college 639. We thank Martina Döhler for excellent technical support and Jacqueline Krämer for critically reading the manuscript.

FIGURE LEGENDS

Figure 1: Generation of *Mlh1*$^{loxPhygro}$ Mice

**A:** Targeting strategy used to introduce the floxed *Mlh1* locus into m*Mlh1*. Schematic representation of the *Mlh1* genomic locus, the *Mlh1*$^{loxPhgro}$ targeting vector and the targeted *Mlh1* locus. The filled boxes represent *Mlh1* exons, filled triangles LoxP sites. Grey arrows indicate PCR primers.

B: PCR analysis of representative *Mlh1*$^{+/+}$ and; *Mlh1*$^{loxPhygro}$ animals. Thymic DNA was amplified using the primers P1 and P2 flanking the 5' LoxP site, as indicated in A. The WT allele is represented by a 400 bp PCR fragment. The *Mlh1*$^{loxPhygro}$ allele, containing the additional LoxP site is indicated by a 600 bp PCR fragment.

Figure 2: Generation of *Mlh1*$^{flox/flox}$, *Mlh1*$^{T\Delta ex4/T\Delta ex4}$ and *Mlh1*$^{\Delta ex4/\Delta ex4}$ Mice

A: Scheme of the expected excision of the hygromycin cassette and exon 4 after Cre mediated recombination

B: PCR analysis of the ΔExon 4 locus in *Mlh1*$^{\Delta ex4/\Delta ex4}$, *Mlh1*$^{T\Delta ex4/T\Delta ex4}$and *Mlh1*$^{+/+}$ mice. Thymic (T) and intestinal (I) DNA was isolated from mice with the indicated genotypes and amplified using the P1 and P3 primers flanking exon 4, indicated in (A). The *Mlh1*$^{+/+}$ locus is represented by a 750bp PCR product, the Δexon 4 locus in *Mlh1*$^{\Delta ex4/\Delta ex4}$ thymocytes by a 350 bp PCR product.

C: Western blot analyses of thymocyte cell extracts using anti-MLH1 and anti-MSH2 antibodies.

Figure 3: Tumorigenesis of *Mlh1*$^{\Delta ex4/\Delta ex4}$, *Mlh1*$^{T\Delta ex4/T\Delta ex4}$ and *Mlh1*$^{-/-}$ Mice.

A: Kaplan-Meier analysis of overall survival up to 80 weeks. The survival curves were generated using SPSS 12.0 software. There are no significant differences between the survival of *Mlh1*$^{\Delta ex4/\Delta ex4}$ (n=35) and *Mlh1*$^{-/-}$ (n=66) tumor mice (p = 0,224; log-rank test). Survival of *Mlh1*$^{\Delta ex4/\Delta ex4}$ and *Mlh1*$^{-/-}$ mice is highly significant reduced compared to *Mlh1*$^{flox/flox}$ mice (n=20) (p> 0,001; log-rank test).

B: Kaplan-Meier analysis for overall survival up to 40 weeks. The survival curves were generated by using SPSS 12.0 software. Significant differences between the survival of *Mlh1*$^{T\Delta ex4/T\Delta ex4}$ and *Mlh1*$^{flox/flox}$ mice compared to *Mlh1*$^{\Delta ex4/\Delta ex4}$and *Mlh1*$^{-/-}$ (p > 0,0001; log-rank test) tumor mice. No significant differences between the survival of *Mlh1*$^{T\Delta ex4/T\Delta ex4}$ compared to *Mlh1*$^{flox/flox}$ mice (p=0,291) and *Mlh1*$^{-/-}$ compared to *Mlh1*$^{\Delta ex4/\Delta ex4}$ mice (p=0,842)

C: Kaplan-Meier analysis for lymphomagenesis. The survival curves were generated by using SPSS 12.0 software. There are no significant differences in the onset of lymphoma development between *Mlh1*$^{T\Delta ex4/T\Delta ex4}$ (n=4) and *Mlh1*$^{-/-}$ (n=27) lymphoma mice (P= 0,56; log-rank-test)

D: Representative microsatellite instability (MSI) analysis for each MSI marker (upper panel). Microsatellite status of tumors derived from *Mlh1*$^{T\Delta ex4/T\Delta ex4}$ mice. Tumors were analyzed

using five independent markers D17Mit132, D7Mit91, U12235, Aa006036 and L24372. High MSI: more than one marker alters, low MSI: one marker alters; no MSI: no marker alters

Figure 4: RT-PCR Analysis of the Δexon4 Locus in *Mlh1*$^{TΔex4/TΔex4}$ Thymocytes.

Double negative (DN) and double positive including single positive thymocytes (DP/SP) have been isolated using MACS technology.

A: FACS analysis of the isolated thymocytes using CD4 and 8 antibodies. 1: whole thymus; 2: DN thymocytes; 3: DP/SP thymocytes.

B: Upper panel: RT-PCR analysis of the thymocyte subfractions of *Mlh1*$^{TΔex4/TΔex4}$ thymocytes and whole mount thymocytes out of *Mlh1*$^{TΔex4/TΔex4}$ and *Mlh1*$^{+/+}$ mice using the indicated primers. *Gapdh* was used as loading control.

Lower panel: scheme of the expected *Mlh1* and *Mlh1* ΔExon 4 transcripts.

Figure 5: Expression of *Mlh1* and *Cre* in *Mlh1*$^{TΔex4/TΔex4}$ Thymocytes.

Expression levels were analyzed by real-time RT-PCR.

A: *Mlh1* expression in subfractioned *Mlh1*$^{TΔex4/TΔex4}$ thymocytes.

Comparison of the *Mlh1* expression change between *Mlh1*$^{TΔex4/TΔex4}$ and *Mlh1*$^{+/+}$ thymocytes subpopulations. *Mlh1* expression in *Mlh1*$^{+/+}$ thymocytes was ascertained as 1. Shown are the results of a representative qPCR analysis after normalization with HPRT. No expressional differences could be observed in the *Mlh1*$^{+/+}$ thymocyte subpopulations. *Mlh1* expression is highly significant downregulated in all *Mlh1*$^{TΔex4/TΔex4}$ T-cell subpopulations ($p>0,001$; t-Test). The *Mlh1* expression in DN *Mlh1*$^{TΔex4/TΔex4}$ thymocytes is significant higher compared to DP/SP *Mlh1*$^{TΔex4/TΔex4}$ thymocytes ($p=0,031$; t-Test).

B: *Cre* Expression levels in subfraktioned *Mlh1*$^{TΔex4/TΔex4}$ thymocytes. *Cre* expression in total thymocytes was ascertained as 100%. Shown are results of a representative qPCR analysis after normalization with *HPRT*. *Cre* Expression is highly significant downregulated in DN *Mlh1*$^{TΔex4/TΔex4}$ thymocytes compared to DP/SP and total thymocytes ($p<0,001$; t-test).

Table I: Tumor Incidences of *Mlh1*$^{TΔex4/TΔex4}$, *Mlh1*$^{flox/flox}$ *Mlh1*$^{-/-}$ and *Mlh1*$^{Δex4/Δex4}$ Mice.

Mice were monitored over a period of 40 weeks. No significant differences in the tumor incidences between *Mlh1*$^{-/-}$ and *Mlh1*$^{\Delta ex4/\Delta ex4}$ mice can be observed (p=0,137; t-test). Lymphoma incidences of *Mlh1*$^{T\Delta ex4/T\Delta ex4}$ mice is highly significant reduced compared to *Mlh1*$^{-/-}$ and *Mlh1*$^{\Delta ex4/\Delta ex4}$ mice (p<0,001; t-test). *Percent of total

Table I: Tumor Incidences of *Mlh1*$^{T\Delta ex4/T\Delta ex4}$, *Mlh1*$^{flox/flox}$ *Mlh1*$^{-/-}$ and *Mlh1*$^{\Delta ex4/\Delta ex4}$ Mice after 40 Weeks of Live.

| | *Mlh1*$^{T\Delta ex4/T\Delta ex4}$ | *Mlh1*$^{flox/flox}$ | *Mlh1*$^{\Delta ex4/\Delta ex4}$ | *Mlh1*$^{-/-}$ |
|---|---|---|---|---|
| n | 64 | 30 | 39 | 62 |
| Tumor free | 60 (94%) | 30 | 14 (36%) | 14 (23%) |
| Tumor animals (n) | 4 (6%) | 0 | 25 (64%) | 48 (77%) |
| Lymphoma | 4 (6%) | 0 | 13 (33%) | 27 (43%) |
| T-cell | 4 (6%) | 0 | n.a. | 16 (26%)* |
| B-cell | 0 | 0 | n.a. | 8 (13%)* |
| Hematopoietic | 0 | 0 | n.a. | 3 (4%)* |
| GI | 0 | 0 | 9 (23%) | 16 (26%) |
| GI + Lymphoma | 0 | 0 | 3 (8%) | 5 (8%) |
| Median survival (weeks) +/- SD | | | | |
| Total | 40 | 40 | 33,6 +/- 3 | 32,6 +/- 1,5 |
| Lymphoma | 21 +/- 0,968 | - | 24,7 +/- 3,9 | 22 +/- 1,2 |
| GI | - | - | 41 | 49,5 +/- 7 |

*Percent of total

[1] F.S. Leach, N.C. Nicolaides, N. Papadopoulos, et al., Mutations of a mutS homolog in hereditary nonpolyposis colorectal cancer. Cell 75 (1993) 1215-25.

[2] N. Papadopoulos, N.C. Nicolaides, Y.F. Wei, et al., Mutation of a mutL homolog in hereditary colon cancer. Science 263 (1994) 1625-9.

[3] M. Pineda, E. Castellsague, E. Musulen, et al., Non-Hodgkin lymphoma related to hereditary nonpolyposis colorectal cancer in a patient with a novel heterozygous complex deletion in the MSH2 gene. Genes Chromosomes Cancer 47 (2008) 326-32.

[4] L.A. Loeb, K.R. Loeb, and J.P. Anderson, Multiple mutations and cancer. Proc Natl Acad Sci U S A 100 (2003) 776-81.

[5] L.S. Chao EC, Molecular models for the tissue specificity of DNA mismatch repair-deficient carcinogenesis. Nucleic Acids Research 34 (2006) 840-52.

[6] P. Karran, Microsatellite instability and DNA mismatch repair in human cancer. Semin Cancer Biol 7 (1996) 15-24.

[7] C. Wada, S. Shionoya, Y. Fujino, et al., Genomic instability of microsatellite repeats and its association with the evolution of chronic myelogenous leukemia. Blood 83 (1994) 3449-56.

[8] H. Kaneko, S. Horiike, J. Inazawa, H. Nakai, and S. Misawa, Microsatellite instability is an early genetic event in myelodysplastic syndrome. Blood 86 (1995) 1236-7.

[9] O.S. Hangaishi A, Mitani K, Hosoya N, Chiba S, Yazaki Y, Hirai H., Mutations and loss of expression of a mismatch repair gene, hMLH1, in leukemia and lymphoma cell lines. Blood 89 (1997) 1740-47.

[10] M.D. Ricciardone, T. Ozcelik, B. Cevher, et al., Human MLH1 deficiency predisposes to hematological malignancy and neurofibromatosis type 1. Cancer Res 59 (1999) 290-3.

[11] D. Whiteside, R. McLeod, G. Graham, et al., A homozygous germ-line mutation in the human MSH2 gene predisposes to hematological malignancy and multiple cafe-au-lait spots. Cancer Res 62 (2002) 359-62.

[12] R. Fishel, M.K. Lescoe, M.R. Rao, et al., The human mutator gene homolog MSH2 and its association with hereditary nonpolyposis colon cancer. Cell 75 (1993) 1027-38.

[13] M.H. Kucherlapati, K. Lee, A.A. Nguyen, et al., An Msh2 conditional knockout mouse for studying intestinal cancer and testing anticancer agents. Gastroenterology 138 993-1002 e1.

[14] W. Edelmann, K. Yang, A. Umar, et al., Mutation in the mismatch repair gene Msh6 causes cancer susceptibility. Cell 91 (1997) 467-77.

[15] T.A. Kunkel, and D.A. Erie, DNA mismatch repair. Annu Rev Biochem 74 (2005) 681-710.

[16] R.R. Iyer, A. Pluciennik, V. Burdett, and P.L. Modrich, DNA mismatch repair: functions and mechanisms. Chem Rev 106 (2006) 302-23.

[17] S.L. Hickman MJ, Role of DNA mismatch repair and p53 in signaling induction of apoptosis by alkylating agents. Proceedings of the National Academy of Sciences 96 (1999) 10764-69.

[18] S. Yanamadala, and M. Ljungman, Potential role of MLH1 in the induction of p53 and apoptosis by blocking transcription on damaged DNA templates. Mol Cancer Res 1 (2003) 747-54.

[19] C.P. Edelmann W, Kane M, Lau K, Morrow B, Bennett S, Umar A, Kunkel T, Cattoretti G, Chaganti R, Pollard JW, Kolodner RD, Kucherlapati R., Meiotic pachytene arrest in MLH1-deficient mice. Cell 85 (1996) 1125-34.

[20] W. Edelmann, K. Yang, M. Kuraguchi, et al., Tumorigenesis in Mlh1 and Mlh1/Apc1638N mutant mice. Cancer Res 59 (1999) 1301-7.

[21] E. Avdievich, C. Reiss, S.J. Scherer, et al., Distinct effects of the recurrent Mlh1G67R mutation on MMR functions, cancer, and meiosis. Proc Natl Acad Sci U S A 105 (2008) 4247-52.

[22] M. Lakso, J.G. Pichel, J.R. Gorman, et al., Efficient in vivo manipulation of mouse genomic sequences at the zygote stage. Proc Natl Acad Sci U S A 93 (1996) 5860-5.

[23] P.C. Orban, D. Chui, and J.D. Marth, Tissue- and site-specific DNA recombination in transgenic mice. Proc Natl Acad Sci U S A 89 (1992) 6861-5.

[24] J. Bertholon, Q. Wang, C.M. Galmarini, and A. Puisieux, Mutational targets in colorectal cancer cells with microsatellite instability. Fam Cancer 5 (2006) 29-34.

[25] G.A. Calin, R. Gafa, M.G. Tibiletti, et al., Genetic progression in microsatellite instability high (MSI-H) colon cancers correlates with clinico-pathological parameters: A study of the TGRbetaRII, BAX, hMSH3, hMSH6, IGFIIR and BLM genes. Int J Cancer 89 (2000) 230-5.

[26] G. Poulogiannis, I.M. Frayling, and M.J. Arends, DNA mismatch repair deficiency in sporadic colorectal cancer and Lynch syndrome. Histopathology 56 167-79.

[27] A.H. Reitmair, R. Schmits, A. Ewel, et al., MSH2 deficient mice are viable and susceptible to lymphoid tumours. Nat Genet 11 (1995) 64-70.

[28] S. Zienolddiny, D. Ryberg, D.H. Svendsrud, et al., Msh2 deficiency increases susceptibility to benzo[a]pyrene-induced lymphomagenesis. Int J Cancer 118 (2006) 2899-902.

[29] M.R. Campbell, P.N. Nation, and S.E. Andrew, A lack of DNA mismatch repair on an athymic murine background predisposes to hematologic malignancy. Cancer Res 65 (2005) 2626-35.

[30] R.M. Nepal, L. Tong, B. Kolaj, W. Edelmann, and A. Martin, Msh2-dependent DNA repair mitigates a unique susceptibility of B cell progenitors to c-Myc-induced lymphomas. Proc Natl Acad Sci U S A 106 (2009) 18698-703.

[31] C. Shimizu, H. Kawamoto, M. Yamashita, et al., Progression of T cell lineage restriction in the earliest subpopulation of murine adult thymus visualized by the expression of lck proximal promoter activity. Int Immunol 13 (2001) 105-17.

[32] J. Laurent, N. Bosco, P.N. Marche, and R. Ceredig, New insights into the proliferation and differentiation of early mouse thymocytes. Int Immunol 16 (2004) 1069-80.

A

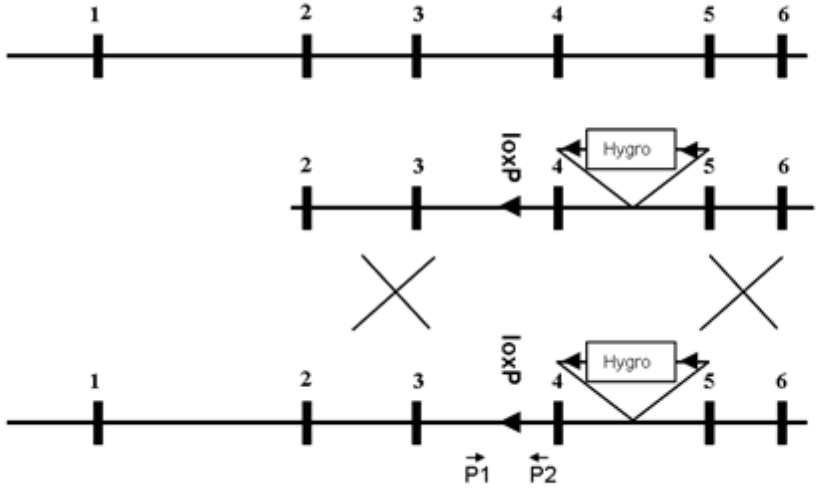


*Mlh1* genomic locus

*Mlh1*$^{loxPhygro}$ targeting Vector

Homologous recombination

*Mlh1*$^{loxPhygro}$ locus

B

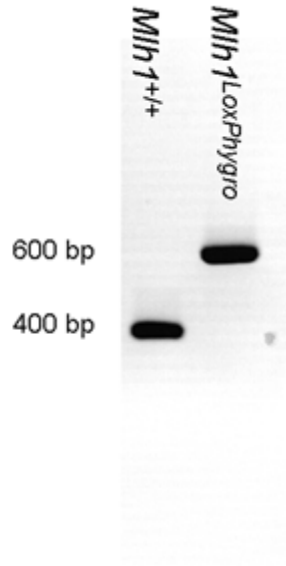

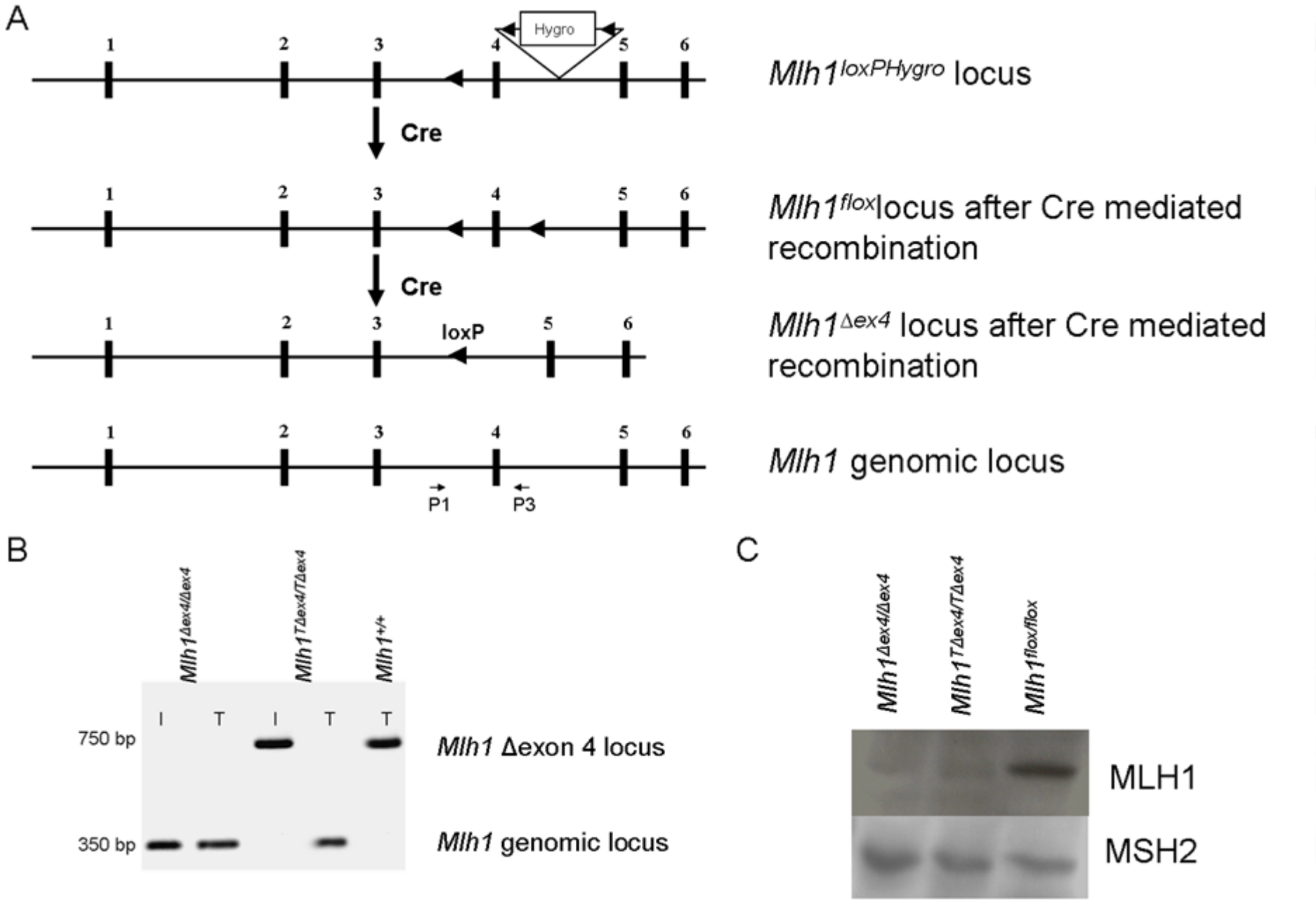
A
Hygro
1
2
3
4
5
6
Cre
Mlh1loxPHygro locus
Mlh1flox locus after Cre mediated recombination
Mlh1Δex4 locus after Cre mediated recombination
loxP
Mlh1 genomic locus
P1
P3
B
Mlh1Δex4/Δex4
Mlh1TΔex4/TΔex4
Mlh1+/+
I
T
750 bp
350 bp
Mlh1 Δexon 4 locus
Mlh1 genomic locus
C
Mlh1Δex4/Δex4
Mlh1TΔex4/TΔex4
Mlh1flox/flox
MLH1
MSH2

A

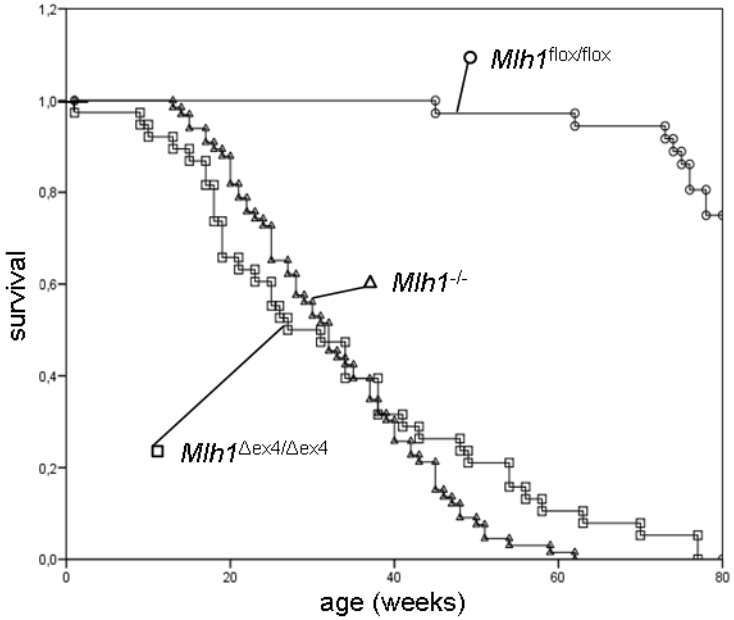


B

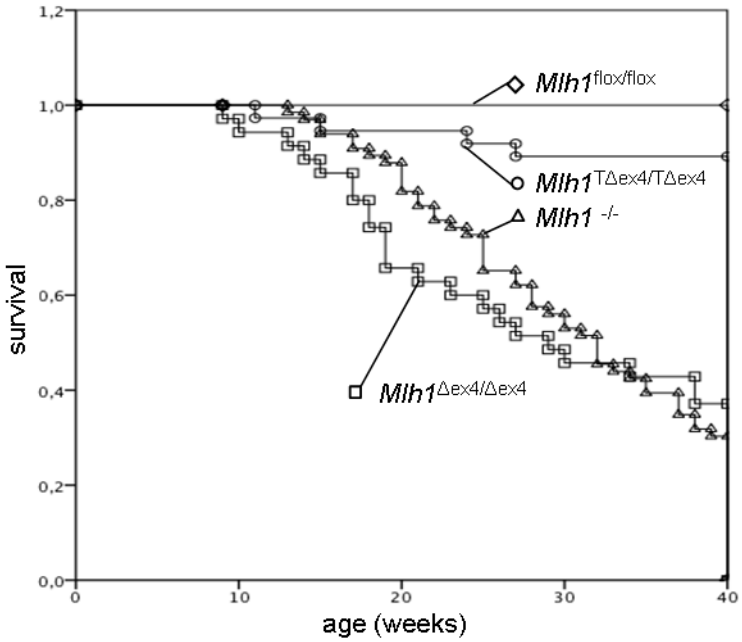


C

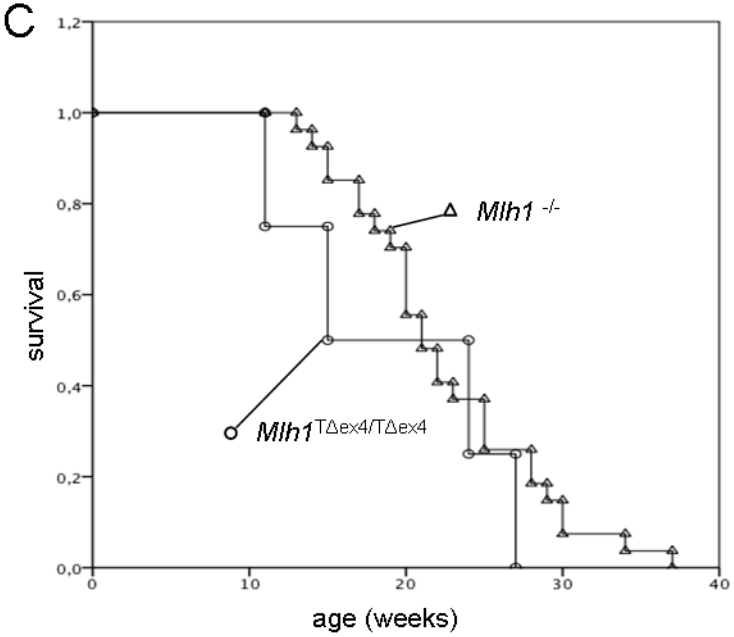


D

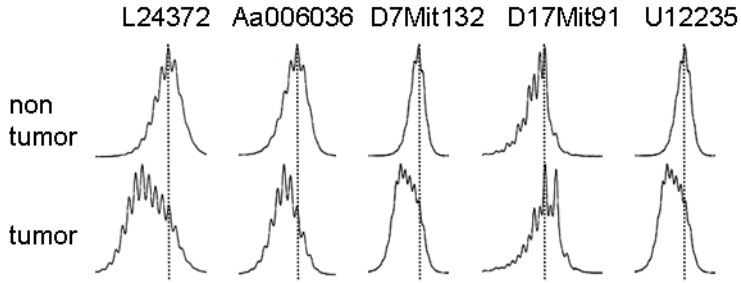


| | n | MS status | | |
|---|---|---|---|---|
| | | high | low | stable |
| *Mlh1 -/-* | 32 | 25 (80%) | 7(21%) | 0 |
| *Mlh1Δex4/Δex4* | 17 | 12 (70%) | 3 (18%) | 2 (12%) |
| *Mlh1TΔex4/TΔex4* | 4 | 1 (25%) | 2 (50%) | 1 (25%) |

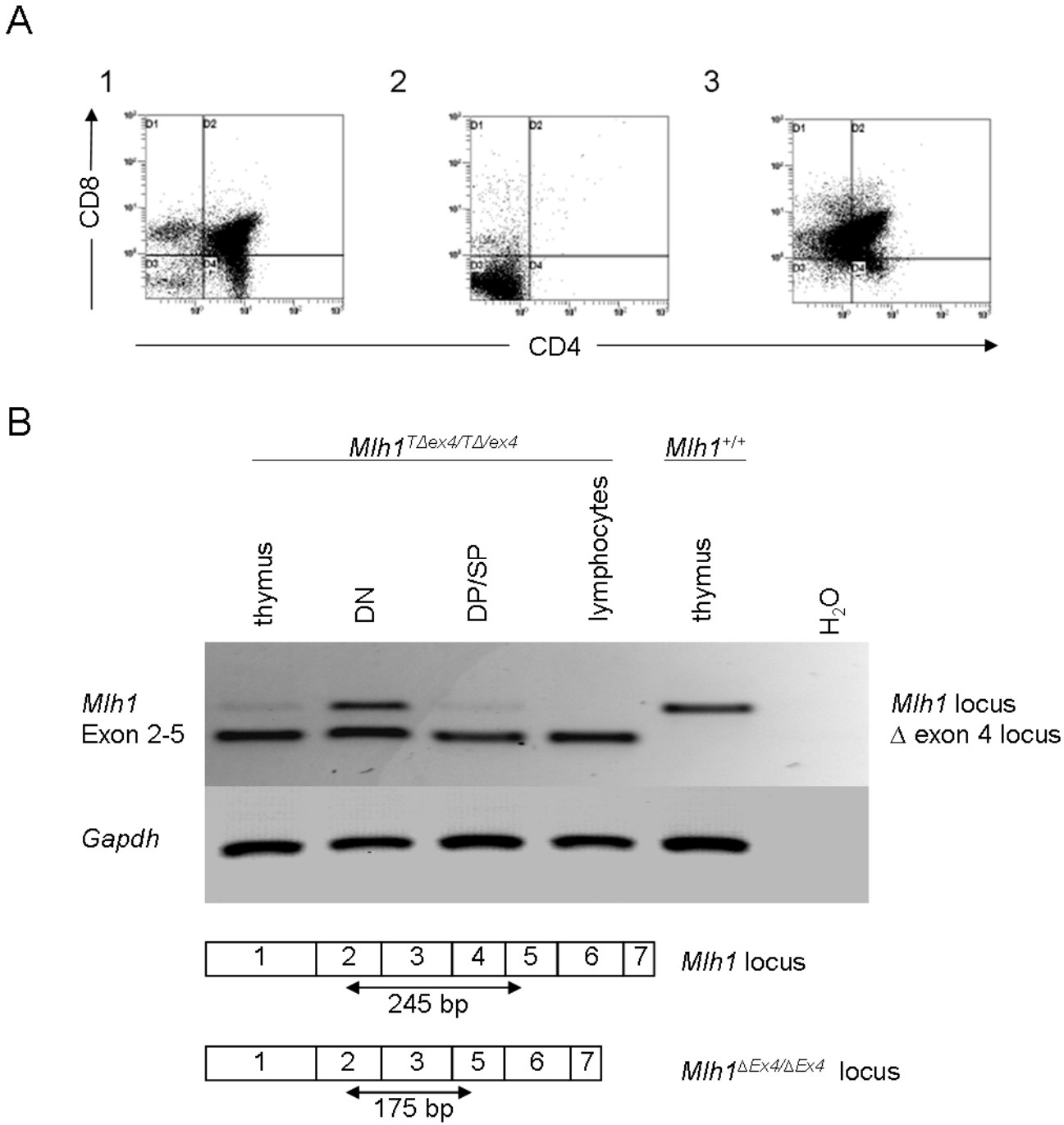
A
1
2
3
CD8
CD4
B
Mlh1TΔex4/TΔ/ex4
Mlh1+/+
thymus
DN
DP/SP
lymphocytes
thymus
H2O
Mlh1
Exon 2-5
Gapdh
Mlh1 locus
Δ exon 4 locus
1 2 3 4 5 6 7
Mlh1 locus
245 bp
1 2 3 5 6 7
Mlh1ΔEx4/ΔEx4 locus
175 bp

A

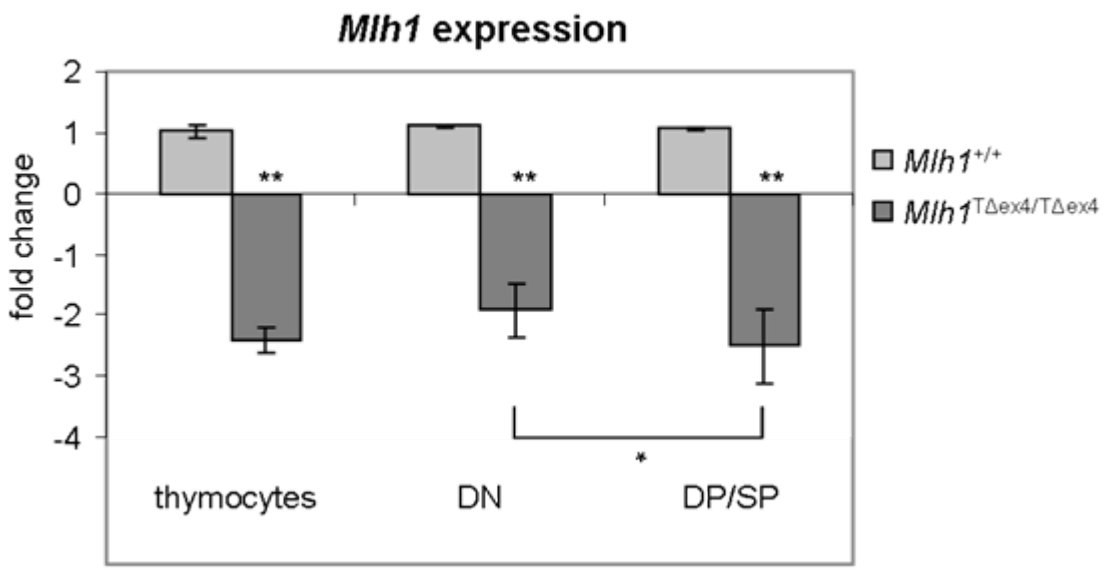
Mlh1 expression
fold change
2
1
0
-1
-2
-3
-4
**
**
**
*
thymocytes
DN
DP/SP
Mlh1+/+
Mlh1TΔex4/TΔex4

B


Cre expression in Mlh1TΔex4/TΔex4 thymocytes
Cre expression (%)
120
100
80
60
40
20
0
**
thymocytes
DN
DP/SP

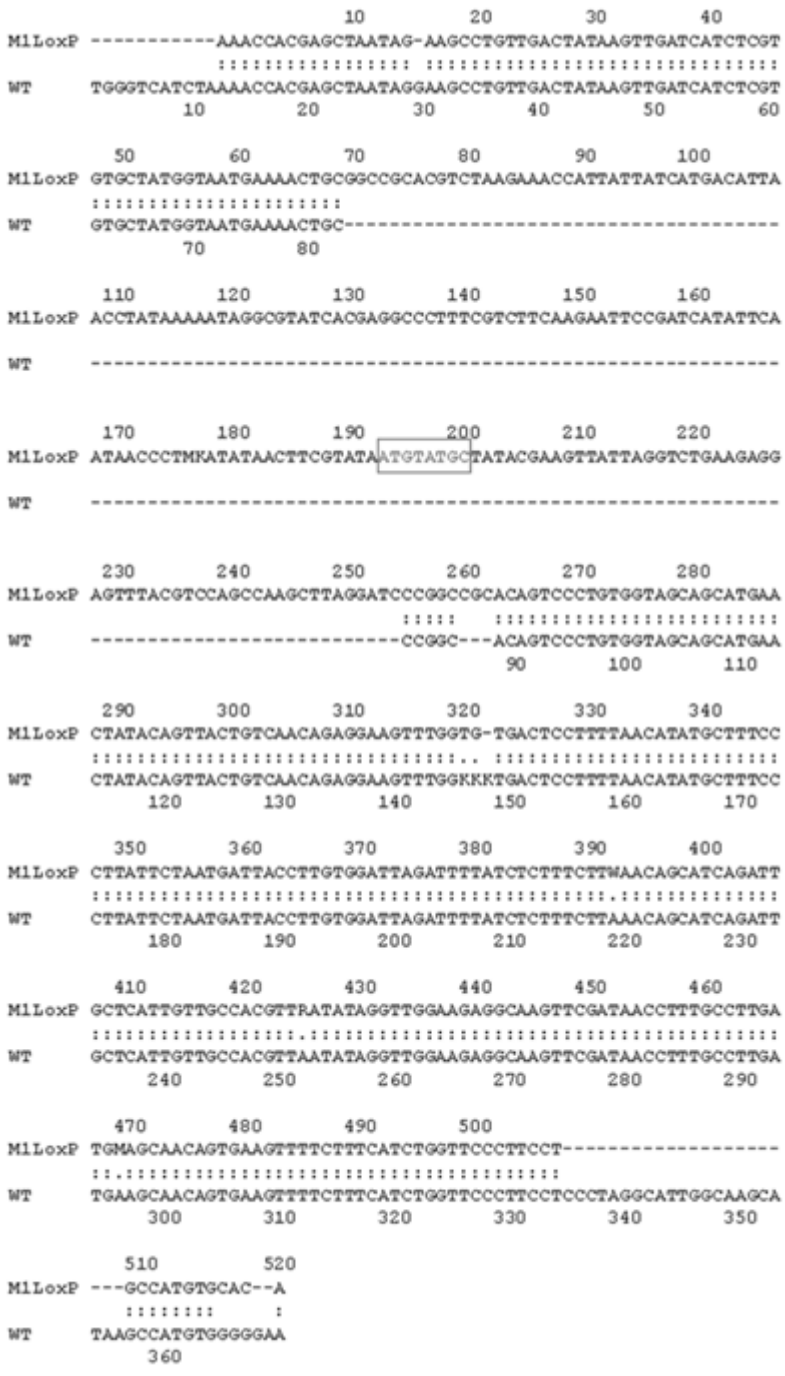
10 20 30 40
M1LoxP ----------AAACCACGAGCTAATAG-AAGCCTGTTGACTATAAGTTGATCATCTCGT
WT TGGGTCATCTAAAACCACGAGCTAATAGGAAGCCTGTTGACTATAAGTTGATCATCTCGT
10 20 30 40 50 60
50 60 70 80 90 100
M1LoxP GTGCTATGGTAATGAAAACTGCGGCCGCACGTCTAAGAAACCATTATTATCATGACATTA
WT GTGCTATGGTAATGAAAACTGC----------
70 80
110 120 130 140 150 160
M1LoxP ACCTATAAAAATAGGCGTATCACGAGGCCCTTTCGTCTTCAAGAATTCCGATCATATTCA
WT ----------
170 180 190 200 210 220
M1LoxP ATAACCCTMKATATAACTTCGTATAATGTATGCTATACGAAGTTATTAGGTCTGAAGAGG
WT ----------
230 240 250 260 270 280
M1LoxP AGTTTACGTCCAGCCAAGCTTAGGATCCCGGCCGCACAGTCCCTGTGGTAGCAGCATGAA
WT ----------CCGGC---ACAGTCCCTGTGGTAGCAGCATGAA
90 100 110
290 300 310 320 330 340
M1LoxP CTATACAGTTACTGTCAACAGAGGAAGTTTGGTG-TGACTCCTTTTAACATATGCTTTCC
WT CTATACAGTTACTGTCAACAGAGGAAGTTTGGKKKTGACTCCTTTTAACATATGCTTTCC
120 130 140 150 160 170
350 360 370 380 390 400
M1LoxP CTTATTCTAATGATTACCTTGTGGATTAGATTTTATCTCTTTCTTWAACAGCATCAGATT
WT CTTATTCTAATGATTACCTTGTGGATTAGATTTTATCTCTTTCTTAAACAGCATCAGATT
180 190 200 210 220 230
410 420 430 440 450 460
M1LoxP GCTCATTGTTGCCACGTTRATATAGGTTGGAAGAGGCAAGTTCGATAACCTTTGCCTTGA
WT GCTCATTGTTGCCACGTTAATATAGGTTGGAAGAGGCAAGTTCGATAACCTTTGCCTTGA
240 250 260 270 280 290
470 480 490 500
M1LoxP TGMAGCAACAGTGAAGTTTTCTTTCATCTGGTTCCCTTCCT----------
WT TGAAGCAACAGTGAAGTTTTCTTTCATCTGGTTCCCTTCCTCCCTAGGCATTGGCAAGCA
300 310 320 330 340 350
510 520
M1LoxP ---GCCATGTGCAC--A
WT TAAGCCATGTGGGGGAA
360

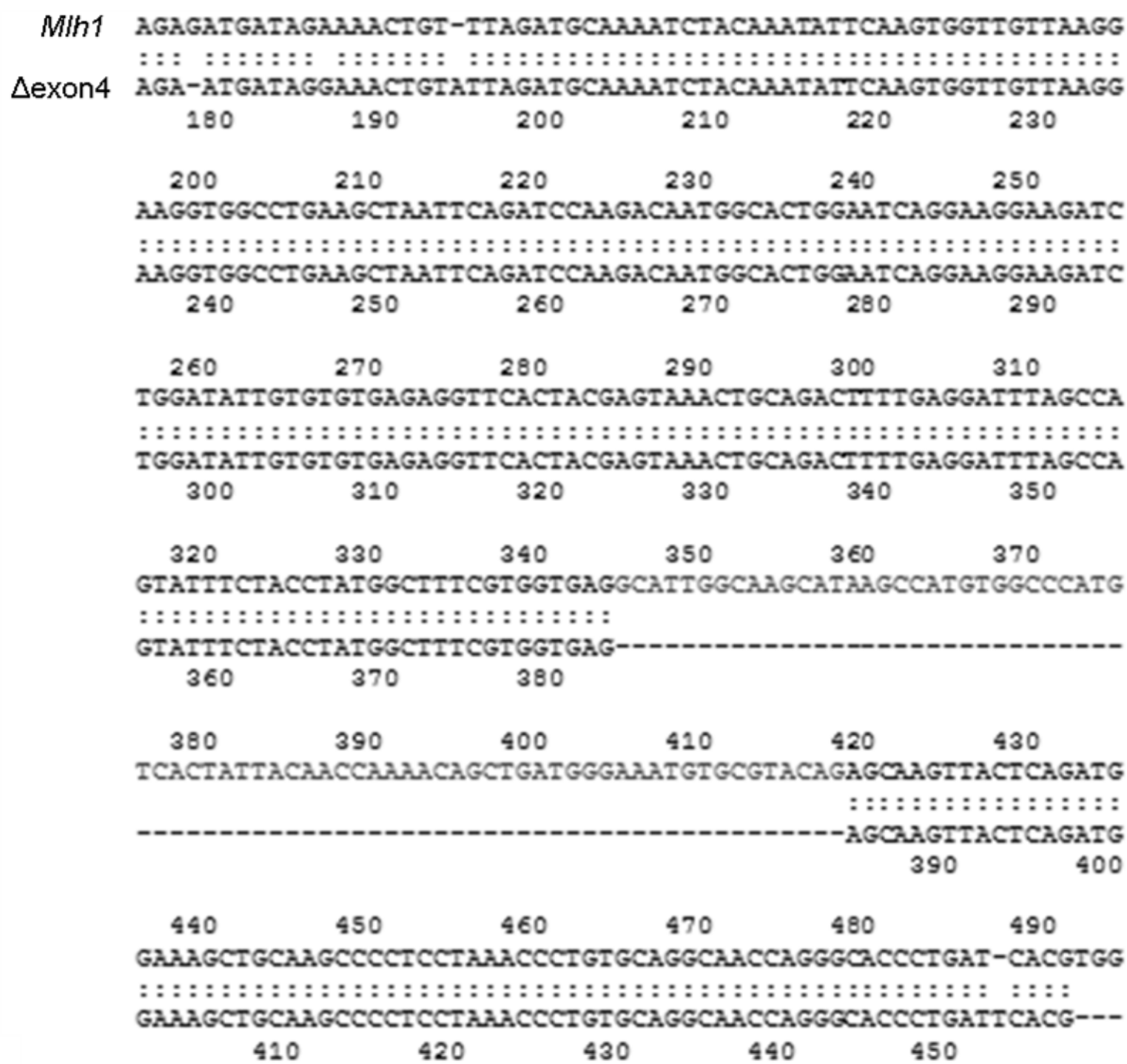
Mlh1
AGAGATGATAGAAAACTGT-TTAGATGCAAAATCTACAAATATTCAAGTGGTTGTTAAGG
Δexon4
AGA-ATGATAGGAAACTGTATTAGATGCAAAATCTACAAATATTCAAGTGGTTGTTAAGG
180 190 200 210 220 230
200 210 220 230 240 250
AAGGTGGCCTGAAGCTAATTCAGATCCAAGACAATGGCACTGGAATCAGGAAGGAAGATC
AAGGTGGCCTGAAGCTAATTCAGATCCAAGACAATGGCACTGGAATCAGGAAGGAAGATC
240 250 260 270 280 290
260 270 280 290 300 310
TGGATATTGTGTGTGAGAGGTTCACTACGAGTAAACTGCAGACTTTTGAGGATTTAGCCA
TGGATATTGTGTGTGAGAGGTTCACTACGAGTAAACTGCAGACTTTTGAGGATTTAGCCA
300 310 320 330 340 350
320 330 340 350 360 370
GTATTTCTACCTATGGCTTTCGTGGTGAGGCATTGGCAAGCATAAGCCATGTGGCCCATG
GTATTTCTACCTATGGCTTTCGTGGTGAG----------
360 370 380
380 390 400 410 420 430
TCACTATTACAACCAAAACAGCTGATGGGAAATGTGCGTACAGAGCAAGTTACTCAGATG
----------AGCAAGTTACTCAGATG
390 400
440 450 460 470 480 490
GAAAGCTGCAAGCCCCTCCTAAACCCTGTGCAGGCAACCAGGGCACCCTGAT-CACGTGG
GAAAGCTGCAAGCCCCTCCTAAACCCTGTGCAGGCAACCAGGGCACCCTGATTCACG---
410 420 430 440 450

# Reactive Antibodies Against Bacillus Calmette-Guerin Heat-Shock Protein-65 Potentially Predict the Outcome of Immunotherapy for High-Grade Transitional Cell Carcinoma of the Bladder

**Publiziert 2010 in Cancer 116, 600-609.**

# Reactive Antibodies Against Bacillus Calmette-Guerin Heat-Shock Protein-65 Potentially Predict the Outcome of Immunotherapy for High-Grade Transitional Cell Carcinoma of the Bladder

Peter U. Ardelt, MD1; Burkhard Kneitz, MD1; Patrick Adam, MD2; Cora Reiss, PhD3; Arkadius Kocot, MD1; Joachim Fensterle, PhD4; Limor Chen, PhD5; Renata Pasqualini, PhD6; Wadih Arap, MD, PhD6; Elmar W. Gerharz, MD1; and Hubertus Riedmiller, MD1

BACKGROUND: Intravesical immunotherapy with Mycobacterium bovis (M. bovis) bacillus Calmette-Guerin (BCG) is the current standard of care against superficial, high-grade transitional cell carcinoma (TCC) of the urinary bladder (carcinoma in situ and pathologic T1, grade 3 disease). However, individual patient outcome is barely predictable because of the lack of serum markers. Consequently, progression to muscle-invasive bladder cancer and critical delay of treatments (such as neoadjuvant combination chemotherapy and/or radical cystectomy) often occur. The objectives of this study were to identify a marker for measuring the BCG-induced immune response and to predict the outcomes and potential improvements of BCG immunotherapy. METHODS: Because host immunoresponse mediates BCG activity, the authors screened a combinatorial random peptide library on the circulating pool of immunoglobulins (Igs) purified from an index patient after successful BCG immunotherapy to identify the corresponding target antigen(s). RESULTS: An immunogenic peptide motif was selected, isolated, and validated from M. bovis BCG heatshock protein 65 (HSP-65) as a dominant epitope of the humoral response to treatment. Increasing IgA and IgG anti- HSP-65 titers specifically predicted a positive patient outcome in a cohort of patients with bladder cancer relative to several cohorts of control patients. CONCLUSIONS: The current results indicated that antibody production against M. bovis BCG HSP-65 can serve as a serologic marker for the predictive outcome of BCG immunotherapy. Subsequent studies will determine the value of this candidate marker to modify BCG-based treatment for individual patients with bladder cancer.

Intravesically administered Mycobacterium bovis bacillus Calmette-Guerin (M. bovis BCG) has become the treatment of choice against superficial, high-grade transitional cell carcinoma (TCC) (carcinoma in situ [Cis] and pathologic T1 [pT1], grade 3 tumors). Repeated intravesical instillations induce a complex immunologic response that results in tumor eradication in ~75% after the induction cycle[1-3] and long-term remission in 50% to 75% of patients.[4,5] Evidence exists that, primarily, a cellular immune response is necessary for successful BCG immunotherapy.[6,7] Interferon c and interleukin 12, both mediators of a T-helper cell 1 (TH1)-mediated immune response, essentially are necessary for a positive BCG effect in vivo.7 However, it also has been demonstrated that intravesical application of M. bovis BCG results in the activation of both TH-1-mediated and TH-2-mediated pathways and that separation is less strict.[7,8] Patients who do not respond to BCG (~30%) are at increased risk of progression to muscle-invasive disease and metastasis. Delays in starting more aggressive treatments, such as neoadjuvant combination chemotherapy and/or radical cystectomy, may lead to potentially worse outcomes. Thus, it is paramount to identify nonresponders to BCG
immunotherapy as early as possible in their clinical course so that these individuals may be considered for more aggressive therapeutic strategies. Several adverse factors
for the outcome of BCG immunotherapy are known, such as age, incomplete tumor resection, and tumor size.[9,10] A second resection before BCG immunotherapy is associated with an improved outcome.10 However, currently, the success of BCG immunotherapy is determined only indirectly according to the presence or absence of tumor at the time of re-evaluation, and the induced immune response cannot be measured directly during or after induction. Because the immune response has an established role as a predictive biomarker in cancer therapy for many tumors,[11-14] including human bladder cancer, and certainly in the setting of BCG therapy,[3,8] we attempted to identify candidate serum markers for measuring the immune response and, thus, the outcome of BCG immunotherapy through combinatorial epitope mapping (‘‘fingerprinting’’) of the antibody response to BCG. In this report, we describe a peptide from M. bovis BCG heatshock protein 65 (HSP-65) that elicits a strong and specific
humoral response to treatment. Reactive serum titers after BCG treatment predicted a positive outcome for a cohort of patients with bladder cancer. If these results are
confirmed in larger, prospective, follow-up studies, then this approach and finding will lead to an antibody-based assay for measuring BCG-induced antitumor response.
This assay should allow for the early detection of nonresponding patients and an immunotherapy designed specifically for each patient.

## MATERIALS AND METHODS

### Collection of Patient Serum Samples

All experiments were reviewed and approved by the Institutional Review Board of the Bavarian Julius Maximilians-University Medical School, Wurzburg, Germany. Written informed consent was obtained from all patients. Sera samples were collected and immediately frozen at -80° after centrifugation from patients who were receiving BCG therapy (n = 16) for superficial high-grade TCC (Cis or pT1/grade 3 tumors) at the time of initial diagnosis, after the induction cycle, and at the first followup. Control samples were obtained from patients who had other stages of TCC (Ta, T2-T4; n ¼ 38), patients who had prostate cancer (n = 40), and age-matched healthy volunteers (n = 40). Standard exclusion criteria for BCG immunotherapy were applied, and only patients
who had not received previous intravesical therapies for urothelial tumors were eligible.

**Screening of the Phage-Display Random Peptide Library**

We used a random peptide phage-display library based on the vector fUSE5, displaying inserts with the general arrangement CX7C (C, cysteine; X, any residue).[15] An insertless phage clone served as a negative control. For all experiments, IgGs were immobilized and/or purified on protein G-agarose beads (Sigma-Aldrich, Taufkirchen, Germany). Screening was performed as described previously. [15] Briefly, 109 transducing units (TU) of the CX7C random peptide phage-display library were precleared for 60 minutes at 4°C on pooled, immobilized IgG from healthy control volunteers. After centrifugation, equal amounts of the supernatant were added to immobilized IgGs from patients with bladder cancer and from healthy control volunteers. After incubation for 2 hours at 4C,
the beads were washed 5 times with phosphate-buffered saline (PBS). Bound phages were eluted with 0.1 M glycine buffer, pH 2.2, and were neutralized with 1 M Tris/
HCl, pH 7.0. Reinfection was performed with 1 mL of log-phase Escherichia coli (E. coli) K91. Sequential rounds of phage amplification were performed as described previously.[15] Serial dilutions were plated in triplicate to determine the ratio of bound phage after each screening round.

**DNA Amplification and Sequencing**

After the second selection round, serial dilutions were plated for single bacterial colony isolation. Individual DNA corresponding to the peptide inserts of randomly picked phage clones (n = 30) was amplified with the primers 5'-AGGTTGGTGCCTTCGTAGTG-3' and 5'-GTTTAGTACCGCCACCCTCA-3' and was purified with EXO SAP IT, (USB, Cleveland, Ohio). Sequencing was performed with the primer 5'-CCCTCATAGT TAGCGTAACGATCT-3', the CEQ 2000 Dye Terminator Cycle Sequencing Kit, and a CEQ 2000 automated sequencer (both from Beckmann Coulter, Fullerton, Calif). Sequences were aligned and compared with online protein databases of the National Center for Biotechnology Information (available at: http://ncbi.nlm.nih.gov/ blast/Blast.cgi accessed January 2008).

**Phage Binding Assay and Competitive Binding Inhibition**

For phage binding assays, 1 µg of purified IgG was immobilized on Nunc Maxisorp plates (Nunc, Wiesbaden, Germany) overnight at 4°C. After blocking wells with PBS that contained 0.1% Tween-20 and 1% nonfat dried milk (NFDM) for 2 hours at room temperature (RT), we added $10^8$ TU of either amplified phage clones or control phage for 2 hours at RT. For inhibition assays, increasing amounts of corresponding glutathione-S-transferase (GST)-fused peptides or wild-type (negative control) GST were preincubated for 30 minutes at RT before the addition of phages. Unbound phages were removed by washing 5 times with PBS that contained 0.1% Tween-20 and 1% NFDM. Bound phages were recovered with 200 µL log-phase E. coli K91 and were plated in serial dilutions (triplicate plates for each dilution).

**Enzyme-Linked Immunoadsorbent Assay and Patient Screening**

For the enzyme-linked immunoadsorbent assay (ELISA), 1 µg of purified M. bovis BCG HSP-65 (StressGen Biotechnologies Corp., Victoria, British Columbia, Canada)
per well was immobilized on Maxisorp plates (Nunc) overnight at 4°C. Wells were blocked with PBS that contained 0.1% Tween-20 and 1% NFDM for 2 hours at
RT. Next, 100 µL of 1:200 diluted serum was added overnight at 4°C. After 5 washes with PBS that contained 0.5% NFDM, bound antibodies were detected with peroxidase-coupled rabbit-antihuman IgG (diluted 1:5.000) or with goat-antihuman IgA secondary antibody (diluted 1:5.000) for 1 hour at RT (both from Sigma-Aldrich). The substrate tetramethylbenzidine (Sigma-Aldrich) was added for 20 minutes, and absorbance at 620 nm was determined in an automated ELISA plate reader (LabSystems, Vantaa, Finland). For competitive inhibition, serum samples were preincubated with HIGAEGR-GST

for 20 minutes at RT.

**Western Blot Analysis**

In total, 150 ng of M. bovis BCG HSP-65 were resolved by electrophoresis on a 12.5% sodium dodecyl sulfatepolyacrylamide gel, and proteins were electrotransferred
onto a polyvinylidene fluoride membrane. After blocking of the membrane with PBS that contained 7% NFDM, 100 µL of patient serum (1:200) were added at 4°C overnight. After washing with PBS that contained 7% powdered milk, bound IgGs were detected with a peroxidase- coupled rabbit-antihuman IgG secondary antibody (Sigma-Aldrich). Detection was performed with the Roti- Lumin reagent (Roth, Karlsruhe, Germany). A monoclonal mouse IgM anti-human HSP-65 (anti-huHSP-65) antibody (StressGen Biotechnologies Corp.) served as a positive control.

**Immunohistochemistry**

HSP detection was performed on archived, formalinfixed, paraffin-embedded tissue sections (1 µm) with a monoclonal mouse IgG anti-huHSP-65 antibody (Stress- Gen Biotechnologies Corp.). The secondary antibody was a horseradish peroxidase, polymerized IgG antibody. Detection was performed with Liquid DABþ Substrate
Chromogen System (DAKO, Glostrup, Denmark), and slides were counterstained with hematoxylin. The intensity of HSP-65 (from 0 to 3 arbitrary units) was graded by a pathologist using similarly treated slides of breast cancer tissue as a positive control.

**Biostatistics**

The optical density (OD) of antibody reactions measured in ELISAs and phage binding were compared with 2-sided Student t tests. Standard deviations are reported as standard errors of the mean.

## RESULTS

**Combinatorial Screening on IgG From a BCG-Responding Bladder Cancer Patient**

A bladder cancer patient with Cis and concomitant T1/grade 2 disease who had a positive clinical outcome after BCG immunotherapy served as the index patient
(Patient 2). The circulating antibody pool from this index patient was probed according to a previous report from a sample that was obtained 3 months after initial diagnosis and 2 weeks after the last weekly BCG instillation.[11] Successive rounds of screening of a 7 mer, cyclic, random peptide phage-display library were performed on IgGs that were isolated in serum from this index patient after the induction cycle of BCG immunotherapy. During the screening, we observed a serial and marked increase in phage binding to the immobilized IgG from the index patient compared with control IgG obtained from healthy volunteers (Fig. 1). This results indicated binding of the selected ligand peptides displayed on the phage to the IgG from the patient. Sequencing the DNA corresponding to the inserts of individually selected phage clones identified an enrichment of the peptide motif HIGAEGR.

**Verification of Binding Specificity**

Specificity of the binding of HIGAEGR to the IgG pool from the index patient subsequently was determined. The binding of HIGAEGR-displaying phage to IgGs from the index patient was significantly greater (Student t test; $P < .05$) relative to that from age-matched and sex-matched, healthy control volunteers (Fig. 2A). Moreover, recombinant fusion HIGAEGR-GST, but not wild-type GST, significantly (t test; $P < .05$) and competitively inhibited the binding of HIGAEGR phage to IgGs from the index patient (Fig. 2B). In contrast, binding of negative control phage was not influenced by either recombinant GST protein. These results indicate that IgG antibodies from the index patient specifically recognizes the selected peptide motif HIGAEGR.

**Identification of the Corresponding Target Antigen**

By homology sequence comparison with online protein databases from the National Center for Biotechnology Information, M. bovis HSP-65 was identified as a possible corresponding antigen to the peptide motif HIGAEGR (Fig. 3A). A high level of similarity (71%) between the selected ligand peptide and HSP-65 was observed. Four residues were identical, and another residue was a conservative replacement with similar physiochemical attributes (histidine vs lysine). To validate HSP-65 as the native antigen binding to the IgG from the index patient, we evaluated immobilized HSP-65 by immunoblotting and in competitive binding inhibition by ELISA. HSP-65 was recognized specifically by the IgGs from the index patient and by the IgGs from another patient after successful BCG immunotherapy, but not by IgGs from healthy control volunteers (Fig. 3B). Binding of the IgGs from the index patient was augmented over binding to the control IgGs; moreover, binding was inhibited competitively by the cognate HIGAEGR-GST, but not by wild-type GST (Fig. 3C). Binding of control IgG was not influenced by any recombinant GSTs. Together, these results indicate that M. bovis BCG HSP-65 is the native antigen corresponding to the peptide sequence HIGAEGR. Thus, the humoral immune response from the index patient specifically targets M. bovis BCGHSP-65.

**Humoral Immune Response Against HSP-65**

We determined the predictive value of IgG and IgA antibodies against M. bovis BCG HSP-65 in a panel of patients who were receiving BCG immunotherapy for superficial, high-grade TCC (n = 16). Antibody titers against M. bovis BCG HSP-65 were measured at initial diagnosis, after the induction cycle, and at the first followup (Table 1).

Eleven patients responded to BCG immunotherapy and remained tumor-free for up to 67 months. Four patients did not respond and underwent radical cystectomies. Another patient required a second induction cycle after an initial clinical failure. Data from the failed and successful induction cycles were added to the nonresponding group and the responding group, respectively. No significant correlation of the clinical outcome with the following clinical features was observed in this small population: age (IgG titer vs age; P = .19), status of the tumor as recurrent or primary (IgG titer vs tumor status; P = .17), and restaging resection before BCG immunotherapy (IgG titer vs status of resection; P = .16). IgG and IgA antibody titers against M. bovis BCG HSP-65 were low in prostate cancer patients and healthy control volunteers. Similarly, titers in patients with bladder cancer other than superficial, high-grade TCC were low. All patients who were receiving BCG immunotherapy had low titers before therapy, regardless of their later clinical outcome (Figs. 4A and 4B) (OD for responders: IgG, 0.32 $\pm$ 0.08; IgA, 0.08 $\pm$ 0.03; OD for nonresponders: IgG, 0.18 $\pm$ 0.01; IgA, 0.01 $\pm$ 0.0). In clinically nonresponding patients, anti-HSP-65-specific antibody titers did not change detectably after the induction cycle (OD: IgG, 0.27 $\pm$ 0.12; IgA, 0.07 $\pm$ 0.04). In contrast, both IgG and IgA antibody titers rose significantly (pre-BCG vs post-BCG: IgG, $P < .01$; IgA, $P < .05$) in clinically responding patients (OD: IgG, 0.95 $\pm$ 0.16; IgA, 0.32 $\pm$ 0.05) and were significantly higher than titers in nonresponding patients (responders vs nonresponders: IgG, $P < .01$; IgA, $P < .05$). Furthermore, titers remained elevated throughout maintenance therapy and declined after up to 47 months and 15 months for IgG and IgA, respectively. These results demonstrate that increasing IgG and IgA antibody titers against M. bovis BCG HSP-65 after a BCG induction cycle exhibit a positive predictive value for clinical outcome. Patient 12 initially failed BCG immunotherapy (identified as Patient 12.1). Here, no significant increase in either antibody titer was observed. However, after a second induction cycle, a strong antibody increase was noted for IgG and IgA (identified

as Patient 12.2), and the patient responded clinically. Another patient terminated the induction cycle because of BCG-induced, irritative side effects (Patient 5)
after 4 instillations. Titers were low after the induction cycle but increased after 3 months, and the patient remained tumor-free.

**Histologic Expression of HSP-65**

Antibodies induced by BCG immunotherapy may target huHSP-65 in bladder tumor cells as a consequence of its similarity to M. bovis BCG HSP-65. Therefore, we examined
the incidence and localization of huHSP-65 in highgrade, superficial TCC (Fig. 5). huHSP-65 was weak in normal urothelium and apparently was elevated in high-grade TCC (Cis). No differences in expression were noted between responding patients and nonresponding patients (Table 1).

DISCUSSION

BCG immunotherapy traditionally has been used for the treatment of superficial, high-grade TCC of the bladder. However, unpredictable failure occurs in approximately 33% of patients after the induction cycle, potentially delays adequate treatment, and is accompanied by the risk of progression to muscle-invasive disease and distant metastasis. Several adverse risk factors, such as incomplete tumor resection and age, and positive factors, such as secondary transurethral resection, have been identified.
[9,10] However, determining the effectiveness of BCG remained indirect and was assessed either cystoscopically according to the absence or presence of tumor at the time of re-evaluation, typically 3 months after the initial diagnosis, or as a statistical factor. Therefore, we sought to identify a serum marker that would directly measure the immunostimulatory effect of BCG and predict the individual outcome of BCG immunotherapy. For our studies, we used patients who had high-risk, superficial TCC (eg, Cis or T1/grade 3 tumors) without distinguishing between tumor stages to rule out the influence of tumor type and to focus on a BCG-specific marker. We used an antibody-fingerprinting approach11 to evaluate the humoral immune response through combinatorial selection of a random peptide phage-display library on IgG isolated from an index patient after a BCG immunotherapy induction cycle.

In contrast to previous studies, which limited the response to a given subset of antigens,[12,16] our unbiased strategy allowed us to probe for the whole range of possible
target antigens, including neoantigens. This approach seems plausible, because humoral antitumor immune responses have been reported previously[13,14,17] and have
led to the identification of HSP-65 from M. bovis BCG as a target of humoral immune response during BCG immunotherapy. HSPs are a large family of highly conserved and immunogenic cytoplasmic components that can augment the immune response against tumor cells.[18] HSP- 65 is involved in protein scaffolding and is a known target of the immune system under several conditions. For example, serum antibodies against HSP-65 have been observed in atherosclerosis and in vasculitis.[19] Furthermore, a cellular polarized immune response against HSP-65 has been observed in mice after intravenous infection with BCG.[20] In our index patient, antibody production remained
dominantly directed against HIGAEGR (residues 16-22), as determined by the presence of antibody titers against both HSP-65 and the HIGAEGR-GST fusion protein. We conclude that this peptide sequence is the dominant epitope of HSP-65 involved in BCG immunotherapy and that this humoral immune response is induced by intravesical application of M. bovis BCG. Indeed, HIGAEGR is part of a highly homologous domain between human and mycobacterial HSP-65. Moreover, molecular mimicry between exogenously administered BCG antigens and huHSP was proposed as a major mechanism of BCG immunotherapy.[16,21]

There is evidence that a mainly cellular immune response is required for successful BCG immunotherapy.[6] However, it has been demonstrated that intravesical application of M. bovis BCG induces TH-2–mediated pathways. Therefore, it is tempting to speculate that BCG immunotherapy activates both cellular and humoral immune effector mechanisms.[8] It is uncertain whether the production of this antibody is therapeutically effective. We propose that it reflects activation of the immune system, and, in contrast to cellular activation, titers can be measured serially to determine the state of immune activation during and after BCG immunotherapy. It is noteworthy that a patient with BCG-induced urosepsis did not exhibit an increase in anti-HSP-65 IgG titers, a result indicating that this immunologic phenomenon is not merely a sign of nonspecific stress (data not shown). Our findings are consistent with those of other investigators. Lamm et al demonstrated a positive clinical outcome in patients who had an increase in anti-BCG IgG antibodies after BCG immunotherapy.[22] Therefore, it was not entirely surprising that an increase in both IgA and IgG titers after immunotherapy had a positive predictive value. However, our findings are in contrast with those of Zlotta et al[12] and van der Meijden et al[23]; both groups have reported antibody production against mycobacterial components as a negative prognostic marker for the outcome of BCG immunotherapy. However, the differences in patient selection could explain the diametrically opposed results: The patients recruited by Zlotta et al had a history of repeated recurrence and repeated futile intravesical therapies (eg, mitomycin). Because 16 of 17 reported patients had low and presumably less aggressive grades (from 1 to 2), we propose that these patients had a high tendency for recurrence.[12,23] In our cohort, all patients had grade 3 disease and had received no prior intravesical therapies. Thus, it is likely that that additional factors are determining the high aggressiveness of some tumors. Amore extensive study with more patients should identify reasons for the opposing results. In addition, the data reported here raise questions about the optimal BCG immunotherapy regimen. Typically, the induction cycle comprises 6 weekly instillations. In 1 patient, BCG immunotherapy was terminated after 4 instillations because of severe side effects. IgG titers against HSP-65 increased moderately after 3 months but were high at the next follow-up after 3 months, and the patient remained tumor-free. Another patient did not exhibit a significant increase in titers after 6 weekly instillations, and that patient developed a clinical recurrence. After a second induction cycle, his titers increased, and he has remained tumor-free since that time. Therefore, we propose an ‘‘individually tailored’’ induction cycle to be achieved by the monitoring of anti-M. bovis BCG HSP-65 titers. In the case of an insufficient increase in titers, additional cycles might be helpful before routine transurethral biopsy after 3 months. This treatment would be consistent with the common clinical practice—in case of failure, a second induction cycle may be performed.[24] The histologic expression of huHSP-65 was heterogeneous; it was elevated in high-grade, superficial TCC, and it was not suitable as a predictive marker of clinical outcome after BCG therapy.

A potential weakness of this study is that it represents results from a single institution and from a relatively small number of patients. However, the results were statistically significant. Because of the rarity of the disease and a tendency toward early cystectomy for T1/grade 3 disease, the patient numbers were low. Therefore, a larger and multicentric study would be desirable to further verify these results. This type of study also can rule out the possible influence of results from a single institution, such as surgical factors. Furthermore, such a study would allow a clear multivariate analysis of additional influencing factors, such as age and second transurethral resection before BCG immunotherapy.

In summary, to our knowledge, this report is the first to demonstrate a humoral immune response against HSP-65 at the time of re-evaluation after the induction cycle as a positive predictive marker for individual patient outcomes from BCG immunotherapy. IgA and IgG titers measured before and after the induction cycle predicted the success of treatment. We propose that monitoring anti-HSP-65 titers during the induction cycle would enable the development of an early assay for the detection of nonresponders and would lead to a treatment regimen designed on an individual basis.

## CONFLICT OF INTEREST DISCLOSURES

This study was supported by a grant from the Interdisciplinary Center for Clinical Research, University of Wurzburg (to P.U.A.).

## REFERENCES

1. Murakami T, Ebara S, Saika T, et al. Routine transurethral biopsy of the bladder is not necessary to evaluate the response to bacillus Calmette-Guerin therapy. Acta Med Okayama. 2007;61:341-344.
2. Morales A, Eideger D, Bruce A. Intracavitary bacillus Calmette- Guerin in the superficial bladder tumor. J Urol. 1976;116:180-183.
3. Sharma P, Old LJ, Allison JP. Immunotherapeutic strategies for high-risk bladder cancer. Semin Oncol. 2007;34: 165- 172.
4. Herr HW, Schwalb DM, Zhang ZF, et al. Intravesical bacillus Calmette-Guerin therapy prevents tumor progression and death from superficial bladder cancer: ten-year follow-up of a prospective randomized trial. J Clin Oncol. 1995;13:1404-1408.
5. Alexandroff AB, Jackson AM, O'Donnell MA, James K. BCG immunotherapy of bladder cancer: 20 years on. Lancet. 1999;353:1689-1694.
6. Saint F, Patard JJ, Maille P, et al. T helper 1/2 lymphocyte urinary cytokine profiles in responding and nonresponding patients after 1 and 2 courses of bacillus Calmette-Guerin for superficial bladder cancer. J Urol. 2001;166:2142-2147.
7. Bohle A, Brandau S. Immune mechanisms in bacillus Calmette- Guerin immunotherapy for superficial bladder cancer. J Urol. 2003;170:964-969.
8. Atkins H, Davies BR, Kirby JA, Kelly JD. Polarisation of a T-helper cell immune response by activation of dendritic cells with CpG-containing oligonucleotides: a potential therapeutic regime for bladder cancer immunotherapy. Br J Cancer. 2003;89:2312-2319.
9. Herr HW. Age and outcome of superficial bladder cancer treated with bacille Calmette-Guerin therapy. Urology. 2007;70:65-68.
10. Herr HW. Restaging transurethral resection of high risk superficial bladder cancer improves the initial response to bacillus Calmette-Guerin therapy. J Urol. 2005;174:2134-2137.
11. Mintz PJ, Kim J, Do KA, et al. Fingerprinting the circulating repertoire of antibodies from cancer patients. Nat Biotechnol. 2003;21:57-63.
12. Zlotta AR, Drowart A, Huygen K, et al. Humoral response against heat shock proteins and other mycobacterial antigens after intravesical treatment with bacille Calmette-Guerin (BCG) in patients with superficial bladder cancer. Clin Exp Immunol. 1997;109:157-165.
13. Hansson Y, Paulie S, Larsson A, Lundblad ML, Perlmann P, Naslund I. Humoral and cellular immune reactions against tumor cells in patients with urinary bladder carcinoma. Correlation between direct and antibody-dependent cell-mediated cytotoxicity. Cancer Immunol Immunother. 1983;16:23-29.

14. Studer UE, deKernion JB, Lovrekovich H, Lovrekovich L. Quantitative measurements of humoral immune response in mice to a FANFT induced bladder tumor. Urol Res. 1985;13:123-130.
15. Pasqualini R, Arap W, Rajotte D, Ruoslahti E. In vivo selection of phage-display libraries. In: Barbas CF 3rd, Burton DR, Scott JK, Silverman GJ, eds. Phage Display: A Laboratory Manual. Cold Spring Harbor, NY: Cold Spring Harbor Laboratory Press; 2000:1-24.
16. Zlotta AR, Van Vooren JP, Denis O, et al. What are the immunologically active components of bacille Calmette- Guerin in therapy of superficial bladder cancer? Int J Cancer. 2000;87:844-852.
17. Troye M, Hansson Y, Paulie S, Perlmann P, Blomgren H, Johansson B. Lymphocyte-mediated lysis of tumor cells in vitro (ADCC), induced by serum antibodies from patients with urinary bladder carcinoma or from controls. Int J Cancer. 1980;25:45-51.
18. Fuller KJ, Issels RD, Slosman DO, Guillet JG, Soussi T, Polla BS. Cancer and the heat shock response. Eur J Cancer. 1994;30A:1884-1891.
19. Schett G, Metzler B, Kleindienst R, et al. Myocardial injury leads to a release of heat shock protein (hsp) 60 and a suppression of the anti-hsp65 immune response. Cardiovasc Res. 1999;42:685-695.
20. Charo J, Geluk A, Sundback M, et al. The identification of a common pathogen-specific HLA class I A*0201-restricted cytotoxic T cell epitope encoded within the heat shock protein 65. Eur J Immunol. 2001;31:3602-3611.
21. Bruno S, Machi AM, Semino C, et al. Phenotypic, functional and molecular analysis of lymphocytes associated with bladder cancer. Cancer Immunol Immunother. 1996; 42:47- 54.
22. Lamm DL, Thor DE, Winters WD, Stogdill VD, Radwin HM. BCG immunotherapy of bladder cancer: inhibition of tumor recurrence and associated immune responses. Cancer. 1981;48:82-88.
23. van der Meijden AP, Steerenberg PA, van Hoogstraaten IM, et al. Immune reactions in patients with superficial bladder cancer after intradermal and intravesical treatment with bacillus Calmette-Guerin. Cancer Immunol Immunother. 1989;28:287-295.
24. van der Meijden AP, Sylvester R, Oosterlinck W, et al. EAU guidelines on the diagnosis and treatment of urothelial carcinoma in situ. Eur Urol. 2005;48:363-371.

FIGURE LEGENDS

**Figure 1.** (A) A random peptide phage-display library (CX7C; C indicates cysteine; X, any residue) was precleared on immunoglobulins from healthy donors before incubation. Selection was then performed on immunoglobulins from an index patient after successful bacillus Calmette-Guerin (BCG) immunotherapy for carcinoma in situ of the bladder. (B) Phage titers during the screening are shown (the asterisk indicates $P < .05$; Student t test). Bars represent binding of selected phage to immunoglobulin G of the index patient (gray bars) or pooled healthy donor volunteers (black bars). cfu indicates colony-forming units.

**Figure 2.** The peptide motif HIGAEGR specifically binds to immunoglobulin G (IgG) isolated from the index patient after successful bacillus Calmette-Guerin (BCG) immunotherapy for carcinoma in situ of the bladder. (A) Significantly more HIGAEGR phage binds to IgG from patients (Patient) than to IgG from age-matched and sex-matched, healthy donor volunteers (Control) (the asterisk indicates $P < .05$; Student t test). (B) The binding of HIGAEGR phage is inhibited competitively by HIGAEGR that displays glutathione-S-transferase (GST) (HIGAEGR-GST) (the asterisk indicates $P < .05$; Student t test) but not by wild-type GST (Control-GST).

**Figure 3.** Mycobacterium bovis (M. bovis) bacillus Calmette- Guerin (BCG) heat-shock protein (HSP)-65 is the antigen corresponding to the peptide HIGAEGR. (A) The selected oligopeptide HIGAEGR exhibits a strong similarity to the N-terminal sequence of M. bovis BCG HSP-65. (B) Western blot analysis demonstrated that, after BCG immunotherapy, 2 patients, but not healthy controls, had immunoglobulin G (IgG) directed against M. bovis BCG HPS-65. (C) Binding of the index patient's IgG (Patient) to M. bovis BCG HSP-65 was competitively inhibited by HIGAEGR/glutathione-S-transferase (GST) (light gray bars) but not by wild-type GST (dark gray bars). The binding of healthy donor IgG (Control) was significantly lower and was not influenced by HIGAEGR/GST (the asterisk indicates $P < .05$; Student t test). KD indicates kilodaltons; O.D., optical density.

**Figure 4.** High antibody titers against Mycobacterium bovis (M. bovis) bacillus Calmette-Guerin (BCG) heat-shock protein 65 (HSP-65) after BCG immunotherapy were identified as predictive of a positive clinical outcome. Bars represent (A) immunoglobulin G (IgG) and (B) IgA antibody response at the time of initial diagnosis (Pre BCG), after a BCG induction cycle (Post BCG), and after 6 monthly BCG maintenance instillations (Maint.) against immobilized M. bovis BCG HSP-65. Single asterisks indicate $P < .05$; double asterisks, $P > .05$ (Student t test). Bars represent standard error of the mean. NS indicates healthy donor sera; PCA, prostate cancer patient sera; Ta, and T2, T3, sera from patients with different stages of transitional cell carcinoma; O.D., optical density.

**Figure 5.** Human heat-shock protein 65 (huHSP-65) is expressed in high-grade, superficial transitional cell carcinoma (TCC). The expression of huHSP-65 was graded from 0 to 3 according to the intensity of staining. Muscle, fat, and connective tissue revealed a faint staining that was barely detectable (grade 0). Expression in normal urothelium was weak and predominantly cytoplasmic (grade 1). In all patients with TCC, levels of huHSP-65 were increased compared with those of normal urothelium (grades 2 and 3). (A) Normal urothelium is shown. (B) Positive control (human breast cancer) tissue is shown. (C,D) Human carcinoma in situ of the urinary bladder is shown (original magnification, x400 in A-D; scale bars = 100 μm).

**Table 1.** Patient Clinical Data

| Patient ID | Sex | Age, y | Tumor Type, Classification/ Grade | Recurrent Tumor | Second Resection Performed | Clinical Outcome | Therapy After Induction Cycle | IgG Response After Induction, OD | Disease-Free Period, mo | Persistence of IgG Titer, mo | Persistence of IgA Titer, mo | Histologic HSP-65 Expression, Grade1-3 | Comments |
|---|---|---|---|---|---|---|---|---|---|---|---|---|---|
| 1 | Man | 77 | Cis | No | No | Remission | BCG maintenance | 1077 | 48 | >26 | >15 | G2 | |
| 2 | Man | 69 | Cis, T1/G2 | No | No | Remission | BCG maintenance | 1162 | 55 | 14 | >14 | ND | Index patient |
| 3 | Man | 58 | Cis | No | Yes | Remission | BCG maintenance | 1452 | 52 | 14 | 14 | G | |
| 4 | Man | 65 | Cis, mTa/G2 | Yes | Yes | Remission | BCG maintenance | 2032 | 37 | 7 | 7 | ND | |
| 5 | Man | 66 | Cis | Yes | Yes | Remission | BCG maintenance | 265 | 55 | 47 | ND | ND | Incomplete induction |
| 6 | Man | 73 | Cis | No | No | Remission | BCG maintenance | 1204 | 43 | >11 | 4 | G1 | |
| 7 | Man | 71 | Cis | No | No | Remission | BCG maintenance | 317 | 67 | 45 | 12 | G3 | |
| 8 | Man | 67 | T1/G3 | No | Yes | Remission | BCG maintenance | 579 | 10 | >4 | ND | ND. | |
| 9 | Man | 72 | Cis | Yes | No | Remission | BCG maintenance | 454 | 55 | >22 | ND | ND | |
| 10 | Man | 73 | Cis | Yes | No | Remission | BCG maintenance | 366 | 15 | >9 | ND | ND | |
| 11 | Man | 80 | T1/G3 | Yes | No | Remission | BCG maintenance | 1585 | 18 | >7 | ND | ND | |
| 12.2 | Man | 68 | Cis | Yes | Yes | Remission | BCG maintenance | 959 | 53 | 36 | 9 | G2 | Second induction cycle |
| 12.1 | Man | 68 | Cis | Yes | No | Recurrence | Second induction cycle | 395 | NA | NA | NA | NA | First induction cycle |
| 13 | Man | 81 | Cis, T1/G3 | Yes | No | Recurrence | Cystoprostatectomy | 173 | NA | NA | ND | ND | |
| 14 | Man | 82 | Cis | Yes | No | Recurrence | Cystoprostatectomy | 9 | NA | NA | NA | G3 | |
| 15 | Man | 65 | Cis, Ta/G2 | Yes | No | Recurrence | Cystoprostatectomy | 124 | NA | NA | NA | ND | |
| 16 | Man | 69 | Cis, T1/G3 | No | No | Recurrence | Cystoprostatectomy | 37 | NA | NA | NA | G3 | |

ID indicates identification number; IgG, immunoglobulin G, OD, optical density; IgA, immunoglobulin A; HSP-65, heat-shock protein 65; Cis, carcinoma in situ; G, grade; BCG, bacillus Calmette-Guerin; ND, not done; NA, not available.

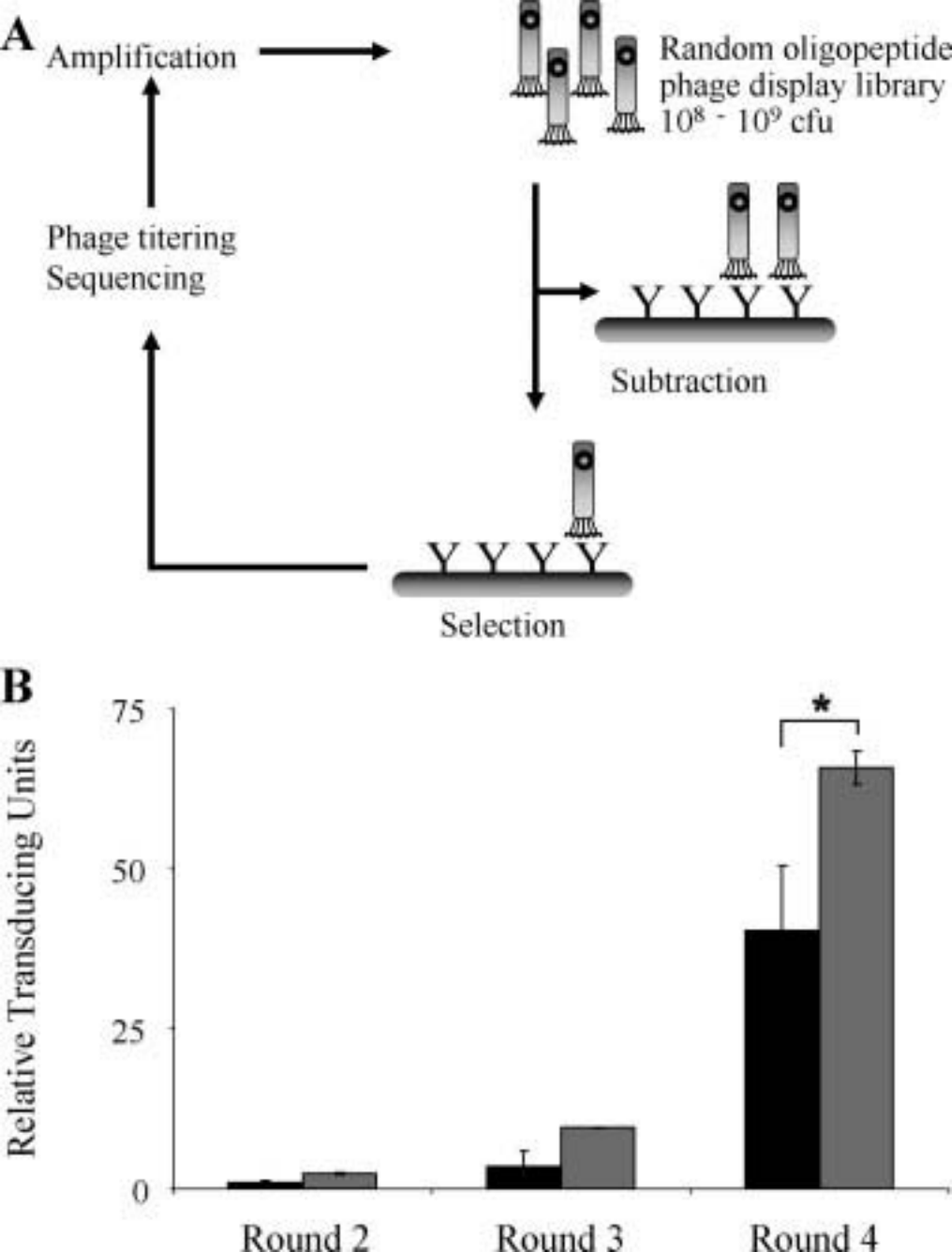
A
Amplification
Random oligopeptide
phage display library
10^8 - 10^9 cfu
Phage titering
Sequencing
Subtraction
Selection
B
Relative Transducing Units
75
50
25
0
*
Round 2
Round 3
Round 4

A

| | |
|---|---|
| Selected clone | 1-HIGAE GR-7 |
| Hsp65 M. bovis BCG | 1-EDPYEKIGAE LVKEVAKKTD DVAGDGTTTA ... |

B

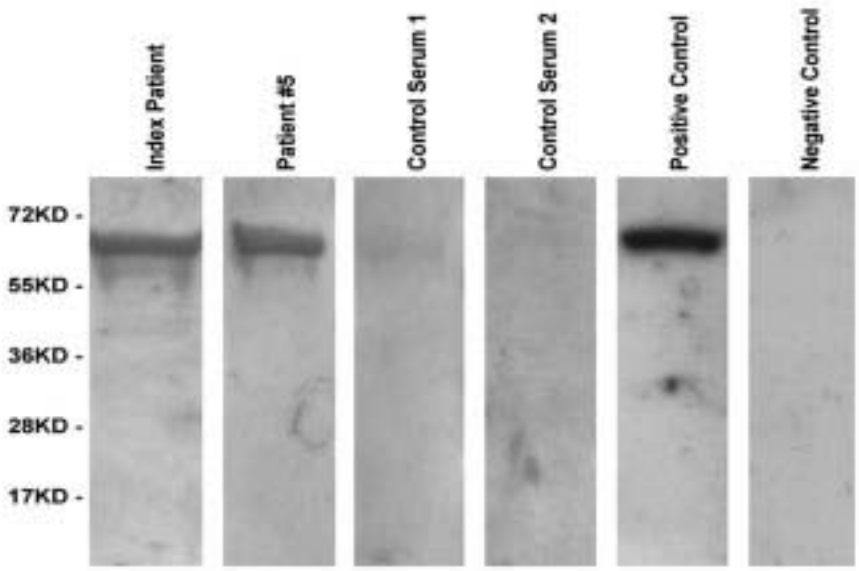


C

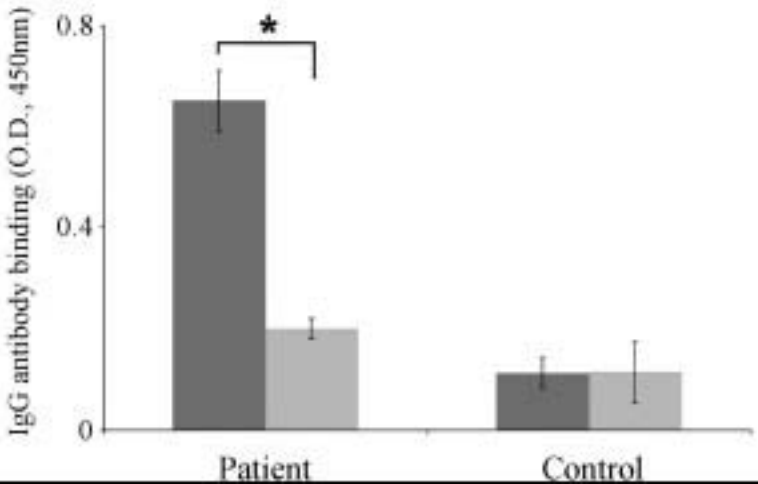

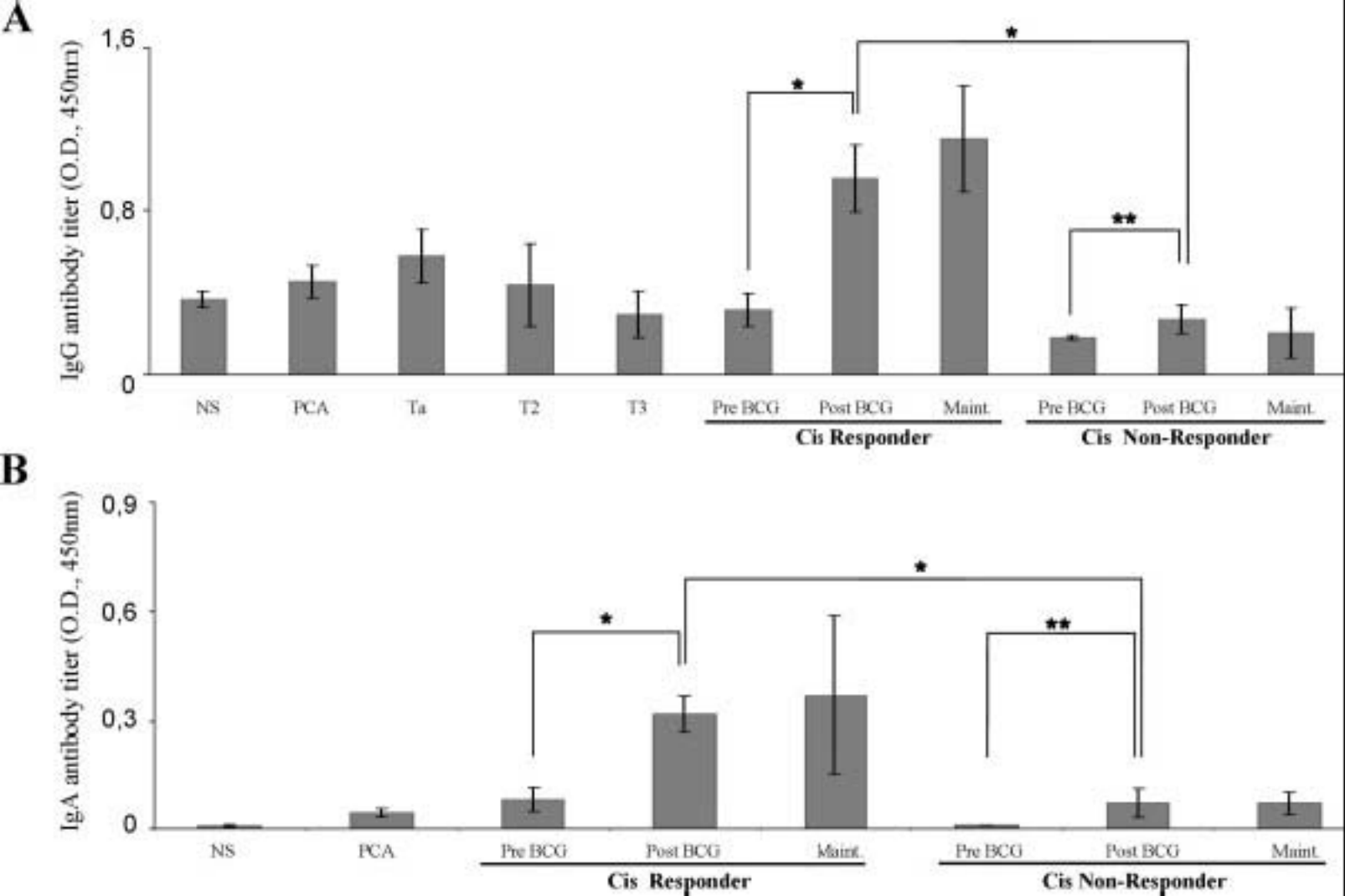
A
IgG antibody titer (O.D., 450nm)
1,6
0,8
0
NS
PCA
Ta
T2
T3
Pre BCG
Post BCG
Maint.
Cis Responder
Pre BCG
Post BCG
Maint.
Cis Non-Responder
*
*
**
B
IgA antibody titer (O.D., 450nm)
0,9
0,6
0,3
0
NS
PCA
Pre BCG
Post BCG
Maint.
Cis Responder
Pre BCG
Post BCG
Maint.
Cis Non-Responder
*
*
**

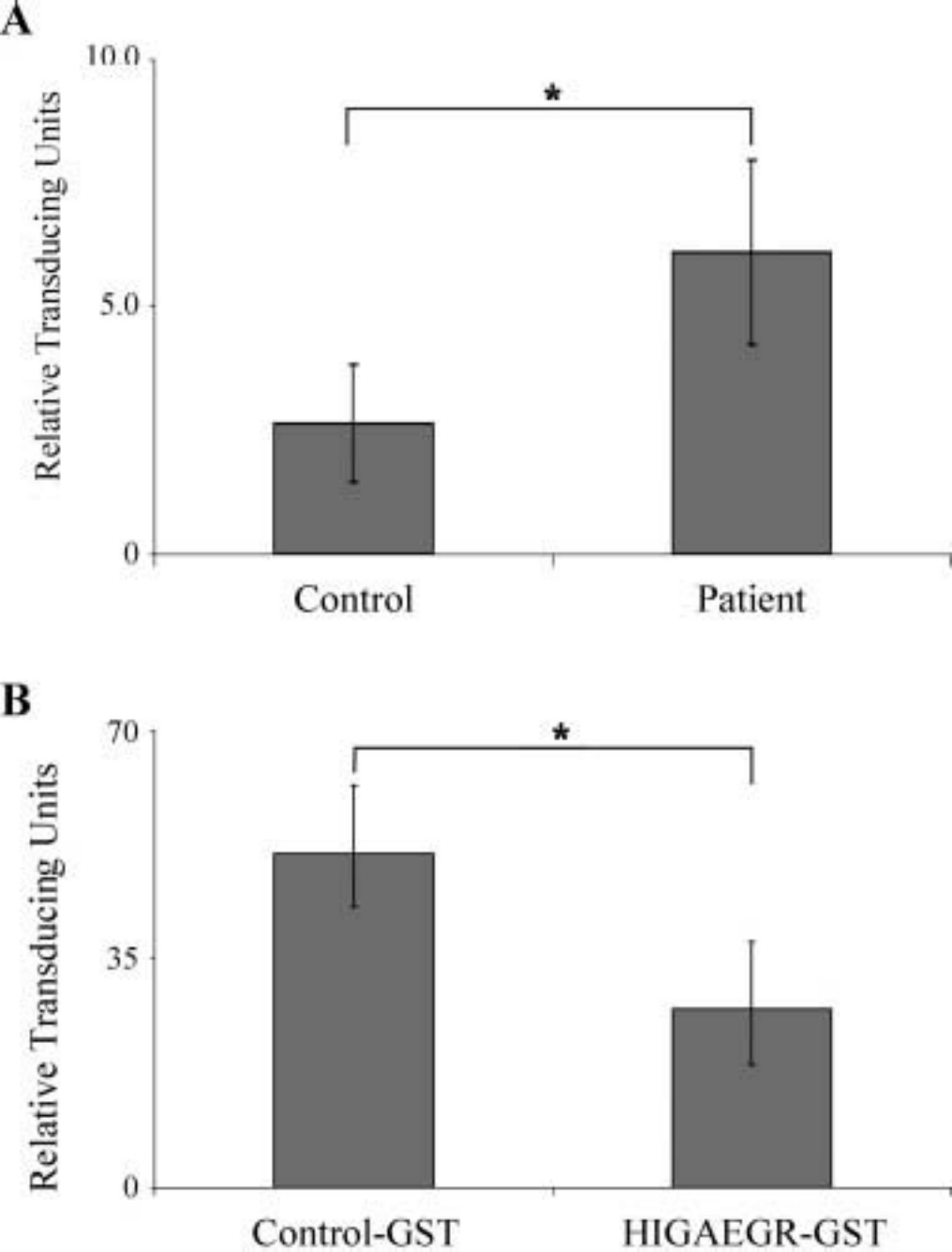
A
10.0
5.0
0
Relative Transducing Units
*
Control
Patient
B
70
35
0
Relative Transducing Units
*
Control-GST
HIGAEGR-GST

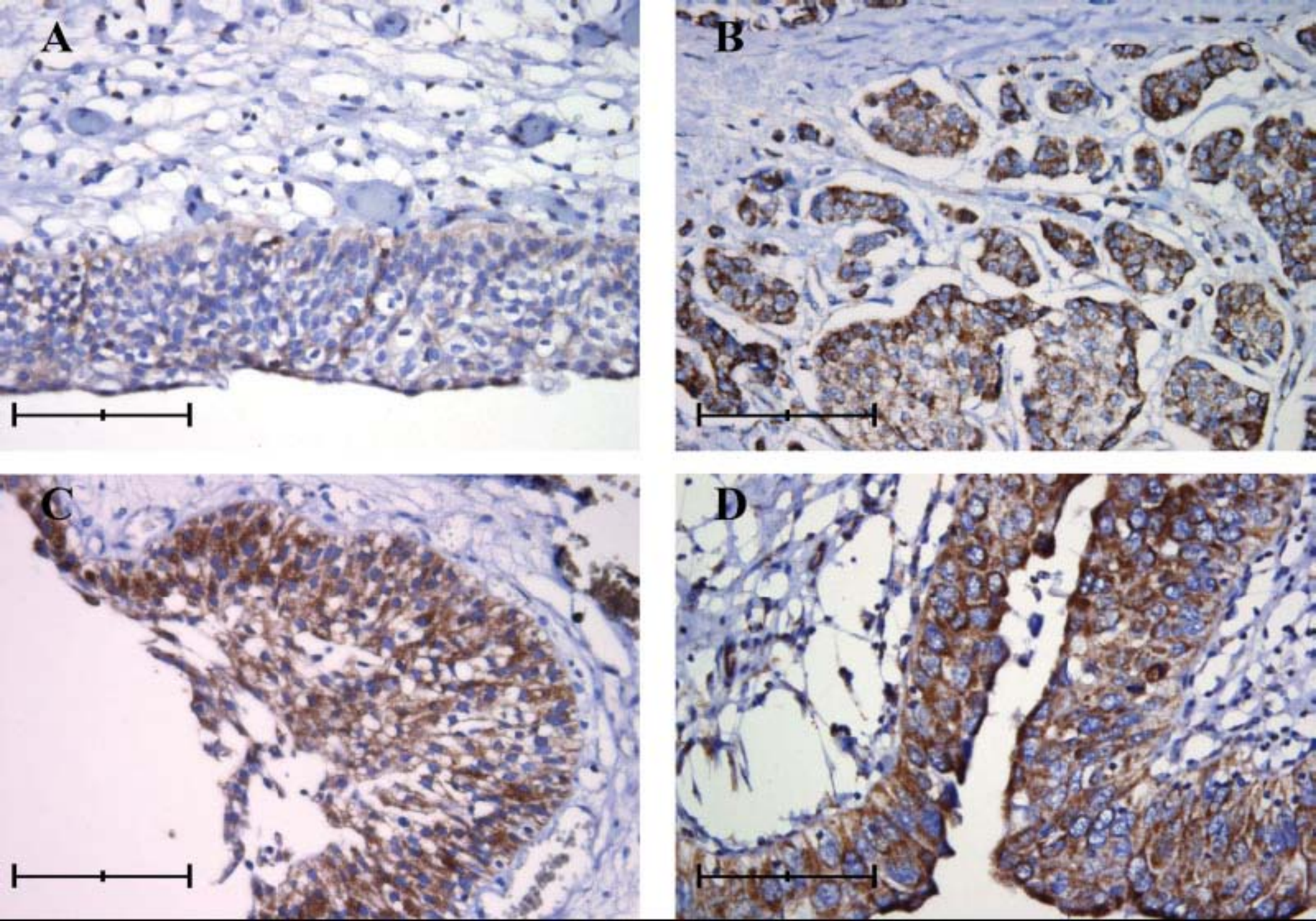
A
B
C
D

# STAT3 and SMAD1 Signalling in Medaka Embryonic Stem-Like Cells and Blastula Embryos

**Publiziert 2009 in Stem Cells and Development. 11; 18(1): 151-160.**

# STAT3 and SMAD1 Signalling in Medaka Embryonic Stem-Like Cells and Blastula Embryos

T.U. Wagner,1 M. Kraeussling,1 L.M. Fedorov,1 C. Reiss,1 B. Kneitz,2 and M. Schartl1

The activation and transcriptional activity of signal transducer and activator of transcription 3 (STAT3) is essential for maintaining mouse embryonic stem (ES) cell cultures in an undifferentiated state. However, reports from human and monkey ES-cell culture suggest that STAT3 is dispensable for pluripotency in these systems. At the same time, BMP signalling via Smad1 was shown to be able to counteract STAT3 signalling in murine ES-cell cultures, while it in: uences differentiation in multifaceted ways in other cellular contexts. Hence, the question arises whether the signalling situation found in mice or primates and human ES-cells represent the rule or the exception. With this study, we want to contribute an answer to this question from an evolutionary perspective. Therefore, we analyzed the expression and activation status of the Medaka (*Oryzias latipes*) STAT3 and SMAD1 in Medaka ES-cell-like cultures and their in vivo counterpart, the Medaka blastula embryo. While SMAD signalling is active in the culture system as well as in blastula embryos, our results indicate that STAT3 is inactive and can thus not be involved in pluripotency control of blastula cells or their derived pluripotent in vitro counterparts. These results suggest that the signalling pathways active in the mouse ES-cell culture system represent the exception, while inactivity of STAT3 is apparently the rule in vertebrate ES-cell cultures.

**Introduction**

Signal transducer and activator of transcription 3 (STAT3) is a member of the signal-transducer-and-activator-of-transcription family of latent transcription factors. It is involved in cellular signalling induced by a variety of cytokine-receptors [1–3]. In its inactive form, STAT3 monomers constantly shuttle between cytoplasm and nucleus, but predominantly localize to the cytoplasm [4,5]. Upon activation of the cytokine receptor common subunit gp130 [6], STAT3 monomers attach to a YXXQ motive [7,8] and become activated through phosphorylation of tyrosine 705 [9] by the receptor associated janus kinase JAK1 [10]. After being released from the receptor complex, phosphorylated STAT3 monomers are able to dimerize, accumulate in the nucleus [11,12] and bind to DNA. STAT3 is constantly shuttling between nucleus and cytoplasm, both in the monomeric and dimeric forms [4], but the transport mode and ef7 ciencies seem to be regulated so that the phosphorylated and dimerized form enriches in the nucleus [3]. Here, they act as transcriptional activators [13]. Inactivation of the

dimer occurs through dephosphorylation by Receptor Protein Tyrosine Phosphatase T [14]. The other latent transcription factor investigated here is Smad1 [15]. Predominantly cytoplasmic in its inactive, monomeric form, Smad1 becomes Serine-phosphorylated by BMP receptor complexes upon their binding of ligand-dimers. Once activated, Smad1 multimerizes with Smad4 and subsequently accumulates in the nucleus, where the complex predominantly acts as a transcriptional activator. Smads have recently been found to be inactivated by dephosphorylation by PPM1a [16]. In murine ES-cell cultures, leukemia-inhibitory-factor (LIF) is able to activate STAT3 [17,18] and thereby triggers a transcriptional programme [19] that maintains the developmental potential of the cultured ES cells [20]. The LIF-STAT3 axis does not fulfil this task on its own. In standard mouse
ES-cell culture, the medium contains several other factors and high amounts of serum. In addition, prolonged pluripotency is achieved by growing the ES-cells on a fibroblast feeder cell. Alternatively, a well-defined culture system was reported to maintain pluripotency of mouse ES-cells [21] by combined addition of BMP4 and LIF; thereby the need for presence of both feeder cells and serum can be alleviated. The pluripotency stabilising mechanism in this system depends on downstream inhibitory effects on differentiationexerted by STAT3 and the ID proteins—direct downstream targets of BMP-Smad signalling [22]. STAT3 and the BMPSmad pathway have been linked—mostly indirectly—in a variety of differentiation models, including fate choice of neural stem cells [23,24]. More recent studies on the molecular basis governing pluripotency in human embryonic stem cells (hESCs) as well as monkey ES-cell cultures revealed that both systems are independent of STAT3 and LIF [25–27]. Accordingly, BMP4 addition to hESC cultures leads to differentiation of the cells, while the BMP antagonist Noggin enhances selfrenewal [28]. It should be mentioned here that BMP4 treatment of mouse ES-cells in the absence of LIF will also lead to differentiation. This is explainable by the absence of active STAT3, and consequently, the lack of a balancing effect for BMP4-induced mes-/endodermal differentiation; the counterinhibition effect of BMP and LIF signalling pathways described for mouse is therefore nonexistent in primates
and humans in this context. These signifcant differences between such closely related
species as mouse and human in the very fundamental biological process of pluripotency control are surprising. They could be due to species-speciec differences in the regulation of pluripotency or in the processes required for the adaptation to the artificial in vitro culture situation. The comparison of the features guiding pluripotency between more distant vertebrate species both in vivo and in vitro could be a reasonable approach to obtain answers to such questions. We chose the Medaka system to compare the activities of STAT3 and SMAD signalling in vitro and in vivo. Being a teleost fish, Medaka is a vertebrate evolutionarily quite distant from mouse and human, but offers pluripotent cell culture systems and easy access to early embryonic stages. Similarly to the well established zebrafish model system, Medaka produces high numbers of offspring on a daily basis. The embryos are largely transparent throughout embryogenesis and, in contrast to zebrafish, their speed of development can be widely
controlled by temperature adjustment. Furthermore, the Medaka genome is available in high quality [29] and a broad spectrum of mutants is available through mutagenesis
screens [30–32]. In addition to the technical advantages as an in vivo model, Medaka also offers a set of well described cell culture lines. Establishment of ES-cell-like cultures derived from Medaka blastula s tage embryos was reported before [33]. When reintroduced into blastula embryos, these cells display a pluripotent differentiation phenotype and contribute to all somatic organs, yet lack the ability to contribute to

the germ line, a feature thus far only reported for ES-cell cultures from mouse. The molecular basis for their self-renewal has, however, not been investigated yet. Furthermore, there is no description of either *stat3* or *smad1* in Medaka. Taking
all these features together, Medaka represents a good model for comparison of pluripotency signalling with data available from mammalian culture systems.
Our aim was to identify the orthologues of both *smad1* and *stat3* in Medaka, and determine their activity status by localising their subcellular distribution in both Medaka stem cell cultures as well as in their embryonic origin, the blastula. We found cytoplasmic accumulation, of STAT3 in pluripotent cells of Medaka blastula embryos and cultures, suggesting low activity or inactivity of the pathway. SMAD1, in contrast, was predominantly found in the nuclei of Mes1 cells, and accordingly, also in all nuclei of early blastula embryos. Altogether, these results make it unlikely that STAT3 is generally involved in pluripotency control in vitro or utilized for that matter in vivo. With teleost 7 sh and humans not relying on STAT3 activity, the strong dependency of murine ES-cells may represent an enigmatic feature of this system.

## Materials and Methods

*Immunofluorescence staining and F uorescence microscopy*
For immunofluorescence experiments, embryos and cells were fixed with 4% paraformaldehyde, permeabilized with 0,1% Triton X in PBS, blocked with 5% BSA in PBS and incubated with anti-STAT3 antibody (SantaCruz Biotechnology, C-20) or anti-Smad1 antibody (SantaCruz Biotechnology, A-4) at 1:1000 dilution in 5% BSA in PBS overnight at 4°C. Detection was done with Alexa594-coupled anti-rabbit secondary
antibody at 1:1,000 in 5% BSA in PBS overnight at 4°C. DNA was stained using Hoechst 33258 (Molecular Probes) at 1:10,000 dilution in PBS for 1 h. For confocal imaging, a Leica SP2 system was used. For normal inverse microscopy, a Leica IM6000 system was used. All images were analyzed and formatted using ImageJ software.

*Cloning and expression patterning by RT-PCR of mfstat3*
Embryos of mixed stages (st.4–st.39) of Medaka (Carbio strain) were used for RNA extraction (ABgene) and cDNA synthesis (Fermentas). PCR with this cDNA as template was performed for 35 cycles at 56°C annealing temperature. Primers MF-STAT3_f04 (5′-AGGACTCGAGATGGCTCAGTGGAA CCAGTTACAGCA-3′) and MF-STAT3_r04 (5′-CTGCAGAATTCGCTTGTCATCGTCGTCCTTGTAGTCCATGGGG GAAGCGACGTCCATGT-3′) were used together with ReproFast (Genaxxon) proof reading polymerase to amplify full-length *stat3*. The PCR products were cloned into pEGFPN1 (ClonTech) and pmOrange-N1, respectively. After restriction digest with *Xho*I and *Eco*RI of PCR fragments and plasmids ligation with T4 Ligase (Fermentas) followed.
Positive clones were veri7 ed by sequencing. To clone MF-Smad1, the procedure was amplification at 56°C for 35 cycles with primers MF_Smad-f01 (5′AAGCTTCGAATTCTGATTACAAGGATGACGACGATAAGATGAATGTCACCTCACT CTTCTCATTCAC-3′) and MF_Smad1-r01(5′-GCCCGGGATCCCTAGGAGACAGAGGA TATAGGGTTGT-3′). Cloning into pEGFP-C1 (ClonTech) was done by ligation of *Eco*RI and *Bam*HI digested fragments. For RT-PCR expression analysis the primers MF_ef1a1-f01 (5′-GCCCCTGGACACAGAGACTTCATCA-3′) and MF_ef1a1- r01(5′-AAGGGGGCTCGGTGGAGTCCAT-3′) were used for the housekeeping gene *elongation factor 1-alpha-1* (*ef1a1*) and MF-STAT3-f04 (5′-AGGACTCGAGATGGCTCAGTGG

AACCAGTTACAGCA-3′) together with MF-STAT3-r02 (5′-CAGGAGATTGTGGAACA CCAGGGT-3′) were used for *stat3*, resulting in a 193 bp cDNA band. Other oligos used for expression a nalyses were: M F-Smad1-f02 (5′-CACCTTTCCTCATTCACC CTCTAG CT-3′) and MF-Smad1-r02 (5′-CTAAGGGCAAGGGTGGAGCCATGA-3′) yielding a 160 bp cDNAproduct, MF-Smad5-f01 (5′-CCGCTTCTGCCTCGGGCTGTTGT-3′) and MF-Smad5-r01 (5′-CACACGGTGGTGGGATGGAAGTTGT-3′) yielding a 195 bp cDNA product, MF-Smad7-f01 (5′-GTGGGTCTACAACCGCAGCTGCT-3′) and MFSmad7-r01 (5′-CTGTGCGAGGCTGCTGCGTGAA-3′ yielding a 185 bp cDNA product, MF_id2-f02 (5′- TCCAGCGTCGCAC TGAGCAGCCT-3′) and MF_id2-r03 (5′-CAGCCCCACTT ACCGCCTTAACGA-3′) yielding a 184 bp cDNA product.
RT-PCR was done with 1 $\mu$g of total RNA and random hexamer primers, resulting in 80 $\mu$l of cDNA of which 1 $\mu$l was used for every PCR reaction. PCRs were run for 32 cycles with an annealing temperature of 58°C and 30 s extension times. Murine STAT3 was cloned into pEGFP-N1 (Clontech) by PCR ampli7 cation with mus_stat3-f03 (5′-AGACG AATTCAGATCTCTCGAG ATGGCTCAGTGGAACCAGCT-3′) and mus_stat3-r04 (5′-CACCATGGATCCCTTATCGTCGTCATCCTTGTAATCTTTCCAAACTGCATCAATGAAT GGT-3′). Vector and PCR product were cut using *Eco*R1 and *Bam*H1 and ligated. A resulting clone was veri7 ed by sequencing.

*Sequence analyses*
Sequences for known genes and proteins were obtained from Ensembl (http://www.ensembl.org). The Medaka genome assembly available at Ensembl website was used for locus analysis and mfstat3 identification by BLAST. Sequences were loaded into BioEdit [34], translated into amino-acid sequences and aligned with CLUSTALW [35] as implemented in BioEdit.

*Animals and cell lines*
Medaka fish of the Carbio strain (Carolina Biological Supplies) used for this study were kept in the aquarium facility of the Biocenter Wurzburg. Mes1 cells, Medaka ES cell line 1 (Mes1), were cultured as described before [36]. Blastocysts were isolated from C57BL/6J females at day 3.5 after positive vaginal-plug. Zona pelucida has been removed by digestion with Tyrode's solution (Sigma-Aldrich, Taufkirchen). Parental mice were kept in the mouse facility of the Biocenter Wurzburg. Transfections of cell lines were done using TransIT-LT1 (MirusBio) or FugeneHD (Roche) according to the manufacturer's protocols. WW6 ES-cells were cultured feeder free on gelatinecoated plates in DMEM medium (Gibco, Karlsruhe) containing 10% FCS, nonessential amino acids, nucleosides and LIF (2 x 104 U/ml).

## Results

*Identication of Medaka stat3 and smad1 genes*
With the recent publication of the Medaka genome sequencing project [29], it became possible to better predict the exact relationships between genes of a large and complex subfamily such as the *stats*. The *mfstat3* gene is highly conserved (84% amino-acid identity with the human sequence) and maps to chromosome 8. It contains 22 coding exons. The amino-acid alignment (Supplementary Fig. 1) between Medaka, mouse and human r evealed that t he major sites for secondary protein modi7 cation known for mammalian STAT3 are conserved in the C-terminal region: the tyrosine residue 705 (mammalian count) is the prime target of activating

phosphorylation, upon which dimerization of STAT3 occurs and leads to nuclear accumulation and transcriptional
activity. There is a 12 AA long stretch of perfect homology between Medaka and human STAT3 surrounding this residue. The second very important site of regulatory phosphorylation in the mammalian protein is serine 727 (mammalian count). At this position, there is again a 10 AA long stretch of perfectly matching residues between all analyzed sequences. These findings suggest that the regulation on protein level is likely conserved at both these sites, and again raises the probability of functional conservation. Due to a genome-wide duplication event that took place during early teleost diversification [37], many mammalian genes have two counterparts in model fish such as zebrafish or Medaka. Such a duplication makes functional comparison between species more complicated as subfunctionalization, neo-functionalization and redundancy in function between both genes need to be analyzed. Hence, it is important to note that no second *stat3* copy was found in the Medaka genome.
The Medaka orthologue of *smad1* was also identified by blasting the Ensembl database with the human protein sequence. The gene maps to chromosome 1 and comprises
6 exons, which translate into 469 amino acids. At more than 89% amino-acid identity, the homology on protein sequence level between human and Medaka is very high
(Supplementary Fig. 2). Importantly, the primary regulatory region, the C-terminal S-S-V-S tail, is perfectly conserved throughout all species. In order to be able to visualize STAT3 and SMAD1 localization, the coding sequence of STAT3 was fused with the
coding sequences for either fluorescent protein variant eGFP or mOrange [38], repectively. As reported in the literature, C-terminal fusions to STAT3 proteins allow full functionality [39]. For SMAD1, the coding sequence for GFP was fused to its N-terminus in order not to interfere with the regulatory C-terminus [40]. Truly monomeric : uorescent protein variants were used [41], so that STAT3 and SMAD1 dimerization will not occur due to the fusions.

*Subcellular localization of MFSTAT3 in Mes1 cells*
Our goal was to clarify the activity status of STAT3 signalling in both Medaka ES cell cultures and also in the blastula embryo. As with most latent transcription factors that
act in signal transduction, the predominant localization of STAT3 to the cytoplasm when inactive, and accumulation in the nucleus when active, allows to infer functional information by determination of subcellular localization [42]. Consequently, immunofluorescence against STAT3 was performed on Mes1 cells held under standard culture conditions (Fig. 1). The nuclei of all Mes1 cells showed very weak or no signal, while the nuclear periphery and other cytoplasmic spots gave strong signals. When murine LIF was added to the cultures, no change in STAT3 distribution could be observed. Human IL-6 did not result in a response either. Hence, it was not possible to show the antibody specificity by translocation studies. An alternative way of verification was the generation of a fusion protein between Medaka STAT3 and GFP (and one with mOrange [38]). In parallel, a murine STAT3-GFP fusion was generated as well. This construct served as a positive control as fusions of GFP variants to murine and human STAT3 have been widely used and proven to reflect endogenous STAT3 behavior [4,39,43–46]. Mes1 cells were subsequently transfected with either variant. As a live marker for the nucleus, a fusion of Histone2B [47] with eBFP2 [48] was cotransfected.
Both combinations clearly localize to the cytoplasm of Mes1 cells (Supplementary Fig. 3A–F). Still, translocation could not be seen when cells were treated with potential ligands. However, a change of growth surface from gelatin-coated plastic to collagen-I-coated glass coverslips resulted in accumulation of STAT3 in prominent spots within Mes1 nuclei (Supplementary Fig. 3G–I). The change of surface apparently induces subnuclear condensation of STAT3 into 2–4

distinct foci, with little signal coming from other areas. Also, the DNA staining in these STAT3-rich areas is very weak. As
further control experiments, immuno: uorescence assays on mouse ES-cells as well as on their in vivo counterpart, 3.5 dpc blastocysts, were performed. Here, mouse ES-cells represent the reference cell culture system with active STAT3 signalling. STAT3 was found to be clearly accumulated in all mouse ES-cell nulcei (Supplementary Fig. 4A–C), with minor staining of the nuclear periphery. Consistent with this finding, ICM cells of 3.5 dpc mouse blastocysts show strong nuclear STAT3 signals—even though the cytoplasm
of these cells is also STAT3 positive. Taken together, these experiments verify that the STAT3 pathway is principally functional in Mes1 cells, and that our methods are able to
detect signalling changes. Furthermore, mouse ES-cells known to strongly depend on STAT3, show a dominant nuclear localization. This again demonstrates that nuclear
STAT3 represents a state of activity in respect to target gene activation documented for mouse ES-cells [11,19,20,49,50]. Consequently, nuclear accumulation is taken as a feature directly correlated to pathway activity. Hence, it can be concluded that STAT3 is mostly inactive under standard growth conditions in Medaka ES cells and is therefore probably not involved in control of the pluripotent state of these cells. In addition, STAT3-related pathway-routes were tested to make sure that the observed inactivity is not simply a result of a transducer switch within a protein family or pathway system. STAT1 is able to signal in response to gp130 ligands [51] and apparently competes with STAT3 for recruitment to receptor complexes. However, STAT1 was, just like STAT3,
predominantly found in the cytoplasmic side of the nuclear periphery of fixed Mes1 cells (Supplementary Fig. 5A–C). MAPK signalling on the other hand was found to be active by western blot analysis of lysates of different cell types with a phospho-Erk1/2 antibody (Supplementary Fig. 5D). This was expected as the growth medium of Mes1 cells contains bFGF.

*Expression and subcellular localization of MFSTAT3 in Medaka blastula embryos*

The results from the in vitro culture were then compared to the embryonic origins of the cell line, the blastula (Fig. 2). Expression analysis of *stat3* mRNA by RT-PCR (Fig. 3A) was positive for all tested developmental stages. Importantly, *stat3* mRNA is readily detectable in unfertilized eggs and also in the subsequent early cleavage stages. During that period of embryonic development there is no active transcription of the zygotic genome. Only around stage 10, when the mid-blastula transition occurs in Medaka, the embryonic transcription is started [52]. Hence, *stat3* mRNA is maternally
deposited in the egg, but also expressed zygotically during later stages of embryogenesis. In order to compare STAT3 signalling status between the Mes1 system and the pluripotent cells of the embryo, Medaka embryos were 7 xed at, and around stage 11 of development, the time point from which stem cell cultures are derived.
Immunofluorescence against STAT3 was performed and the embryos were analyzed with a confocal microscope. Interestingly, not a single cell of the Medaka blastula embryo shows accumulation of STAT3 in its nucleus (Fig. 4). When an overlay of the DNA staining and the STAT3 localization was done (Fig. 4C), there is no overlap detectable. In order to independently verify these data, mRNAs for H2BGFP and
MFSTAT3-mOrange were prepared in vitro and coinjected into one-cell stage Medaka embryos. Again, there was a clear distinction between nuclear GFP signal and cytoplasmic mOrange localization (data not shown). Thus, like in the stem cell culture system, the pluripotent cells of the early Medaka embryo do not show STAT3 activity. In order to make sure that stage 10–11 is not simply a short window of STAT3 inactivity,

we also looked at embryos of stages 8 and 9. Again, no cell with nuclear STAT3 was found (Supplementary Fig. 7).

*Expression of smad1 during embryogenesis*

Next, BMP-SMAD signalling, the second pathway involved in control of stemness in mouse ES-cell culture, was analyzed. RT-PCR on a series of early embryonic stages of Medaka was performed in order to determine expression of *smad1* (Fig. 3B). No maternally deposited mRNA was detectable. Zygotic transcription of *smad1* does not start directly with mid-blastula transition, but only during early patterning. Hence, expression analyses were extended and cDNAs were assayed for *smad5*, *smad7* and the direct BMP2/4-Smad target gene *id2*. Strong signals for all three mRNAs were detected during both maternal and zygotic phases of development (Fig. 3B), similar to what has been reported for early zebrafish development [53]. However, in murine ES-cell cultures, SMAD1 is the primary BMP signal transducer. Furthermore, Mes1 cells strongly express *smad1*, *smad5*, and *smad7* (Fig. 3C). When available within a cell, SMAD1, SMAD5, and SMAD7 will all react to BMP receptor activation with nuclear enrichment. Hence, investigation of BMP signal activity in both ES-cells and blastula embryos of Medaka is possible by determination of the subcellular distribution of ectopically expressed MFSMAD1-GFP.

*BMP signalling activity as determined by SMAD1 localization*

We used immuno: uorscence with a SMAD1/5/7 antibody (Santa Cruz) to determine the activity status of the canonical BMP signalling cascade. A strong nuclear enrichment of MF-SMAD1 was found in Medaka ES-cell cultures under standard growth conditions (Fig. 4A–C). To verify this result, we cloned a fusion protein of GFP and MFSmad1 and transfected the construct into Mes1 cells (Supplementary Fig. 6A and C). As a live marker for the nucleus, cotransfection of a construct encoding Histone2B-eBFP2 (Supplementary Fig. 6B and C) was used. To employ an already verified tool, we also used human Smad1 fused to CFP [54] in the same assay (Supplementary Fig. 6D and F). In all cases, a predominant nuclear localization of Smad1 was found. It should be noted that in contrast to STAT3, in the case of SMAD1, no change of localization was observed upon changing the growth surface from gelatine-coated plastic to collagen-coated glass.

*BMP signalling activity during early blastula stages of Medaka*

Prompted by the activity of the BMP cascade in cultured ES-cells, we investigated their embryonic origin, the early blastula, using injection of in vitro transcribed mRNA coding for GFP-MF-SMAD1. As a nuclear marker, mRNA coding for a fusion of Histone2B and eBFP2 was coinjected. Embryos were allowed to develop until early blastula stage, fixed, and imaged with a confocal microscope. All cells of all embryos imaged at stage 10 displayed nuclear accumulation of GFP-MF-SMAD1 (Fig. 5A–C), strongly suggesting active BMP signalling—probably transduced by a different SMAD in vivo. There is a considerable amount of nonnuclear GFP signal, but this is expected as SMADs constantly shuttle between nucleus and cytoplasm, even when phosphorylated [40]. Together, these results confirm that the BMP-SMAD signalling status of the Medaka culture system matches that found in the blastula embryo in vivo.

## Discussion

The control of the undifferentiated state of stem cells is a very basal process in all multicellular organisms. Alterations in this system are hard to establish, because of the dependency of all other cell types on the validity of the pluripotency of the stem cells. Studies on different mammalian ES-cell culture systems unveiled a strong discrepancy in the molecular control of the undifferentiated state. While mouse ES-cells depend on STAT3 activity [18,20], this is completely dispensable for upkeep of monkey and hES
cultures [25–27]. Looking at a lower vertebrate model system, the Medaka, it was possible to gain insight into the evolution of STAT3 function in ES-cells. Medaka represents a powerful model system for such analyses. These fish belong to the teleost lineage. The Medaka contains no extra copies of *stat3* or *smad1/5/7.* This fact, together with very high conservation level of the amino-acid sequences between Medaka and human (>80%)—especially around the known sites for regulatory secondary modi7 cations—strongly suggest a functional conservation as well. We hence reasoned
that it would be possible to assess the signalling status of two major pathways involved in pluripotency control in the mouse in the Medaka system both in culture and in the
embryo. In both cases, the subcellular localization of the signal transducer proteins is directly related to the signalling status of the respective pathway [39,55–57]. Therefore, *stat3* and *smad1* genes were isolated from Medaka and used as live reporters for signalling activity by fusing them to fluorescent proteins [4,40].
Next, Medaka ES cells were transfected with MFSTAT3-GFP and imaged live under standard culture conditions. Alternatively, a murine STAT3-GFP fusion and a STAT3-
antibody were used for verification of the results. In all cases, STAT3 strictly localized to the cytoplasm of Mes1 cells. While addition of mammlian ligands known to induce
STAT3 activation (mLIF and hIL6) did not result in a change of localization in Mes1 cells, a change of growth surface lead to STAT3 activation and cellular redistribution. The mechanisms behind this surface-induced STAT3 activation remain elusive. However, the fact that STAT3 can be found in its active form in Mes1 cells under these conditions suggests that the detection strategies used throughout this study are valid. We furthermore looked at the situation in mouse to be able to compare the Medaka system with a STAT3-dependent one. There, strong nuclear accumulation of STAT3 in the nuclei of mouse ES-cells was detected. In summary, signalling pathways utilising STAT3 as transducer should be considered inactive under normal growth conditions of Medaka ES-cells. This result is in strong contrast to the situation in mouse ES-cell cultures, but matches results from studies done with human ES-cells as well as monkey ES-cells. As Medaka ES-cell cultures were derived from blastula embryos, it was essential to compare the signalling status of STAT3 between the in vivo origin and the culture system. Therefore, STAT3 protein localization in these embryonic stages was analyzed. Exclusive cytoplasmic localization of STAT3 perfectly fit with the cultured stem cell situation. In comparison, mouse blastocysts (3.5 dpc) showed nuclear STAT3 in the ICM cells, albeit the cytoplasmic levels were also significant. Hence, the inactivity of STAT3 signalling in Mes1 cells does not represent a culture-induced artefact, but resembles the status of the embryonic origin of the cells in this respect. We also looked at the distribution of SMAD1 in both ES-cell culture and blastula embryos of Medaka. Here,
the results were uniform again: SMAD1 is enriched in the nuclei of ES-cells and early blastula embryos. Change of the growth surface of Medaka ES-cells d id not result in a
relocation of SMAD1. These observations are supported by readily detectable expression in Mes1 cells and blastulae of the direct SMAD1 target gene *id2* [22], which is principally a negative regulator of many bHLH transcription factors involved in differentiation [58]. BMP-SMAD1

signalling is generally considered to induce mes-/endodermal differentiation of stem cells when not counteracted [59,60].
We thus hypothesize that BMP-SMAD signalling at the detected level does not lead to differentiation of Mes1 cells, even though it is not counteracted by STAT3 as needed in the mouse culture system. From these data, it is not possible to tell whether other signalling pathways are actively inhibiting BMP-induced differentiation. The concept of counterinhibition of differentiation by STAT3 and SMAD1 described for mouse ES-cells [21] is not applicable to the Medaka system. In conclusion, the mouse ES-cell system can be kept in pluripotency by activation of STAT3 and SMAD1, while Medaka, monkey and human cultures a re independent of STAT3. Still, it is important to note that mouse ES-cells are by far the best characterized system and still the only one able to contribute to the germ line upon reintroduction into early embryos. Other pathways including Wnt >β -catenin, PI3K and Notch are known to play important roles in pluripotency
control as well, but these have not been analyzed in great detail outside of the mouse [61–66]. To understand the extrinsic regulation of pluripotency and discriminate culture-artefacts from in vivo relevance, a combinatorial approach between cell culture experiments and verification in early embryos is AQ3 necessary. Furthermore, the largely view of isolated, rather canonical signalling pathways has to be changed to one of broader signalling networks [67–69]. Examples for system-wide analyses [19,70] followed by in-depth characterization of interesting data are the successes in reprogramming of 7 broblasts into pluripotent cells [71,72]. Outlining of transcriptional networks guiding pluripotency was possible due to advances in genomics— mainly through methods such as microarrays [73], chromatin-immunoprecipitation [74], and their combinations [75]. Deciphering signalling networks is yet more challenging, as
methods to assess signalling status of a series of different pathways such as antibody-arrays are so far not widely available. However, only more detailed knowledge of the mechanisms involved in signal integration will make it possible to understand extrinsically guided and induced pluripotency, carrying along the ability to manipulate the differentiation status of cells with nongenetic means.

**Acknowledgments**
We would like to thank the EU for funding through the Plurigenes project. Furthermore, thanks go to Dr. S. Meierjohann for f ruitful discussions throughout the work and to EC. Thoma for practical help. We thank Dr. Michael Davidson for kindly providing plasmids encoding EBFP2. We thank Dr. Gregory Harms for providing the phSmad1-L-CFP construct and helpful discussion. We thank Dr. Roger Tsien for providing mOrange and other mFruit plasmids. We also thank the Ensembl team and the Japanese Sequencing
Consortium for compiling a high quality Medaka genome.

**References**
1. Boulton TG, Z Zhong, Z Wen, JE Darnell, Jr., N Stahl and GD Yancopoulos. (1995). STAT3 activation by cytokines utilizing gp130 and related transducers involves a secondary modi7 cation requiring an H7-sensitive kinase. Proc Natl Acad Sci USA
92:6915–6919.
2. Hebenstreit D, J Horejs-Hoeck and A Duschl. (2005). JAK/STATdependent gene regulation by cytokines. Drug News Perspect 18:243–249.
3. Vinkemeier U. (2004). Getting the message across, STAT! Design principles of a molecular signaling circuit. J Cell Biol 167:197–201.

4. Pranada AL, S Metz, A Herrmann, PC Heinrich and G Muller-Newen. (2004). Real time analysis of STAT3 nucleocytoplasmic shuttling. J Biol Chem 279:15114–15123.
5. Reich NC and L Liu. (2006). Tracking STAT nuclear traf7 c. Nat Rev Immunol 6:602–612.
6. Kishimoto T. (1994). Signal transduction through homo- or heterodimers of gp130. Stem Cells 12 (Suppl. 1):37–44; discussion 44–35.
7. Abe K, M Hirai, K Mizuno, N Higashi, T Sekimoto, T Miki, T Hirano and K Nakajima. (2001). The YXXQ motif in gp 130 is crucial for STAT3 phosphorylation at Ser727 through an H7-sensitive kinase pathway. Oncogene 20:3464–3474.
8. Zhang T, WH Kee, KT Seow, W Fung and X Cao. (2000). The coiled-coil domain of Stat3 is essential for its SH2 domainmediated receptor binding and subsequent activation induced by e pidermal g rowth factor a nd i nterleukin-6. Mol C ell Biol 20:7132–7139.
9. Sasse J, U Hemmann, C Schwartz, U Schniertshauer, B Heesel, C Landgraf, J Schneider-Mergener, PC Heinrich and F Horn. (1997). Mutational analysis of acute-phase response factor/Stat3 activation and dimerization. Mol Cell Biol 17:4677–4686.
10. Lutticken C, UM Wegenka, J Yuan, J Buschmann, C Schindler, A Ziemiecki, AG Harpur, AF Wilks, K Yasukawa, T Taga, T Kishimoto, G Barbieri, S Pellegrini, M Sendtner, PC Heinrich and F Horn. (1994). Association of transcription factor APRF and protein kinase Jak1 with the interleukin-6 signal transducer gp130. Science 263:89–92.
11. Sato N, R Tsuruma, S Imoto, Y Sekine, R Muromoto, K Sugiyama and T Matsuda. (2005). Nuclear retention of STAT3 through the coiled-coil domain regulates its activity. Biochem Bioph Res Co 336:617–624.
12. Ushijima R, N Sakaguchi, A Kano, A Maruyama, Y Miyamoto, T Sekimoto, Y Yoneda, K Ogino and T Tachibana. (2005). Extracellular signal-dependent nuclear import of STAT3 is mediated by various importin alphas. Biochem Bioph Res Co 330:880–886.
13. Becker S, B Groner and CW Muller. (1998). Three-dimensional structure of the Stat3beta homodimer bound to DNA. Nature 394:145–151.
14. Zhang X, A Guo, J Yu, A Possemato, Y Chen, W Zheng, RD Polakiewicz, KW Kinzler, B Vogelstein, VE Velculescu and ZJ Wang. (2007). Identi7 cation of STAT3 as a substrate of receptor protein tyrosine phosphatase T. Proc Natl Acad Sci USA 104:4060–4064.
15. Massague J, J Seoane and D Wotton. (2005). Smad transcription factors. Gene Dev 19:2783–2810.
16. Duan X, YY Liang, XH Feng and X Lin. (2006). Protein serine/ threonine phosphatase PPM1A dephosphorylates Smad1 in the bone morphogenetic protein signaling pathway. J Biol Chem 281:36526–36532.
17. Smith AG, JK Heath, DD Donaldson, GG Wong, J Moreau, M Stahl a nd D R ogers. ( 1988). I nhibition of p luripotential embryonic stem cell differentiation by puri7 ed polypeptides. Nature 336:688–690.
18. Williams RL, DJ Hilton, S Pease, TA Willson, CL Stewart, DP G earing, EF W agner, D M etcalf, NA N icola and NM Gough. (1988). Myeloid leukaemia inhibitory factor maintains the developmental potential of embryonic stem cells. Nature 336:684–687.
19. Sekkai D, G Gruel, M Herry, V Moucadel, SN Constantinescu, O Albagli, D Tronik-Le Roux, W Vainchenker and A Bennaceur- Griscelli. (2005). Microarray analysis of LIF/Stat3 transcriptional targets in embryonic stem cells. Stem Cells 23:1634–1642.
20. Niwa H, T Burdon, I Chambers and A Smith. (1998). Self-renewal of pluripotent embryonic stem cells is mediated via activation of STAT3. Gene Dev 12:2048–2060.
21. Ying QL, J Nichols, I Chambers and A Smith. (2003). BMP induction of Id proteins suppresses differentiation and sustains embryonic stem cell self-renewal in collaboration with STAT3. Cell 115:281–292.

22. Hollnagel A, V Oehlmann, J Heymer, U Ruther and A Nordheim. (1999). Id genes are direct targets of bone morphogenetic protein induction in embryonic stem cells. J Biol Chem 274:19838–19845.
23. Nakashima K, M Yanagisawa, H Arakawa, N Kimura, T Hisatsune, M Kawabata, K Miyazono and T Taga. (1999). Synergistic signaling in fetal brain by STAT3-Smad1 complex bridged by p300. Science 284:479–482.
24. Rajan P, DM Panchision, LF Newell and RD McKay. (2003). BMPs signal alternately through a SMAD or FRAP-STAT pathway to regulate fate choice in CNS stem cells. J Cell Biol 161:911–921.
25. Daheron L, SL Opitz, H Zaehres, WM Lensch, PW Andrews, J Itskovitz-Eldor and GQ Daley. (2004). LIF/STAT3 signaling fails to maintain self-renewal of human embryonic stem cells. Stem Cells 22:770–778.
26. Humphrey RK, GM Beattie, AD Lopez, N Bucay, CC King, MT Firpo, S Rose-John and A Hayek. (2004). Maintenance o f pluripotency in human embryonic stem cells is STAT3 independent. Stem Cells 22:522–530.
27. Sumi T, Y Fujimoto, N Nakatsuji and H Suemori. (2004). STAT3 is dispensable for maintenance of self-renewal in nonhuman primate embryonic stem cells. Stem Cells 22:861–872.
28. Xu RH, RM Peck, DS Li, X Feng, T Ludwig and JA Thomson. (2005). Basic FGF and suppression of BMP signaling sustain undifferentiated proliferation of human ES cells. Nat Meth 2:185–190.
29. Kasahara M, K Naruse, S Sasaki, Y Nakatani, W Qu, B Ahsan, T Yamada, Y Nagayasu, K Doi, Y Kasai, T Jindo, D Kobayashi, A Shimada, A Toyoda, Y Kuroki, A Fujiyama, T Sasaki, A Shimizu, S Asakawa, N Shimizu, S Hashimoto, J Yang, Y Lee,
K Matsushima, S Sugano, M Sakaizumi, T Narita, K Ohishi, S Haga, F Ohta, H Nomoto, K Nogata, T Morishita, T Endo, IT Shin, H Takeda, S Morishita and Y Kohara. (2007). The medaka draft genome and insights into vertebrate genome evolution. Nature 447:714–719.
30. Taniguchi Y, S Takeda, M Furutani-Seiki, Y Kamei, T Todo, T Sasado, T Deguchi, H Kondoh, J Mudde, M Yamazoe, M Hidaka, H M itani, A Toyoda, Y S akaki, RH Plasterk and E Cuppen. (2006). Generation of medaka gene knockout models by target-selected mutagenesis. Genome Biol 7:R116.
31. Furutani-Seiki M, T Sasado, C Morinaga, H Suwa, K Niwa, H Yoda, T Deguchi, Y Hirose, A Yasuoka, T Henrich, T Watanabe, N Iwanami, D K itagawa, K S aito, S Asaka, M Osakada, S Kunimatsu, A Momoi, H Elmasri, C Winkler, M Ramialison, F Loosli, R Quiring, M Carl, C Grabher, S Winkler, F Del Bene, A Shinomiya, Y Kota, T Yamanaka, Y Okamoto, K Takahashi, T Todo, K Abe, Y Takahama, M Tanaka, H Mitani, T Katada, H Nishina, N Nakajima, J Wittbrodt and H Kondoh. (2004). A systematic genome-wide screen for mutations affecting organogenesis in Medaka, *Oryzias latipes*. Mech Dev
121:647–658.
32. Loosli F, RW Koster, M Carl, R Kuhnlein, T Henrich, M Mucke, A Krone and J Wittbrodt. (2000). A genetic screen for mutations affecting embryonic development in medaka 7 sh (*Oryzias latipes*). Mech Dev 97:133–139.
33. Hong Y, C Winkler and M Schartl. (1996). Pluripotency and differentiation of embryonic stem cell lines from the medakafish (*Oryzias latipes*). Mech Develop 60:33–44.
34. Hall TA. (1999). BioEdit: a user-friendly biological sequence alignment editor and analysis program for Windows 95/98/NT. Nucl Acids Symp Ser 41:98, 95.
35. Thompson JD, DG Higgins and TJ Gibson. (1994). CLUSTAL W: improving the sensitivity of progressive multiple sequence alignment through sequence weighting, position–speci7 c gap penalties and weight matrix choice. Nucleic Acids Res 22:4673–4680.

36. Hong Y, C W inkler a nd M S chartl. (1998). Production of medakafish chimeras from a stable embryonic stem cell line. Proc Natl Acad Sci USA 95:3679–3684.
37. Hoegg S, H Brinkmann, JS Taylor and A Meyer. (2004). Phylogenetic timing of the fish-specific genome duplication correlates with the diversification of teleost fish. J M ol E vol 59:190–203.
38. Shu X, NC Shaner, CA Yarbrough, RY Tsien and SJ Remington. (2006). Novel chromophores and buried charges control color in mFruits. Biochemistry 45:9639–9647.
39. Kretzschmar AK, MC Dinger, C Henze, K Brocke-Heidrich and F Horn. (2004). Analysis of Stat3 (signal transducer and activator of transcription 3) dimerization by fluorescence resonance energy transfer in living cells. Biochem J 377:289–297.
40. Nicolas FJ, K De Bosscher, B Schmierer and CS Hill. (2004). Analysis of Smad nucleocytoplasmic shuttling in living cells. J Cell Sci 117:4113–4125.
41. Giepmans BN, SR Adams, MH Ellisman and RY Tsien. (2006). The fluorescent toolbox for assessing protein location and function. Science 312:217–224.
42. Simeoni I and JB Gurdon. (2007). Interpretation of BMP signaling in early Xenopus development. Dev Biol 308:82–92.
43. Watanabe K, K Saito, M Kinjo, T Matsuda, M Tamura, S Kon, T Miyazaki and T Uede. (2004). Molecular dynamics of STAT3 on IL-6 signaling pathway in living cells. Biochem Bioph Res Co 324:1264–1273.
44. Herrmann A, U Sommer, AL Pranada, B Giese, A Kuster, S Haan, W Becker, PC Heinrich and G Muller-Newen. (2004). STAT3 is enriched in nuclear bodies. J Cell Sci 117:339–349.
45. Huang Y, J Qiu, S Dong, MS Redell, V Poli, MA Mancini and DJ Tweardy. (2007). Stat3 isoforms, alpha and beta, demonstrate distinct intracellular dynamics with prolonged nuclear retention of Stat3beta mapping to its unique C-terminal end. J Biol Chem 282:34958–34967.
46. Herbst A, M Koester, D Wirth, H Hauser and K Welte. (1999). G-CSF receptor mutations in patients with severe congenital neutropenia do not abrogate Jak2 activation and stat1/ stat3 translocation. Ann N Y Acad Sci 872:320–325; discussion 325–327.
47. Kanda T, KF Sullivan and GM Wahl. (1998). Histone-GFP fusion protein enables sensitive analysis of chromosome dynamics in living mammalian cells. Curr Biol 8:377–385.
48. Ai HW, NC Shaner, Z Cheng, RY Tsien and RE Campbell. (2007). Exploration of new chromophore structures leads to the identification of improved blue fluorescent proteins. Biochemistry 46:5904–5910.
49. Raz R, CK Lee, LA Cannizzaro, P d'Eustachio and DE Levy. (1999). Essential role of STAT3 for embryonic stem cell pluripotency. Proc Natl Acad Sci USA 96:2846–2851.
50. Liu L, KM McBride and NC Reich. (2005). STAT3 nuclear import is independent of tyrosine phosphorylation and mediated by importin-alpha3. Proc Natl Acad Sci USA 102:8150–8155.
51. Qing Y and GR Stark. (2004). Alternative activation of STAT1 and STAT3 in response to interferon-gamma. J Biol Chem 279:41679–41685.
52. Aizawa K, A Shimada, K Naruse, H Mitani and A Shima. (2003). The medaka midblastula transition as revealed by the expression of the paternal genome. Gene Expr Patterns 3:43–47.
53. Dick A, A Meier a nd M Hammerschmidt. (1999). Smad1 a nd Smad5 have distinct roles during dorsoventral patterning of the zebrafish embryo. Dev Dyn 216:285–298.
54. Gromova KV, M Friedrich, A Noskov and GS Harms. (2007). Visualizing Smad1/4 signaling response to bone morphogenetic protein-4 activation by FRET biosensors. Biochim Biophys Acta 1773:1759–1773.

55. Rakemann T, M Niehof, S Kubicka, M Fischer, MP Manns, S Rose-John and C Trautwein. (1999). The designer cytokine hyperinterleukin- 6 is a potent activator of STAT3-dependent gene transcription in vivo and in vitro. J Biol Chem 274:1257–1266.
56. Sapkota G, C Alarcon, FM Spagnoli, AH Brivanlou and J Massague. (2007). Balancing BMP signaling through integrated inputs into the Smad1 linker. Mol Cell 25:441–454.
57. Xiao Z, AM Brownawell, IG Macara and HF Lodish. (2003). A novel nuclear export signal in Smad1 is essential for its signaling activity. J Biol Chem 278:34245–34252.
58. Ghil SH, YJ Jeon and H Suh-Kim. (2002). Inhibition of BETA2/NeuroD by Id2. Exp Mol Med 34:367–373.
59. Friedman MS, MW Long and KD Hankenson. (2006). Osteogenic differentiation of human mesenchymal stem cells is regulated by bone morphogenetic protein-6. J Cell Biochem 98:538–554.
60. Suzuki A, E Kaneko, J Maeda and N Ueno. (1997). Mesoderm induction by BMP-4 and -7 heterodimers. Biochem Bioph Res Co 232:153–156.
61. Boiani M and HR Scholer. (2005). Regulatory networks in embryo-derived pluripotent stem cells. Nat Rev 6:872–884.
62. Feng GS. (2007). Shp2-mediated molecular signaling in control of embryonic stem cell self-renewal and differentiation. Cell Res 17:37–41.
63. Hao J, TG Li, X Qi, DF Zhao and GQ Zhao. (2006). WNT/betacatenin pathway up-regulates Stat3 and converges on LIF to prevent differentiation of mouse embryonic stem cells. Develop Biol 290:81–91.
64. Liu N, M Lu, X Tian and Z Han. (2007). Molecular mechanisms involved in self-renewal and pluripotency of embryonic stem cells. J Cell Physiol 211:279–286.
65. Ogawa K, R Nishinakamura, Y Iwamatsu, D Shimosato and H Niwa. (2006). Synergistic action of Wnt and LIF in maintaining pluripotency of mouse ES cells. Biochem Bioph Res Co 343:159–166.
66. Watanabe S, H Umehara, K Murayama, M Okabe, T Kimura and T Nakano. (2006). Activation of Akt signaling is suf7 cient to maintain pluripotency in mouse and primate embryonic stem cells. Oncogene 25:2697–2707.
67. Dreesen O and AH Brivanlou. (2007). Signaling pathways in cancer and embryonic stem cells. Stem Cell Rev 3:7–17.
68. Kachalo S, R Zhang, E Sontag, R Albert and B Dasgupta. (2007). NET-SYNTHESIS: A software for synthesis, inference and simpli7 cation of signal transduction networks. Bioinformatics 24:293–295.
69. Katoh M. (2007). Networking of WNT, FGF, Notch, BMP, and Hedgehog signaling pathways during carcinogenesis. Stem Cell Rev 3:30–38.
70. Loh YH, Q Wu, JL Chew, VB Vega, W Zhang, X Chen, G Bourque, J George, B Leong, J Liu, KY Wong, KW Sung, CW Lee, XD Zhao, KP Chiu, L Lipovich, VA Kuznetsov, P Robson, LW Stanton, CL Wei, Y Ruan, B Lim and HH Ng. (2006). The Oct4 and Nanog transcription network regulates pluripotency in mouse embryonic stem cells. Nat Genet 38:431–440.
71. Takahashi K and S Yamanaka. (2006). Induction of pluripotent stem cells from mouse embryonic and adult fibroblast cultures by defined factors. Cell 126:663–676.
72. Wernig M, A Meissner, R Foreman, T Brambrink, M Ku, K Hochedlinger, BE Bernstein and R Jaenisch. (2007). In vitro reprogramming of fibroblasts into a pluripotent ES-cell-like state. Nature 448:318–324.

73. Schena M, D Shalon, RW Davis and PO Brown. (1995). Quantitative monitoring of gene expression patterns with a complementary DNA microarray. Science 270:467–470.
74. Orlando V, H Strutt and R Paro. (1997). Analysis of chromatin structure by in vivo formaldehyde cross-linking. Methods 11:205–214.
75. Horak C E, M C Mahajan, NM Luscombe, M G erstein, SM Weissman and M Snyder. (2002). GATA-1 binding sites mapped in the beta-globin locus by using mammalian chIpchip analysis. Proc Natl Acad Sci USA 99:2924–2929.

**Fidure Legends**

**FIG. 1.** Localization of STAT3 in Medaka ES-cells grown under standard culture conditions. Antibody staining of STAT3 is shown in red (**A**) and DNA is visualized in blue by Hoechst (**B**). The overlay of both channels is given in (**C**). Scale bars represent 20 $\mu$m.

**FIG. 2.** Confocal section of an immunofluorescence staining for STAT3 in Medaka blastula embryos. STAT3 is shown in red (**A**) and DNA is visualized in blue (**B**) by DAPI staining. The overlay of both channels is given in (**C**). Scale bars represent 100 $\mu$m.

**FIG. 3.** (**A**) RT-PCR for stat3 during Medaka development. Lane 1 shows stat3 PCR products after 30 cycles. As reference, lane 2 shows the housekeeping gene elongation factor 1 alpha. PCR primers were designed to discriminate between genomic DNA and cDNA as shown in the last row of both lanes. In the first row of both lanes water-template controls are depicted. (**B**) RT-PCR for smad1/5/7 and id2 during Medaka development. Lanes show PCR products a fter 30 cycles. As reference, lane 1 shows the housekeeping gene elongation factor 1 alpha. Discrimination between genomic DNA and cDNA is possible due to primers spanning small introns for all cDNAs except for smad7, for which no intron was found. cDNA contamination of PCRs is excluded by water-template controls shown in row 1 of all lanes. (**C**) RT-PCR for stat3, smad1/5/7 and id2 in Mes1 cells. Lanes show PCR products after 30 cycles. As reference, lane 1 shows the housekeeping gene elongation factor 1 alpha. In the last lane water was used as a negative control template for ef1a1 PCR.

**FIG. 4.** Representative confocal section of an immuno: uorescence staining for SMAD1 in Medaka ES-cells. The SMAD1 signal is depicted in red (**A**) and DNA is shown in blue after DAPI staining (**B**). The overlay of both channels is given in (**C**). Scale bars represent 20 $\mu$m.

**FIG. 5.** Confocal image of GFP-MFSMAD1 in Medaka blastula embryos. As typical example, the same confocal section is displayed for both channels. The SMAD1 signal is depicted in red (**A**) and DNA is shown in blue (**B**) after DAPI staining. The overlay of both channels is given in (**C**). Scale bars represent 100 $\mu$m.

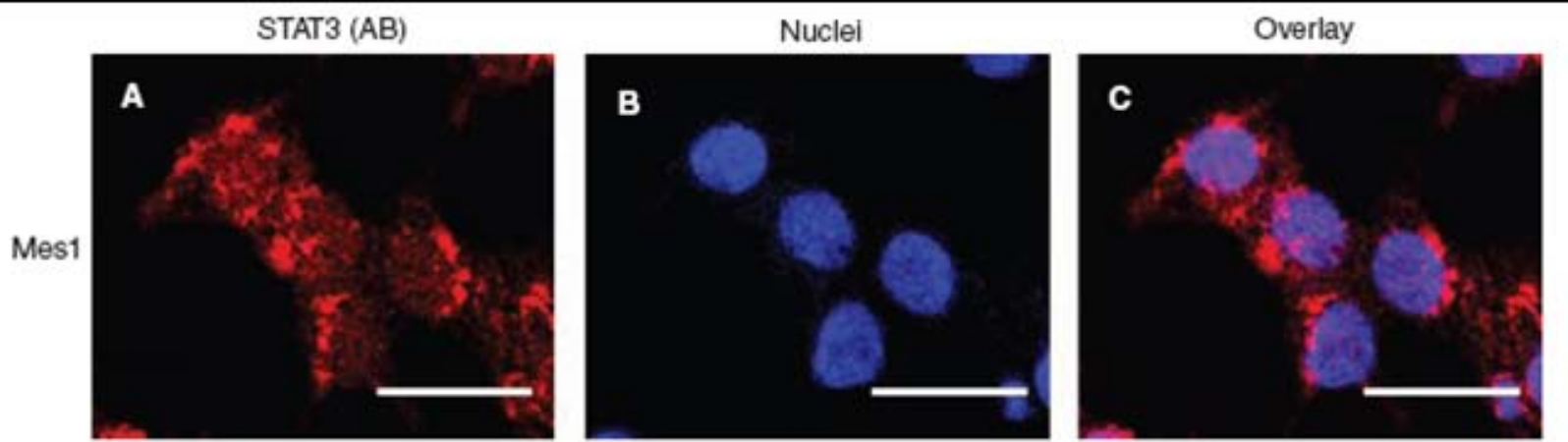
STAT3 (AB)
Nuclei
Overlay
A
B
C
Mes1

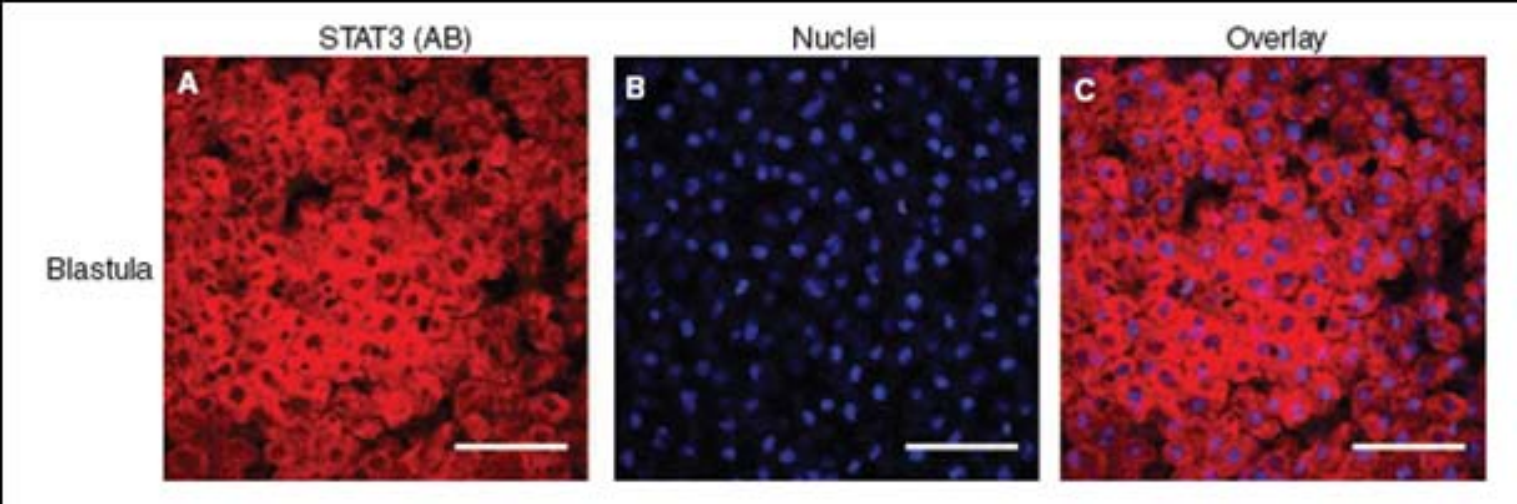
STAT3 (AB)
Nuclei
Overlay
Blastula
A
B
C

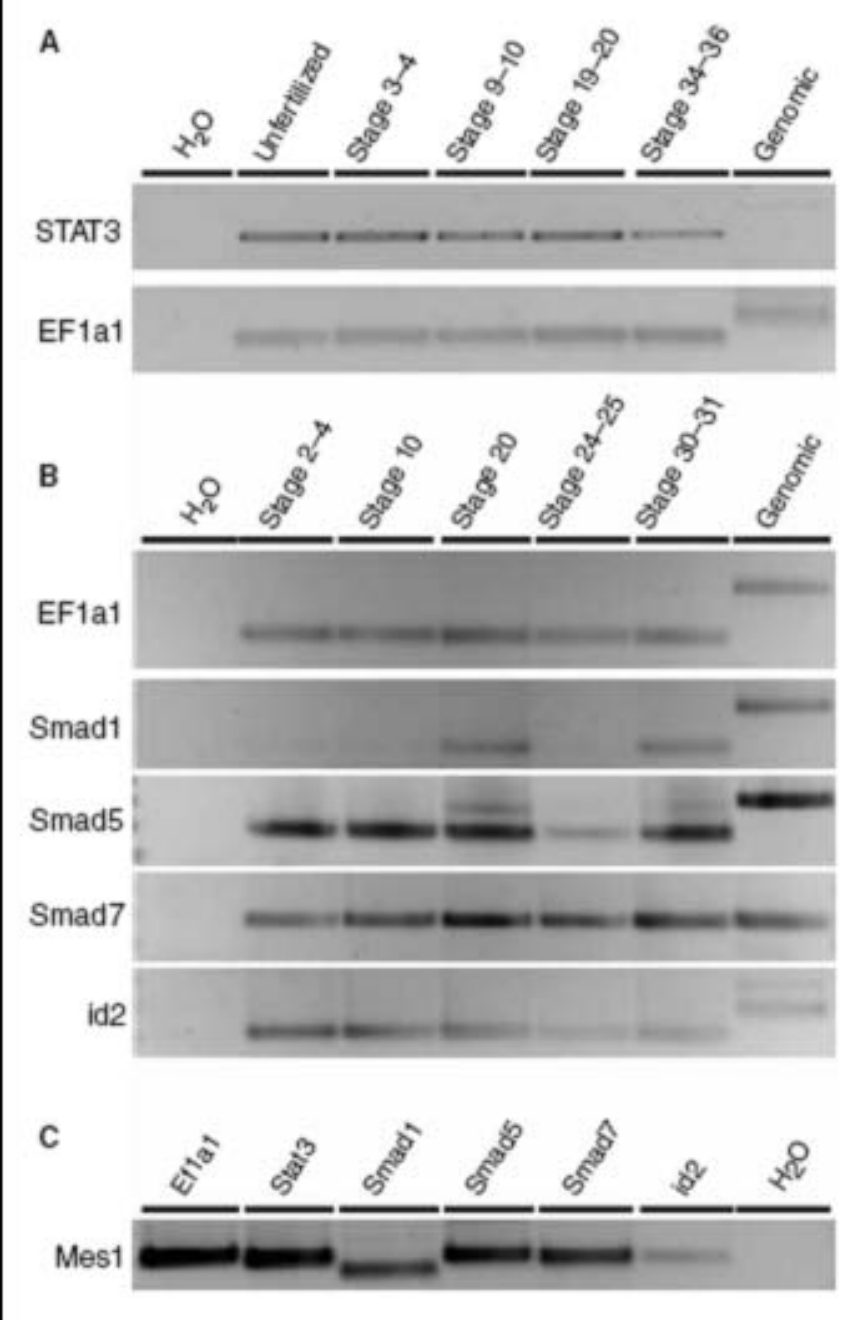
A
H2O
Unfertilized
Stage 3–4
Stage 9–10
Stage 19–20
Stage 34–36
Genomic
STAT3
EF1a1
B
H2O
Stage 2–4
Stage 10
Stage 20
Stage 24–25
Stage 30–31
Genomic
EF1a1
Smad1
Smad5
Smad7
id2
C
Ef1a1
Stat3
Smad1
Smad5
Smad7
id2
H2O
Mes1

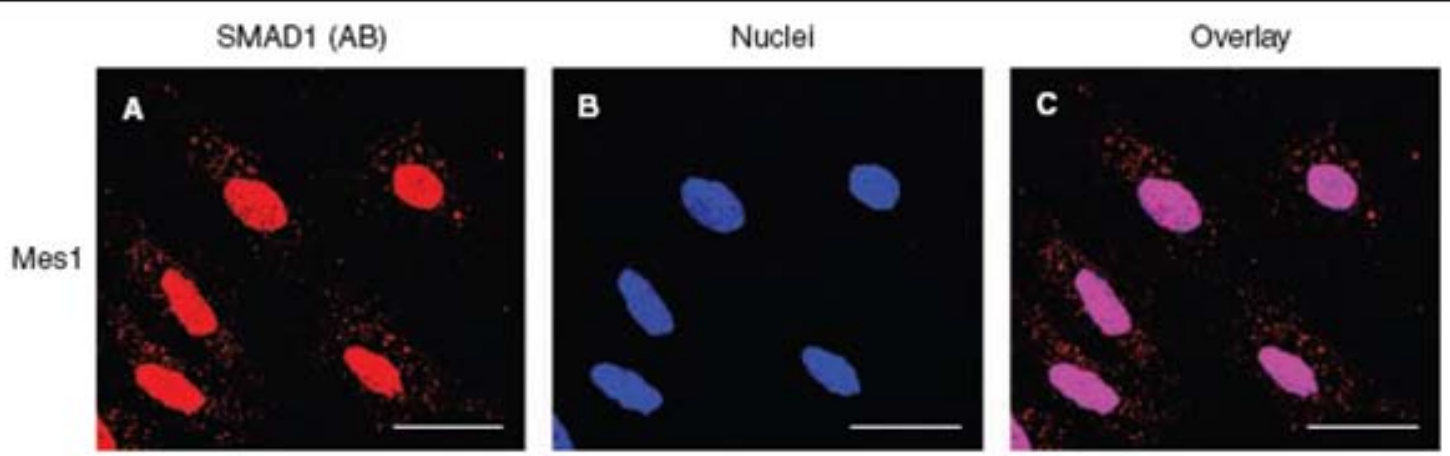
SMAD1 (AB)
Nuclei
Overlay
A
B
C
Mes1

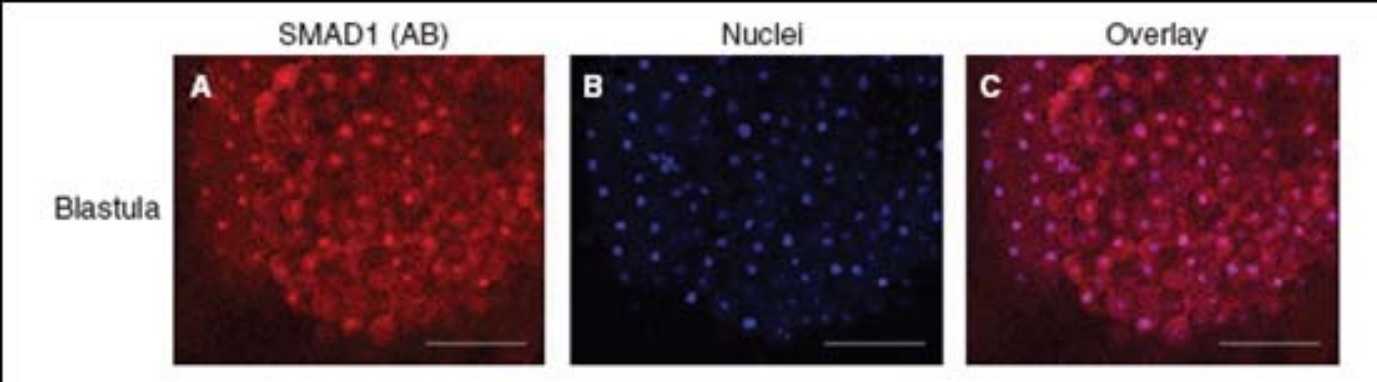
SMAD1 (AB)
Nuclei
Overlay
Blastula
A
B
C